THE OPTIMUM LASER TREATMENT OF PORT-WINE STAINS

A thesis
submitted in partial fulfilment
of the requirements for the Degree
of
Doctor of Philosophy in Physics
in the
University of Canterbury
by
Derek J. Smithies

University of Canterbury
1995

Abstract

A port-wine stain is a visually obtrusive cosmetic defect of the skin. There is a desire for a removal process that is effective with a minimal risk for the patient.

The laser treatment of port-wine stains has been the most effective method so far. Further improvements in this technique may be attained by adjustment of the treatment parameters.

In this thesis, we numerically model the treatment process. The passage of the laser light through skin is simulated with the Monte Carlo method. Our simulation is superior to those of other workers as we use a more realistic model of skin with the minimum of assumptions. These results are used to predict the temperature change in skin. The effect of conduction is included, so we can calculate the ideal illumination time.

The illumination time should be in the range of 1-10 ms. For vessels with a diameter of 50 μm, the ideal illumination time is close to 4 ms. The calculations show that the fluence should be around 3 J/cm^2. When the vessel diameter is larger, a longer illumination time and a higher fluence will be necessary.

To provide these illumination times, a computer controlled scanning device was designed and built. The light from a copper vapour laser is scanned over the port-wine stain to form a rasterscan like pattern on the lesion. The user determines what part of the lesion is treated, so the light never scans over normal skin.

Following treatment with illumination times of 4 ms and a fluence of 10 J/cm^2, the skin blanches, and then turns red as a result of erythema. The blanching response is not related to non-selective damage within the skin but is attributed to constriction of the blood filled vessels. We describe the probable mechanism that causes the constriction.

Our calculations predict that a fluence that is approximately one fifth of the fluence that is used in the clinic. We discuss the validity of the optical parameters that were used in our calculations. The effect of changing these parameters by a factor of five is shown. One possible explanation is that the model of skin used does

not include the effect of the superficial layers of the epidermis. We suggest that these layers prevent some of the incident beam from reaching the vessels below the laser beam.

The time before the blanching response commences is calculated from measurements of the quantity of light backscattered from the skin. The blanching occurs between 8 and 13 ms after the spot is incident on a region of skin. This is 4 ms, or more, after sufficient energy has been deposited in the skin to cause the desired response.

Contents

List of Tables

List of Figures

Chapter 1

Introduction

We briefly describe what a port-wine stain is. Such a mark may cause psychological or social problems for the bearer, which forms the motivation to have the mark removed. Several techniques have been tried, with varying degrees of success. The use of lasers to remove these marks has provided some very encouraging results.
The motivation for this thesis is to obtain an improvement in the clinical results. We aim to achieve this by understanding the physical processes involved, and from this predict and trial different treatment protocols.

A port-wine stain is a red, or purple, discolouration of a region of skin, and is present through the entire lifetime of those so afflicted. They consist of ectatic (swollen or enlarged) capillaries in the skin, most of which contain blood (Barsky *et al*, 1980). Thus, a larger fraction of the skin is blood, and so the discolouration. This discolouration is visually obtrusive, and forms a cosmetic defect. With age the port-wine stain tends to form nodules.

Several studies on the incidence of port-wine stains have been carried out (Jacobs and Walton, 1976; Osburn *et al*, 1987; Karvonen *et al*, 1992). In the combined results, 18 (0.3%) of the 6234 babies examined had port-wine stains. From the work reported in these papers, it is usually stated in the literature that 0.3% of the population have port-wine stains. The validity of this extrapolation is questionable and remains to be proven in larger studies.

The cause of the blemish is uncertain. It seems that it is linked to a problem in the nervous system. Ohtsuka (1990) notes that the distribution pattern is said to correspond roughly to that of the sensory branches of the trigeminal nerve. The findings of Smoller and Rosen (1986) showed that there is a deficit in the number of

perivascular nerves in port-wine stains. From this, they raise the possibility that a lack of neural modulation of the vascular flow may be involved in the pathogenesis of port-wine stains.

Sadly, there are mothers of those with port-wine stains that blame themselves for the port-wine stain. They point to a trauma during the pregnancy as the cause. Such a belief is wrong, as there are many mothers who had similar or worse experiences during pregnancy and their children were unmarked.

A port-wine stain may cause psychological or social problems for the person so afflicted. These problems are briefly discussed in section 1.1. There is a need for treatment of port-wine stains, and patients are prepared to pay thousands of dollars for partial removal. We describe the various techniques that have been used in section 1.2. The use of a laser to remove port-wine stains is the preferred technique. Several terms which describe the treatment process with a laser are defined in section 1.3.

When seeking to find the method of delivering the laser beam onto the skin that gives the best possible outcome, a knowledge of the physics involved will aid the interpretation of the results. This will reduce the number of clinical trials needed. In the search for the appropriate treatment there are several questions which have been raised. These questions are listed in section 1.4, and the need for answers has formed the motivation for the work contained in this thesis. Section 1.5 lists the chapters in this thesis and describes how they fit into the calculation of, and the use of, the optimal treatment parameters for port-wine stains.

1.1 Motivation for treatment

In this brief section, we give a few of the psychological and social problems that the presence of a port-wine stain may cause a person. These examples illustrate the point that there is a need to remove port-wine stains from those so afflicted.

Several studies on the effect of a port-wine stain on a person have been carried out. Dixon *et al* (1984b), Lanigan and Cotterill (1989) and Pickering *et al* (1990a) have sent questionnaires to people who presented for treatment of their port-wine stain. The results from these studies show a clear need for the the port-wine stain to be removed. The respondents in the third study stated that they had difficulties with interpersonal relationships, particularly with members of the opposite gender.

In these studies, people with port-wine stains who had undergone laser treatment were questioned. The people involved in the questionnaire must have disliked their

port-wine stain, as this dislike would have formed the motivation to seek treatment. That a person with a port-wine stain is willing to undergo treatment, with the associated risk of an untoward result, is further evidence of the need for an effective treatment.

Wagner and Wagner (1990) review results of various studies in the literature. They describe the parental reactions and the psychological implications of untreated port-wine stains in children. From these results, they conclude that the presence of a port-wine stain adversely affects the psychological development of a child.

An illustration of the psychological harm caused by a port-wine stain comes from the experience of one lady who presented for treatment. Her port-wine stain was dark red in colour, covering one cheek, the jaw and neck. When, as a child, she was at assembly in school, a teacher called her to the side with a loud, authoritative voice. She was then told by the teacher, without reducing the volume, "to remove the lipstick from her face". One can only speculate on the feelings of embarrassment created in this child.

1.2 Overview of the treatment of port-wine stains

In this section, we describe the techniques that have been used, and those currently used, to remove port-wine stains.

1.2.1 Prior to the use of lasers

Some of the methods described in this subsection are *macro* in nature. These methods result in damage to both the non-vascular and vascular tissue.

cause non-specific necrosis	remove the skin	cover the skin
x-ray irradiation	surgery and skin graft	tattooing
electrocautery	dermabrasion	makeup
cryosurgery		

Table 1.1. The various techniques that were used prior to the advent of the laser to cover or remove a port-wine stain.

Tan (1992) lists the various treatments that have been used. They are listed in table 1.1. These techniques fall into three categories.

The techniques in the first category cause non-specific necrosis of the tissue. This is a very destructive approach to removing the offending mark. Following treatment,

the desire is that the appearance of the port-wine stain will be less objectionable. This may not be the case, as the tissue below the skin is damaged.

In the second category, the skin is removed with surgery. Partial excision may not give much improvement of the appearance as the patient will end up with a square or rectangular section of normal skin inside, or adjacent to, an irregularly shaped port-wine stain. Goldman *et al* (1976) notes that "Excisional surgery is often done in adult life when connective tissue changes in the port-wine mark result in nodular pendulous areas which can be ablated."

The two techniques in the third category differ from the rest as they attempt to cover the ectatic vessels, so that they are not seen. Goldman *et al* (1976) states in their description of the results obtained, "Tattooing with barium dioxide or zinc oxide particles is still done occasionally by some plastic surgeons. This procedure results in an irregular mottled pattern".

The use of heavy "theatrical" makeup is common among females. It is hot, uncomfortable and greasy. Carruth *et al* (1992) states "It has been estimated, however, that only one-third of patients use special makeup to cover the port-wine stain, and many of those who do use makeup are distressed to be seen by others without this protection."

1.2.2 Laser treatment

In this subsection, we give an overview of the laser treatment of port-wine stains.

One desires that the large vessels within the skin are thermally damaged, so that they are no longer viable. As these vessels no longer contain blood, there will be less blood in the skin, so the colour of the port-wine stain will fade. It is the action of the laser beam that damages the large vessels in the skin. This process is summarised below.

The laser light is directed onto the skin. It may have passed through a fibre or the laser beam was reflected off a mirror. Most of the laser light travels into the skin, while some is reflected at the surface. The epidermis, non-vascular dermis and the blood in the dermis absorb a fraction of the incident light. The remainder of the laser light is backscattered out of the skin.

Typically, yellow light (577 or 585 nm) is used when treating port-wine stains. These wavelengths are strongly absorbed in the haemoglobin, and less strongly absorbed in the non-vascular components in the skin. The temperature of the blood rises as a result of absorbing some of the energy in the laser beam. Thermal conduction will cause the temperature of the blood vessel wall and adjacent tissue to rise.

If there is a sufficient rise in the temperature of the vessel walls, then the cells in the vessel wall will become necrotic, and the vessel will no longer be viable. After the healing process has occurred, the vessel will no longer contain blood.

We require that the non vascular structures in the skin are undamaged. If this requirement is met, laser treatment is *micro* in nature. Such a treatment will minimise the risk of untoward results, and is regarded as optimal.

Several different laser types have been used, argon-ion, CO_2, continuous wave dye, copper bromide, copper vapour, excimer, Nd:YAG, pulsed dye, and ruby. In many cases, it seems that the choice of laser was determined not by physical principles but by the availability of a particular type of laser. From an argument based on physical principles, Anderson and Parrish (1981b) stated that lasers producing yellow light (577 nm) should be used as this will cause selective heating of the blood in the skin. In the following years, there has been a gradual shift in the literature towards the use of this wavelength.

Recently, some have claimed that 585 nm will provide superior results to the 577 nm wavelength. The literature is in general agreement that yellow light, either 577 or 585 nm will provide the best results. There is an ongoing disagreement about the merits of 585 nm over 577 nm.

When the exposure time is less than 0.5 ms, the skin turns purple as a result of treatment. This is described in the literature as purpura. With exposure times longer than 4 ms, the skin is whitened by the laser beam. This is described as blanching.

1.3 The terms used to describe the laser treatment

In this section, we give a glossary of the words that are used to describe the laser treatment of port-wine stains.

Spot diameter or spotsize
The diameter of the spot formed when the laser beam is incident on the skin. In this thesis, we assume that the spot has a uniform intensity and the laser beam is normal to the skin surface. We use the units of millimetres, (mm). In clinical practice, the laser beam can be far from uniform, perhaps gaussian. The laser beam may be divergent or convergent, which is determined by the focussing of the laser beam.

Laser power
The power contained in the laser beam, which is measured in watts. In this thesis,

we have assumed that the power output of the laser is constant during the exposure time, as shown in figure 1.1a. However, Dinehart *et al* (1993) report that the power output of this laser is not constant, which is shown in figure 1.1b.

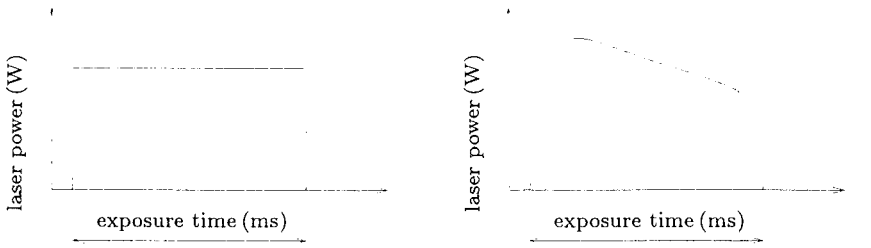

(a) Theoretical pulse profile (b) Pulse profile of pulse dye laser

Figure 1.1. Theoretical and actual pulse profile of the pulsed dye laser from Dinehart *et al* (1993).

We describe the results from the copper vapour laser. The laser that we use in our clinic generates a series of pulses at a frequency of 15 kHz, so the output appears to be continuous. Consequently, the laser has been described in the literature as "quasi continuous" (Neumann *et al*, 1992). The individual pulses last, approximately, 0.000 02 ms (20 ns). Between each pulse there is a 0.067 ms interval. The haemoglobin, which absorbs the incident light, does not cool to its initial temperature by conduction during the interval between pulses. Thus, the temperature of the haemoglobin will rise in a staircase manner. Conduction effects will (mostly) remove the effect of the non-uniform energy input so the temperature rise in the other components of blood will be a smoother function of time.

Wavelength

This term is used when describing the laser beam that is incident on the skin during treatment. It has been defined as "the distance, measured in the direction of propogation, between two points of the same phase in consecutive cycles of a wave." (Hanks, 1986). We have used the units of nanometres, (nm), in this thesis when describing the wavelength of the laser beam. By specifying the wavelength, we specify the position of the laser beam on the electromagnetic spectrum.

There is, essentially, no difference in the absorption properties of the haemoglobin and epidermis at the wavelengths 577 and 578 nm. Thus, when we describe the use of the 578 nm wavelength light generated by a copper vapour laser, the results would be unchanged if the wavelength was switched to 577 nm.

The copper vapour laser generates green (510.55 nm) and yellow (578.21 nm) light. These wavelengths results from two particular transitions of the electrons in the copper atom. The motion of the copper atoms in the laser tube cause the light generated to be Doppler shifted, so the wavelengths generated will vary by fractions of a nanometer. For our purposes, we may regard the output as fixed at 510 and 578 nm.

In contrast, the pulsed dye laser produces a range of wavelengths. Hulsbergen-Henning *et al* (1984) reports that with a Phase R flash-lamp pumped dye-laser, Rhodamine 575 dye, the power produced is spread over a range of wavelengths. Peak power is at 577 nm, and the full width of this range at half maximum is 5 nm. In our theoretical calculations, we ignore this spread.

In a personal communication to my thesis advisor, Prof. Martin J. C. van Gemert stated that with some models of a tunable pulsed dye laser there may be a difference of 5 nm between the stated output wavelength and the generated wavelength. Such a difference is unfortunate, as this change in the wavelength affects the amount of light absorbed in the haemoglobin. We do not consider the effect of this problem when examining the literature.

The argon-ion laser generates a number of wavelengths in the visible region, most of which are around 500 nm. The two principal wavelengths at 488.0 and 514.5 nm are used when treating port-wine stains. The absorption properties of skin for these two wavelengths are similar, so the output of this laser may be considered to be at 500 nm.

Illumination time

The maximum period of time that the laser beam is incident on any one point in the skin. The illumination time is set by several factors, the design of the laser, the action of shutters in the laser, and the method of directing the beam onto the skin.

With a pulsed dye laser, the laser generates a pulse of light that lasts for less than a millisecond. This light is passed down a fibre and directed at one region of the port-wine stain. The illumination time is equal to the duration of the light pulse.

The light from a continuous wave laser may be chopped by the action of shutters within the laser so that pulses of light are generated. Each individual pulse is directed at a different point on the skin, which can be achieved with a device such as the Hexascan (Rotteleur *et al*, 1988). Typically, the illumination time, or pulse length, is longer than 20 ms (Neumann *et al*, 1993).

The light from a continuous wave laser may be scanned in a rasterscan like fashion

over the port-wine stain. In this case, the illumination time is the time required for the spot to move a distance equal to the diameter of the spot.

Throughout this thesis, we use the units of milliseconds, (ms).

Fluence

The amount of energy deposited on a region of tissue. In the literature, the units used are J/cm^2. When the laser beam is pulsed by the action of shutters or the design of the laser, this is determined from

$$\text{fluence} = \frac{\text{illumination time} \times \text{laser power}}{\text{area of laser spot}} \tag{1.1}$$

If the laser beam is scanned over the port-wine stain, the average fluence is calculated. That is

$$\text{fluence} = \frac{\text{time to scan a region of skin} \times \text{laser power}}{\text{area of the region scanned}} \tag{1.2}$$

To illustrate the case for when the beam is continuous, we take the data from figure 2 of Pickering *et al* (1990b). When the laser power is 5 W, 4.5 s are required to scan 1 cm^2. Consequently, the fluence is 22 J/cm^2. The lines on the skin which the spot travels over are separated by a gap so that no part of the skin is accidentally treated twice. The size of this gap is less than one spot diameter.

1.4 The motivation for this thesis

In this section, we describe the motivation for the work contained in this thesis.

In the absence of knowledge of the processes involved in the laser treatment, one approach to finding a satisfactory treatment is to

> Take a set of treatment parameters, and use it on a group of patients. Alter the parameters and treat another set of patients. Repeat this process. When the incidence of untoward results has been minimised with a particular set of parameters, use this on all subsequent patients.

This type of approach has been effective when testing and improving drugs to treat illnesses. However, we understand part of the damage process and a little of the repair process from clinical and histological studies. With this knowledge we can estimate which treatment parameters should be tested and better interpret the results from the trials that are carried out.

Consequently, the optimal treatment parameters can be determined with the minimum of clinical trials. This is beneficial, as it means that fewer patients will receive a non-optimal treatment.

The theoretical model must be able to answer questions such as the effect of beam diameter, capillary geometry, wavelength, skin pigmentation, and scattering model on the distribution of absorbed light in skin. Such a model did not exist in the literature when my Ph.D. commenced in 1989. The desire to fill this gap formed the motivation for some of the work contained in this thesis.

Part of the goal of my Ph.D. resarch was to answer several questions about the treatment of port-wine stains, specifically:

1. What is the clinical effect when illumination times in the 1–10 ms range are used?

2. Is there an increase in the depth of penetration when the wavelength is changed from 577 to 585 nm?

3. Can a computer program be written so that the surgeon, who is not computer literate, may successfully operate a computer controlled treatment device?

4. When the skin blanches after treatment, what processes occur in the skin, and how quickly do these processes occur?

1.5 Contents of this thesis

We desire to find the optimal treatment for port-wine stains. Improved treatment protocols for port-wine stains can be deduced with an understanding of the physics and biology involved in the laser treatment of port-wine stains. By adding to this knowledge, we can better interpret the results from clinical trials, and reduce the number of clinical trials that are necessary to test our calculations and understanding.

In chapter 2, we examine the structure of skin, both normal and where there is a port-wine stain. We look at skin from a clinical viewpoint, where the various structures within it are described. For theoretical simulations, skin is described with a model which is a simplification of skin. We describe the model that we use, which is superior to those of previous workers.

With a model of skin chosen, one can determine the passage of light through it. The various methods of simulating the passage of light through our model of skin are described in chapter 3. The complexity of our model is such that only one method, Monte Carlo, is suitable.

The Monte Carlo technique is described in detail in chapter 4. The methods used to reduce the necessary computer time are explained. In this chapter we show

the distribution of absorbed light in skin for a variety of vessel geometries and the wavelengths 577 and 585 nm.

From a knowledge of where the light is absorbed in the skin, we examine the effect of adjusting the illumination time in chapter 5. The effect of changing the wavelength from 577 to 585 nm is shown. A range of vessel configurations is used.

The computed temperature changes in the skin are much higher than those obtained clinically. We examine several possible reasons for this in chapter 6.

The results from the theoretical simulations state that the illumination time should be in the range of 1-10 ms. In chapter 7, we describe the computer controlled scanning (SCANALL) system that was designed and built to provide these illumination times.

In chapter 8, we describe the clinical results from other workers and our treatment protocol. These results are evaluated in the light of the theoretical work in the previous chapters.

Chapter 9 contains a description of the photodiode unit that was used to obtain a measurement of the rate at which the skin turns white after treatment with the computer controlled scanner.

Finally, in chapter 10, we summarise the findings of this research.

Chapter 2

Skin

In this chapter, we describe the structure of normal skin.
The differences between normal and port-wine stain skin
are explained.
The optical properties of the various components used
in models that represent skin are listed.
From the biological information, the basis for the various
representations of skin in the literature is described.

In section 2.1 we describe the physiology of skin. The optical properties of the components in skin are listed in section 2.2.

The description of skin shows that it is a complex organ, far more complex than the various models that have been used to describe it. Most of the models that have been used in the literature are given in section 2.3.

2.1 Physiology of human skin

In our simulations of the treatment process, we require a model of skin that represents reality. To develop a realistic model, we first examine the structure of normal and port-wine stain skin. From a knowledge of the structure of skin, we can set criteria for what components in the skin the laser beam should thermally damage.

In writing this review of the physiology of human skin, we have used the relevant information in the work of the following authors (Montagna, 1956; Marples, 1965; Rushmer, 1972; Jarrett, 1973; Ryan, 1973; Goldsmith, 1983; Parrish and Deutsch, 1984; Wood and Bladon, 1985). For further information, the reader may examine these references.

Skin is a continuous covering of the human body with an area of $1.8\,\mathrm{m}^2$, and constitutes 10% of the total adult body weight. It is a complex organ, varying in

thickness from 1 mm on the eyelids to 4 mm on the back, palms of the hands, and soles of the feet.

The skin over the body is furrowed by a specific pattern of grooves called the "lines of Langer". These lines are roughly similar, but not identical, in all individuals, and they are so orientated as to indicate the direction of elastic tension of skin.

In figure 2.1, we show the various components in skin. It is clear from this diagram that skin consists of three main layers: the epidermis, the dermis, and the subcutaneous tissue.

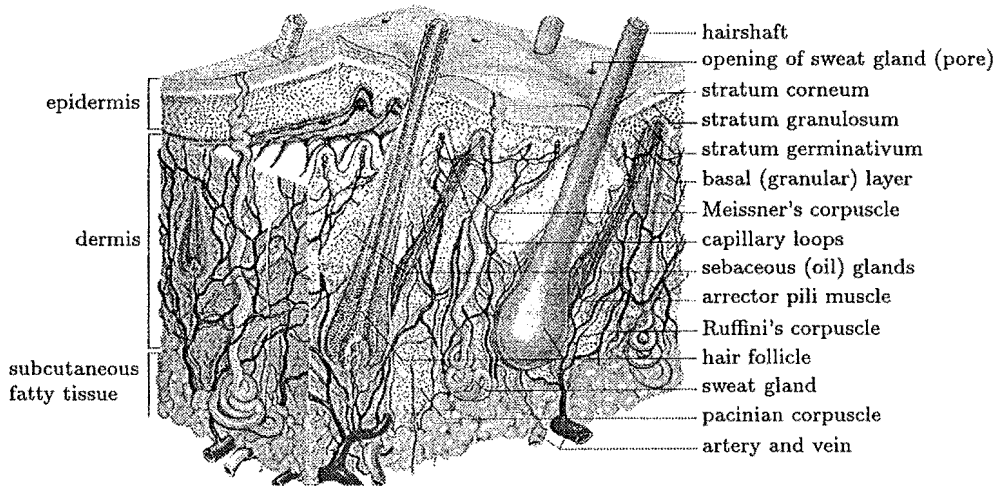

Figure 2.1. The various components in skin. Picture supplied courtesy of Glaxo New Zealand Limited.

2.1.1 Epidermis

The epidermis is the most superficial layer of the skin. It is cellular in structure and entirely avascular. The composition of the epidermis is shown in figure 2.2. We have used the diagram of skin from Marples (1965) which contains the stratum lucidum layer. Jarrett (1973) has noted that the stratum lucidum is only clearly evident in palmar and plantar epidermis where it is evident by a poorly staining hyalin zone immediately above the stratum granulosm.

Marples (1965) quote the work of Leider and Buncke (1954), who measured the thickness of the epidermis, and found it to be between 0.42 and 1.56 mm. These figures do not appear to include the stratum corneum as the authors state that the thickness of this layer has a range of 0.03 to 2.0 mm. The stratum spinosum ranges from 0.03 to 1.0 mm, the average thickness being about 0.07 mm.

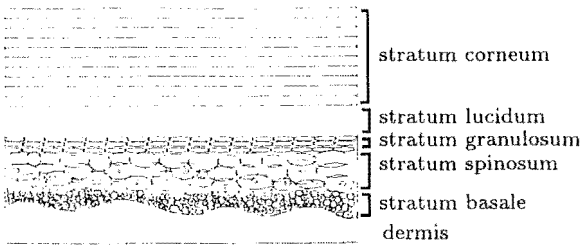

Figure 2.2. The layered structure of the epidermis.

The basal layer is only one cell thick and contains two types of cells: keratinocytes and melanocytes. The keratinocytes are so named because they produce keratin, the fibrous protective proteins of skin. The melanocytes produce melanosomes, small (0.3 μm to 1.0 μm) egg-shaped sacks that contain the chromophore melanin.

The keratinocytes in the basal layer divide, causing the daughter cells to be pushed towards the surface of the skin. Melanosomes are linked to the keratinocytes, so the upward movement of the keratinocytes spreads melanasomes throughout the epidermis. As the keratinocytes cells progress higher in the epidermis they become flatter, and the nucleus becomes more condensed. When the cells reach the the stratum granulosum, or granular layer, they die and form keratin. This material continues to move upwards, where it is eventually sloughed off. The entire process from basal cell formation to keratin shedding takes 45 to 75 days, depending on the thickness of the epidermis.

The melanosomes contain melanin, a complex macromolecular protein derived from tyrosine, which strongly absorbs visible light and ultraviolet radiation. It is the level of melanin in skin which determines how much ultraviolet and visible radiation reaches the dermis. Also, the melanin in the epidermis provides skin with its yellow, brown, or black pigmentation. The melanin content in the epidermis may vary by a large fraction between any two sites on the skin of an individual. Further, the melanin concentration at any site may change over a period of days or weeks depending on the exposure to ultraviolet light the skin receives.

For our purposes, the temperature of the skin is relevant. A summary of some of the results of Burton (1934) and Gagge *et al* (1938) is contained in the work of Marples (1965). When a nude patient is in an environment at 22.8 °C, the temperature of the skin on the head is between 33 and 33.4 °C. In contrast, the temperature on the palm of the hand is in the range, 32.5-32.9 °C. With clothing, these temperatures rise by 2 °C (approx).

2.1.2 Dermis

The dermis forms the bulk of the skin. It is a tough, resilient tissue that cushions underlying organs against mechanical injury and provides nutriment for the epidermis and cutaneous appendages. The dermis contains few cells, in contrast to the epidermis which is almost entirely cellular.

The main structural feature of the dermis is a network of mechanically strong fibres, mostly collagen, but with some elastin, embedded in a matrix of amorphous ground substance (polysaccharide). Collagen has a high tensile strength. This strength, along with the elasticity provided by elastin, creates a network of strong fibres which are able to protect underlying organs from mechanical injury.

Somewhat arbitrarily, the dermis can be divided into two layers, the superficial papillary layer and the deeper reticular layer. Between these two layers there is no clear dividing line. The papillary dermis contains the capillaries that provide nutrients for the epidermis. The lower layer extends inwards towards the fatty layer, and contains the larger blood vessels.

2.1.3 Cutaneous vascular system

The cutaneous blood supply serves a dual purpose. First, it provides nourishment to both the surrounding dermis and the avascular epidermis. However, the skin has a larger blood supply than is needed to satisfy its oxygen requirements. The large volume of blood which flows through the skin plays an important role in regulating the temperature of the body. On exposure to heat, a larger than normal volume of warm blood flows to the peripheral regions of the body through a widely dilated vascular network. In contrast, the rate of blood flow falls upon exposure to cold.

Marples (1965) has drawn a representation of the distribution of blood vessels within the skin, which we have shown in in figure 2.3. Ryan (1973) gives a different view, where the various loops in the papillary dermis are shown (figure 2.4). It is clear that the blood has many possible routes to take from when it enters the skin, to when it leaves the skin. Selection of the route is determined by the small arteries, which can close and block the flow of blood. When these shunts open, the blood does not pass through the shallow vessels.

The sizes of the vessels within the skin at different levels is shown in figure 2.5. An artery approximately 100 μm in diameter enters the lower dermis through the subcutaneous fat. This artery may divide once or twice before reaching the mid-dermis where the branches are approximately 50 μm in diameter and are called arterioles.

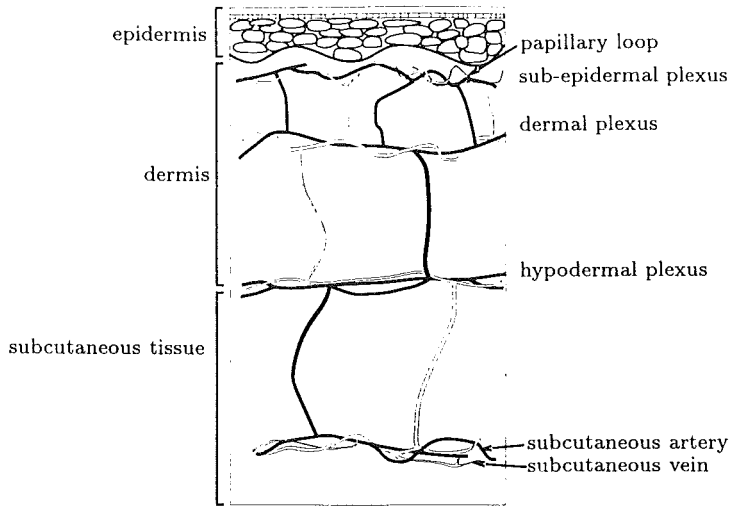

Figure 2.3. The blood vessels within skin.

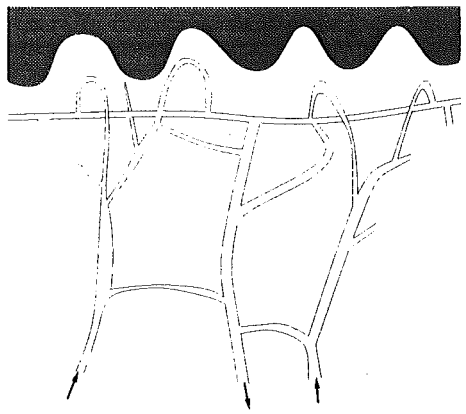

Figure 2.4. The various routes available to the blood when it flows through the skin.

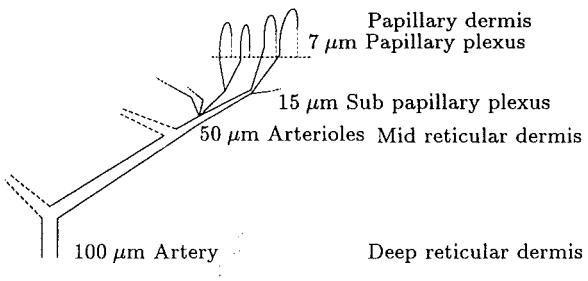

Figure 2.5. The size of the vessels within the dermis (Ryan, 1973).

More branching occurs as the arterioles reach upwards until they begin to form one or two plexi (the sub-papillary plexi) of small capillaries that lie approximately parallel to the surface. Extending from these plexi into the dermal papilla are the papillary (or terminal) capillaries. These are vertical loops in the shape of a hair pin, which supply the papillae. The papillary capillaries are only 5 μm to 10 μm in diameter and a typical papilla contains only one such vessel. The capillaries drain into venules which lead to larger and larger veins deeper within the dermis.

Capillaries are formed of a single layer of entwined endothelial cells. Unlike other types of blood vessel, capillaries have no surrounding muscle tissue to control vessel diameter and hence blood flow. At the join of the capillary and arteriole there is a pre-capillary sphincter muscle. It is this muscle which determines if the blood flows through the capillary. Only a fraction of the capillaries carry blood at any one time, since there is insufficient blood to fill every blood vessel in the body at the same time (Chaffee and Lytle, 1980). The fraction varies throughout the body and also varies with body temperature and emotional state.

The endothelial cells resemble lightly fried eggs rolled over to form a tube. The yoke represents the nucleus and may be up to 6 μm thick. The egg-white represents the cytoplasm of the cell and may be found in any shape and is only 1 μm thick. The volume enclosed by the endothelial cells is called the lumen.

Blood, which is contained within the lumen of the vessel, is a collection of many components but the main components are, by volume, 55% plasma, 40% erythrocytes (red blood cells), and 5% leukocytes (white blood cells). The erythrocytes move in single file along the capillary, separated by other blood elements. In the process the erythrocyte's outer surface is left in contact with the vessel wall allowing, among other processes, the transfer of oxygen from oxyhaemoglobin (HbO_2) within the cell to the surrounding tissues.

Erythrocytes contain haemoglobin, the oxygen carrying pigment that is responsible for the red colour of blood (Ganong, 1965). During laser treatment, it is the haemoglobin that absorbs the laser light. The erythrocytes are bi-concave discs that are manufactured in the bone marrow, averaging about 7.5 μm in diameter and 2 μm in thickness.

For the blood to flow from the arteries to the veins, a pressure gradient exists. The average value is approximately 100 mm Hg., which fluctuates in response to beating of the heart. The capillaries are required to support pressures of 20-30 mm at heart level. When a person stands, capillaries in the lower extremities must support pressures of 100 mm Hg., so the blood will return to the heart.

2.1.4 Port-wine stains

In this subsection, we describe the probable cause, frequency of occurrence and structure of port-wine stains.

Port-wine stains are areas of skin which are abnormally red in colour. They vary in size from a few square millimetres to over 10% of the body surface area (approximately 2000 cm^2). They are present at birth, and do not involute (disappear) with time.

In figure 2.6, we have shown a port-wine stain that extends over most of a pa-

Figure 2.6. A typical port-wine stain.

tients face. Of those who present for treatment, most have a port-wine stain on the face. This implies that most port-wine stains are on the face or port-wine stains on the limbs and torso do not cause sufficient personal turmoil to warrant treatment. Port-wine stains, such as those shown in figure 2.7, are a product of the cartoonists imagination.

The red colour of the port-wine stain is due to the surplus of blood within the skin. This blood is contained in the abnormally large capillaries within the sub-papillary or papillary plexus. The diameter of these large, or ectatic, capillaries ranges from 20 μm to over 150 μm. The colour of a port-wine stains varies between salmon pink and purple.

For the remainder of this thesis the only blood vessels of interest are these ectatic vessels. To be consistent with the literature we refer to them simply as vessels.

The cause of the ectasia is uncertain, but the literature suggests that the ectasia is linked to the neural control of blood flow. Smoller and Rosen (1986) performed

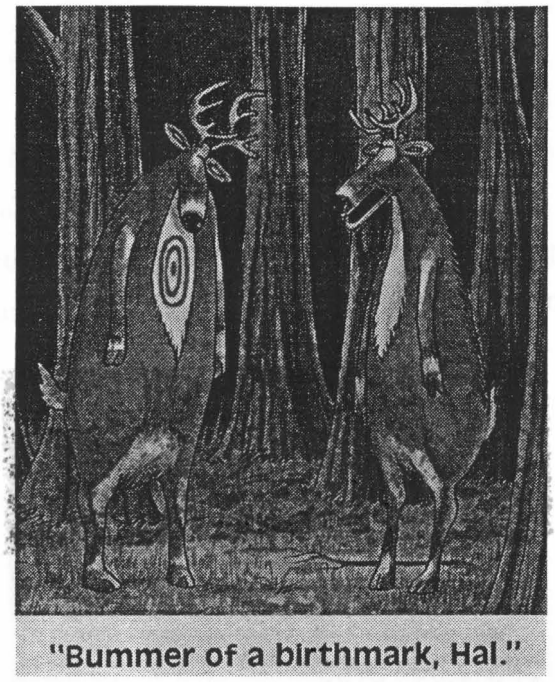

Figure 2.7. This post-card cartoon in the Far Side series by Gary Larson illustrates the public recognition of port-wine stains but depicts an atypical port-wine stain.

histologies of vascular lesions and examined the distribution of nerves and vessels within the skin. Port-wine stains showed a significant decrease in nerve density and increase in the vessel to nerve ratio. Pickering *et al* (1991) showed that the position of the port-wine stains on the face is related to the nerve regions on the face. Rydh *et al* (1991) stated that "the pathologically dilated vessels in the middle and deep dermis were found to have defective innervation with only single or no nerve fibres in their vicinity, while other structures in the skin showed a normal density of fibres".

Several studies of the incidence of port-wine stains among babies less than 48 hours old have been carried out. We summarise these results in table 2.1.

Table 2.1. The incidence of port-wine stains

contributing paper	sample size	port-wine stain
Jacobs and Walton (1976)	1058	3 (0.30%)
Osburn *et al* (1987)	830	5 (0.60%)
Karvonen *et al* (1992)	4346	10 (0.23%)

The frequency at which port-wine stains occur varies between studies. The rate of occurrence for port-wine stains is sufficiently low that statistical variation makes

the result reliable to within a factor of two only. It would be useful to have studies with a larger sample size, and ones that look for genetic, ethnic variations.

Ohmori and Huang (1981) have classified port-wine stains into four types: constricted, intermediate, dilated, and deeply located. These four types are shown in figure 2.8. The main differences are in the subpapillary layer. With the constricted type, there was the same density of blood vessels, except that they are slightly larger. The dilated type consists of much larger vessels that often contained red blood cells. The intermediate category is a combination of the dilated and constricted types. Lastly, the deeply located type contains ectatic vessels throughout the dermis. Niechajev and Clodius (1990) note that the deep type barely exists, and that port-wine stains should be classified on the diameter of the vessels to give three morphologic groups: narrow, intermediate, and wide.

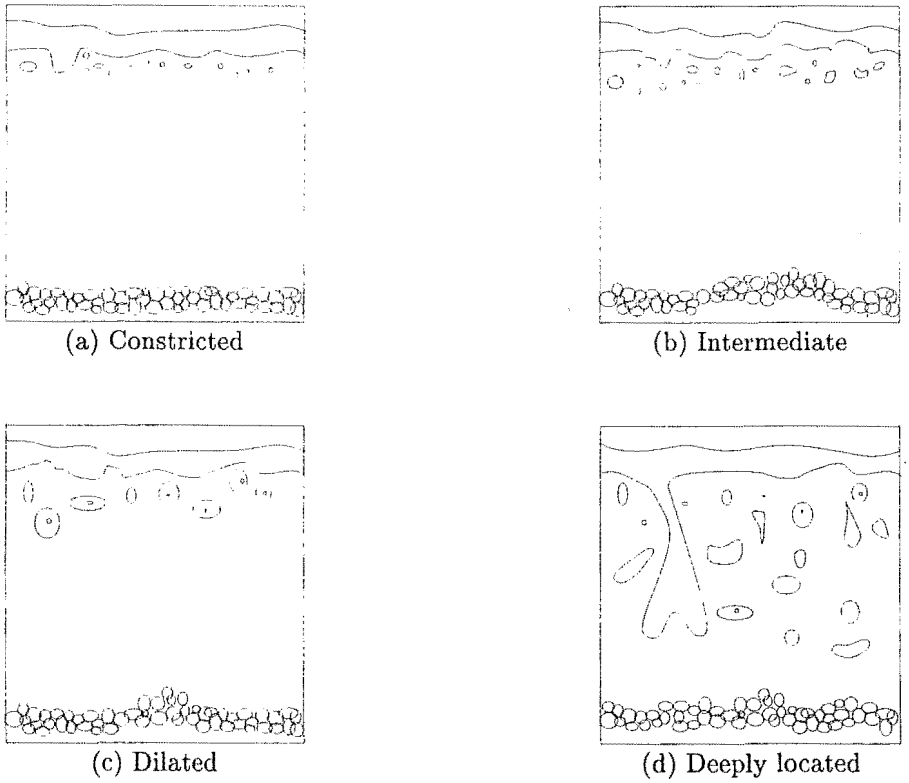

Figure 2.8. The four different types of port-wine stains, as classified by Ohmori and Huang (1981).

The colour of the port-wine stain can be used as a method of classification. Ginsbach (1991) describe the use of the MUNSELL colour standards. With these standards, a quantitative assessment is provided at relatively low cost that is reproducible at other treatment centres.

"Ageing occurs with the passage of time" (Ryan, 1973), and its effects are seen

in the colour of port-wine stains. Children tend to have salmon pink coloured stains while the port-wine stains in adults are often dark purple in colour.

Noe *et al* (1980), and Barsky *et al* (1980) state that with increasing age the number of ectatic vessels remains constant but they become progressively dilated. Niechajev and Clodius (1990) have criticised the work of Noe *et al* (1980) and Barsky *et al* (1980) as they analysed biopsies obtained from port-wine stains. They state that the biopsies are not representative of the entire port-wine stain, and obtaining and preparing the sample affects the percentage of vessels that contain blood.

Niechajev and Clodius (1990) examined the skin obtained when subtotal or total excision of a port-wine stain had been carried out. Such a technique ensures that a more representative picture of the port-wine stain is obtained. Their results confirmed that port-wine stains do darken with age, but could not link age with an increase in the size of the vessel lumen or increase in the percentage of vessels containing blood.

2.2 The optical properties of skin

Experimental problems make it difficult, if not impossible to determine the optical properties of skin components such as a hair follicle. Skin is therefore considered as consisting of three components: epidermis, dermis and blood. Measurement of the optical properties of these components has been carried out by several authors. In the following paragraphs, we describe some of the results and the uncertainties in these results.

Analysis of the optical properties of the skin components show that the only significant differences arise for visible wavelengths (Parrish and Deutsch, 1984). In the visible wavelengths, the parameters that can be used to describe the absorption and scattering of light by the different skin components have been published by several authors. For example, Anderson and Parrish (1981a) plotted the absorption coefficients for haemoglobin (with and without oxygen) and melanin over the wavelengths 300 to 800 nm. This graph (and caption) has been reproduced in figure 2.9.

More recently, Verkruysse *et al* (1993a) have listed the optical properties of the epidermis, dermis and blood for a number of wavelengths. These values have been repeated in table 2.2. The parameters μ_a and μ_s are the absorption and scattering coefficients respectively. The anisotropy factor, g, is the average cosine of the deflection angle. These parameters are used when describing the passage of light through our model of skin in subsequent chapters. Unfortunately, Verkruysse *et al* (1993a) did not give the definition that they used for pigmentation level.

Table 2.2. The optical parameters that are used when describing the passage of light through the epidermis, dermis, and blood.

wavelength (nm)	μ_a (mm^{-1})	μ_s (mm^{-1})	g
Epidermis			
415	3.30	80	0.743
500	2.40	59	0.760
532	2.30	53	0.775
545	2.00	50	0.780
560	1.9	49	0.785
577	1.9 (3.6)[a]	48	0.787
585	1.9 (3.6)[a]	47	0.790
590	1.9 (3.6)[a]	47	0.800
Dermis			
415	0.35	32.0	0.743
500	0.26	25.5	0.760
532	0.24	24.0	0.775
545	0.23	23.0	0.780
560	0.22	22.0	0.785
577	0.22	21.0	0.787
585	0.22	20.5	0.790
590	0.22	20.0	0.800
Blood			
415	300.0	48.0	0.995
500	11.5	47.5	0.995
532	26.6	47.3	0.995
545	33.0	47.2	0.995
560	20.0	47.0	0.995
577	35.4	46.8	0.995
585	19.1	46.7	0.995
590	6.9	246.6	0.995

[a]heavily pigmented epidermis

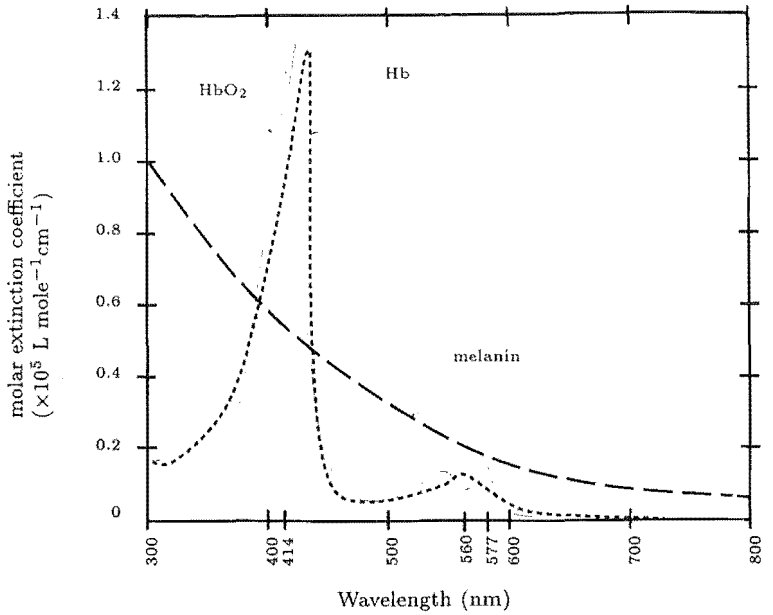

Figure 2.9. Absorption spectra of the oxygen carrying haemoglobin (solid line), oxygen deficient haemoglobin (dotted line), and melanin (dashed line). In all cases, the pigments have been dissolved in water. The spectrum shown for melanin is the absorbance for 1.5mg% aqueous solution

The values listed in table 2.2 have been compiled from the work of several authors. We have assumed that they are correct. The literature shows that these values, which were determined from *in vitro* work, may be in error.

Several sources of error exist. For example, Jacques *et al* (1987) measured the angular dependence of scattering of a He-Ne laser beam by human dermis. The prepared tissue was soaked in a saline solution to standardise the degree of hydration, which increased the amount of light reflected back from the sample.

Graaff *et al* (1993) measured the quantity of light that is reflected back from *in vivo* skin and compared this with the theoretically predicted result. Their theoretical calculations used the values published in the literature that had been derived from *in vitro* work. They showed that the correct values for the optical parameters are much smaller than the values obtained from *in vitro* work.

Torres *et al* (1994) showed that unacceptable errors can occur when integrating spheres are used to measure the amount of light transmitted and reflected from a sample. Pickering *et al* (1993) showed that this happens when the port of the sphere is not significantly larger than the beam diameter. With a ratio of 10:1, up to 30% of the light is lost. When the port size was increased to 25 mm, the amount of light lost became negligible.

The technique used to determine the optical properties may require a sample of uniform thickness (Cheong *et al*, 1990), which is easier to acquire if the sample is frozen. Çilesiz and Welch (1994) showed that the absorption properties of human aorta decreases by 5-11% over much of the 300-800 nm wavelength range when the sample is kept frozen in liquid nitrogen for 1 month. This finding is unsurprising, as freezing will cause the water in the tissue to turn to ice, and the subsequent expansion will disrupt the cell membranes. We are therefore uncertain of all results obtained after the tissue is frozen.

The results obtained from calculations with these numbers will be dependent on the validity of the optical parameters. For example, if the true value for the absorption coefficient in the epidermis is lower than the figure given in table 2.2, then more light will reach the dermis. In a later chapter, Chapter 6, we examine how sensitive our simulation is to the absorption and scattering parameters.

2.3 Representation of skin

To simulate the processes that occur in skin during treatment, we must first develop a model of skin. Once we have a model that provides a representation of skin, we can calculate where the light is absorbed within the skin. With this information, we can calculate the flow of heat within the skin, and so determine the appropriate treatment parameters.

The diagram of skin in figure 2.1 shows the complexity of skin. Structures such as nerve fibres, basal cells, hair follicles are evident. The intrinsic biological variation in skin means that this diagram is a representation of typical skin.

When the passage of light through skin is calculated, several simplifying assumptions about the structure of skin are made. There are two main reasons for use of a simplified model, 1) any variation within the skin that is on the microscopic scale is averaged out and 2) knowledge of the optical parameters cannot support a more accurate study. We review several of the skin models reported in the literature below.

Several different layered models have been used with varying degrees of success. For example, van Gemert *et al* (1989) describe a model with two layers, as shown in figure 2.10a. In this model, the blood is uniformly distributed throughout the dermis. The epidermis has a thickness of 65 μm. Verkruysse *et al* (1993a) used this model and altered the percentage of blood contained in the dermis.

Instead of distributing the blood uniformly in the dermis, some authors have placed it all in one layer in the dermis, (see for example van Gemert *et al*, 1982). The skin is then as shown in figure 2.10b. In this case, the blood plexus has a thickness

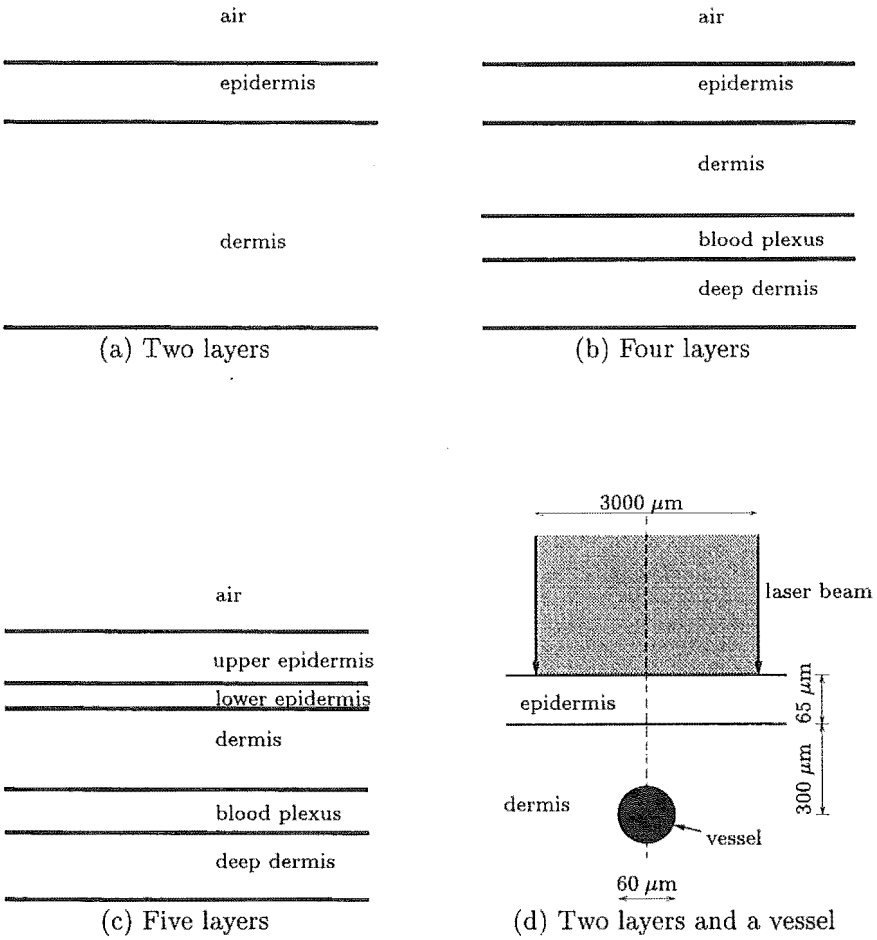

(a) Two layers (b) Four layers

(c) Five layers (d) Two layers and a vessel

Figure 2.10. The various models of skin that that have been described in the literature.

of 100 μm, at a variable distance from the epidermis/air boundary.

Clinical work showed that the temperature rise at the top of the epidermis was much lower than the results from a four layer model predicted. This is not surprising as melanin, the major chromophore in the epidermis is not evenly distributed throughout the epidermis. There is a high concentration at the base of the epidermis. For this reason, Miller and Veitch (1993) separated the epidermal layer into two layers. This five layer model is shown in figure 2.10c. The lower layer in the epidermis represents the melanin rich basal layer. The shallow layer represents the remainder of the epidermis. The upper layer of the epidermis has a thickness of 50 μm, while the bottom layer has a thickness of 10 μm. With this model, the temperature rise at the top of the epidermis was closer to that measured clinically.

van Gemert *et al* (1986) proposed a model containing one vessel, as shown in figure 2.10d. It is a modification of the model containing several layers, as it has represented the blood vessel by a cylinder.

The model shown in figure 2.10d can be extended by adding many vessels, at different heights, as shown in figure 2.11. The blood vessels do not need to be the same diameter, or parallel. We have drawn the vessels in this manner for reasons of clarity. It does not include a basal layer, the non planar interface between the epidermis and dermis. We have chosen to use this model for our theoretical calculations, as it is as complete as the available optical parameters allow.

We set the thickness of the epidermis to be 65 μm (van Gemert *et al*, 1986). However, in subsection 2.1.1 the epidermis was reported to be much thicker, between 420 and 1 560 μm. It appears that van Gemert *et al* (1986) considered only the parts of the epidermis that contain melanin, the principal chromophore in the epidermis. The melanin is contained within the stratum spinosum and stratum basale, which have a combined thickness of around 65 μm.

The model dermis has an infinite depth since, as Graaff *et al* (1993) showed, the subcutaneous tissue below the dermis has a minimal effect on the quantity of remitted light.

We use the skin model shown in figure 2.11 and optical parameters in table 2.2 in the following chapters. First, we digress and examine the methods that can be used to simulate the passage of light through a medium. From this information we calculate where the light is absorbed in the skin.

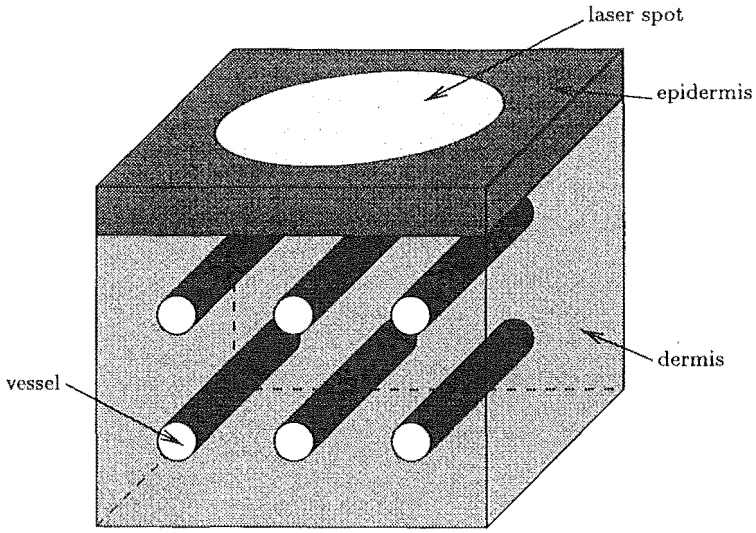

Figure 2.11. Model of skin showing the incident laser spot, the epidermis, dermis, and two layers of capillaries.

Chapter 3

The Transport of Light through Skin

In this chapter, we review the techniques that can be used to determine the passage of light through skin. The drawbacks and advantages of each technique will be described.
From the description of the techniques used to model the passage of light through skin and the model of skin that is used in this thesis the motivation to use the Monte Carlo technique is clear.

Maxwell's equations, which have been given by Doughty (1990) describe the passage of light through a known medium. Presupposing we know enough about the medium, all effects of diffraction, interference, anqd polarisation are included. Ishimaru (1977) notes that, "In practice, it is impossible to obtain a formulation which completely includes all these effects, and various theories which yield useful solutions are all approximate, each being useful in a specific range of parameters."

We therefore make the approximation that the wave aspects of light can be ignored, and regard light as consisting of discrete, noninteracting and neutral particles travelling through a stationary medium. This description is similar to that of neutrons, except that the light particles travel at the one speed. The techniques used to describe the transport of neutrons in the study and design of nuclear reactors have been applied to the transport of light through a scattering media.

In chapter 2 we chose a model of skin that consists of three different structures, epidermis, dermis and blood vessels. The simulation of the passage of light through this model of skin must include several effects, which we list below.

1. The optical properties of each of the skin components are different, so the simulation must take this into account when the light moves from one component of skin to another.

2. When the light is incident on the epidermis/air boundary from the epidermis, some (or all) of the light will be internally reflected.

3. The light is scattered in three dimensions when it travels in skin. Many workers have used a two or a one dimensional scattering model. We want to see the effect of this approximation, so our simulation must be able to describe 1D, 2D and 3D scattering.

In section 3.1, we give a brief description of the derivation of the transport equation, which is used to describe the passage of the particles that represent the light. In section 3.2, we show that reducing the number of dimensions in the simulation drastically reduces the computer requirements. The effects of this simplification on the results obtained are explained. Section 3.3 lists the various approximations to the transport equation in the literature.

3.1 Transport equation

We show the underlying physical principles involved in the equation of transport and give the basis for the derivation of this equation. The work of Glasstone and Edlund (1953), Tait (1964), Ishimaru (1977), and Ishimaru (1978) has been drawn on for the material in this section.

As the light travels through the medium, some is scattered into a new direction, some is absorbed by the medium and some is unscattered. Consider a cylindrical elementary volume with unit cross section and length ds, at the point $\boldsymbol{r}$, as shown in figure 3.1.

As the intensity $I(\boldsymbol{r}, \hat{\boldsymbol{s}})$ traverses the distance ds, there is a reduction in the intensity due to the absorption of energy in the medium and the scattering of some of the energy away from the direction $\hat{\boldsymbol{s}}$.

There is incoming light in a direction $\hat{\boldsymbol{s}}'$ that is scattered in the direction $\hat{\boldsymbol{s}}$ at the point $\boldsymbol{r}$. The probability that this will happen is given by $p(\hat{\boldsymbol{s}}, \hat{\boldsymbol{s}}')$. To find the total contribution in the direction $\hat{\boldsymbol{s}}$, one must sum over all possible values of $\hat{\boldsymbol{s}}'$.

In the volume ds, there may be some fluorescence. This is described by the source term, $\varepsilon(\boldsymbol{r}, \hat{\boldsymbol{s}})$.

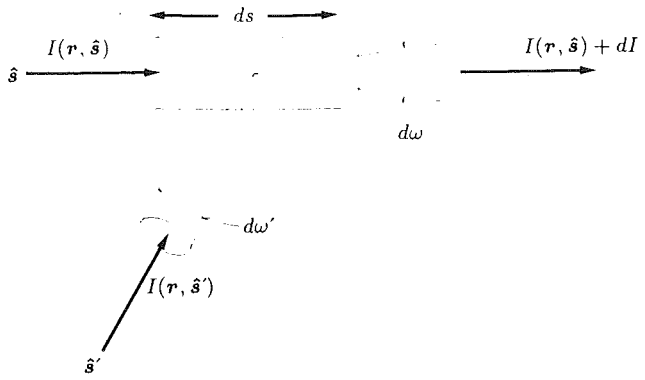

Figure 3.1. The incident light in the direction $\hat{s}$ is supplemented by the scattering of light from the direction $\hat{s}'$.

Putting these three effects together, the equation of transfer can be obtained and is as follows:

$$\frac{d}{ds}I(\boldsymbol{r}, \hat{\boldsymbol{s}}) = -\rho\sigma_t I(\boldsymbol{r}, \hat{\boldsymbol{s}}) + \frac{\rho\sigma_t}{4\pi}\int_{4\pi} p(\hat{\boldsymbol{s}}, \hat{\boldsymbol{s}}')I(\boldsymbol{r}, \hat{\boldsymbol{s}}')d\omega' + \varepsilon(\boldsymbol{r}, \hat{\boldsymbol{s}}) \tag{3.1}$$

where,

ρ number of particles per unit volume

σ_t the total cross section, and is related to the mean free path of the light particles in the tissue

Ishimaru (1977) notes that this equation is identical to the Boltzmann transport equation which is used in neutron transport theory. To solve this equation either analytically or numerically is a daunting task and one looks for some simplifications.

3.2 Dimensions of the model

The scattering model can be designed so that the light will only scatter in one or two dimensions. Significant reductions in the computing resources necessary to solve the transport equation are obtained on making this simplification. Further, reducing the number of dimensions in the model will increase the distance that the photons travel into the model. Finally, the representation of the laser beam lacks validity when the beam diameter is small.

If the light scatters in 2D, it will travel in a plane and never leave the plane.

A 1D scattering model is even simpler. The light always travels in a direction parallel to the direction of propagation.

3.2.1 Computing resources required

Reducing the dimensions of the model reduces the computing resources required, which we show in this subsection.

With a numerical solution of the transport equation, information on the intensity at every point in the skin is required. Thus, the skin is represented by a three dimensional array in the computer. The size of this array may well be too large for the computer to handle.

Suppose a $(1\text{ mm})^3$ section of skin is represented by a $400\times400\times400$ element array. Each element in the array corresponds to a $(2.5\ \mu\text{m})^3$ cube, which is much smaller than the diameter of a blood vessel. Each element of the array is one floating point number, which requires eight bytes of memory. Two copies of this array are required so that numerical differentiation can be carried out. In total, 1024 megabytes of memory are required. These memory requirements can only be met by large computers. In contrast, only 2.6 megabytes are required if a two dimensional model is used.

As a first approximation, the computer time required will be proportional to the number of elements in the array. Reducing the number of dimensions drastically reduces the computer time required.

3.2.2 Penetration of the light into the skin

Reducing the number of dimensions that the light can scatter in will mean that more photons will reach the deeper regions of the model. We will show this in the following argument.

Suppose the light, which is represented by particles, is scattered at the origin. The particles travel a fixed distance, l. The direction of the scattered particles is such that the next scattering point will be somewhere on the hemisphere centred at the origin, which is shown in figure 3.2. Averaging over many particles that are scattered at the origin, the next scattering point is uniformly distributed over the hemisphere.

The average distance $\bar{d}$, travelled in the vertical direction will be

$$\bar{d} = \frac{2\,l}{3} = \frac{\int_{-l}^{l}\int_{-l}^{l}\sqrt{l^2-(x^2+y^2)}\,dx\,dy}{\pi l^2} \tag{3.2}$$

which is equal to the volume of the hemisphere divided by the area of the base.

If the light scatters in two dimensions, then it will travel an average distance of

$$\bar{d} = \frac{\pi\,l}{4} = \frac{\int_{-l}^{l}\sqrt{l^2-x^2}dx}{2\,l} \tag{3.3}$$

which is equal to the area of a semi circle divided by the length of the base.

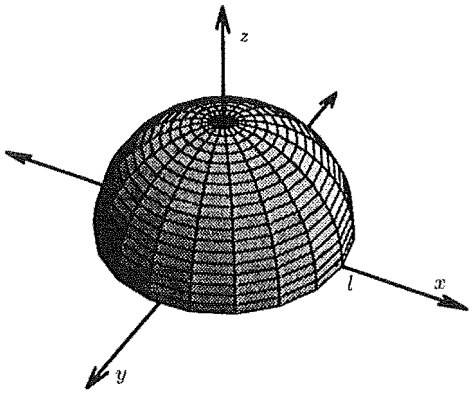

Figure 3.2. The light travels a distance l, after being scattered in three dimensions from the origin. It reaches some point on the hemisphere shown.

Finally, when the light scatters in one dimension, it must travel a distance of l.

If the scattering is more forward orientated, it is less likely that the particles will be scattered to the side. Consequently, the light will travel further in the z direction.

3.2.3 Representation of the laser beam

Reducing the dimensions in the scattering model drastically effects the representation of the laser laser beam, which we show in this subsection.

With a three dimensional scattering model, any laser beam profile can be accurately represented.

In a 2D scattering model, the light travels within a plane. A circular laser beam, such as that shown in figure 2.10d, is identical to a rectangular beam of infinite length with a width equal to the beam diameter. The absorption in the skin immediately below the edge of the beam will be quite different for the 2D and 3D scattering models.

The use of a one dimensional scattering model cannot describe the broadening of the laser beam in the tissue. This may not matter, particularly if the diameter of the laser beam is large compared to the broadening experienced. When the laser beam is large, the intensity of the beam at its centre will be slightly reduced by beam broadening.

3.3 Simplifications to the transport equation

We describe in this section the various simplifications to the transport equation that are reported in the literature. The source term, $\varepsilon(\boldsymbol{r}, \hat{\boldsymbol{s}})$, has been ignored, because

we assume that fluorescence is negligible.

3.3.1 Beer's Law

If the light is assumed to travel in a straight line, with no scattering but only absorption, one obtains Beer's Law. The integral term in the equation of transport is ignored, so the intensity at a depth z is given by $I = I_0 e^{-\rho\sigma_t z}$, where I_0 is the intensity of the beam at the surface of the skin. Pickering *et al* (1989a) have used this model, which is simple to implement, when determining the distribution of light within skin. We want to see the effect of scattering in the skin, which this model cannot show.

3.3.2 Kubelka Munk, or two flux theory

This theory was developed by Kubelka (1948) and it is based on a model of two diffuse light fluxes travelling in the forward and backward directions. Ishimaru (1977) note that this theory adequately describes the experimental results if the illumination is diffuse and the medium is dull so that the light is diffusely scattered. Thus, regular reflections occurring at the boundaries of a sample can be neglected. This approximation is not applicable when a collimated beam is incident upon a medium.

In figure 3.3, the various fluxes when incident on a medium of thickness D are shown. The light travels in two directions, upwards and downwards, so this is a one dimensional model. The fraction of the incident beam that is reflected from the

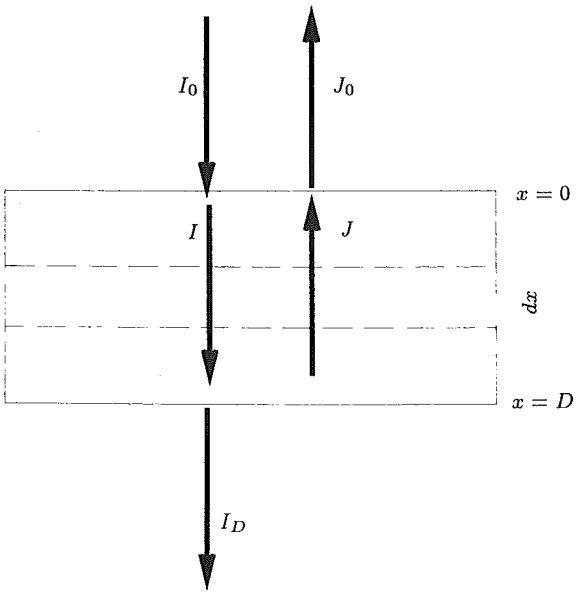

Figure 3.3. The Kubelka Munk model for radiation transfer in a turbid, absorbing medium (Anderson and Parrish, 1981a).

media is given by

$$R = \frac{J_0}{I_0} \tag{3.4}$$

and the fraction of the incident beam that is transmitted is

$$T = \frac{I_D}{I_0} \tag{3.5}$$

If S is the scattering coefficient and K is the absorption coefficient then we can write the following equations:

$$\frac{dI}{dx} = -SI - KI + SJ \tag{3.6a}$$

$$\frac{-dJ}{dx} = -SJ - KJ + SI \tag{3.6b}$$

Equation (3.6a) states that the change dI in the flux I over some layer of thickness dx is equal to the fraction removed by absorption and backscattering plus the the contribution of the scattered flux travelling in the opposite direction. Equation (3.6b) is identical to the previous equation, except that it describes the change in the flux travelling in the opposite direction. Equations (3.6) can be solved for S and K using the measured values of R and T.

This formalism is not easily applied to an inhomogeneous medium, nor can it be used to describe the case when collimated laser beam is incident on tissue.

3.3.3 Four flux theory

This model is an improvement to the two flux model, in that it can be used to describe the case when a collimated laser beam is incident on tissue. Two additional fluxes are included, which describe a collimated beam of light travelling in the forward and backward directions. The collimated beam in the forward and backward directions is reduced by absorption and scattering into the diffuse fluxes. Mudgett and Richards (1971) provide further details on the use of this model. They used this model to accurately predict ($\pm 2\%$) the transmission and reflectance through plastic discs. Again, this formalism is not easily applied to an inhomogeneous medium.

3.3.4 Seven flux model

The material in this subsection is from Yoon *et al* (1987) who have described this approximation to the transport equation. In figure 3.4, the seven fluxes that are considered are shown. Unlike the models described previously, this is a three dimensional model.

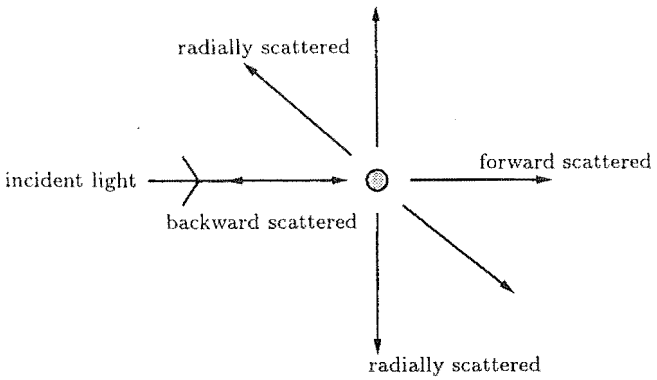

Figure 3.4. Representation of the scattered light by six directional fluxes in the seven flux model (Yoon *et al*, 1987).

The incident flux is scattered into six directions, represented by fluxes. A seventh flux is included to describe the collimated light. As such, it is not exact, but an approximation. However, it does provide a practical model from which the fluence within a medium can be determined.

Seven first order coupled linear differential equations are obtained when the the collimated flux, $I_c(x, y, z)$ travelling in the z direction is incident on the material. For I_{+z}, the flux in the positive z direction,

$$\frac{\partial I_{+z}(x,y,z)}{\partial z} + \rho\sigma_t I_{+z} = P_{z,z} I_c(x,y,z) + \rho\sigma_t [P_{z,x} I_{+x} + P_{z,-x} I_{-x} + P_{z,y} I_{+y} + P_{z,-y} I_{-y} + P_{z,z} I_{+z} + P_{z,-z} I_{-z}]. \quad (3.7)$$

The function $P_{z,x}$ is the portion of the flux scattered from the direction given by x into the z direction. The five equations describing the fluxes in the remaining five directions are similar. The seventh equation describes the attenuation of the collimated beam:

$$\frac{\partial I_c(x,y,z)}{\partial z} = -\rho\sigma_t I_c(x,y,z) \quad (3.8)$$

Welch *et al* (1987) describe how they used numerical methods to solve the seven equations that describe the fluences within skin. Numerical methods were used as the authors stated that it is difficult to solve the seven equations analytically. To simplify the problem, isotropic scattering was used and the change in refractive index at the tissue/air boundary was ignored. Further, the model chosen by these authors was homogeneous.

We desire a solution of the transport equation where the light scatters in three dimensions. A numerical solution based on this technique with the chosen model of skin is beyond our available computing resources.

3.3.5 Diffusion approximation

We have relied upon the work of Welch *et al* (1987), Star *et al* (1988) and Keijzer *et al* (1988) for the material in this subsection.

The light is assumed to be scattered almost uniformly after numerous scattering events. Some anisotropy is retained, as energy is transported in the $\hat{z}$ direction. When a laser beam is incident on a turbid material, the radiance inside the medium can be divided into the coherent intensity and the diffuse intensity. We write this as

$$\begin{aligned} I_d(\boldsymbol{r}, \hat{\boldsymbol{s}}) &= I_{\text{isotropic}} + I_{\text{coherent}} && (3.9) \\ &= \frac{1}{4\pi}\int_{4\pi} I_d(\boldsymbol{r}, \hat{\boldsymbol{s}})d\omega + \frac{3}{4\pi}\int_{4\pi} I_d(\boldsymbol{r}, \hat{\boldsymbol{s}})\hat{\boldsymbol{s}}\cdot\hat{\boldsymbol{z}}d\omega && (3.10) \\ &= U_d(\boldsymbol{r}) + \frac{3}{4\pi}F_d(\boldsymbol{r})\cdot\hat{\boldsymbol{s}} && (3.11) \end{aligned}$$

The first term on the right hand side of equation (3.6) represents the average diffuse intensity of the light. The righthand term describes the net flow of energy in a specific direction, in this case the $\hat{z}$ direction.

In figure 3.5, we have shown a representation of the diffuse intensity $I_d(\boldsymbol{r}, \hat{\boldsymbol{s}})$.

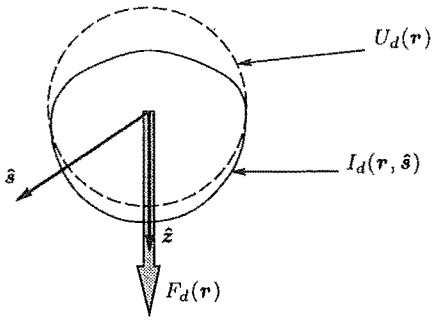

Figure 3.5. The diffuse intensity $I_d(\boldsymbol{r}, \hat{\boldsymbol{s}})$ is the sum of the isotropic irradiance $U_d(\boldsymbol{r})$ and a peak flux $F_d(\boldsymbol{r})$ in the direction $\hat{\boldsymbol{z}}$ direction.

This approximation is valid for an optically dense and highly scattering medium. As the model requires diffuse light in the tissue, the results are not as accurate near boundaries and internal light sources. With this condition, it cannot be used in a medium such as blood or epidermis as these skin components weakly scatter the laser beam.

3.3.6 Monte Carlo technique

The Monte Carlo technique differs from the above techniques in that it is a stochastic (statistical) method.

In this technique, the particles which represent the laser beam travel along straight paths (without energy loss) between collision points. On collision, the particle is absorbed, or else scattered into a new direction. Each particle will travel along a different path, which is determined from probability statistics and the optical parameters of the medium. By compiling the results for many millions of particles, a map of absorption in the skin is available. In this way, we obtain a numerical solution to the transport equation.

This technique does not require that all of the absorption events in the skin model are recorded. Indeed, the program need only record the absorption in some part of the model, as specified by the user. For this reason, simulations that allow the scattering of light in three dimensions can be carried out with minimal memory requirements.

Effects such as changes in the refractive index when the particles move between different components in the medium can be added simply and easily. Thus, the passage of light through a medium consisting of several different components, each with different optical properties can be simulated.

The Monte Carlo technique satisfies the criteria set down at the beginning of this chapter. None of the previously described techniques meet these criteria. In the next chapter there is a complete description of how we used this technique to determine where the light is absorbed in the skin.

Chapter 4

Monte Carlo

In this chapter, we describe in detail how the Monte Carlo technique was used to obtain the distribution of light within skin.
Our implementation of this technique is compared with that of other workers, and the differences are discussed. We use this technique with several different scattering and skin models.

The Monte Carlo technique is statistical, or stochastic in nature. With this technique, it is possible to replicate the path of light through tissue by representing the light with independent particles. The path of millions (or billions) of particles through the skin is individually generated. Once the path of the every particle has been generated, a map of where the particles were absorbed in the tissue is available. In this way, we can perform an experiment with the aid of a computer to determine where the light is absorbed.

This technique has been used by many workers in different fields of physics. For example, Witt (1977) reported the use of this method to calculate the surface brightness distribution on a plane-parallel reflection nebula of uniform density, illuminated by a single star.

In the section 4.1, we describe what the Monte Carlo technique is and how it was implemented in our work. This method is compared with the methods that have been used by other workers in section 4.2. The differences are discussed. The results that were obtained with our method are described in section 4.3. Finally, in section 4.4 we discuss the results that we obtained, and compare them with those published in the literature.

4.1 Implementation of the Monte Carlo technique

In this section, we describe how we use the Monte Carlo technique to determine the passage of light through skin.

In subsection 4.1.1 we describe the model of skin that is used. We must first describe the skin, as the choice of model influences the implementation of the Monte Carlo technique.

In subsection 4.1.2, we explain how the continuous laser beam is represented by discrete particles.

As we have stated above, the Monte Carlo technique relies upon the computer generating the path of the individual particles. Each particle travels a distance, l, between interactions. At an interaction point, it may be absorbed or scattered. If it is absorbed, a record is kept of the absorption event and a new particle is simulated. If the particle is scattered, the azimuthal and deflection angles are calculated and the particle moves in the new direction to the next interaction point.

The distance between interactions, the probability of scattering, and the scattering angles must be determined so that they represent what a particle would experience in reality. For example, in an optically dense medium one would not expect the particles to travel a long distance between scattering events. In subsections 4.1.3, 4.1.4, 4.1.5, and 4.1.6 the calculation of these variables is described.

In subsection 4.1.7, we describe how particles incident on the epidermis/air boundary (from the epidermis) are processed.

Subsection 4.1.8 describes how the results from this model are presented.

Finally, subsection 4.1.9 describes the simplifications that were made to reduce the computer time required to a more acceptable level.

The description of the Monte Carlo method has been derived from the following authors, Cashwell and Everett (1959), Hammersley and Handscomb (1964), Buslenko *et al* (1966), Profio (1979), Freund and Walpole (1987), Witt (1977), and Keijzer *et al* (1989).

4.1.1 Model of skin

The choice of model is limited by the available knowledge of the optical properties of the components in the skin. The model of skin in our simulation is more complete than those used by previous workers. Our model is shown in figure 2.11. It consists

of two layers of infinite extent which represent the epidermis and dermis with layers of ectatic (enlarged) capillaries, represented by cylinders of infinite length.

In figure 4.1 we give a more detailed view of the skin geometry shown in figure 2.11. The axis of the laser beam is at $x, y = 0$ μm. The vessels are parallel to the y axis.

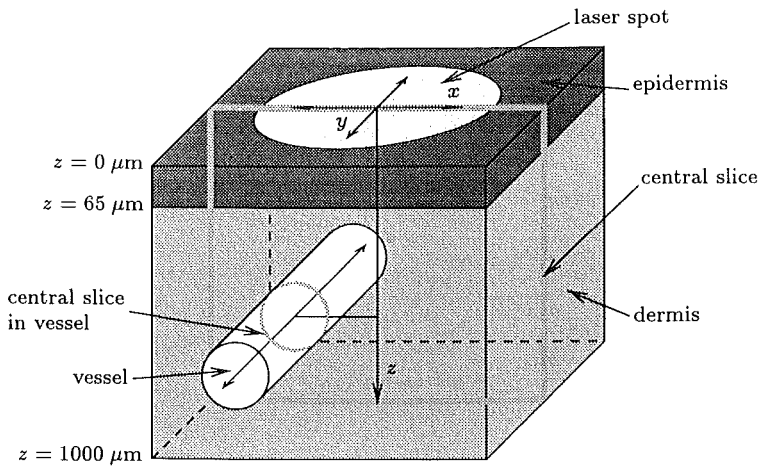

Figure 4.1. The three dimensional model of skin with the coordinate system used, epidermis, dermis, and the central slice in which we record absorption. For reasons of clarity, this figure shows only one vessel.

The histological findings of Niechajev and Clodius (1990) were used to determine the appropriate vessel placement and size for a base model of skin which is referred to in the text as the "reference model". The vessels are positioned in layers with a vessel at the centre of the spot. The distance between the axes of the vessels in each layer is 150 μm. Since there are vessels in a layer that are outside of the laser spot we include the effect of such vessels on the distribution of light. Our reference model has six layers of vessels with a diameter of 50 μm, at depths of 200, 350, 500, 650, 800, and 950 μm. For some of the simulations we used over five hundred vessels.

4.1.2 Representation of the incident laser beam

The laser beam that is incident on the skin is continuous in nature. To represent the laser beam with discrete particles we deposit them on the surface of the skin, arranged as in figure 4.2.

The collimated laser beam of uniform intensity is represented by many thousands of particles. The initial position of the particles form a uniform grid pattern with a circular perimeter on the air/epidermis boundary. The path of each particle in the skin is generated by the computer, using the technique explained in the subsequent subsections.

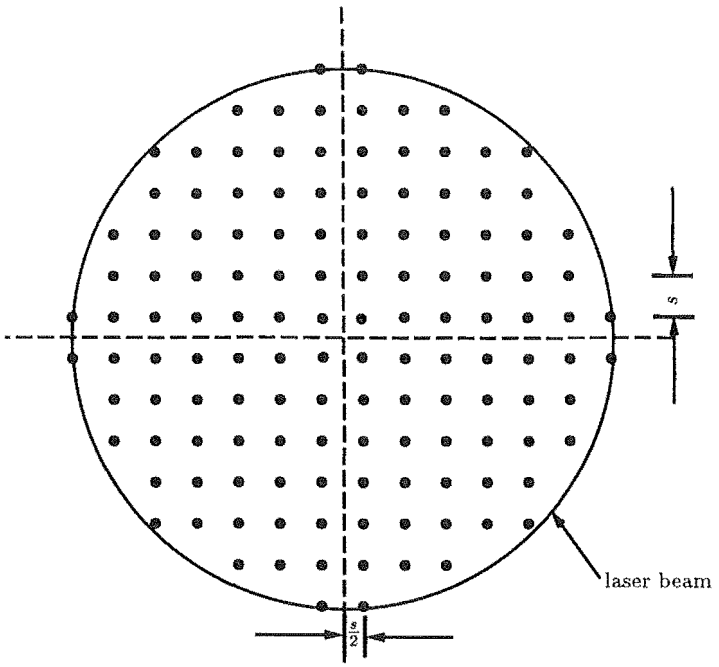

Figure 4.2. The position of the particles that represent the laser beam on the skin surface.

As the separation between the particles on the surface of the skin decreases, the representation of the laser beam improves. However, the simulation requires more computer time when the separation is decreased as there are more particles to follow.

4.1.3 Generation of random quantities

In this subsection, we explain how the computer generates values of the quantities that are used to describe what the particles experiences in reality.

Suppose that one of the quantities that is used to describe the path of the particles is represented by the symbol ξ. The physical quantity represented by ξ will have a frequency distribution which is described by the probability density function, $P(\xi)$. We note that $P(\xi)$ is normalised, so

$$1 = \int_a^b P(\xi) d\xi \tag{4.1}$$

where a and b are the minimum and maximum values of ξ.

For the simulation to represent reality, the simulation must generate values of ξ that have a frequency distribution identical to that of the physical quantity. The values generated, ξ_r, are obtained by solving the following equation

$$r = \int_a^{\xi_r} P(\xi) d\xi \tag{4.2}$$

where r is a random number uniformly distributed between 0 and 1.

As an aside, we note that the average value of ξ can be determined from the probability density function with the following equation,

$$\xi_{\text{ave}} = \int_a^b P(\xi)\xi \, d\xi \tag{4.3}$$

4.1.4 Path length

To determine the distance between interaction points in a medium that consists of several different homogeneous zones, we use the concept of optical thickness. Optical thickness, τ, is equal to the product of the total attenuation coefficient, μ_t ($\mu_t = \mu_a + \mu_s$) and distance. The probability density function for the distance between interactions is

$$P(\tau) = \exp(-\tau) \tag{4.4}$$

This equation states that it is more likely for the particle to travel a shorter distance than a longer distance.

The minimum and maximum thickness the particle can travel through is 0 and ∞ respectively. The average value of τ is obtained by substituting equation (4.4) into equation (4.3), and we obtain

$$\tau_{\text{ave}} = 1 \tag{4.5}$$

so

$$l_{\text{ave}} = 1/\mu_t \tag{4.6}$$

This is expected, as $1/\mu_t$ is the mean free path.

To determine l, the distance between scattering events, we substitute equation (4.4) into equation (4.2) and obtain

$$r = 1 - exp(-\tau_r) \tag{4.7}$$

On rearranging, and noting that $1 - r$ is equivalent to r,

$$\tau_r = \ln \frac{1}{r} \tag{4.8}$$

For a medium that is homogeneous, the distance between scattering events is:

$$l = \frac{\tau_r}{\mu_t} \tag{4.9}$$

When the medium consists of several different homogeneous components, the particle may travel through several components before arriving at the next interaction point. We write in this case,

$$\tau_r = \sum^{i<j} \mu_{ti} l_i + l_j \mu_{tj} \tag{4.10}$$

This formula takes into account the possibility that the particles may travel through several skin components, labelled by the subscripts i, before reaching the next interaction point in the skin component labelled by the subscript j. The particle will travel a distance l_i in the skin component labelled i. If the particle does not move to a different skin component when travelling between interaction points, equation (4.10) reduces to equation (4.9).

4.1.5 Scattering angles

When an event occurs, the particle may be scattered. It is assumed that the deflection angle α is given by the Henyey Greenstein distribution (Henyey and Greenstein, 1941), which is written by Keijzer *et al* (1989) as:

$$P(\alpha) = \frac{1-g^2}{2(1+g^2-2g\cos\alpha)^{3/2}} \tag{4.11}$$

where g is the mean cosine of the deflection angle. With this distribution, the deflection angle ranges from 0 to π. For equation (4.11) to be normalised, it must be a function of $\cos\alpha$, not α.

The average value of $\cos\alpha$ is g, which is expected as g is the mean cosine of the scattering angle. The deflection angle is calculated by substituting the modified form of equation (4.11) into equation (4.2), from which one obtains (Keijzer *et al*, 1989; Witt, 1977)

$$\alpha = \arccos\left(\frac{1}{2g}\left[1+g^2-\left(\frac{1-g^2}{1-g+2g\,r}\right)^2\right]\right) \tag{4.12}$$

which was verified with the aid of Mathematica®.

The azimuthal deflection angle, ϕ is assumed to be isotropic and it is calculated from the next equation,

$$\phi = 2\pi\, r \tag{4.13}$$

If the direction cosines of the photon packet before a scattering event occurs are (u_0, v_0, w_0) then the direction cosines after scattering will be (u_1, v_1, w_1). The new direction cosines are calculated from the following equations (Cashwell and Everett, 1959)

$$u_1 = \frac{w_0 u_0 \sin\alpha\cos\phi - v_0\sin\alpha\sin\phi}{\sqrt{1-w_0}} + u_0\cos\alpha \tag{4.14a}$$

$$v_1 = \frac{w_0 v_0 \sin\alpha\cos\phi + u_0\sin\alpha\sin\phi}{\sqrt{1-w_0}} + v_0\cos\alpha \tag{4.14b}$$

$$w_1 = w_0\cos\alpha - \sin\alpha\cos\phi\sqrt{1-w_0} \tag{4.14c}$$

As w_0 approaches unity, equations (4.14) break down. When $w_0 \geq 0.99$ the following equations are used instead.

$$u_1 = \sin\alpha\cos\phi \tag{4.15a}$$

$$v_1 = \sin\alpha\sin\phi \tag{4.15b}$$

$$w_1 = w_0\cos\alpha \tag{4.15c}$$

In the above description, we have described the situation when the light can scatter in three dimensions. The light scatters in one dimension when the deflection angle is limited to 0 or π. Setting the azimuthal scattering angle to zero or π gives the two dimensional results.

4.1.6 Absorption or scattering

The probability of scattering is equal to the albedo, a which is defined as

$$a = \frac{\mu_s}{\mu_t} \tag{4.16}$$

Thus, the probability of absorption at each event is equal to $1-a$. To determine if the particle is absorbed, the computer generates a random number r which is uniformly distributed between 0 and 1. If r is greater than the albedo, the particle will be absorbed.

All absorption events in a $4000 \times 1000 \times 3\ \mu\text{m}^3$ slice of skin through the centre of the laser spot are recorded. This skin slice is shown in figure 4.1 and given as

$$-2000\ \mu\text{m} < x < 2000\ \mu\text{m} \tag{4.17a}$$

$$-1.5\ \mu\text{m} \leq y \leq 1.5\ \mu\text{m} \tag{4.17b}$$

$$0\ \mu\text{m} \leq z < 1000\ \mu\text{m} \tag{4.17c}$$

The total number of particles absorbed in the epidermis is recorded. That is, those absorbed in the infinite layer where z is in the range $0 \leq z \leq 65\ \mu$m. From this, we determine the fraction of the beam absorbed in the epidermis.

4.1.7 Transmission through the epidermis/air boundary

When the light is incident on the epidermis/air boundary total or partial internal reflection may occur. We follow the example of Keijzer *et al* (1989) and use Fresnel's law for unpolarised light to calculate the probability that the particle is transmitted. This approximation does not include the effect the uneven surface of the skin will

have on the fraction transmitted. Reflection increases with angle of incidence. Nor does it include scattering by dry surface keratinocytes. Thus, at normal incidence, fewer particles will cross the epidermis/air boundary than are determined from this approximation. However, the situation is more complicated at other angles of incidence.

4.1.8 Presentation of results

The absorption events in each 3 μm cube in the skin slice are recorded in one element of the 1333 $\times$ 333 element array in the computer program. The results contained in this array are displayed in a three dimensional surface plot created with Mathematica®.

For the presentation of quantitative results we use the total number of particles absorbed in the part of a vessel that is in the skin slice (equation 4.17). This part is referred to as the "central section" in the text. In figure 4.1, the central section in one vessel has been marked. When the simulation is repeatedly executed with different values of one parameter, the total absorption in the central section can be plotted against the different values of the parameter on a line graph.

The total number of particles absorbed in the epidermis is recorded. That is, those absorbed in the infinite layer where z is in the range $0 \leq z \leq 65\ \mu$m. From this, we determine the total fraction of the beam absorbed in the epidermis.

4.1.9 Computer enhancements

The computer time required is reduced by following packets of particles (Kahn, 1954). At each interaction point, a fraction of the packet is scattered and the remainder is absorbed. The fraction scattered is equal to the albedo (equation 4.16). Similarly, the fraction of the packet transmitted through the epidermis/air boundary is equal to the probability that the particle will be transmitted. In our calculations, each packet contains 100 000 particles. When the packet size is less than 10, we use the technique of Russian Roulette described by Cashwell and Everett (1959) to terminate the nearly empty packets without introducing a statistical bias or violating energy conservation.

There is mirror symmetry about the x and y axes in our model with this choice for the position of the vessels. Therefore, particles need only to be released in the $x, y > 0$ quadrant on the skin surface as the absorption for particles released in the remaining quadrants can be deduced from the results of this quadrant.

When a one or two dimensional scattering model is used, the particles cannot scatter into, or out of, the skin slice. Consequently, particles are only released above the skin slice, with a significant reduction in the computer time required.

The separation between packets on the skin surface is 0.1 μm. Tests showed that this choice of packet size and separation did not introduce a computational error. Increasing the number of photons incident on the skin by decreasing the separation increased the absorption in all of the vessels in proportion to the number of photons simulated.

As the separation of the packets on the skin surface is constant, increasing the spot diameter will place more packets on the skin. Therefore, the energy density (fluence) of the laser spot that is simulated is constant. On the other hand, increasing the spot diameter in the treatment clinic will deposit the same amount of energy over a larger area, decreasing the fluence on the surface of the skin. To maintain constant fluence in the clinic the laser power has to be increased. We describe the results for both cases, constant fluence and constant total incident energy. The results for constant total incident energy are obtained by multiplying the results for constant fluence with a scaling factor determined from the spot diameter.

4.2 Alternative implementations

The description of the Monte Carlo technique in section 4.1 is computationally expensive. Other workers have used the Monte Carlo technique, but with a different approach with significant savings in computer requirements. In the following subsections, we give a summary of the different methods that have been used.

4.2.1 Isotropic scattering, homogeneous tissue

Wilson and Adam (1983) represented the tissue with a homogeneous structure, and assumed that the light was scattered isotropically. That is, the probability of a particle scattering in one direction is equal to the probability of the particle scattering in any other direction. The scattering angle is therefore independent of the direction of the particle prior to the scattering event. the reflection of light from the interface between tissue and air was ignored. These assumptions reduce the computational requirements as the calculation of the distance between interaction points and the direction of the particles after a scattering event becomes very simple.

Hasegawa *et al* (1991) used a slightly improved model to investigate the transmission of light through a scattering/absorbing medium. In this case, the direction

of the scattered particles at an interaction depends on the phase functions of the interacting particles. The authors noted that when non-isotropic scattering is used, a transformation of the coordinate system is required to calculate the new direction. The general form of the coordinate transformation required is given by Cashwell and Everett (1959), and the results are repeated in equations (4.14) and (4.15).

4.2.2 Non-isotropic scattering, homogeneous tissue

The work of Keijzer *et al* (1989) provides an excellent example of when scattering is non-isotropic and the tissue is homogeneous,

This model includes the effect of reflection and refraction at the surface of the tissue. To calculate the fraction of particles transmitted at the tissue surface, Fresnel's laws for unpolarised light are used, which are given by Keijzer *et al* (1988). Snell's laws are used to determine when total internal reflection occurs.

The tissue is illuminated by a collimated beam of light, which is normal to the surface of the tissue. A cylindrical coordinate system is used, as shown in figure 4.3. The position of the particles which represent the light is given by the coordinates (r, θ, z_d). Spherical coordinates, (r, θ, ψ) are used to describe the direction of the particles. This model has rotational symmetry about the z axis, so changes in the angle θ will not affect the result.

The path of the particles is generated in a similar manner to that described in section 4.1. Every absorption event is recorded in an array where one element of the array corresponds to the tissue in the ring $(r, r + \delta r, z, z + \delta z)$. The dimensions of each element is not given. Such a system means that more particles will be absorbed in the outer rings, as the volume of these rings will be greater. The volume of the rings is $\pi \delta z \, \delta r (2r + \delta r)$, and on making the approximation that δr^2 is 0, we find that the volume is proportional to r. Consequently, the volume elements should be scaled in proportion to r, yet Keijzer *et al* (1989) states that "These element volumes are logarithmically scaled: small near the source and large far from the source".

The computation of the light distribution in the tissue was simplified by taking advantage of the geometry used, and noting that the path of a particle is independent of its initial position on the tissue surface. Initially, the particles are released at the origin. The results from these particles are then translated to represent the results that would be obtained from particles released at other points on the skin surface. Combining the results from all particles released at the surface of the tissue yields the distribution of absorbed light within the tissue for a beam of arbitrary diameter.

This is calculated by convolving the incident beam, with an intensity profile

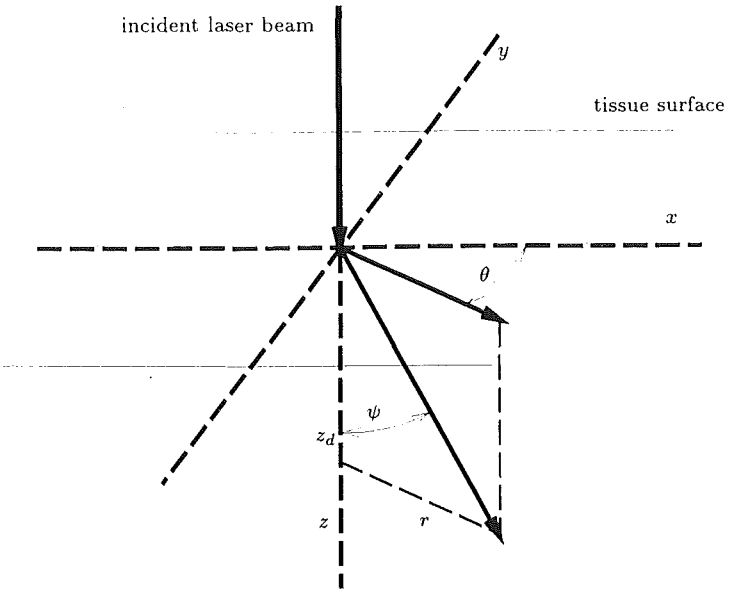

Figure 4.3. The coordinate system used by Keijzer *et al* (1989).

$E(r,\theta)$, and the fluence in the tissue resulting from the particles released at the origin. The fluence in the tissue resulting from the particles released at the origin, $G(r,\theta,z_d)$, is determined from the number of particles absorbed in the tissue, $Q(r,\theta,z_d)$, with the following equation,

$$G(r,\theta,z_d) = \frac{Q(r,\theta,z_d)}{\mu_a} \tag{4.18}$$

In cylindrical coordinates, the convolution is given by Keijzer *et al* (1989) and is:

$$\Psi(r,\theta,z_d) = \int_0^{2\pi}\int_0^{\infty} E(r',\theta')G(\sqrt{r^2+r'^2-2rr'\cos(\theta-\theta')},z_d)r'dr'\,d\theta' \tag{4.19}$$

where $\Psi(r,\theta,z_d)$ is the fluence in the tissue resulting from the incident laser beam. The first parameter of G in equation (4.19) is the distance between the points (r,θ) and $(\acute{r},\acute{\theta})$.

The convolution in cylindrical coordinates can be compared with the convolution in cartesian coordinates, which is given by Bracewell (1978) in the following equation,

$$\Psi(x,y,z_d) = \int_{-\infty}^{\infty}\int_{-\infty}^{\infty} E(x',y')G(x-x',y-y',z_d)dx'\,dy' \tag{4.20}$$

Use of this technique places the restriction on the tissue model that it is invariant under rotations and translations. The computing time required is minimal, as only the particles incident at the origin are simulated. A convolution in two dimensions is also required, but this is relatively quick.

4.2.3 Epidermis, dermis and blood vessel

In 1991, Keijzer *et al.* published the results from a Monte Carlo simulation where a three component model was used, similar to that in figure 2.10d. The authors state that the method has been described elsewhere, (Keijzer *et al*, 1989) and (Prahl, 1988). The method of Keijzer *et al* (1989) requires homogeneous tissue and cylindrical symmetry about the z axis, a requirement not met with this geometry. In the Ph.D. thesis of Prahl (1988), many methods are described. The method that was used by Keijzer *et al* (1991) is therefore uncertain but additional information is provided in the literature that was subsequently published by the authors of this paper.

In 1991, Pickering and van Gemert published the results of Monte Carlo calculations where the differences between 577 nm and 585 nm wavelength light were examined. The blood was considered to be uniformly scattered throughout the dermis. With this two component model, the fluence was calculated. The authors state that, "The fluence rate within the vessel is proportional to the fluence rate immediately outside the vessel, as calculated above, and is exponentially attenuated by absorption of the light with the blood". No description of the Monte Carlo method was given. It is probable that the program developed by Marleen Keijzer (principal author of Keijzer *et al.* 1991) was used as the help of this person was acknowledged.

Later, in 1993, Verkruysse *et al.* published the results of Monte Carlo calculations for a range of wavelengths. The "Fluence rate light distributions for a two-layer model (as in figure 2.10a) were computed by using the Monte Carlo algorithm and beam diameter convolution algorithm described by Keijzer *et al* (1989)". The fluence rate within the vessel is assumed to be attenuated according to Beer's law. This is probably the same method as used by Pickering and van Gemert (1991) and Keijzer *et al* (1991).

Several problems with this implementation are apparent.

The distribution of light within the dermis is affected by the presence (or absence) of vessels. Suppose several vessels are placed in the dermis after the simulation. The absorption in any one vessel will not depend on the location of the other vessels. Our results show that the absorption in a vessel may be significantly altered by other vessels in the model.

Further, there are problems with energy conservation. Particles will be created, or lost, which we have shown in the following explanation. The number of particles absorbed within the dermis is given by

$$Q^{\text{dermis}}(r, \theta, z_d) = \mu_a^{\text{dermis}} \Psi^{\text{dermis}}(r, \theta, z_d) \tag{4.21}$$

As Verkruysse *et al* (1993a) state, the fluence within the vessel will be

$$\Psi^{\text{vessel}}(r, \theta, z, z_{bl}) = \Psi^{\text{dermis}}(r, \theta, z) \exp(-\mu_a^{\text{blood}} z_{bl}) \tag{4.22}$$

where $z = z_d - z_{bl}$, and z_{bl} is the distance from z_d to the top of the vessel. Consequently, the number of particles absorbed within the vessel at the point (r, θ, z_d) will be

$$\mu_a^{\text{blood}} \Psi^{\text{dermis}}(r, \theta, z) \exp(-\mu_a^{\text{blood}} z_{bl}) \tag{4.23}$$

This is not equal to $Q^{\text{dermis}}(r, \theta, z_d)$, the number of particles absorbed in the dermis at the point (r, θ, z_d).

4.2.4 Models containing layers

Gouw *et al* (1991) used a four layer model, similar to that in figure 2.10b. The path of 10^5 particles were simulated. No further information about the simulation process was given. It is unlikely that the convolution algorithm of Keijzer *et al* (1989) was used as there is noise present in the graphs. Lateral scattering must have been considered, as the absorption at the middle of the laser beam is higher than at the side.

They showed the difference in the energy distribution in the skin for four lasers, Nd:YAG, CO_2, argon-ion, and dye laser (577 nm). The light from the CO_2 laser was strongly absorbed in the epidermis, with no absorption in the layer of blood. Conversely, the 577 nm wavelength gave the maximum absorption in the layer of blood. Interestingly, use of the Nd:YAG laser resulted in absorption in the dermis below the layer of blood. None of the other lasers caused absorption in this part of the dermis.

Miller and Veitch (1993) extended the work of Gouw *et al* (1991). The temperature rise in the tissue was calculated with the results of the simulation. Their results, redrawn in figure 4.4, were compared with those obtained in the clinic.

The temperature rise in the epidermis is too high, as this will result in the vaporisation of the epidermis, and is not observed clinically. It was noted that the epidermis will not uniformly absorb light as the melanin is concentrated in the basal layer. Consequently, the epidermis was split into two layers, and the optical parameters of these layers were derived from a simple approximation.

With this revised model, the temperature rise in the epidermis was concentrated in the basal layer. The peak temperature was close to 300 °C, but this occurred in the basal layer. The temperature of the top of the epidermis rose by 15 °C with this model. This result is consistent with that measured clinically.

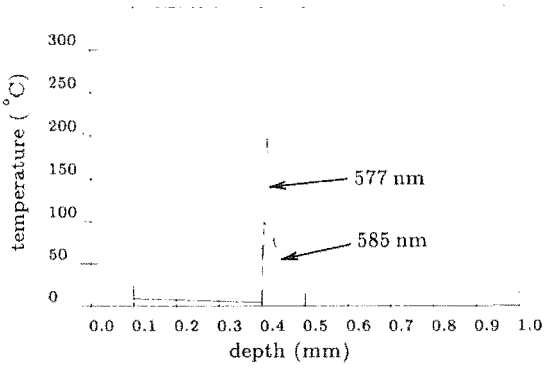

Figure 4.4. The calculated temperature rise in a four layer model of skin following treatment with 577 or 585 nm wavelength light (Miller and Veitch, 1993).

4.3 Results

In this section, we describe the results obtained after we implemented the Monte Carlo technique described in section 4.1. These results, with the exception of those in subsection 4.3.9 have been published (Smithies and Butler, 1995).

4.3.1 The computer program

In this subsection, we describe the computer program, the checks used to verify the results, and the speed of execution.

The program was written in C and executed on a SUN® SPARC STATION 10. The intrinsic random number generator has a period of 2^{32} and satisfies the tests for randomness described by Knuth (1971). The operation of each subroutine in the program was checked with the aid of a debugger and the expected output was obtained.

The results obtained are in agreement with those estimated from physical principles. These include symmetrical absorption patterns, greater absorption in the central vessel than in the vessels at the periphery of the laser spot, and reduced absorption in the deeper vessels. Further evidence of how the results of the program are consistent with those estimated from physical principles is provided in the following subsections, where different skin and scattering models are used.

The computer time required depends, primarily, on the number of particles that are followed. For the 0.4 mm spot diameter simulation with the 3D scattering model, 20 hours of computer time is required. With the 2D scattering model, the number of particles that must be followed is much less (1%) and the program requires 11 minutes of computer time.

4.3.2 Scattering in one, two, or three dimensions

The results for the 1D, 2D, and 3D scattering models for spot diameters between 0.1 and 1.6 mm are described in this subsection. These results show that the 3D scattering model should be used for small spot diameters (< 1 mm). For large spot diameters (> 1 mm), the results from the 2D scattering model are approximately the same as those obtained from the 3D scattering model. The 1D scattering model is inadequate. We use our reference model of skin with 577 nm wavelength light.

Example results from the program for the spot diameter of 0.2 mm are shown in figure 4.5. In this figure, we show the absorption in a small section of the skin slice when the light can scatter in one, two, and three dimensions. The lack of uniformity in the absorption in the epidermis and vessels is a result of the stochastic nature of the Monte Carlo technique. The vertical axis in these surface plots shows the percentage of the incident beam absorbed in the 3 μm cubes in the central skin slice. The percentage is calculated from the number of photons absorbed in the 3 μm cubes in the skin slice divided by the number of photons released over a 3 μm square area of skin.

To help the reader to interpret these surface plots, we ask the reader to estimate the amount of energy absorbed in the epidermis. The scale shows that the absorption in each of the 3 μm cubes in the epidermis is approximately 1%. The epidermis is 65 μm thick (that is 22 cubes), so we see that approximately 22% of the incident light is absorbed in the epidermis. This fraction is given more precisely in subsection 4.3.8.

Absorption in the skin slice when the 1D scattering model is used (figure 4.5a) is quite different from the 2D and 3D models. In the 1D model, only the vessels immediately below the laser spot are illuminated and absorb some of the laser light. There is no absorption in the vessels to the side of the laser spot. The absorption in the central sections of the central vessels is constant when the spot diameter is increased past the diameter of the central vessels. These effects happen because the light travels in a direction perpendicular to the surface of the skin model. There is no lateral, or sideways, scattering.

There is a trough in the absorption in the epidermis with the 1D scattering model. There is less light back-scattered through this part of the epidermis as the central vessels have absorbed some of the incident light. With less light passing through the epidermis, the absorption in the epidermis decreases.

The absorption in the central vessel at a depth of 350 μm is very different from the absorption in the shallow central vessel. Absorption in this vessel is one quarter of the absorption in the shallow vessel. This is mainly due to the shadowing effect

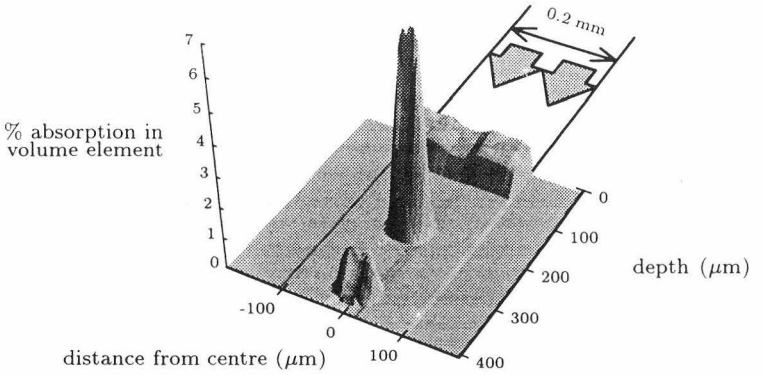

(a) 1D scattering model

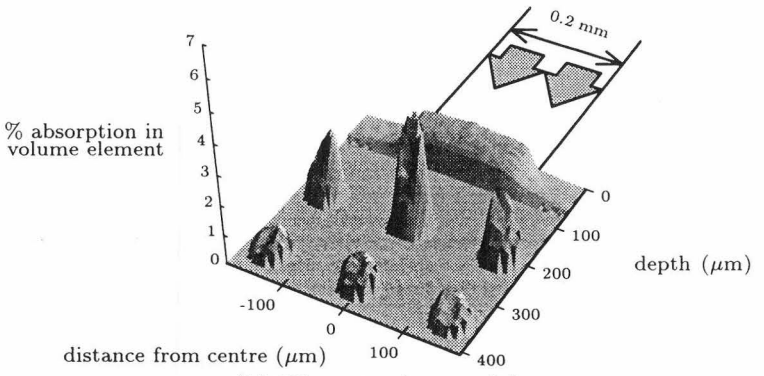

(b) 2D scattering model

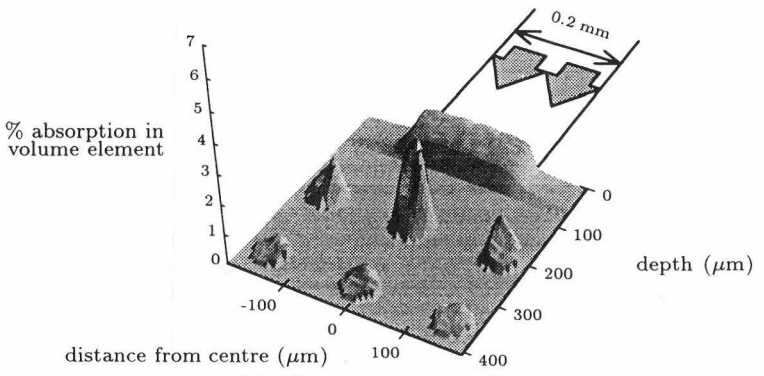

(c) 3D scattering model

Figure 4.5. Surface plots of the results for the three different scattering models. In these and subsequent surface plots, the arrows and black lines at the top right of each graph mark the position of the laser beam. The absorption in the epidermis gives a roughly box shaped structure, and the absorption in the vessels gives the cone shaped peaks.

from the shallow vessel. There is more absorption at the side of the vessel than at the centre. More light reaches the side of the deep vessel than the centre because the distance the light must travel through the shallow vessel is less.

The results for the 2D and 3D scattering models are similar to each other (figures 4.5b and 4.5c). Little variation in the absorption in the epidermis can be seen, except at the boundary of the laser beam. The side of the vessels closest to where the laser beam enters the epidermis has the maximum absorption.

However, there are two factors that create some differences. Firstly, with the 3D model, the light scatters into, and out of, the skin slice. For small spot diameters, the light that scatters out of the central slice is not replaced by light scattering back in from neighbouring slices in the 3D model. This reduces the absorption in all the vessels. As the spot diameter increases, more of the light that scatters out of the slice will be replaced.

The second factor affects the fraction of the laser beam absorbed in each layer of vessels. On average, the particles must undergo fewer scattering events to reach the deeper vessels with the 2D scattering model. Thus, it is more likely that the particles will reach the deeper vessels, and so the absorption in these vessels will be increased. For the 3D scattering model, and with our interpretation of the experimental scattering parameters, the particles travel a shorter distance into the skin. This will increase the absorption in the shallow vessels. This factor is independent of spot diameter.

To show these effects, we plot the total absorption in the central sections of three of the central vessels for spot diameters between 0.1 and 1.6 mm in figure 4.6. In these and similar line graphs, the vertical axis shows the fraction of the incident beam absorbed in the central section of the vessels. This is the number of particles absorbed in the central section of the vessel divided by the number of particles incident on the skin surface above the central section.

There are large differences in the results for the 2D and 3D scattering models when the spot diameter is close to 0.1 mm. For spot diameters above 1 mm, the results for these two scattering models converge. The rate of increase in the absorption in the central vessels reduces as the spot diameter increases with the 2D and 3D scattering models. As the spot diameter approaches 1.3 mm, the rate of change in the absorption is minimal. For larger spot diameters, there is no change.

The first factor has caused the large percentage difference in the results for the 2D and 3D scattering models when the spot diameter is close to 0.1 mm. The effect of the second factor can be seen when the spot diameter is increased beyond 1 mm.

Absorption in the vessel at a depth of 500 μm will always be higher when the 2D

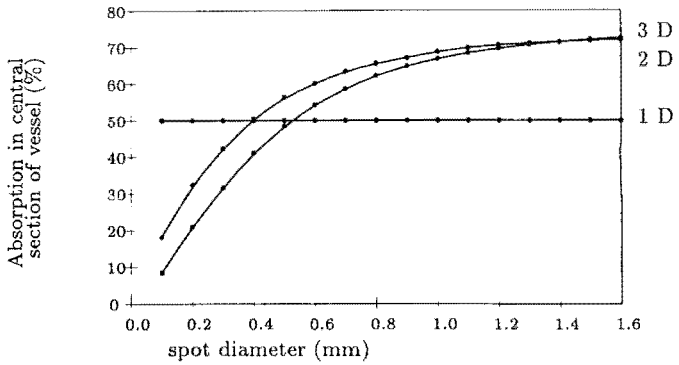

(a) Absorption in the central vessel at a depth of 200 μm.

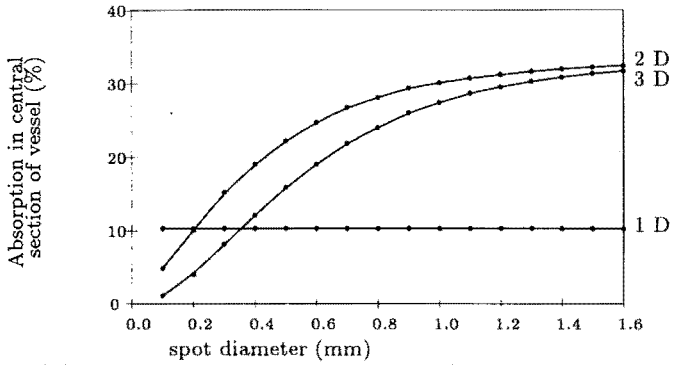

(b) Absorption in the central vessel at a depth of 350 μm.

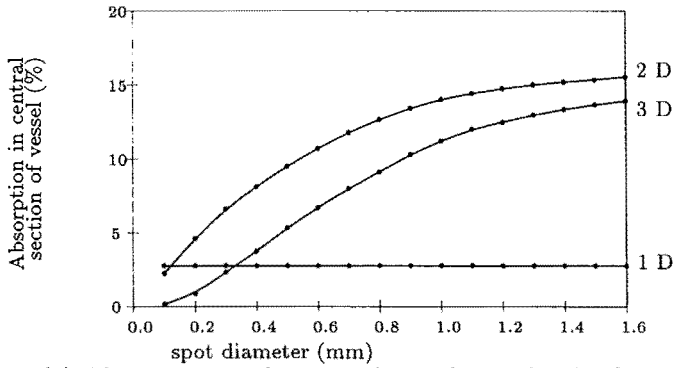

(c) Absorption in the central vessel at a depth of 500 μm.

Figure 4.6. The spot diameter is varied from 0.1 mm to 1.6 mm, with the 1D, 2D, and 3D scattering models.

scattering model is used. In contrast, absorption in the vessel at a depth of 200 μm is higher with the 3D scattering model when the spot diameter is greater than 1.4 mm.

From table 2.2 we see that the total of μ_a and μ_s, which is the mean distance between scattering events in the epidermis, is similar in size to the thickness of the epidermis. A particle that is normally incident on the epidermis will undergo, on average, one scattering event when travelling through the epidermis. Thus, most of the incident beam will be transmitted through into the dermis with the 1D, 2D, and 3D scattering models as the incident beam (in our model) is normally incident on the skin.

The number of dimensions in the model affects the probability of a particle travelling from the dermis through the epidermis. Increasing the dimensions in the scattering model increases the average number of scattering events a particle must undergo to pass through the epidermis. For example, with the 1D scattering model the distance the particle must travel is equal to the thickness of the epidermis. With the 2D or 3D scattering models the particles travel a greater distance as they are deflected sideways while moving through the epidermis.

As the fraction of the incident beam that reaches the dermis is largely independent of the dimensions in the model, we expect that reducing the number of dimensions in the model will increase the fraction of the incident beam back-scattered out of the skin. For the 1D, 2D, and 3D scattering models, 37%, 25%, and 17% respectively of the incident beam is back-scattered from the skin.

4.3.3 Shadowing of the deeper layers

In our reference model, placing the deeper vessels directly below the shallow vessels may have cast a "shadow" on the deeper vessels and reduced the absorption in these vessels. We examine this by comparing the results of the reference model with the results from a variation of the reference model.

The reference model is changed by moving every alternate layer of vessels a lateral distance of 75 μm. The spot diameter is 3 mm so that any change in absorption in the central vessels must be attributed to the shadowing effect of the shallow vessels, and not to the vessels moving into or out of the laser beam. The 1D and 2D scattering models are used with the 577 nm wavelength. The 2D scattering model is used, as the 2D and 3D scattering models are essentially equivalent for the 3 mm spot diameter.

In figure 4.7 we have given surface plots of the absorption in the central region of the skin slice. The distribution of absorbed light inside the vessels is unchanged when the skin model is changed with the 2D scattering model. There is a minimal

(± 2%) difference in the total absorption in the central sections of the vessels close to the centre of the beam.

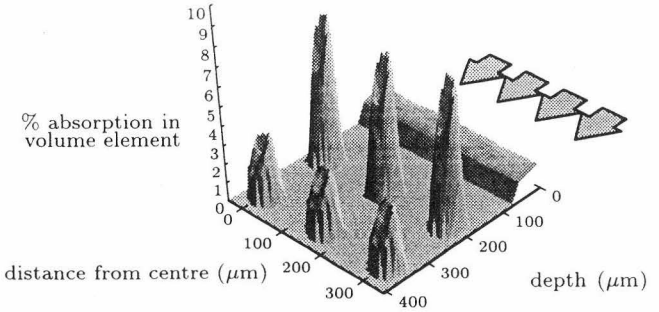

(a) Reference model, 2D scattering model.

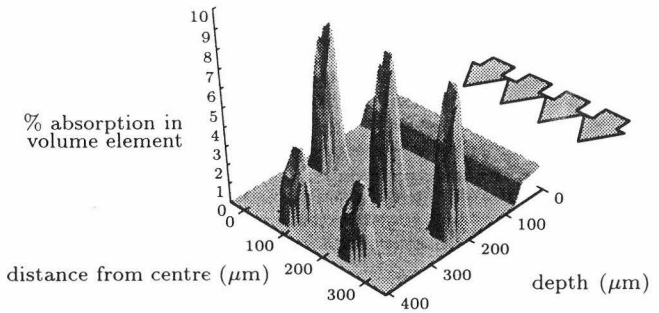

(b) Variation of the reference model, 2D scattering model.

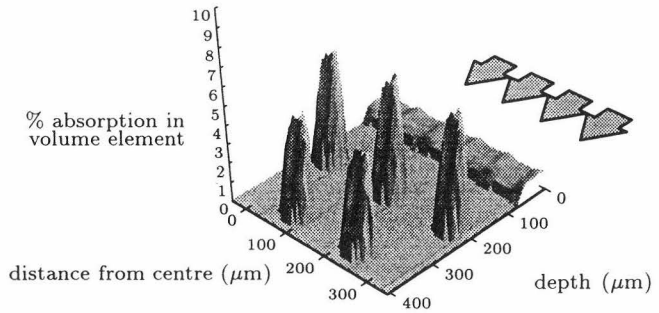

(c) Variation of the reference model, 1D scattering model. This surface plot should be compared with figure (4.5a)

Figure 4.7. In these surface plots, we show the shadowing effect of the shallow vessels, near the centre of a 3 mm beam.

The particles which represent the light have scattered many times and typically have travelled around the shallow vessels before reaching the deeper vessels. As some of the incident light is absorbed in the shallow vessels there is a reduction in the quantity of light present that can reach the deeper vessels. The shallow vessels have reduced the absorption in the deeper vessels for both the reference model of skin and

this variation of the reference skin model (figures 4.7a and 4.7b). The shallow vessels have not cast a clearly defined shadow on the deeper vessels.

After comparing the 1D results in figure 4.7c for the variation of the skin model with figure 4.5a it is clear that the shallow vessels of the reference model have cast a shadow on the deeper vessels. Absorption in the vessels at a depth of 350 μm is significantly higher when the variation on the reference model is made.

For the 1D scattering model, the absorption in the vessels at a depth of 350 μm was expected to be slightly less than the absorption in the shallow vessels. The vessels in the second layer are no longer shadowed by the shallow vessels but there will be some absorption in the dermis, giving a slight decrease in the absorption. However, absorption in these vessels is 84% of the absorption in the shallow vessels. The back-scattering of light in the skin has reduced the quantity of light that reaches the deeper vessels, and so reduced the absorption in the deeper vessels.

4.3.4 The effect of fluence

This subsection shows the effect of fluence on the distribution of absorbed light within the skin for several spot diameters.

Increasing the spot diameter with the same total incident energy spreads the incident energy over a larger area, so the fluence is reduced. A doubling of the spot diameter increases the area four-fold, and so reduces the fluence four-fold. Alternatively, if the fluence is kept constant, the energy in the incident beam must be increased four-fold when the spot diameter is doubled.

Changing the fluence of the incident beam does not affect the height of the graph when the dimensionless units of "% absorption ..." are used. Altering the fluence does change the amount of heat generated within the tissue during laser treatment. In order to show the effect of fluence we plot "heating effect", rather than fractional absorption.

The "heating effect" is a measure which describes the temperature change within the skin. It is proportional to the number of particles which are absorbed at a point within the skin.

We first show the effect of changing the spot diameter from 0.2 mm to 0.4 mm when the fluence is constant, and when the incident energy is constant. The reference model was used with the 3D scattering model, and the results are displayed in figure 4.8.

Increasing the spot diameter from 0.2 mm to 0.4 mm with constant fluence has deposited more energy (and consequently heat) into all of the vessels illuminated.

When the same change to the spot diameter is made without altering the incident energy has reduced the size of the temperature change in the central vessels.

To examine what happens in a quantitative manner for many spot diameters, we take the results in figure 4.6 for the 3D scattering model and scale them to simulate constant total incident energy. The heating effect in the central sections of the central vessels for when the total incident energy is constant and for when the fluence is constant is shown in figure 4.9. Note that the units of "heating effect" have been chosen so that the constant fluence curves in figure 4.9 are the same as the curves in figures (4.6a and 4.6b) for the 3D scattering model.

When the fluence of the incident beam is kept constant, increasing the spot diameter increases the amount of energy that is deposited on the skin. More energy is absorbed in all of the vessels, and so there is more heating of the vessels. The rate of increase becomes less as the spot diameter increases.

When the total incident energy is constant the heating effect in the central vessels decreases as the spot diameter increases. The heating effect in the vessel at a depth of 200 μm decreases by a factor of 30 when the spot diameter is changed from 0.1 mm to 1.6 mm. In contrast, the heating effect in the vessel at a depth of 350 μm decreases by a factor of 10. For the vessels that are deeper in the skin, the change in the heating effect is smaller.

Absorption in the central shallow vessel is strongly affected by the fraction of the beam that is above the vessel. When the spot diameter is close to 0.1 mm, most of the incident laser beam is directed at the central shallow vessel. There are relatively few scattering events before the light reaches the central shallow vessel. Some of these events will scatter the light out of the beam and away from the central shallow vessel, but most of the incident beam will be absorbed in the shallow vessel. This accounts for the significant change in the absorption in the central shallow vessel when the spot diameter is changed from 0.1 to 0.4 mm.

In contrast, the vessel immediately below the central vessel is not illuminated by the unscattered beam. Consequently, the change in absorption when the beam diameter is altered is less.

The amount of heating in all of the central vessels is affected by the average distance the light must travel to reach these vessels. Increasing this distance will decrease the probability that the light entering the skin at the periphery of the beam will reach these vessels. Consequently, for constant total incident energy, there will be less heating of these vessels with increasing spot diameter. Alternatively, if the fluence is kept constant, the rate of rise in the level of heating in the central vessels

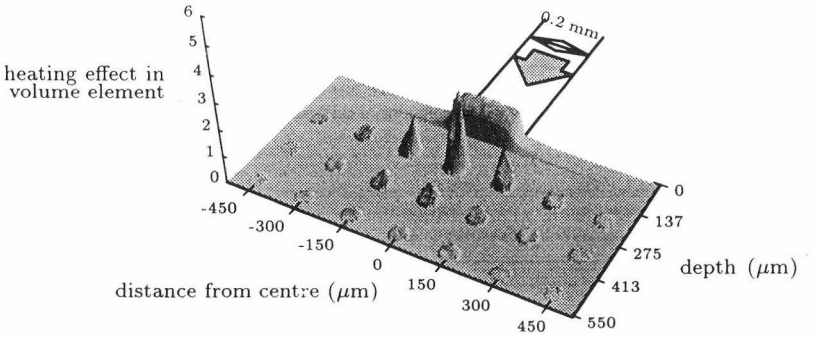

(a) heating effect of a 0.2 mm diameter spot

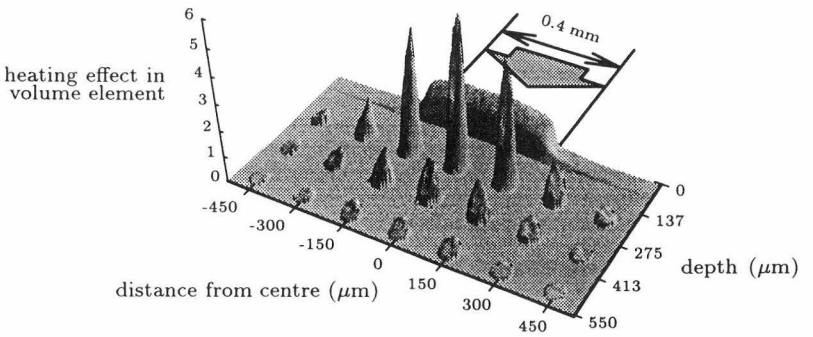

(b) 0.4 mm diameter spot, same fluence as (a).

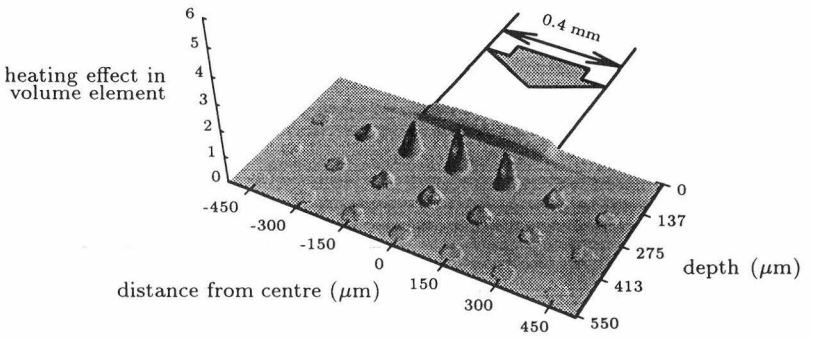

(c) 0.4 mm diameter spot, same total incident energy as (a).

Figure 4.8. In these surface plots we show the heating in the skin slice when the spot diameter and fluence is changed.

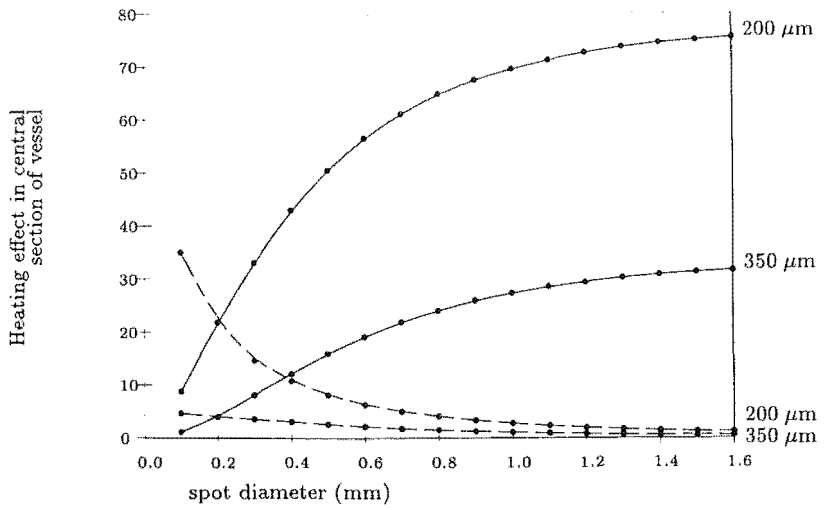

Figure 4.9. The heating in the central sections of the central vessels at depths of 200 and 350 μm as the diameter of the laser spot is increased. For constant total incident energy, (dashed line) the heating effect decreases when the spot diameter is increased. For constant fluence (solid line) more heating is obtained with increasing spot diameter.

will decrease as the spot diameter increases.

4.3.5 Comparison of the wavelengths 577 and 585 nm

From clinical work with a pulsed dye laser, Tan *et al* (1990a) reported that the 585 nm wavelength is more effective in clearing port-wine stains than 577 nm. This was attributed to the increased depth of penetration of the 585 nm light. We examine this conclusion by simulating the passage of light through three different models of skin for both wavelengths.

The spot diameter is 3 mm, as this is a typical size with the pulsed dye laser (Tan and Stafford, 1992). The 2D scattering model is used.

For the first skin model, the reference model is used. Figures 4.10a and 4.10b show surface plots of the absorption in the vessels at depths of 200, 350, 500, and 650 μm with 577 and 585 nm wavelength light respectively. To reduce the amount of detail in this figure, we have shown a region at the edge of the beam. The absorption (due to lateral scattering) in vessels that are outside the laser spot is evident. There is more light absorbed in the shallow vessels with 577 nm. Careful inspection shows that the absorption pattern in the vessels is more uniform with 585 nm than with 577 nm wavelength light.

The differences in the absorption pattern within the central shallow vessel are shown in figure 4.11. There is more absorption close to the wall of the vessel than in

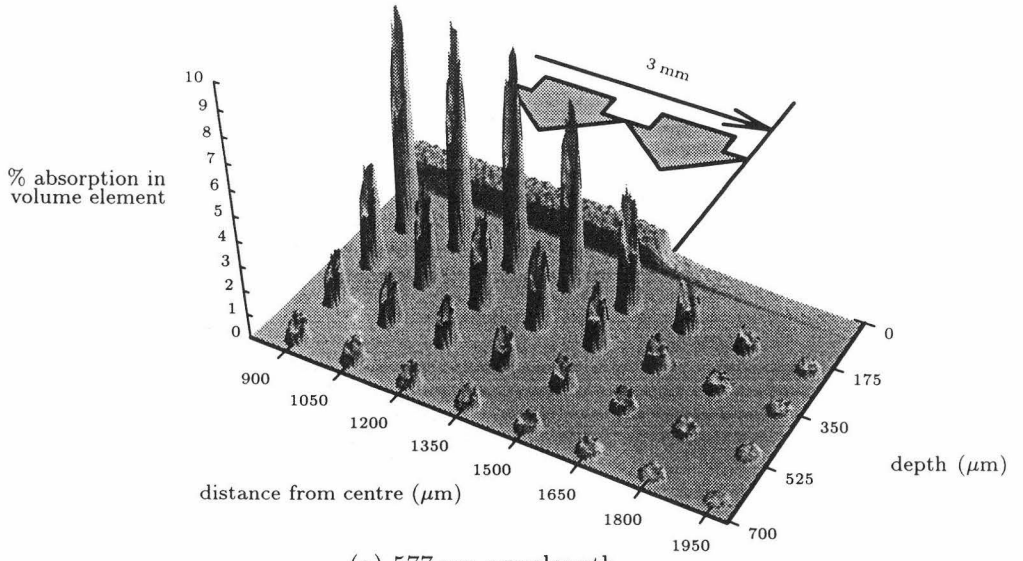

(a) 577 nm wavelength

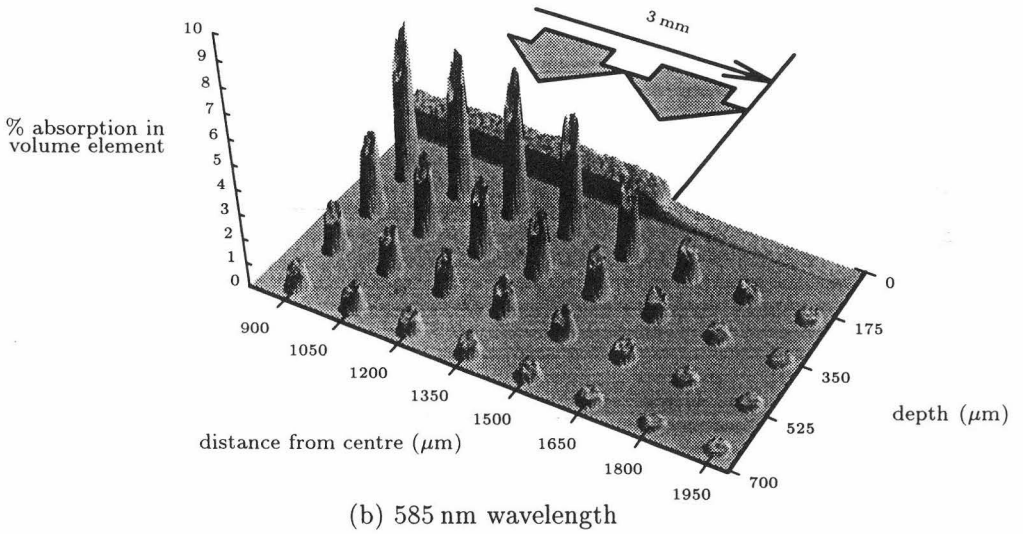

(b) 585 nm wavelength

Figure 4.10. Surface plots of the absorption in the reference model of skin for two wavelengths. Thirty two vessels at depths of 200, 350, 500, and 650 μm are visible. The edge of the incident laser beam is shown.

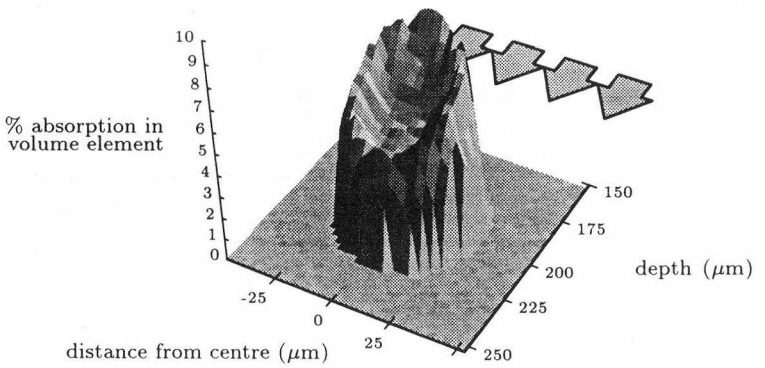

(a) 577 nm wavelength

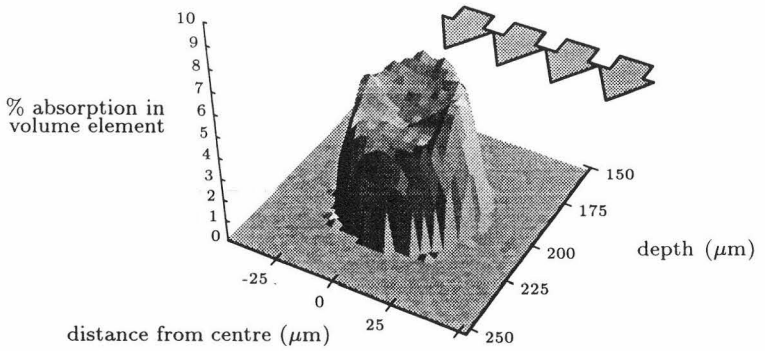

(b) 585 nm wavelength

Figure 4.11. Surface plots of the absorption in the central shallow vessel when the wavelength is 577 and 585 nm, with the reference model of skin.

the centre with 577 nm. The blood is a strong absorber of this wavelength and will attenuate the laser beam. Consequently, less light reaches the centre of the vessel, and so the absorption at the centre is less than at the top, sides, and sometimes the bottom. The 585 nm wavelength is less strongly absorbed in blood than is 577 nm, and so proportionally more light reaches the centre of the vessel, resulting in a more uniform absorption pattern.

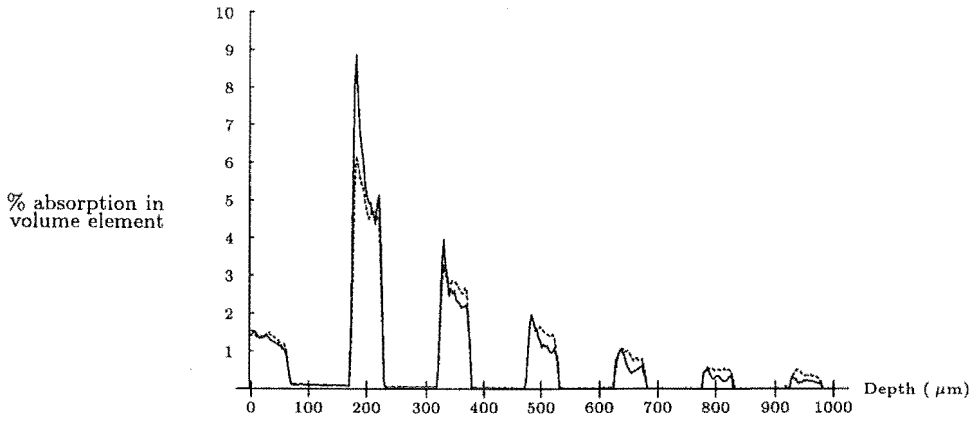

Figure 4.12. The absorption at $x, y = 0\ \mu$m for the wavelengths 577 nm (solid line) and 585 nm (dashed line) with the reference model of skin.

To help show some of the differences in the absorption patterns for the two wavelengths (figure 4.10), we plot the fractional absorption in each volume element along the line $x, y = 0\ \mu$m for both wavelengths in figure 4.12. This graph shows the absorption through the centre of the vessel and it favours 585 nm, as for this wavelength the absorption in the centre is more often higher. There is essentially no difference in the epidermal absorption. The shallow vessels absorb considerably more with the 577 nm wavelength. At a depth of 500 μm there is no difference in the absorption between the two wavelengths. The vessels at a depth of 950 μm absorb twice as much when the wavelength is 585 nm.

For the second skin model, the lateral distance between the centres of the vessels in the reference model is doubled. This simulates a lighter port-wine stain than is represented by the reference model as the percentage of blood in the skin is changed from 9% to 4.5%. Consequently, more laser light should reach the deeper vessels as there are fewer shallow vessels to absorb the incident beam. With this model of skin, the difference in the absorption at $x, y = 0\ \mu$m for the wavelengths 577 nm and 585 nm is shown in figure 4.13.

The absorption in the vessels down to a depth of 650 μm is higher when 577 nm

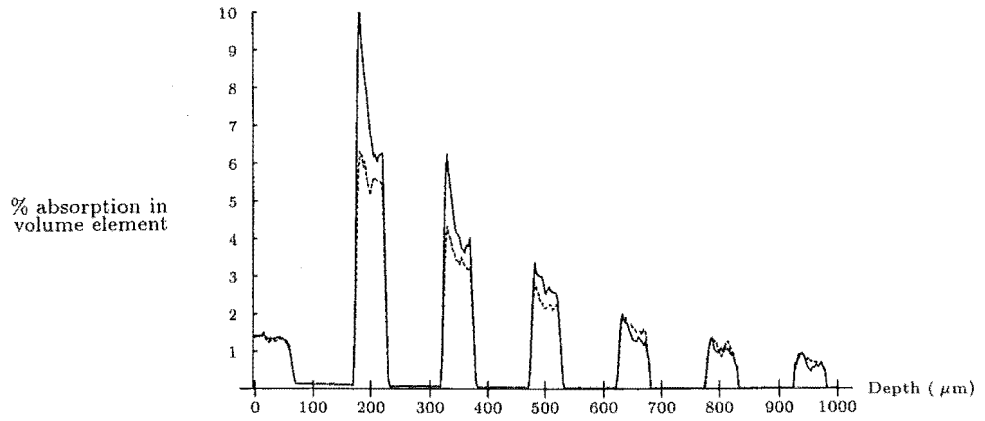

Figure 4.13. The absorption at $x, y = 0\,\mu$m for the wavelengths 577 nm (solid line) and 585 nm (dashed line) when the lateral separation between the vessels is 250 μm.

wavelength light is used. There is no significant difference (<1%) in the absorption in the deeper vessels. The absorption pattern within the vessels is again more uniform when the 585 nm wavelength light is used.

With the third skin model, we envisage a port-wine stain that has had several treatments. The shallow vessels have been thermally necrosed and are no longer present. The top two layers of vessels in the reference model were removed. The absorption along the line $x, y = 0\,\mu$m for this model is shown in figure 4.14.

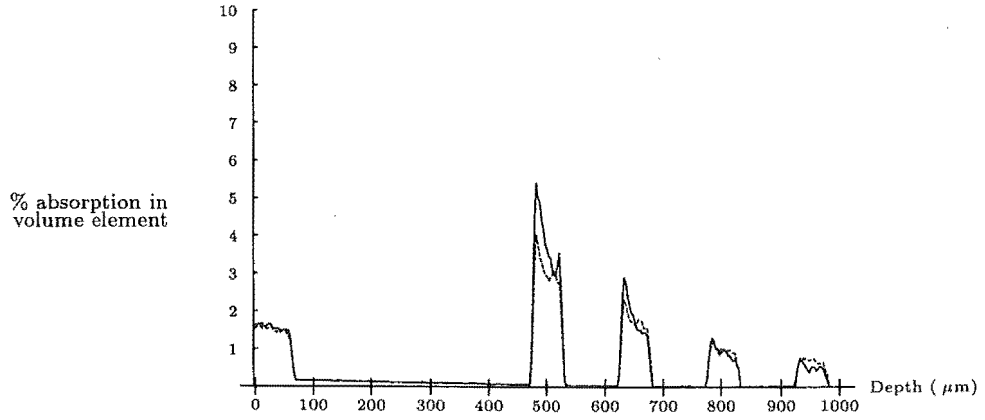

Figure 4.14. The absorption at $x, y = 0\,\mu$m for the wavelengths 577 nm (solid line) and 585 nm (dashed line) when the top two layers of vessels in the reference model are removed.

Alternatively, one may envisage that after laser treatment the shallow vessels have been replaced by capillaries of a normal diameter. Each of the vessels in the top two layers of the reference model would then be replaced by a capillary with a diameter of

5 μm. This reduces the cross sectional area of the shallow vessels to 1% of its previous value. Consequently, the probability that light will be absorbed in these vessels is significantly reduced. The presence of capillaries will not change (significantly) the absorption in the vessels.

Indeed, tests showed that replacing the two shallow layers of vessels in the reference model with capillaries changed the absorption in the vessels at a depth of 500 μm by 1% or less. The capillaries can therefore be ignored, as their effect on the absorption in the vessels is less than the random variations associated with the Monte Carlo technique.

From the three skin models used in this section, absorption in the top layer of vessels is higher with 577 nm light, but less in the very deep vessels. The differences between the two wavelengths are discussed in subsection 4.4.5, where we point out that this finding is not important.

!

4.3.6 Vessel separation

The effect of neighbouring vessels on the absorption in the central vessels is shown in this subsection.

Two types of changes were made to the reference model. Either the separation between the layers of vessels was altered or the lateral separation of the vessels was changed. Increasing the separation, either between the layers or between the vessels in a layer, reduces the percentage of blood in the skin model. The model therefore represents a paler port-wine stain. Conversely, decreasing the separation will increase the percentage of blood in the skin and the skin model represents a darker port-wine stain.

The spot diameter is 3 mm so that any change in absorption in the central vessels must be attributed to the presence (or absence) of neighbouring vessels, and not to the vessels moving into or out of the laser beam. The wavelength is 577 nm, and the 2D scattering model is used.

Figure 4.15 contains the results for when the separation of the layers in the reference model of skin is changed. The shallow layer is not moved when the separation between the layers of the reference model is changed from 0 to 500 μm. That is, the vertical distance between the axes of the vessels is changed from 50 to 550 μm.

The surface plot, figure 4.15a, is the result for when the separation is 500 μm and should be compared with the result from the reference model with the same scattering model, spot diameter, and wavelength (figure 4.10a). The absorption in

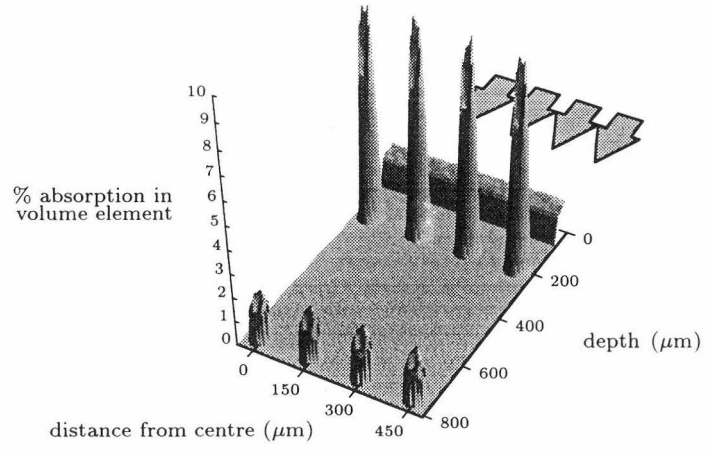

(a) Surface plot for when the separation between the layers is 500 μm.

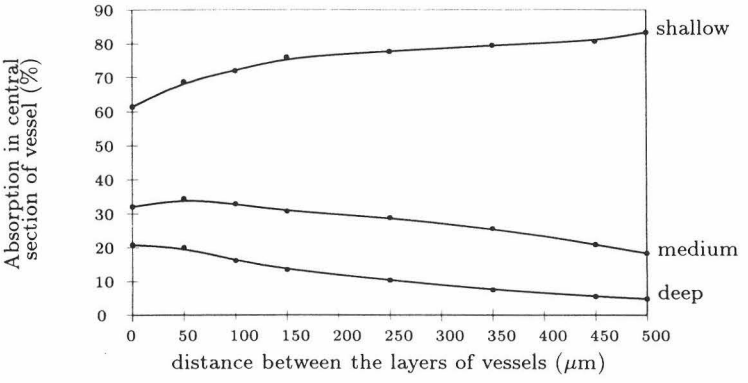

(b) Absorption in the central sections of the central vessels at depths of 200, 350, and 500 μm when the separation between the layers is changed from 0 to 500 μm.

Figure 4.15. The effect of changing the separation of the vessel layers in the reference model of skin.

the second layer of the vessels is much less than in figure 4.10a. As the distance between the layers of vessels is increased, the particles must undergo, on average, more scattering events before being absorbed in a vessel that is moved deeper into the skin. Consequently, the probability that the particles will reach such a vessel is reduced, and so the absorption in these vessels decreases.

Increasing the average number of scattering events that the particles undergo will increase the probability that any given particle will move upwards through the skin, towards the shallower vessels. The absorption at the bottom of the shallower vessels will be increased. This will reduce the difference in absorption between the top and bottom of every vessel, making the absorption pattern within the vessel more uniform.

In figure 4.15b, we have plotted the absorption in the central sections of the three central vessels for when the separation between the layers is changed from 0 to 500 μm. Absorption in the vessels immediately below the shallow vessels decreases by a factor of 2 when the separation of the vessel layers is changed from 0 to 500 μm. The absorption in the shallow vessels is doubled when this change is made.

Generally, vessels that are moved deeper into the skin absorb fewer photons. The decrease in absorption is due to the effect described above, where the particles are less likely to reach the deeper vessels. The particles that are scattered upwards are absorbed in the shallow vessels, increasing the absorption in these vessels. The upward scattering of light accounts for the small increase in absorption in the second layer when the separation is changed from 0 to 50 μm.

In figure 4.16, the effect of changing the lateral separation of the vessels in the reference model is shown.

The surface plot, figure 4.16a, is the result for when the lateral separation is 500 μm and should be compared with the results for the reference model with the same scattering model, spot diameter, and wavelength (figure 4.10a). There is an increase in the absorption in the vessels, as there are fewer vessels in the skin model to absorb the incident particles. The particles will, on average, undergo more scattering events before reaching a vessel. The probability that the particles will enter a vessel from the side, or below, is increased. This accounts for the increase in the absorption at the wall of the vessels.

As the lateral separation increases, the absorption in the central sections of the central vessels should increase. This is shown in figure 4.16b. There is an eight fold absorption increase for the vessels at a depth of 350 μm when the separation of the vessels is changed from 0 μm to 200 μm. When making this change to the lateral separation, the absorption in the vessels at a depth of 500 μm increases by a factor

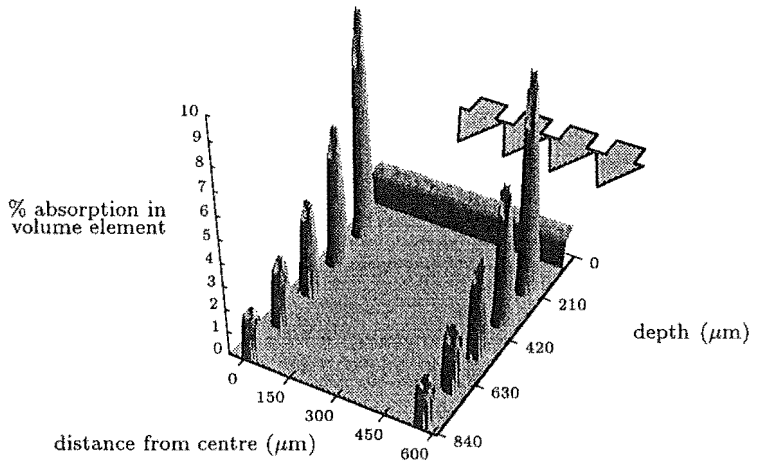

(a) Surface plot for when the lateral separation is 500 μm

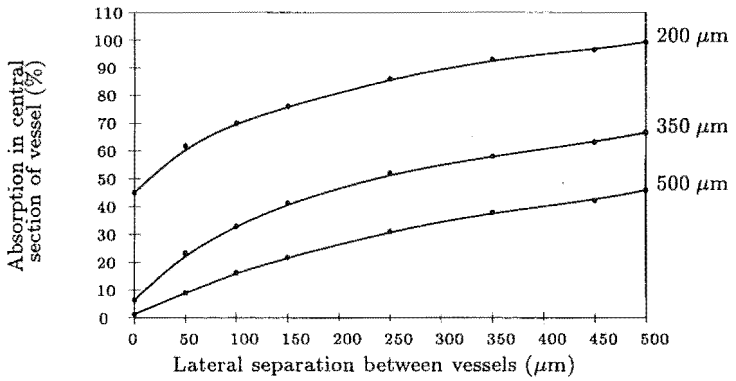

(b) Absorption in the central sections of three central vessels when the lateral separation is changed from 0 to 500 μm.

Figure 4.16. The effect of changing the lateral separation of the vessels in the reference model of skin.

of thirty. As the lateral separation is increased beyond 200 μm the rate of increase in the absorption in every vessel decreases.

From figure 4.16b, it is clear that absorption in the deeper vessels is significantly affected by the lateral separation of the vessels. When the lateral separation is small, a large fraction of the incident beam is absorbed in the layer of shallow vessels, so there is less light available to be absorbed in the deeper layers.

4.3.7 Vessel diameter

The effect of the diameter of the vessels on the transmission of light through the skin is examined in this subsection. Two types of changes were made to the reference model. Either the diameter of every vessel was altered, or the diameter of the shallow vessels was changed. Increasing the diameter of a vessel places more blood in the skin, so a darker port-wine stain is represented.

The spot diameter is 3 mm so that any change in absorption in the central vessels must be attributed to the change in the diameter of the vessels. The 2D scattering model is used with the 577 nm wavelength.

The diameter of all of the vessels in our reference model of skin was varied from 0 to 150 μm. The fractional absorption in the central section of the vessels at depths of 200, 350, and 500 μm is plotted in figure 4.17a. For small vessel diameters ($<$ 25 μm) the absorption in all of the vessels increases as the diameter of the vessels is increased. The shallow vessels do not significantly affect the quantity of light reaching the deeper vessels and the absorption in all of the vessels will depend on the size of the vessels. For larger vessel diameters, absorption in the deeper vessels is determined more by the fraction of the beam absorbed by the shallow vessels than by the size of the vessels. Consequently, the absorption in the deeper vessels rises to a maximum at some diameter and then decreases.

The number of particles absorbed in the central section of the shallow vessels continues to rise as the diameter of the vessels increases. The fractional absorption in the shallow vessels reaches a maximum when the diameter of the vessels is 70 μm, and then decreases. This decrease occurs because the rate of increase in the number of particles absorbed is less than the rate of increase in the number of particles incident on the skin surface above the central section.

The diameter of the vessels which are closest to the skin surface in the reference model was varied from 0 to 150 μm. The diameter of the other vessels is fixed at 50 μm. The fractional absorption in the central section of the vessels at depths of 200, 350, and 500 μm is plotted in figure 4.17b. When the diameter of the shallow

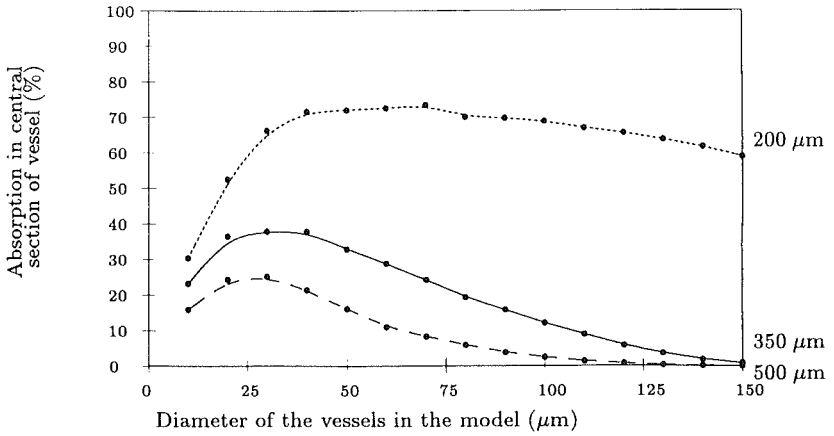

(a) The diameter of every vessel in the reference model is changed.

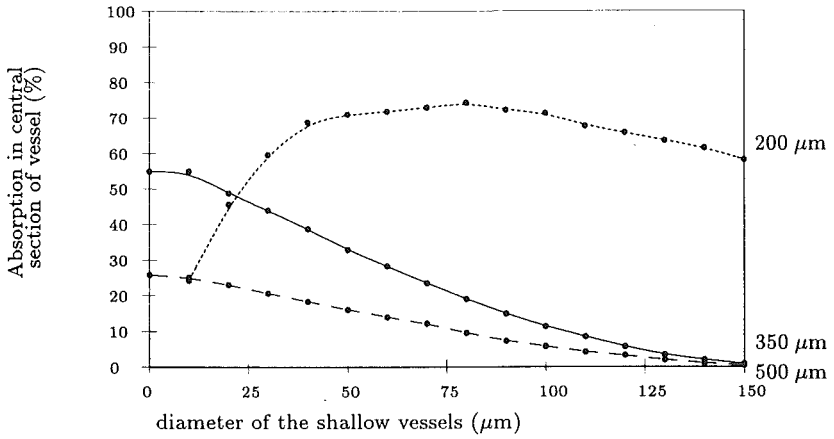

(b) The diameter of the shallow vessels in the reference model is changed.

Figure 4.17. The fractional absorption in the central sections of the three central vessels at depths of 200 μm (short dashes), 350 μm (solid line), and 500 μm (long dashes) when the diameter of some or all of the vessels in the reference model is changed.

The fractional absorption is calculated as stated before, where the number of particles absorbed in the central section is divided by the number of particles incident on the skin surface above the central section.

vessels is zero, no light is absorbed in these vessels and thus more light can reach the deeper vessels. As the diameter of the shallow vessels increases, less light reaches the deeper vessels and so the absorption in these vessels decreases.

The deeper vessels will absorb less than the shallow vessels, even when there are no overlying vessels. This effect is shown in the model of skin where the layer of vessels at a depth of 200 μm was removed by setting their diameter to 0 μm. The fractional absorption in the central vessel at a depth of 350 μm is 55%. In contrast, the fractional absorption in the central vessel at a depth of 200 μm in the reference model is 70%. This difference occurs because the particles are less likely to reach a deep vessel than they are to reach a shallow vessel.

4.3.8 Epidermal absorption

In this subsection, we describe the change in the absorption pattern when the epidermis is heavily pigmented. Also, the absorption in the epidermis for the various skin models and scattering models used in the previous subsections is reported.

When the skin is "heavily pigmented" as defined by Verkruysse *et al* (1993a), the absorption coefficient in the epidermis is increased by 90%, to give the alternative optical properties in table 2.2. We have simulated such a skin model with a 3 mm spot diameter, 577 nm wavelength, and 2D scattering model. The results, figure 4.18, should be compared with the results for skin with a normal level of pigmentation in figure 4.10a.

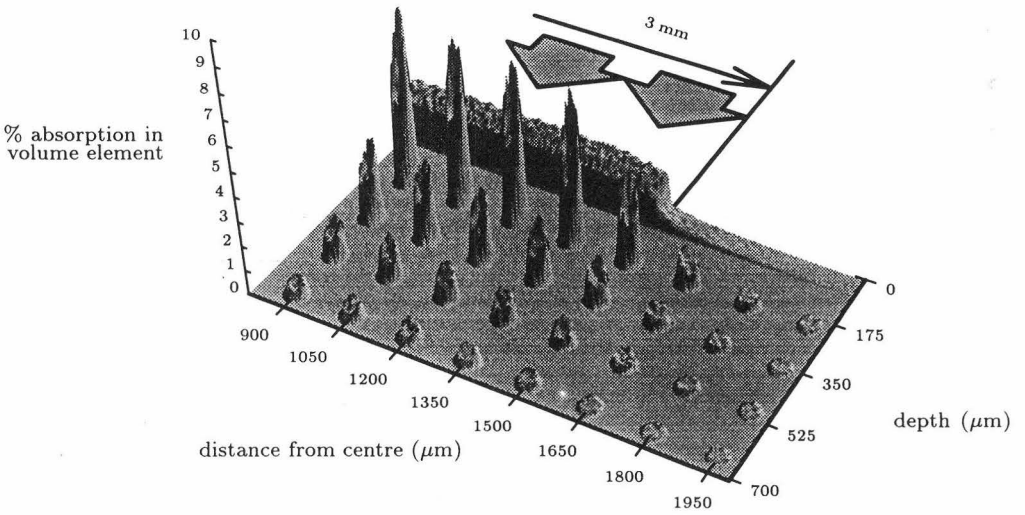

Figure 4.18. Surface plot when the epidermis is heavily pigmented.

For normal and heavily pigmented skin, 23% and 37% respectively of the incident

beam is absorbed in the epidermis. Increasing the level of pigmentation, or melanin, in the epidermis has led to the absorption of more light in the epidermis and so less light passes through into the dermis. As a consequence, absorption in all of the vessels is reduced by, on average, 20% when the skin is heavily pigmented.

Depending on the vessel geometry used in subsections 4.3.6 and 4.3.7, the fraction of the laser beam absorbed in "normal" epidermis was between 20 and 28%. This fraction depends mainly on the diameter and lateral separation of the shallow vessels. Increasing the size of the vessels or reducing the separation between the vessels increases the blood content in the dermis. A larger fraction of the laser beam is absorbed in the vessels, so the fraction of the beam backscattered through the epidermis is reduced. This will reduce the absorption in the epidermis as there is less light passing through it.

Changing the scattering model affects the epidermal absorption. For the 1D, 2D, and 3D scattering models, 16%, 23%, and 26% respectively of the incident beam is absorbed in the epidermis. Increasing the dimensions in the scattering model has increased the average number of scattering events a particle must undergo to pass through the epidermis. Thus, it will be more likely that the particles will be absorbed in the epidermis, and so the fraction of the beam absorbed in the epidermis will increase. Further, it is more likely that a particle will be scattered upwards before it reaches a vessel, increasing the probability that a particle will be absorbed in the epidermis.

4.3.9 The effect of wavelength

In this subsection, we describe the percentage of the beam absorbed in the epidermis, and in the central shallow vessel for the visible wavelengths that are of interest to us: 415, 500, 532, 545, 560, 577, 585, and 590 nm. The wavelengths 415, 545, and 577 nm correspond to three absorption peaks for visible light in oxygen carrying haemoglobin. The 500 nm wavelength may be regarded as the average of the 488 and 515 nm wavelengths which are produced by the argon laser. The 532 nm wavelength is of interest as this wavelength is generated by a frequency doubled Nd:YAG laser, which is used for treatment of port-wine stains. The wavelength 560 nm corresponds to a peak in the absorption of oxygen depleted haemoglobin. The wavelengths 577 and 585 nm are used for treatment of port-wine stains, and are included to provide a comparison.

The parameters in table 2.2 were used in this calculation for each of the wavelengths simulated. The reference model of skin was used, and the light could scatter

in two dimensions. A 3 mm spot diameter was used, so the effect of lateral scattering could be ignored.

The fraction of the beam absorbed in the epidermis, and in the central section of the central shallow vessel was recorded. These results are plotted in figure 4.19.

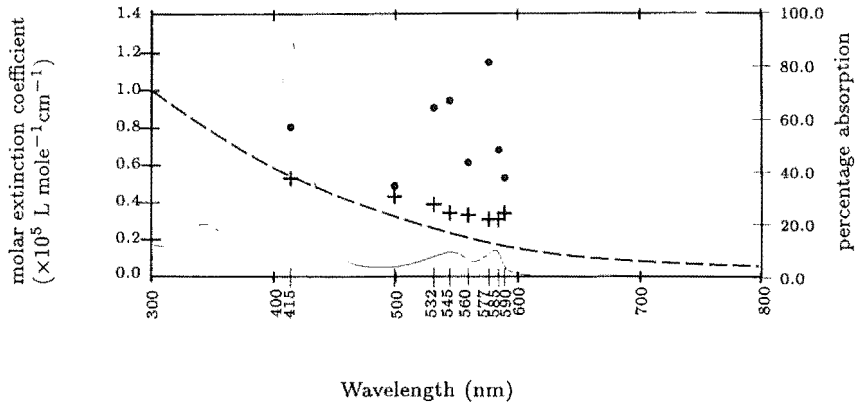

Figure 4.19. The absorption coefficients for oxygen rich haemoglobin (solid line) and dopa-melanin (dashed line) are plotted, where the vertical axis on the left side describes the scale. From the optical properties of the epidermis and blood, the absorption in these structures is determined with the Monte Carlo technique for the wavelengths of interest to us. The absorption in the epidermis (crosses) and the central shallow blood vessel (filled circles) is plotted. For this data, the vertical axis on the right side should be referred to.

Superimposed over the results obtained with the Monte Carlo technique in figure 4.19, we have plotted figure 2.9, which shows the absorption in melanin and haemoglobin for the visible wavelengths. The units for the absorption in the melanin and haemoglobin make this a log scale, unlike the linear scale on the vertical axis on the right hand side.

Consider first the absorption in the epidermis which is, to a large extent, determined by the absorption coefficient of the melanin. However, when the absorption in the blood below the epidermis is increased, less light is backscattered up through the epidermis. As less light passes through the epidermis, less is absorbed there. Consequently, at 577 nm where the absorption in the blood is maximised, there is a corresponding but slight dip in the absorption in the epidermis.

The absorption in haemoglobin is very high at 415 nm, much higher than the absorption in the melanin. This would suggest that 415 nm should be used for the laser treatment of port-wine stains. The results from the Monte Carlo simulation show that with this wavelength, absorption in the epidermis is very high. Therefore, too much of the incident beam is absorbed in the epidermis, and less light is able to reach the blood vessels where it may be absorbed.

4.4 Discussion

We have presented the results of Monte Carlo simulations of the absorption and scattering of laser light in skin. While there are differences between our model and human skin, we have gained insight about the scattering and absorption of laser light in skin.

4.4.1 Comparison with published theoretical results

In this subsection we compare the results from our model with those from other workers who used the Monte Carlo technique. Our model is an improvement over those used by previous workers as it contains multiple blood vessels and allows us to examine how the absorption in one vessel is affected by neighbouring vessels.

Keijzer *et al* (1989) calculated the distribution of absorbed light within homogeneous tissue with a 3D scattering model, but translated the absorption at a point in space back to the plane in which the results were recorded. Hence, the distance between scattering events is shorter than the optical parameters predict. Their results were similar to ours as the absorption decreased as the distance from the skin surface increased. Like us, they showed that the absorption near the centre of the beam was similar in size and profile to the absorption at the centre of the beam.

Keijzer *et al* (1991) used a model of skin that contained an epidermal layer and one vessel at a depth of 410 μm. The inadequacies of this model were described earlier, in subsection 4.2.3. With this model, they reported a 2.5 fold increase in absorption in the vessel when the spot diameter was increased from 0.2 mm to 1 mm. With our 2D scattering model, the results show a 2–3 fold absorption increase for the central vessels at at a depth of 200 and 350 μm respectively. With our 3D model, there is a 3–6 fold absorption increase for the vessels at a depth of 200 and 350 μm respectively.

Pickering and van Gemert (1991) used a 2D scattering model that has epidermal and dermal layers. The absorption and scattering coefficients for the dermis were scaled to simulate blood uniformly distributed throughout the dermis. The thermal damage model of van Gemert *et al* (1991b) was used, so the depth at which the temperature rise in the dermis is equal to the temperature rise at the base of the epidermis was found. This work was extended by Verkruysse *et al* (1993a), who examined a range of wavelengths between 415 and 590 nm with various vessel diameters. Both reports show that the "absorption depth" in the skin was increased when the wavelength is changed from 577 to 585 nm and claimed that this explained the increase in the penetration depth observed clinically by Tan *et al* (1990a).

We agree with Pickering and van Gemert (1991) and Verkruysse *et al* (1993a) that the absorption in the deeper vessels is increased for some vessel geometries with 585 nm. These conclusions are incomplete, as they ignore the absorption and consequent temperature rise in the shallower vessels. As we will discuss in subsection 4.4.4, the required thermal damage in the deep vessels will only occur when the shallow vessels have been removed. When the shallow vessels have been removed, both wavelengths will penetrate to the required depth.

Miller and Veitch (1993) used a model of skin that contained five layers: epidermis, basal layer, shallow dermis, layer of blood, and a deeper layer. From this model, they showed that 585 nm is more uniformly absorbed in the layer of blood. Further, they showed that when the beam diameter is increased past 1 mm, there is a minimal increase in the fluence at the layer of blood. While there are significant differences between this model and ours, we are in agreement with the results of Miller and Veitch (1993).

4.4.2 Two and three dimensional models

One possible justification for ignoring the scattering of light in the third dimension is that the mean free path of light in skin is considerably smaller than the spot diameter modelled. We have shown that this is a poor approximation for small spot diameters (< 1 mm). The optical properties of skin listed in table 2.2 show that yellow laser light is weakly absorbed in the dermis. Particles can then scatter distances far greater than one mean free path in the dermis. Thus, for small spot diameters the calculated absorption with a two dimensional scattering model is significantly different from the results obtained with a three dimensional scattering model.

With the advances in available computing power seen in the last decade, the scattering of light in three dimensions can be calculated in a reasonable time. We can, and should, use the more accurate three dimensional model of scattering for spot diameters less than 1.0 mm.

4.4.3 Spot diameter

We have calculated the effect of the spot diameter for when the total incident energy is constant and for when the fluence is constant.

With constant fluence, increasing the spot diameter will increase the absorption in all of the vessels that are illuminated. When the spot diameter is larger than 1 mm, further increases in the spot diameter have a minimal effect on the absorption in the

vessels near the surface of the skin. We are in accord then with the clinical findings of Tan *et al* (1988) that there is a small increase in the depth of damage when the spot diameter is increased beyond 3 mm.

When the total incident energy is kept constant, reducing the spot diameter increases the absorption in the vessels below the spot. The required illumination time will decrease as the rate of energy deposition into the vessel is increased. Reducing the illumination time reduces the heating in the non vascular tissue. From clinical work, see for example Adams *et al* (1987), reducing the heating in the non vascular tissue will reduce the risk of an untoward result.

From the theoretical work of several workers (van Gemert *et al*, 1986; Pickering *et al*, 1989b) and the results in chapter 5, we see that the illumination time should be in the range of 1–10 ms. This will minimise the heating of the non vascular tissue, while giving sufficient time for the entire vessel wall to be damaged. The spot diameter should therefore be chosen, for a given laser power, so that the fluence on the skin is sufficiently high to give the appropriate response with an illumination time in the optimal range.

4.4.4 Treatment of the deeper vessels

One approach to the treatment of port-wine stains is to place sufficient energy into the skin so that all of the vessels below the laser spot are thermally damaged. The shallow vessels will absorb an order of magnitude more energy than the vessels at depths of 500 μm or more. As we will discuss in the next subsection, vaporisation of the blood in the upper vessels will occur long before the deeper vessels reach the damage threshold. Before the deeper vessels can be treated, the shallow vessels must be removed.

At any given time, some of the vessels in a port-wine stain are empty (Niechajev and Clodius, 1990). Thus, in any one treatment, not all of the shallow vessels will be thermally damaged. These vessels will need to be thermally damaged in a subsequent treatment session. Only when the shallow vessels have been removed, or when the upper part of the dermis consists of empty vessels, will sufficient light reach the deeper vessels to enable treatment of the deeper vessels. The effect of the shallow vessels is shown in figures 4.14 and 4.17b.

After removing the shallow vessels, it is possible to treat the deeper vessels. However, we see from figures 4.12 and 4.14, that the absorption in the shallowest vessel depends on depth. This is true for both the wavelengths 577 and 585 nm. The light is less likely to reach the deeper, but topmost vessels, because the light must undergo

more scattering events to reach these vessels. At each scattering event, the light may be scattered upwards, away from the vessels. The probability that the light will reach a deeper vessel is less, and so the absorption in such a vessel is less.

4.4.5 The differences between 577 and 585 nm wavelength light

There are three observable differences in the absorption patterns for the two wavelengths. First, there is an increase in the absorption in the deeper vessels with 585 nm. Second, the distribution of absorbed light within the vessels is more uniform with 585 nm.

Tan *et al* (1990a) assert that the ideal wavelength light for the treatment of port-wine stains is 585 nm, not 577 nm, because the penetration depth is increased. Our results do show that absorption in the deeper vessels is increased with 585 nm. But, we stress that the shallow vessels have absorbed an order of magnitude more energy than the deeper vessels. Consequently, if enough energy is deposited on the skin so that the average temperature of the blood in the vessels at a depth of 950 μm reaches 70 $^{\circ}$C, then the average temperature of the blood in the shallow vessels will be several hundreds of degrees (ignoring phase changes). The surplus of energy in the shallow vessels will be conducted to, and thermally damage, the surrounding non-vascular tissue.

To carry out optimal treatment, there should be no damage to the non-vascular tissue. Sufficient energy, at either wavelength, should therefore be placed in the skin so that only the uppermost vessels are damaged. Some energy will be absorbed by the deeper vessels but it will be insufficient to cause thermal damage. When the uppermost vessels have been removed in previous treatments, both wavelengths will penetrate to the same depth in the dermis.

From the results of our Monte Carlo model, we state that the important difference in the absorption patterns for the two wavelengths is that with 585 nm the absorption pattern in the vessels is more uniform. In the subsequent chapter of this thesis, (chapter 5), we show why the more the uniform absorption pattern may be important.

4.4.6 Absorption in the epidermis

Miller and Veitch (1993) note that the epidermis is not homogeneous and that there is a high proportion of melanin in the basal layer. Also, the level of melanin can vary between different points on the skin, as observation shows. Of the various components

in the epidermis, melanin is the principal absorber of visible light (Anderson and Parrish, 1981a). Thus, the laser light will not be uniformly absorbed in the epidermis during laser treatments. Our model does not take this into account, so the epidermal absorption shown in the surface plots should be regarded as an approximation.

We have shown that the epidermal absorption is strongly dependent on the level of melanin in the epidermis and, to a lesser extent, on the backscattering of light from the dermis.

4.5 Conclusion

In our calculations, we have shown the effect of the spot diameter, the scattering model of light, position of the vessels, vessel diameter, the level of pigmentation in the epidermis, and the wavelength on the distribution of absorbed light in skin.

The choice of scattering model affects the calculated absorption. Increasing the number of dimensions in the scattering model reduces the distance the light travels into the skin, so the fraction of the beam absorbed in the epidermis is highest when the 3D scattering model is used. The 1D scattering model does not describe the lateral scattering of light, so absorption in the vessels is not increased due to light entering the vessel from the side. For small spot diameters, eg 0.2 mm, absorption in every vessel is higher with the 2D model because the scattering of light in the third dimension is ignored. When the spot diameter is greater than 1 mm, the difference is much less.

Increasing the spot diameter while keeping the fluence constant leads to an increase in the absorption in all vessels since it represents an increase in the total energy supplied. The rate of increase in the absorption becomes negligible for spot diameters larger than 1 mm. Alternatively, if the total incident energy is kept constant, absorption in the central vessels increases when the spot diameter is decreased. This increases the fluence, or energy density, on the skin above the central vessels.

While examining the effect of the spot diameter, the validity of the scattering model and other simpler models were tested. When the spot diameter is less than 1 mm the computer model should simulate the scattering of light in three dimensions if it is to give acceptable results. For larger spot diameters adequate results are obtained in the minimum of computer time when a two dimensional scattering model is used.

Increasing the level of melanin in the epidermis reduces the amount of light that penetrates through the epidermis as more light is absorbed in the epidermis. When

the light levels in the dermis are reduced, there is less light to be absorbed in the vessels, and so the absorption in the vessels is reduced.

Increasing the separation between the vessels increases the absorption in all of the illuminated vessels. Increasing the separation between the vessels means that the light must undergo, on average, more scattering events before reaching a vessel. Consequently, more light is remitted from the skin and the absorption in the epidermis is increased. The absorption in each vessel is increased as the incident light is spread amongst fewer vessels. For these pale port-wine stains, the energy density on the skin that is required to cause the appropriate damage to the vessels will be reduced.

The effect of the vessel geometry on distribution of absorbed light in the skin is larger than that of changing the wavelength from 577 to 585 nm.

Using 585 nm instead of 577 nm does increase the absorption in the vessels several layers below the shallow vessels. We have shown that this is not relevant. The relevant difference is that with 585 nm the absorption in the vessels is more uniform than with the 577 nm wavelength. With exposure times of 0.45 ms or less, the use of 585 nm wavelength may be better as there will be more heating of the bottom of the vessel, for the same heating of the top.

Our model predicts that regardless of what treatment parameters are used, the process of removing the vessels will take numerous treatments. A port-wine stain that consists of vessels in a single layer will require several treatments as some of the vessels will be empty during any given treatment session. For thick port-wine stains, the vessels must be removed "layer by layer". A layer in this context consists of a two to three hundred micron thick slab of the dermis. Attempting to thermally damage all of the vessels in one treatment session will vapourise the blood in the uppermost vessels and cause untoward damage in the non-vascular tissue.

Chapter 5

Calculation of the optimum illumination time

We describe in this chapter the results from two methods for calculating the optimal illumination time. Both methods describe the conduction of heat within the skin by solving the heat transfer equation. The merits of each method is described. We conclude that with exposure times longer than 10 ms, there is heating of the vascular and non-vascular skin components. When the illumination time is less than 1 ms there is an insufficient temperature rise, and consequent damage, at the bottom of the vessel.

When the illumination is less than 1 ms, there is more heating at the bottom of the vessel when the wavelength is shifted from 577 to 585 nm. This effect is small, and may explain why some clinicians claim that 585 nm is superior to 577 nm.

As stated in the introduction to this thesis, the immediate goal of laser treatment is to thermally damage the walls of the oversized vessels in the skin, with a minimum of damage to the surrounding non-vascular tissue.

One of the conditions for this goal to be achieved, is the laser beam must illuminate the skin for some optimal time. We take this as our definition of the optimal illumination time. van Gemert *et al* (1992) gives a similar definition, which is

> The exposure time should be long enough to accomplish irreversible damage of the wall by heat conduction, and short enough to prevent conduction of heat too far into the surrounding dermis.

When the illumination time is shorter than optimal, insufficient heat is conducted from the blood to the vessel walls during the exposure time and the temperature in the vessel rises beyond boiling point. The vessel cannot contain the steam and there is rupture of the vessel wall. The endothelial cells that make up the vessel wall are not thermally damaged, and there is no long term colour change. Increasing the illumination time, without increasing the fluence does not result in damage to the vessel walls as too much heat is conducted away from the blood and blood vessel to the surrounding tissue. Increasing both the illumination time and the fluence results in the required damage to the vessel wall, but more damage to the surrounding tissue.

We need to find the optimal illumination time so that the patients receive the best possible treatment. Two techniques are contained in the literature for calculating the optimal time. We describe both techniques in this chapter. The results from these techniques are given.

Both techniques rely on a solution of the heat transfer equation, which describes the conduction of heat within the skin. It is:

$$\frac{\partial T(x,y,z,t)}{\partial t} = \frac{1}{\rho C_v}\Phi(x,y,z) + \frac{\eta}{\rho C_v}\nabla^2 T(x,y,z,t) \tag{5.1}$$

where ρ, C_v, and η are the tissue density, heat capacity, and conductivity respectively. $T(x,y,z,t)$ is the temperature at the coordinate, (x,y,z), at some time t. The first term on the right hand side, $\Phi(x,y,z)$, is the laser power absorbed at the coordinate, (x,y,z), which is determined from a solution of the equation that describes the transport of light through skin (equation 3.1). The second term on the right hand side of the equation represents the energy change per unit time from coordinate (x,y,z) due to the heat conduction.

The cutaneous tissue characteristics are listed in table 5.1. These values are from a paper by van Gemert *et al* (1986), who examined the flow of heat within tissue. In this paper, the authors stated that the thermal properties of water were used, which was assumed to represent the thermal properties of tissue. The value for the heat capacity of water is 4.2×10^3J kg^{-1} °C^{-1}. It appears that van Gemert *et al* (1986) modified this parameter, but did not mention this in their paper. Liquids, such as water have a higher heat capacity than solids (in general) so it is probable that the heat capacity of tissue was modified to reflect this. The initial temperature of the skin and blood is verified by the results listed in subsection 2.1.1.

Parameter	Value
Density (ρ)	10^3 kg m^{-3}
Heat Capacity (C_v)	3.5×10^3J kg^{-1} °C^{-1}
Thermal Conductivity (η)	0.62 W m^{-1} °C^{-1}
Initial skin and blood temperature (T_0)	35 °C

Table 5.1. Tissue parameters used in the calculation of the flow of heat within the skin.

Two methods for finding the optimal illumination time have been described in the literature, which are described below. With both methods, some approximations are made, which we first describe.

1. The thermal properties of skin are known.

2. The removal of heat by blood flow can be ignored (Welch *et al*, 1980).

3. The skin is regarded as homogeneous. Both solutions of equation (5.1) in the literature require this approximation, but it can be dispensed with if the algorithm used is complex enough.

4. The heat is assumed to be conducted in two dimensions, that is the flow of heat in the direction that is parallel to the axis of the cylindrical blood vessel is ignored. Such an approximation will be valid away from the edge of the laser beam.

5. The optical and thermal properties of the skin components do not change during, or after, the laser illumination.

6. A criteria is used to relate the temperature changes in the skin to tissue damage. The input parameters are then adjusted until the required damage is sustained by the tissue.

Various techniques for relating temperature changes to damage have been used in the literature. We describe the method used in this thesis, and the reasons for choosing this method in section 5.1.

In section 5.2, we describe the results of an analytical technique that has been used to determine the optimal illumination time. These results can be compared with those in section 5.3, where a numerical method is used to determine the optimal illumination time.

With the numerical technique, and the results from the Monte Carlo method that is described in chapter 4, we give a quantitative description of the effect of various illumination times in section 5.4. These results graphically show how increasing the illumination time with a corresponding increase in the fluence results in more heating of the surrounding tissue.

In chapter 4 we examined the differences between the wavelengths 577 and 585 nm. It was noted that when the wavelength is 585 nm, the light distribution in the vessel is more uniform. We examine the effect that changing the wavelength has on the temperature distribution in, and around, the vessel for different illumination times.

These results are discussed in section 5.5.

5.1 Relationship between temperature and damage

In this section, we first briefly describe two techniques in the literature for relating temperature changes within the skin to tissue damage. These can be described as damage prediction models. From this description, the motivation for the technique used in this thesis becomes clear.

The work of Welch (1984) provides a summary of the derivation of the damage integral, an equation that can be used to relate temperature to tissue damage. We repeat the relevant parts of this summary below.

Based on experimental data, Arrhenius has postulated a reaction rate of the form

$$A \exp\left(\frac{E}{RT}\right) \tag{5.2}$$

where

R is the universal gas constant

T is the temperature in degrees Kelvin

E is related to the activation energy

A a rate constant, and is approximately $\frac{kT}{\hbar}\exp(\frac{\Delta S}{R})$

where

k is Boltzmann's constant

$\hbar$ is Planck's constant

ΔS is the entropy of activation

From this, Henriques (1947) postulated and tested an equation of the form

$$\Omega(r,z) = A\int_{t_i}^{t_f} \exp\left(-E/RT\right)dt \tag{5.3}$$

Here,

$\Omega(r, z)$ The value of this function determines the level of injury sustained. Erez and Shitzer (1980) have defined three regions that describe the damage inflicted on the tissue,

$\Omega < 0.53$	damage is reversible, complete healing will occur in time
$0.53 < \Omega < 1$	tissue damage might be irreversible
$1.0 < \Omega$	complete irreversible damage with a coagulation type of necrosis transforming the cells in a homogeneous mass of proteins

t_i the time at which the laser beam is turned on

t_f the time at which the tissue temperature returns to the pre-exposure temperature

The values of the constants A and E are uncertain. In the experiments of Henriques (1947), the following values were obtained

A	$3.1 \times 10^{98} \mathrm{s}^{-1}$
E	630 k J/Mole

Welch (1984) quote the work of Takata (1974), who adjusted the rate coefficients for various ranges of tissue temperatures to obtain the following values,

T <44 °C	was not stated	
44< T <50 °C	A	$4.3 \times 10^{64} \mathrm{s}^{-1}$
	E	420 k J/Mole
T >50 °C	A	$9.4 \times 10^{104} \mathrm{s}^{-1}$
	E	670 k J/Mole

These values are obtained from experiments in which tissue samples are heated for periods of time longer than 1 s. Sometimes, the tissue was heated for more than a thousand seconds. Information on the value of these constants is not available when the heating time is in the order of milliseconds, which is the case in our simulations. It is questionable whether these results can be used to predict the tissue damage when the time scale is of the order of milliseconds, which is the case in our simulations. Further, there is no experimental evidence that the damage integral can be applied to our simulations.

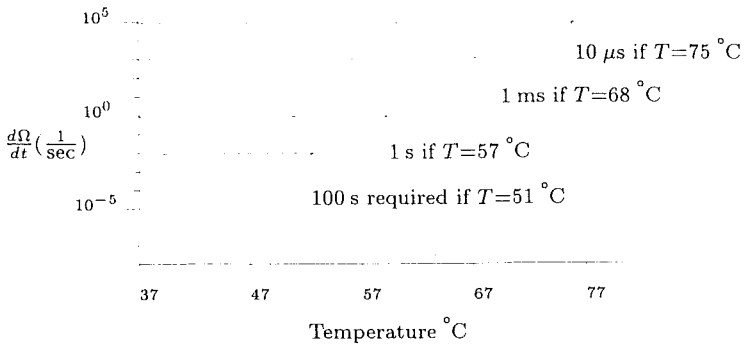

Figure 5.1. The time required for irreversible damage to occur in tissue at various temperatures.

Welch (1984) put these considerations aside and plotted the time taken for Ω to change from 0 to 1 using the values for A and E determined by Henriques (1947). This graph is reproduced in figure 5.1. From this graph, it is clear that the rate at which damage is sustained by the tissue increases as the temperature increases. For temperatures in excess of 70 °C, the time required for threshold damage is less than 0.4 ms, which is the minimum illumination time simulated in this thesis.

A simpler approach, rather than use the damage integral, is to define a threshold temperature, T_c, at which threshold damage is obtained. Such an approach has been used by van Gemert *et al* (1982), Lahaye and van Gemert (1985), and Pickering *et al* (1989b). Following these workers, we set the threshold temperature for the necessary level of damage to be 70 °C.

During the treatment of port-wine stains with a laser, the aim is to thermally damage the wall of the vessel by the conduction of heat from the blood. How much of the endothelial cells that must be damaged for the treatment to be effective is an unanswered question.

We noted in chapter 2 that the endothelial cells extend around the wall of the normal sized capillaries. For the small ectatic capillaries, such as those with a diameter of 30 μm, the endothelial cells will extend around part of the wall. For these vessels, it may only be necessary to heat the top and side of the vessel for all of the endothelial cells in the vessel to be damaged. This is probably not the case for large vessels (200 μm) where the endothelial cells do not extend as far around the wall of the vessel.

From subsection 2.1.3, we see that the nucleus of the endothelial cells have a thickness of 6 μm. We make the requirement in this thesis that all of the endothelial cells in the vessel wall must be thermally damaged. Thus, the temperature at every point at a distance of 10 μm from the vessel lumen must exceed 70 °C, which is our

threshold temperature for damage.

In contrast, van Gemert (1992) proposed that some critical temperature must be reached somewhere inside the vessel, which was taken to be at the centre of the vessel. This requirement does not show that the endothelial cells which make up the vessel wall are damaged, which is the aim of the laser treatment.

5.2 Calculation of the thermal relaxation time

An analytical solution to equation (5.1) has been published by Anderson and Parrish (1981b).

In this paper, Anderson and Parrish (1981b) made the approximation that the illumination time is very short, so the conduction of heat away from the vessel during the illumination time can be ignored. The conduction of heat away from the vessel after the illumination time was determined with the heat transfer equation. From this result, they calculated the thermal relaxation time, which is the time taken for temperature at the centre of the vessel to fall half way from the peak temperature to that of the surroundings. They then stated that the illumination time should be less than, or equal to the thermal relaxation time.

Such an argument has two significant flaws, which we first describe. For vessels with a diameter in excess of 50 μm, the thermal relaxation time is longer than 1 ms. If the illumination time is 1 ms or more, the conduction of heat during the illumination time cannot be ignored. Also, the temperature rise of the endothelial cells in the vessel walls is not shown. It is uncertain whether the temperature rise in these cells is sufficient to cause thermal damage, which is the aim of the laser treatment.

Calculation of the thermal relaxation time is a useful calculation though as it provides an estimate of the ideal illumination time. As Anderson and Parrish (1981b) argue,

> "if the incident energy is delivered within a period of time corresponding to retention of heat within the target structure, a maximum transient temperature differential between the target structure and its surroundings will be achieved, potentially damaging the target structures only".

As such, calculation of the thermal relaxation time is useful to us so we describe the steps in the calculation of the thermal relaxation time below. This description is from Anderson and Parrish (1981b).

Equation (5.1) when expressed in cylindrical coordinates is

$$\frac{\partial T(r,\vartheta,t)}{\partial t} = \frac{\Phi(r,\vartheta)}{\rho C_v} + \frac{\eta}{\rho C_v}\left[\frac{\partial^2 T(r,\vartheta,t)}{\partial r^2} + \frac{\partial T(r,\vartheta,t)}{r\partial r}\right] + \frac{\eta}{\rho C_v}\frac{\partial^2 T(r,\vartheta,t)}{r^2\partial\vartheta^2} \tag{5.4}$$

Here, r is the distance from the origin, which is the centre of the vessel. The angle ϑ indicates a point on the circle of radius r.

Anderson and Parrish (1981b) labelled the fraction $\frac{\eta}{\rho C_v}$ the "thermal diffusivity", and denoted it by α. From table 5.1, the value of the fraction is 1.8×10^{-3} cm^{2}s^{-1}. However, Anderson and Parrish (1981b) used a value of 1.3×10^{-3} cm^{2}s^{-1}, which was obtained from the results of Balasubramanium and Bowman (1976).

We desire to calculate the time taken for the vessel to cool to halfway between the peak temperature and that of its surroundings. Consequently, the source term, $\Phi(r,\vartheta)$, in equation (5.4) is zero. Further, we make the approximation that the temperature distribution within the vessel has rotational symmetry. Thus, the temperature distribution does not depend on ϑ, and so equation (5.4) reduces to

$$\frac{\partial T(r,t)}{\partial t} = \frac{\eta}{\rho C_v}\left[\frac{\partial^2 T(r,t)}{\partial r^2} + \frac{\partial T(r,t)}{r\partial r}\right] \tag{5.5}$$

The solution of equation (5.5) is given by

$$T_{(r,t)} = k_1\left[\frac{4}{16\pi\alpha t + \pi d^2}\exp\left(\frac{-4r^2}{16\alpha t + d^2}\right)\right] + T_0 \tag{5.6}$$

Here, k_1 is determined from the peak temperature within the vessel, and T_0 is the temperature of the region of interest before illumination with the laser beam. It is at the time $t = 0$ that the laser beam is turned off, and the vessel is allowed to cool. The diameter of the blood filled region inside the vessel is given by d.

In this solution, the temperature distribution in the tissue is assumed to have a Gaussian distribution. The term in the square brackets is normalised over two dimensional space, that is

$$1 = \int_{-\infty}^{\infty}\int_{-\infty}^{\infty}\frac{4}{16\pi\alpha t + \pi d^2}\exp\left(\frac{-4(x^2+y^2)}{16\alpha t + d^2}\right)dx\,dy \tag{5.7}$$

After a period of time equal to the thermal relaxation time, t_r, the temperature at the centre of the vessel will be halfway between the peak temperature and the surroundings. So

$$\frac{T_{(0,0)} - T_0}{2} = T_{(0,t_r)} - T_0 \tag{5.8}$$

After some manipulation of equation (5.8), we find that

$$t_r = \frac{d^2}{16\alpha} \tag{5.9}$$

Table 5.2. The thermal relaxation time for vessels of different diameters.

diameter (μm)	time (ms)
10	0.035
20	0.14
50	0.87
100	0.35
200	14

With this result, Anderson and Parrish (1981b) calculated the thermal relaxation time for vessels of different sizes. We have repeated these calculations using a value for α that has been derived from table 5.1. These results are listed in table 5.2.

In figure 5.2, we have plotted the temperature profile in the vessel at $t = 0$ and $t = t_r$. Vaporisation effects are avoided by stating that the peak temperature within the vessel is 100 °C. As expected, at the time $t = t_r$ the temperature at the centre of the vessel has fallen to 67.5 °C which is half way between 100 °C and 35 °C.

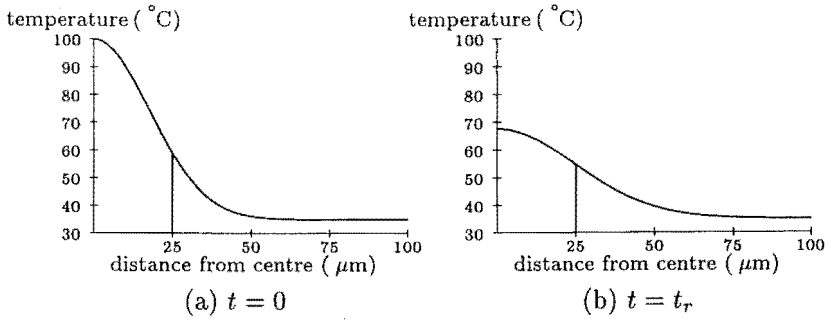

Figure 5.2. The temperature within and around the vessel when it cools after being illuminated by the laser beam, as determined by calculation of the thermal relaxation time . The diameter of this vessel is 50 μm. The vertical line indicates the boundary between the blood and the endothelial cells of the vessel wall.

For the vessel to be damaged, we require that the vessel wall is heated sufficiently to cause thermal necrosis. Heating the blood at the centre of the vessel to 100 °C does not necessarily damage the wall of the vessel. We take equation (5.6) and plot the temperature at the boundary between the blood and the vessel wall as a function of time in figure 5.3.

The temperature at the boundary between the vessel lumen and the endothelial cells of the vessel wall never exceeds 60 °C with this calculation. There is an insufficient temperature rise across the entire vessel wall for thermal damage to occur. The

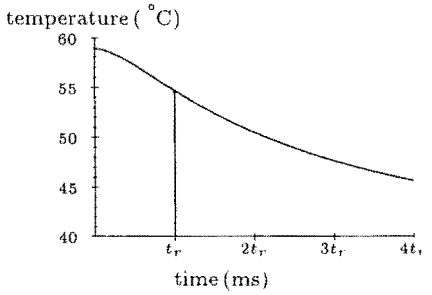

Figure 5.3. The temperature at the interface between the blood and the vessel wall when the 50 μm diameter vessel cools after being illuminated with the laser beam, as determined from the thermal relaxation time calculation. The vertical line indicates when $t = t_r$.

decay in the temperature is quite slow, falling by 4 °C (or less) in a time period equal to t_r. With this calculation, there is insufficient damage inflicted on the vessel wall. We desire a better calculation so that a more realistic answer is provided.

5.3 Numerical solution of the heat transfer equation

Several workers have solved the heat transfer equation with numerical methods, and applied the results to determining the appropriate illumination time. For example, see Lahaye and van Gemert (1985), and Pickering *et al* (1989a). In these works, the authors made the approximation that the tissue contained one blood vessel. The distribution of light within the vessel was calculated using the Kubelka-Munk theory, or Beer's law.

We improve on the methods of both workers in that we use the distribution of light within the vessels as from the Monte Carlo method. These results are more "believable" than those of other models, and have been presented in chapter 4 of this thesis.

We numerically solve the heat transfer equation, equation (5.1) over a time interval that is longer than the illumination time so we are able to examine both the heating and cooling processes. Thus, our solution is superior to the calculation of Anderson and Parrish (1981b) who did not include the effect of conduction during the illumination time. We examine the effect of the illumination time for 50 and 200 μm diameter vessels and when the wavelength is 577 and 585 nm. These results are presented with high quality graphics generated by Mathematica®.

From the results in chapter 4, we see that more light will be absorbed at the top of

the vessel lumen than at the bottom. This shows that two of the assumptions in the calculation of thermal relaxation time are wrong. The distribution of temperature within the vessel when the laser beam is turned off is a) not gaussian and b) does not have rotational invariance. The flow of heat in the skin will be as shown in figure 5.4. Heat flows from the top of the vessel lumen to the bottom, and from the vessel to the surrounding tissue.

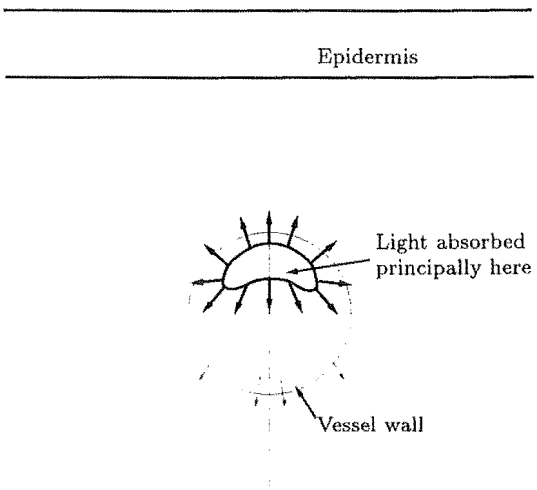

Figure 5.4. A representation of the flow of heat within the vessel, and from the vessel to the surrounding tissue.

Our numerical solution of equation (5.1) allows us to examine the evolution of temperature in the skin that is caused by the incident laser beam. It is not possible to show the temperature at every point in the skin over the time interval that the heat transfer equation is solved using a single graph. This would require a four dimensional structure, and cannot be displayed on paper. Three techniques are used to show the temperature distribution.

With the first two methods, we take a vertical line through the top and bottom of the vessel, which is shown in figure 5.4. In the first method, we show the temperature distribution along this line at the end of the illumination period. The second method is more complex in that we report the temperature distribution along this line over the time interval that the heat transfer equation is solved with contour maps and surface plots. These techniques show the temperature reached by the endothelial cells at the top and bottom of the vessel. For the third technique, we plot a contour map of the temperature within the skin at the end of the illumination period.

5.3.1 Calculation details

A SPARC STATION 10 was used to carry out the calculations. The numerical calculation uses grids of 230 × 230 or 280 × 280 points. The grid spacing, or distance between adjacent points on the grid is 3 μm. The larger grid is used when the vessel diameter is 200 μm. The vessel is positioned at the centre of this grid. The effect of heat conduction from neighbouring vessels and the epidermis is ignored. The time interval between successive calculations of temperature rise due to light absorption and temperature change due to conduction was 0.001 ms. Heat conduction was calculated at each grid point using a second order two dimensional method of finite differences (Carslaw and Jaeger, 1967). The new temperature due to conduction at each grid point (n, m) after each time interval is,

$$T_{n,m}^{\text{new}} = \frac{\eta}{\rho C_v} \frac{1}{(\text{grid spacing})^2} [T_{n+1,m}^{\text{old}} + T_{n,m+1}^{\text{old}} + T_{n-1,m}^{\text{old}} + T_{n,m-1}^{\text{old}} - 4T_{n,m}^{\text{old}}] \qquad (5.10)$$

Conduction of heat from the pixels at the edge of the grid is not calculated. The edges of the pixel array are then infinitely conducting, removing heat from the simulation as their temperature is fixed at T_0. This is an insignificant source of error as the grid has been set sufficiently large so that there is no conduction of heat from the vessel to the edge during the time intervals simulated.

The energy, E (J), deposited in each point of the grid during each time interval of the calculation when the laser beam is on is calculated using a formulae similar to that used by Miller and Veitch (1993). It is:

$$\text{E} = \frac{\text{duration of time interval} \times \text{photons absorbed in the grid element} \times \text{laser power}}{\text{number photons simulated}} \qquad (5.11)$$

The energy deposited in each voxel causes a temperature change δT, which is given by

$$\delta T = \frac{\text{E}}{C_v \rho \times \text{volume of voxel}} \qquad (5.12)$$

In this case, the volume of one voxel is $(3\ \mu\text{m})^3$.

We used the program that was written by Dr. J. Pickering in C(Pickering, 1990). This program was extended so that a larger grid was used. The section which reads the input data was modified so that the results from Monte Carlo calculations could be used. As part of the verification process, the code was altered so that a greater use of procedures was made. Finally, the program was altered so that all calculations were carried out in double precision arithmetic. Thus, all calculations in the program used 16 digit numbers.

Several different checks of the program were carried out. First, the operation of each subroutine in the program was checked with the aid of a debugger and the expected output was obtained. Second, the time interval used in the numerical solution was changed, and the effect was noted. Initially, the time interval was 0.001 ms. Reducing it to 0.0 001, or setting it to one ten thousandth of the time range the equation was solved over affected the temperatures calculated by, at most, half of a degree. Third, the precision of the floating point numbers was changed from sixteen to thirty two digits. This change was made to ensure that roundoff errors were not present. Again, the difference in the calculated temperatures was less than one degree. Fourth, the sum of the temperature change in every grid point at the end of the simulation was proportional to the fluence used. These checks give us confidence that the simulation program operates correctly.

5.4 Results

We show in this section how the choice of illumination time affects the distribution of temperature within the skin. Reducing the illumination time confines the energy deposited in the vessel to the vessel. Further, when the illumination time is decreased the necessary fluence to obtain the desired endpoint is less, which is consistent with clinical results in the literature.

Finally, we examine the effects of the wavelengths 577 and 585 nm for various vessel geometries. The results show that there is a case for using 585 nm with illumination times that are less than 4 ms.

The simulation of a particular illumination time was repeatedly run with various fluences, until the peak temperature in the central shallow capillary was 100 °C. In this way, the effect of vaporisation is ignored.

For the simulations used, we use the reference model of skin, or variations of this model. A description of the reference model is contained in chapter 2, with additional information in chapter 4. We examine the temperature distribution within the central shallow capillary, as the peak temperature within the skin is found in this vessel.

The vessel is at the centre of 3 mm diameter beam. With such a large beam, conduction of heat along the axis of the vessel can be ignored. The wavelength used is 577 nm, unless stated otherwise.

All of the graphs in this section were obtained from vessels at a depth of 200 μm. Compared with the deeper vessels, the light entering the vessel will have been scattered fewer times. We expect that difference in absorption between the top and the

bottom of the vessel will be higher with the shallow vessels.

5.4.1 Immediately after laser illumination

In this subsection, we report the temperature along the vertical line through the centre of the shallow capillary when the laser beam is turned off. The illumination times used are 0.4, 4, and 40 ms and the wavelength is 577 nm. These results are shown in figure 5.5.

The fluence and the power density used for each illumination time are listed in table 5.3. The fluence used in the clinic is listed for comparison. The fluences used by the simulation are lower than those used in the clinic and the explanation for this difference is provided in subsection 5.5.4.

Table 5.3. The clinical and simulation treatment parameters for the reference model of skin with the three different illumination times.

clinical fluence (J/cm^2)	simulation fluence (J/cm^2)	simulation power density (W/cm^2)	illumination time (ms)	figure no.
6.0	1.12	2800	0.4	5.6
12	2.48	620	4.0	5.7
22	11.3	283	40	5.8

When the illumination time was altered, it was necessary to adjust the fluence to keep the maximum temperature within the vessel at 100 °C. Suppose the fluence was kept at 2.48 J/cm^2, which was used in the 4.0 ms illumination case. Reducing the illumination time to less than 4.0 ms would cause the peak temperature in the blood to exceed 100 °C, and there would be boiling of the blood. Conversely, increasing the illumination time to more than 4.0 ms will reduce the peak temperature in the blood. The maximum temperature reached in the walls of the vessel will be reduced, and so the vessel wall may not be thermally damaged.

Several conclusions can be reached from the results in this section, which we give below.

1. The fluence required to bring the peak temperature in the blood to 100 °C is reduced by reducing the illumination time.

2. As the illumination time is increased, with a corresponding increase in the fluence, the temperature difference between the top and the bottom of the vessel decreases.

   Further, the peak temperature reached at the boundary of the vessel lumen and

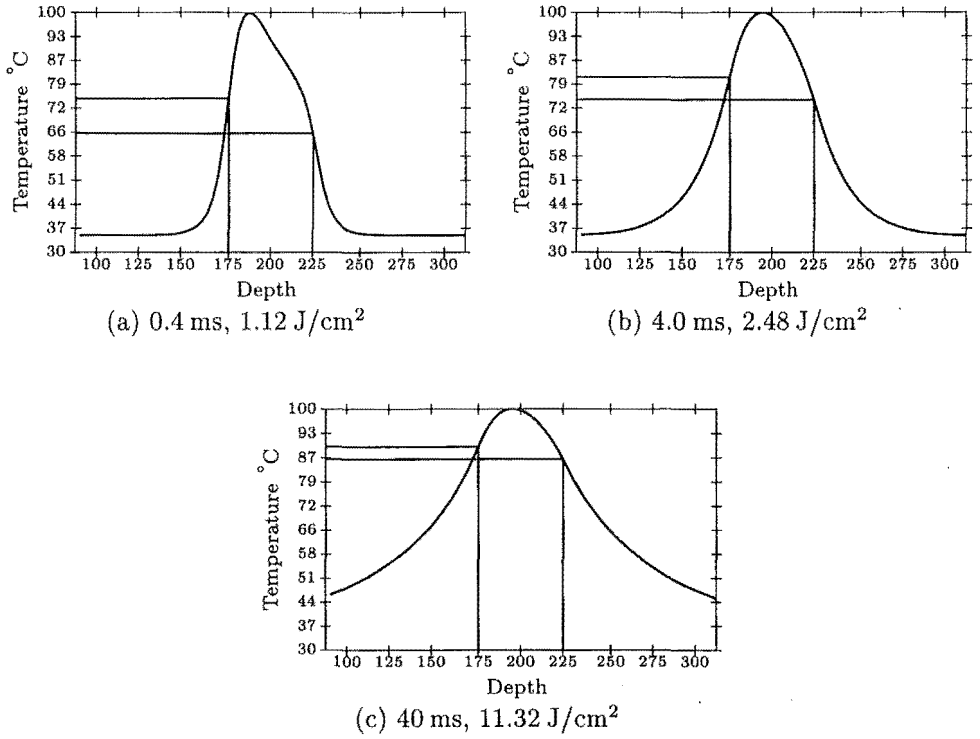

(a) 0.4 ms, 1.12 J/cm^2

(b) 4.0 ms, 2.48 J/cm^2

(c) 40 ms, 11.32 J/cm^2

Figure 5.5. The temperature distribution along the vertical line through the central shallow vessel immediately after the laser beam is turned off. The temperature reached by the vessel walls is marked by the lines drawn on the graph.

the vessel wall is increased.
Also, there is more heating of the surrounding tissue.

3. From our damage criteria, there is insufficient damage to the vessel wall when the illumination time is 0.4 ms.

4. When the illumination time is reduced, the power density (W/cm^2) on the skin surface must be increased to keep the peak temperature in the vessel at 100 °C. This can be achieved by reducing the laser spot size, or increasing the power output of the laser.

5. With a short illumination time (0.4 ms), the energy deposited in the blood has had insufficient time to spread throughout the vessel.

However, figures 5.5a, 5.5b, and 5.5c do not show what happens immediately after the illumination period. This is shown in the next subsection.

5.4.2 The evolution of temperature in the skin

In this subsection, we extend the results in the previous subsection (subsection 5.4.1). We report the evolution of temperature along the vertical line through the centre of the shallow capillary during and after the illumination time.

The temperature distribution along the vertical line through the centre of one vessel over a period of time is plotted as a contour map. An example of this is in figure 5.6a, where the illumination time is 0.4 ms. The central axis of the vessel is at a depth of 200 μm. This vessel has a diameter of 50 μm. Thus, the horizontal lines at a depth of 175 and 225 μm represent the top and bottom of the vessel.

During the first 0.4 ms, the vessel is illuminated by the laser beam. The temperature within the vessel rises, and heat is conducted to the surrounding tissue. After 0.4 ms, the laser beam is turned off, which is marked by the vertical black line. The part of the vessel at a depth of 182 μm has reached 100 °C. The vessel wall at the top of the vessel has reached 86 °C, but at the bottom it has reached 49 °C. After the laser has illuminated the skin, the vessels in the skin cool by the conduction of heat to the surrounding tissue.

To help visualise the data contained in the contour map, we have included surface plots of the the results contained in the contour map. The three black lines in the contour map are included in the surface plot and should be interpreted in the same manner.

More light is absorbed at the top of the vessel lumen than at the bottom, so the temperature reached at the top of the vessel lumen will be higher that at the bottom. This difference in temperature is reduced by the conduction of heat from the top of the vessel lumen to the bottom. However, when the illumination time is 0.4 ms, as shown in figure 5.6, there is minimal conduction of heat within the vessel. This accounts for the significant difference in temperature between the top of the vessel and the bottom. The cells at the bottom of the vessel will not undergo the desired damage. Further, there is minimal heating of the surrounding dermal tissue, and so this tissue will not be damaged.

The results for when the illumination time is 4 ms are shown in figure 5.7. The illumination time has been long enough to allow the heat generated at the top of the vessel lumen to be conducted to the bottom of the vessel lumen. The endothelial cells at the top and the bottom of the vessel reach a temperature greater than 70 °C. We conclude that irreversible tissue damage to the vessel wall does occur. More of the surrounding tissue is heated than when the illumination time is 0.4 ms, but the extent is acceptable.

The results for an illumination time of 40 ms in figure 5.8 show that there has been conduction of heat from the top of the vessel to the bottom. The vessel wall at the top and bottom has been thermally necrosed. There is significant conduction of heat from the vessel to the surrounding non–vascular tissue. With even longer illumination times, heating of the surrounding tissue will be more widespread.

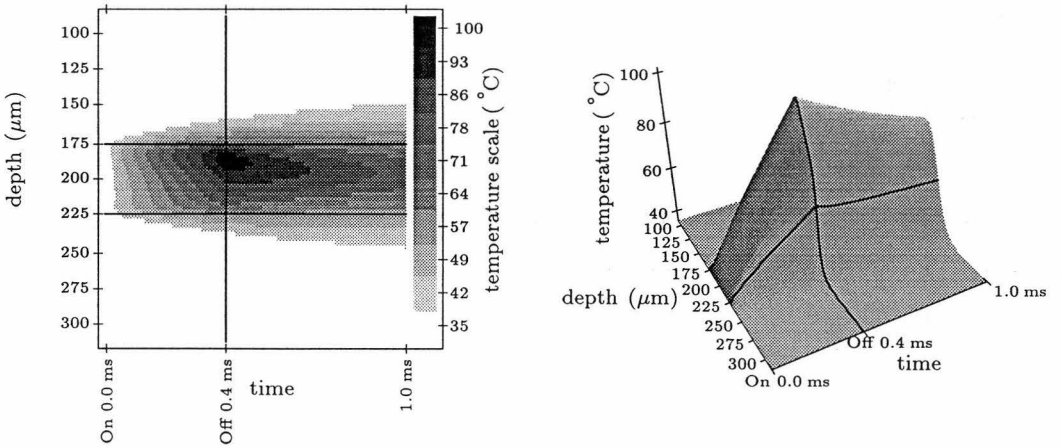

(a) Contour map of the temperature distribution.

(b) Surface plot of the temperature distribution

Figure 5.6. The temperature distribution along the line from the top of the vessel to the bottom. The vessel is heated for 0.4 ms. The flow of heat in the vessel is simulated for a further 0.6 ms.

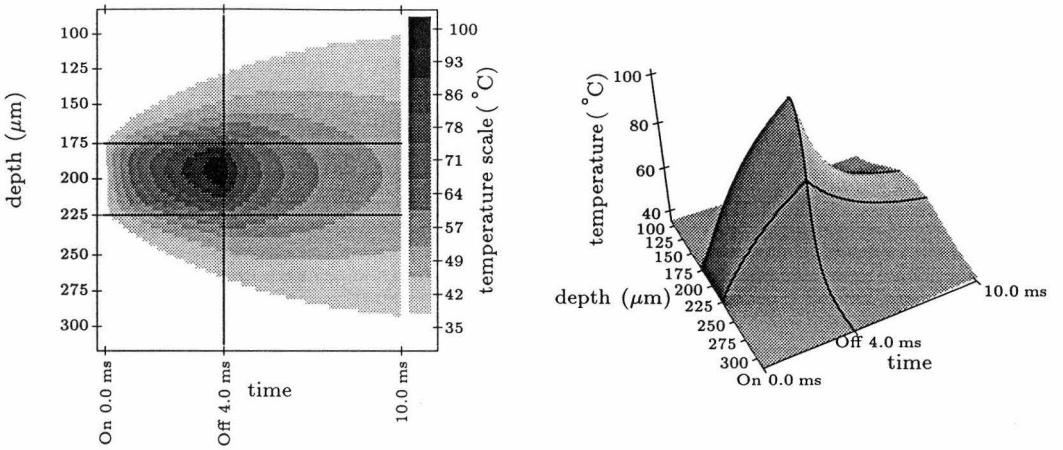

(a) Contour map of the temperature distribution.

(b) Surface plot of the temperature distribution

Figure 5.7. The temperature distribution along the line from the top of the vessel to the bottom. The vessel is heated for 4 ms. The flow of heat in the vessel is simulated for a further 6 ms.

5.4.3 Comparison of the wavelengths 577 and 585 nm

The literature shows that some workers are now advocating the use of 585 nm, see for example Tan *et al* (1990a). These workers are using pulsed dye lasers, with illumination times of 0.45 ms or less. In chapter 4 we stated that the important difference between the two wavelengths is that there is a more uniform absorption pattern within the vessel when the wavelength is 585 nm. In this subsection, we use the numerical solution of the heat transport equation to show the effect of the more uniform absorption pattern.

We use the results of the Monte Carlo simulation from four models of skin with the wavelengths 577 and 585 nm. The illumination times 0.4 and 4.0 ms are used, as the results in the previous subsection show that the 40 ms illumination time causes widespread heating of the dermis.

The four models of skin are

1. The reference model, where all the vessels are 50 μm in diameter. There are layers of vessels at depths of 200, 350, 500, 650, 800, and 950 μm. The distance between the center of the vessels in each layer is 150 μm.

2. A paler port-wine stain is envisaged, where the distance between the centres of the vessels in each layer is 300 μm.

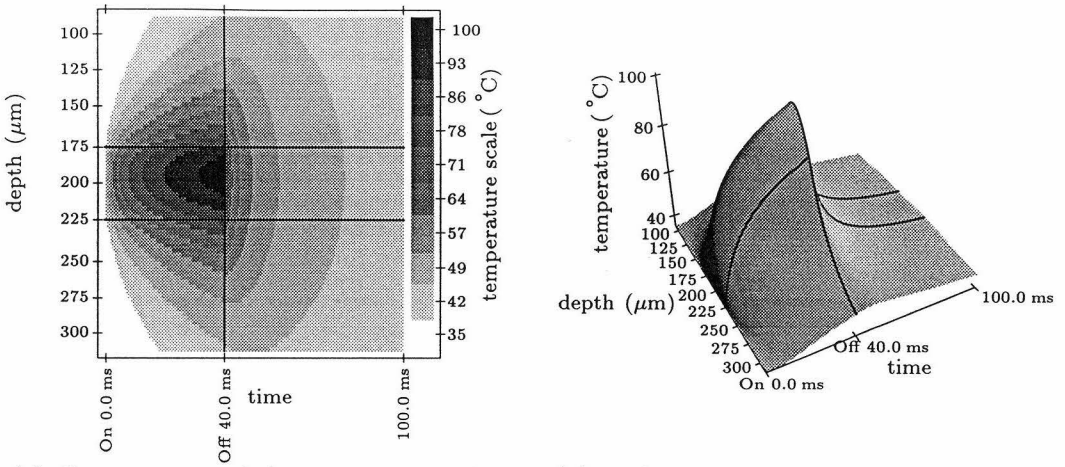

(a) Contour map of the temperature distribution.

(b) Surface plot of the temperature distribution

Figure 5.8. The temperature distribution along the line from the top of the vessel to the bottom. The vessel is heated for 40 ms. The flow of heat in the vessel is simulated for a further 60 ms.

3. This port-wine stain has received several treatments, so the shallow vessels have been thermally damaged and are no longer present. Thus, the layers of vessels at a depth of 200 and 350 μm has been removed.

4. A port-wine stain that contains vessels with a large diameter, 200 μm, is simulated. The separation between the layers and the separation between the vessels in a layer is doubled. With these changes, this model of skin contains four times as much blood as the reference model.

In figure 5.9, we show the effect on the temperature distribution within the vessel when the wavelength is changed from 577 to 585 nm with the reference model. There is slightly more heating at the bottom of the vessel lumen, but the temperature change is less than 10 °C. When the illumination time is in the optimal range of 1-10 ms, there is sufficient heating of the top and bottom of the vessel walls to cause the required thermal damage.

The results from the reference model are essentially the same as those for the pale port-wine stain and the port-wine stain that has had several treatments. When the vessel diameter is 200 μm, changing the wavelength significantly affects the results obtained. In figure 5.10 we show the differences between the two wavelengths for a 200 μm diameter vessel.

The results in figures 5.9 and 5.10 do not show the temperature at the side of the vessel. We show these differences in figures 5.11 and 5.12, where we use a contour

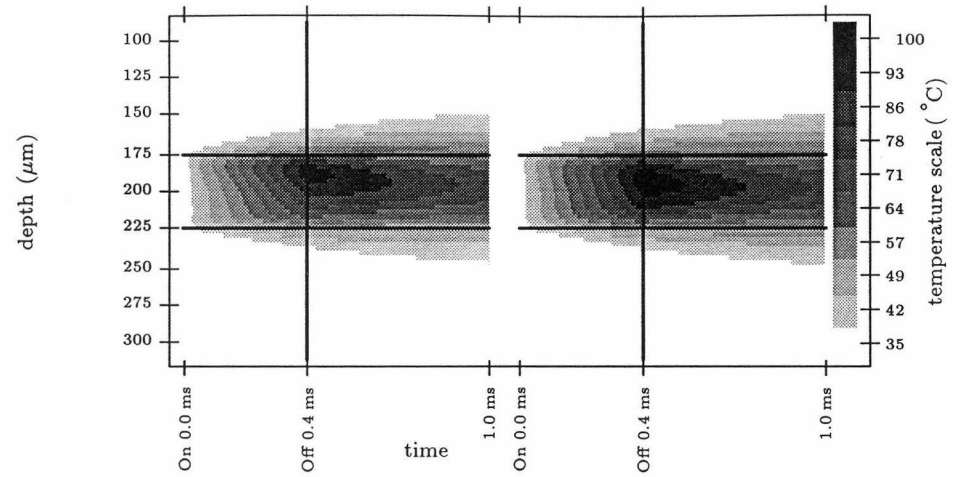

(a) 0.4 ms illumination time

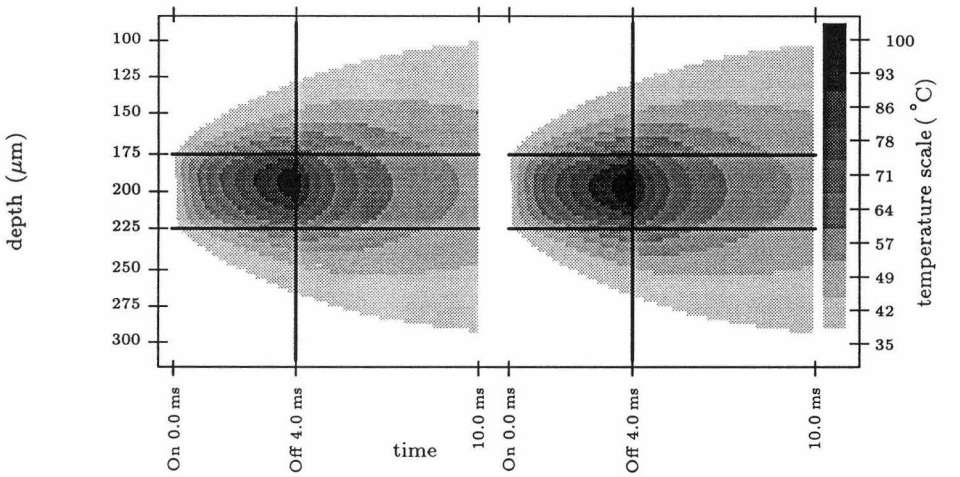

(b) 4 ms illumination time

Figure 5.9. The reference model of skin is used, with the results for the wavelengths 577 nm (left) and 585 nm (right).

Table 5.4. The treatment parameters for two models of skin, the untreated reference model and the skin model with large vessels.

skin model	fluence (J/cm^2) (577 nm)	(585 nm)	illumination time (ms)	figure no.
reference model	1.12	1.48	0.4	5.9a
"	2.48	3.56	4.0	5.9b
large vessels	6.12	9.04	0.4	5.10a
"	10.4	13.6	4.0	5.10b

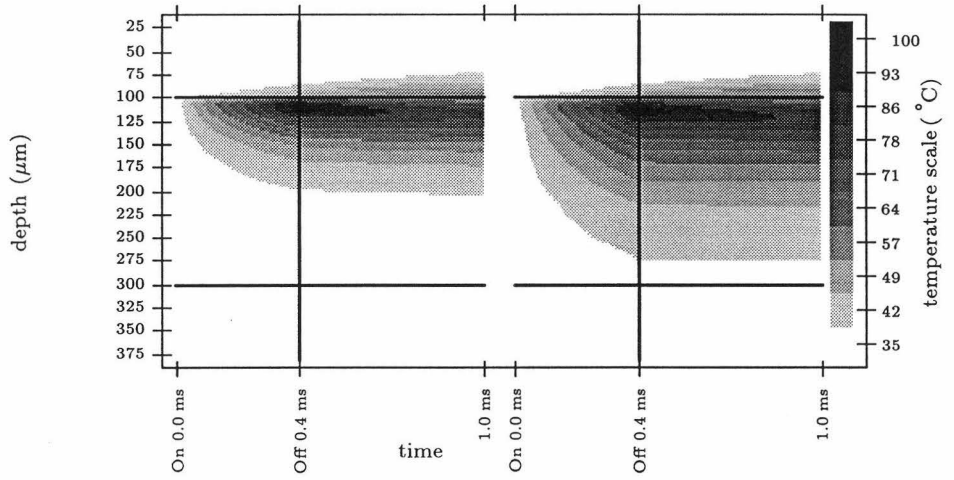

(a) 0.4 ms illumination time

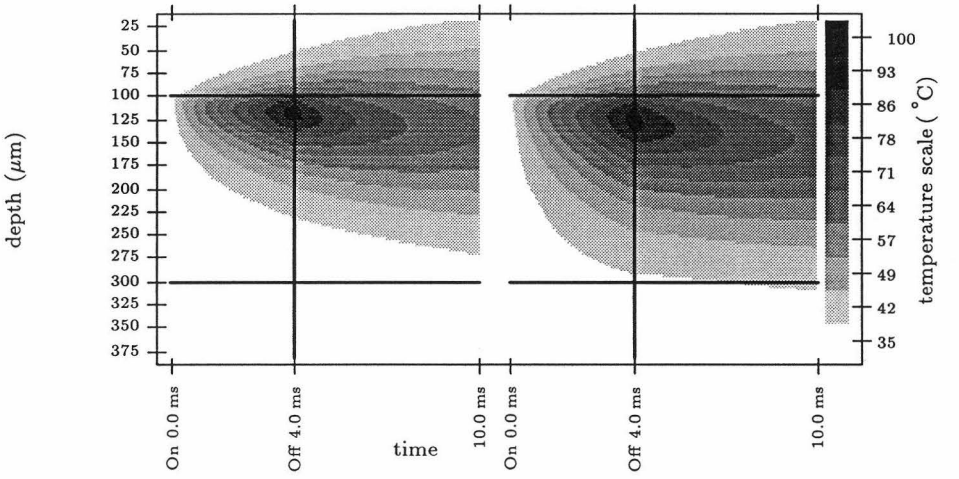

(b) 4 ms illumination time

Figure 5.10. A port-wine stain with large vessels (200 μm diameter) is simulated. Again, the results for the wavelengths 577 and 585 nm are on the left and right sides respectively.

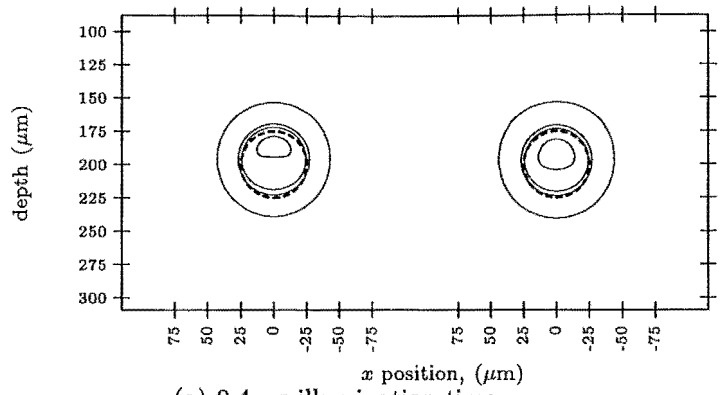

(a) 0.4 ms illumination time

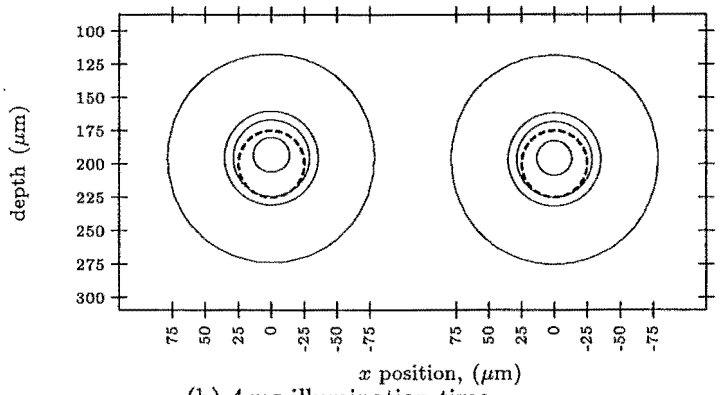

(b) 4 ms illumination time

Figure 5.11. The reference model of skin is used, with the results for the wavelengths 577 nm (left) and 585 nm (right). The contour lines indicate the temperatures 37, 60, 70, and 95 °C. The dashed line marks the interface between the blood and the vessel wall.

map to plot the maximum temperature reached in the region of the vessel when the laser beam is turned off.

From these graphs and the table, we can see several differences in the temperature profiles for the two wavelengths. These differences are described below.

Fluence required

Less light is absorbed in the shallowmost vessel with 585 nm. To cause the vessel to reach the same peak temperature as with 577 nm, the fluence used needs to be increased by 15 to 30%. This is not advantageous, as increasing the amount of energy deposited on the skin increases the absorption in the epidermis.

Temperature distribution

With 585 nm, the position within the vessel at which the peak temperature is reached

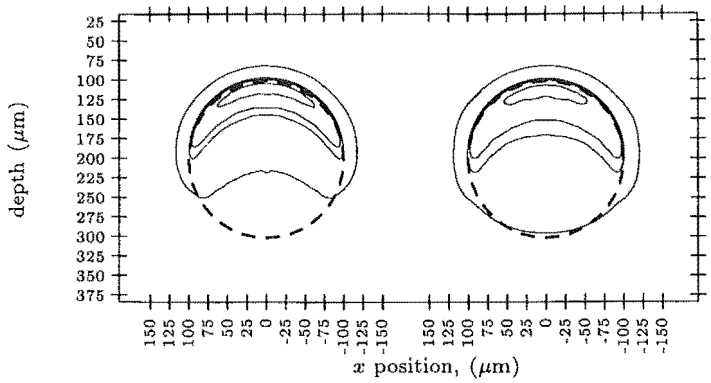

(a) 0.4 ms illumination time

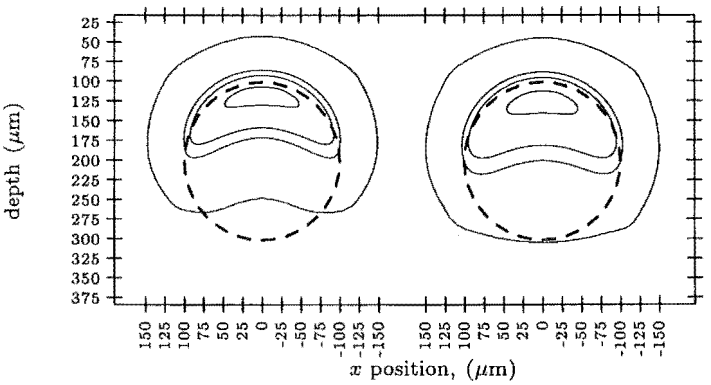

(b) 4 ms illumination time

Figure 5.12. A port-wine stain with large vessels (200 μm diameter) is simulated. The interpretation of this graph is the same as in figure 5.11.

is lower, closer to the centre of the vessel.

Temperature rise in the endothelial cells at the bottom of the vessel

Changing the wavelength from 577 to 585 nm has increased the size of the temperature rise in the endothelial cells at the bottom of the vessel. When the illumination time is 0.4 ms, this may be important. For illumination times in the ideal range or longer, this effect is not significant.

Increasing the diameter of the vessel from 50 to 200 μm has reduced the temperature rise at the bottom of the vessel for both wavelengths.

If the fluences used for the wavelengths 577 and 585 nm are identical, as is the case in the clinic, then with illumination times of 0.4 ms, 577 nm is the superior wavelength as there is more heating at the bottom of the vessel.

5.5 Discussion

In this section, we explain the effect of the illumination time on the conduction of heat within the blood vessel. We use the results from clinical and theoretical work to show that absorption in the epidermis is reduced when the illumination time is reduced.

We suggest reasons as to why the fluences that the simulation used are much lower than those used in the clinic.

Finally, we compare our results with those in the literature.

5.5.1 Short, ideal and long illumination times

The haemoglobin in the red blood cells is the principal absorber of yellow light in the blood. During laser treatment, the haemoglobin will absorb the light and be heated. This heat is conducted from the haemoglobin to the surrounding plasma, to the walls of the vessel, and then to the surrounding tissue. From this process we define three different illumination times. They are: short, optimal, and long.

The volume of the haemoglobin is a tiny fraction of the volume of the vessel lumen, which limits the amount of heat that can be conducted away from the haemoglobin. Further, when extremely short exposure times are used, say 0.001 ms, there is minimal time available for the conduction of heat from the haemoglobin to the surrounding plasma. With extremely short exposure times, essentially it is the haemoglobin which is heated. The temperature rise in the haemoglobin is large enough to generate steam, which ruptures the red blood cells and then the enclosing vessel. There has been no heating of the endothelial cells of the vessel wall, so these cells will not be thermally

damaged. We expect then that there will be no long term colour change after treating port-wine stains with an illumination time of 0.001 ms, which Hulsbergen-Henning *et al* (1984) verified.

With illumination times of 0.4 ms, the temperature rise in the haemoglobin in the red blood cells is low enough that steam is not generated. Consequently, the red blood cells are not ruptured. However, our theoretical results show that the temperature rise in the endothelial cells at the bottom of the vessel is insufficient to cause thermal damage. Our theoretical results in fig 5.6 show that an illumination time of 0.4 ms is too short when used to treat a vessel with a diameter of 50 μm. Sufficient heat has been conducted from the haemoglobin to thermally damage the endothelial cells at the top of the vessel, but those at the bottom remain undamaged.

With 200 μm diameter vessels, the temperature rise at the bottom of the vessel is negligible. This is true for the wavelengths 577 and 585 nm. To heat the endothelial cells at the bottom of the vessel, the exposure time needs to be longer so that there is conduction of heat from the top of the vessel lumen to the bottom.

With optimal illumination times there is sufficient time for the heat generated in the haemoglobin to be conducted to, and thermally damage, the entire wall of the vessel. In fig 5.7 we see the effect of a 4 ms illumination time, which is optimal for this 50 μm diameter vessel. The endothelial cells at the top and the bottom of this vessel reach a temperature that is high enough to ensure thermal necrosis occurs.

When long illumination times are used, the vessel walls are heated by thermal conduction from the haemoglobin and will be thermally damaged. Unfortunately, too much heat is conducted from the vessel wall to the surrounding tissue, and this tissue is thermally damaged. This process is shown in fig 5.8, where the use of 40 ms exposure time has resulted in the thermal damage of tissue adjacent to vessel. We expect the clinical findings of Neumann *et al* (1992), who reported a cuff of damaged collagen around the illuminated vessels when the exposure time was 50 ms. For even longer illumination times, such as 300 ms, there will be more heating of the non-vascular tissue. Damage to the non vascular tissue is not the goal of treatment and increases the risk of undesired changes in the appearance of the skin (Adams *et al*, 1987).

5.5.2 The effect of wavelength for sub millisecond illumination times

In this subsection, we give possible reasons why the 585 nm wavelength is claimed to be superior to 577 nm when the pulsed dye laser is used to treat port-wine stains.

When a pulsed dye laser is used to treat port-wine stains, the illumination times are 0.45 ms or shorter. From the numerical results in this chapter we see that with such short illumination times there is minimal thermal averaging. That is, the flow of heat from the top to the bottom of an ectatic capillary is too slow for all of the capillary to be sufficiently heated during laser treatment with illumination times of 0.45 ms and a wavelength of 577 nm. Changing the wavelength to 585 nm, or using a longer illumination time, are alternative means of ensuring that there is sufficient heating of all of the endothelial cells in the vessel wall.

The clinical work of Tan *et al* (1990a) with a pulsed dye laser supports this argument. It was noted that a larger number of capillaries were damaged completely with the 585 nm wavelength than with 577 nm. These capillaries showed "endothelial cell injury, and perivascular collagen denaturation around the *whole* blood vessel".

Indeed, this conclusion that the use of the 585 nm wavelength rather than 577 nm will result in a more uniform temperature distribution can be obtained from results in the literature. From histological studies, such as those carried out by Walker *et al* (1989) with 578 nm wavelength light, there are vessels in the skin that are damaged on the top surface only. As the wavelength 585 nm is less strongly absorbed in the blood as 578 nm, more 585 nm light will reach the bottom of the vessel. We expect then that the temperature distribution in the vessel to be more uniform with the 585 nm wavelength.

5.5.3 Epidermal absorption

One side effect of using exposure times longer than optimal is that the energy absorbed in the epidermis is greater than it need be. We explain why in this subsection.

We showed before that a long exposure time results in widespread heating of the non vascular tissue. The energy required to heat the non vascular tissue has passed through the epidermis. The results from the Monte Carlo simulation in chapter 4 show that when there is an increase in the energy that passes through the epidermis, more energy is absorbed in the epidermis. Thus, increasing the exposure time, with a corresponding increase in the fluence, increases the absorption in the epidermis.

This provides a further reason why long exposure times must be avoided. The use

of such times will result in unnecessary, and unwanted, heating and thermal damage in the epidermis.

5.5.4 The fluence used in the simulation

In tables 5.3 and 5.4, we see that the fluence used by the simulation is much lower than the typical fluence used in the clinic. We explain why this difference arises in this subsection.

The fluences used in the simulation follow the same trend as those used in the clinic: short illumination times correspond to a low fluence.

However, the clinical and simulated fluences are different. A thorough search for mistakes in the computer code that simulates the conduction of heat was carried out. An order of magnitude estimate of the results, which we describe here, shows that the code which describes conduction gives the correct fluence from the Monte Carlo results.

The Monte Carlo calculation shows that 75% of the 577 nm wavelength light that is incident on the skin above the central section of the shallow vessel is absorbed in the central section of the shallow vessel. For the 0.4 ms illumination case, there is minimal heating of the non vascular tissue. When the fluence is 1.12 J/cm^2, the average temperature change in the central section of the central vessel is (using the parameters from table 5.1) 63 °C. If the incident fluence is 7.5 J/cm^2, which is typical when these illumination times are used, the average temperature change in the central shallow vessel will be 420 °C. If this temperature change was obtained in the clinic, there would be rupture of the vessels due to the generation of steam. Clinical experience shows that the vessels are not ruptured, which indicates that the temperature rise is much less. Presumably, vaporisation of the blood occurs at 100 °C, so the maximum temperature change is 65 °C.

We conclude that the results of the Monte Carlo calculation are in error. In chapter 6 we examine the possible reasons why the absorption of light in the shallow vessels is much higher than expected.

5.5.5 Comparison with other workers

In this subsection, we compare our results with those from other workers who have numerically solved the heat transfer equation.

Lahaye and van Gemert (1985) used a one dimensional form of this equation, and showed that the illumination time should be several milliseconds when the wavelength

is 577 nm.

Pickering *et al* (1989b) used Beer's law to calculate the distribution of absorbed light within the skin. The vessel has a diameter of 50 μm, at a depth of 415 μm. They showed that with 577 nm an illumination time of 5.5 ms results in the 6 μm thick endothelial cell at the top of the vessel reaching a temperature of 70 $^{\circ}$C. Our results are similar, as we see in figure 5.5a that an illumination time of 4 ms will cause the same temperature change.

In contrast to Pickering *et al* (1989b), we predict a much lower fluence on the skin surface is necessary to cause the required temperature change. We predict a fluence of 1.1 J/cm^2, whereas they predicted a fluence between 6.3 and 8.8 J/cm^2. This variation arises from the uncertainty in the absorption in the epidermis and dermis. The differences between Pickering *et al* (1989b) and our results result from several factors which we list below.

1. In the work of Pickering *et al* (1989b), it was assumed that 30-50% of the incident beam was attenuated before reaching the vessel.

2. Use of Beer's law ignores the scattering of light from the side and below the vessel. This scattering may double or triple the absorption in the vessel.

3. The absorption coefficient used by Pickering *et al* (1989b) was 43.0 mm^{-1}, and is less than the value we used, 47.0 mm^{-1}. Thus, even more light will be absorbed in the vessel with our simulation, lowering the necessary fluence.

4. Our vessel was closer to the surface than the vessel simulated by Pickering *et al.*, so a larger fraction of the incident beam is absorbed in the vessel in our simulation.

Our results are consistent with the theoretical results of other workers. They predict that there will be insufficient damage to the vessels in the skin when the exposure time is 0.4 ms.

From a clinical trial, Tan *et al* (1989) reports that an average of 6-7 treatments are necessary to remove a port-wine stain when the illumination time is 0.36 ms and the wavelength is 577 nm. This finding implies that there is sufficient thermal damage to the endothelial cells of the vessels in the skin with illumination times of 0.45 ms.

It is possible that our damage criteria is too strict, and damage to most of the vessel wall is sufficient. In this case, we expect that use of 0.45 ms illumination times will result in sufficient thermal damage to the vessel. However, on the basis of our

modelling we would not expect a large vessel (200 μm diameter) to undergo sufficient thermal damage with illumination times of 0.45 ms.

Clinical results in the literature verifies this.

Fitzpatrick *et al* (1994) reports on the use of a flashlamp pumped dye laser (0.45 ms, 585 nm) to treat port-wine stains. They stated, "The purple lesions with a deep dermal component often respond poorly because many vessels are too deep in the dermis and too large for this laser to eradicate."

Waner *et al* (1993) used the pulsed dye laser (0.45 ms, 585 nm) and the copper vapour laser (578 nm, 200 ms) to treat telangiectasia, a condition with a similar nature to port-wine stains. They reported that "a patient with large vessels (approximately 0.5 to 1.0 mm) on the dorsum, tip, and alae of his nose, experienced a greater degree of clearance with the copper vapour laser."

5.6 Conclusion

Our theoretical results support the use of illumination times in the range of 1-10 ms. With illumination times in this range, all of the endothelial cells in vessel wall are thermally damaged.

Illumination times of 0.4 ms result in damage to the endothelial cells at the top of the blood vessel. There is minimal thermal damage to the cells at the bottom of the vessel. There is more damage to the cells at the bottom of the vessel with this illumination time if the wavelength is changed from 577 to 585 nm.

With both wavelengths, the bottom half of vessels that have a diameter of 200 μm is not damaged when the illumination time is 0.4 ms. The temperature rise at the bottom of the vessel which is due to conduction and absorption is too low. For the endothelial cells at the bottom of the vessel to be damaged, the illumination time needs to be more than 4 ms. This finding explains why the pulsed dye laser is ineffective with such large vessels.

If the illumination time is longer than 10 ms, there is damage to the tissue surrounding the vessel. Too much energy is deposited in the epidermis, resulting in excessive damage. The chance of an untoward result is increased.

Chapter 6

Modification of the optical parameters

When the optimal illumination time was calculated in chapter 5 with the results from the Monte Carlo technique, it was shown that the absorption in the blood vessels is much higher than that obtained in the clinic. In this chapter we suggest several reasons for this discrepancy.

Results in an earlier chapter show that human epidermis is about 1 mm thick. Our model represents the epidermis by a much thinner layer. We examine the effect of this approximation.

It is possible that the optical parameters used in the simulation are not correct, a conclusion supported by the literature. We report the results obtained after the use of modified optical parameters.

Exhaustive checks of the computer program which implements the Monte Carlo technique did not reveal any errors. As we stated in subsection 4.3.1, the results from the program are consistent with those estimated from physical principles.

One further check, which is described for the benefit of the reader, is to ensure that the simulation does not create, or lose, particles in the simulation. In a simple check, we see what happens to the fraction of the beam incident on a 150×3 μm region at the centre of a 3 mm diameter beam, 2D scattering model. Epidermal absorption and remission from the skin accounts for 23% and 25% respectively. In the vessels at depths of 200, 350 and 500 μm, 25%, 11%, and 5% respectively of the beam is

absorbed. In total, 89%, which is close to the expected 100%. The remaining 11% will have been absorbed in the surrounding dermis and the deeper vessels. This result shows that the simulation is not creating particles and then reporting an absorption in the vessels that is a factor of five too high.

We are confident that the simulation functions as it was designed to, and that there is no error in the code. There are several possible reasons why our simulation determines a fluence that is quite different from that used in the clinic. It is possible that several of the approximations that we made when the Monte Carlo technique was implemented are wrong, for example that the skin has a uniform refractive index. Further, the description of the epidermis is inadequate, which we explain in section 6.1. Results in the literature suggest that measurement errors have effected the calculation of the optical parameters. We test several different variants of the optical parameters, and report the results in section 6.2.

Finally, in section 6.3 we combine the results presented in this chapter in a short summary.

6.1 Representation of the epidermis

In section 2.3, we stated that the thickness of the epidermis in our model is 65 μm. This thin layer represents the melanin containing components of the epidermis. The remaining layers of the epidermis, stratum corneum, stratum lucidum, and stratum granulosum are ignored. These layers will scatter the incident laser light. There will be some broadening of the laser beam, but this should not be significant when the spot diameter is 3 mm or more.

It is possible that these shallow layers backscatter some of the incident light out of the skin. To reduce the amount of light that reaches the shallow vessels so the calculated maximum temperature is 100 °C, over 80% of the incident light will be backscattered out of the skin.

From the results of the Monte Carlo simulation, 23% of the incident beam is absorbed in the epidermis. Using the tissue constants in table 5.1, the average temperature rise in the 65 μm thick layer will be 75 °C when the incident fluence is 7.5 J/cm^2. As the initial temperature of the skin is 35 °C, this will result in the vaporisation of this layer.

In a clinical trial, Shakespeare *et al* (1991) measured the temperature rise on the surface of the skin following treatment with a pulsed dye laser with a thermographic camera. After treatment with a fluence of 7.5 J/cm^2, the temperature at the surface

of the skin rose by 10 °C. This is much lower than the predicted rise. It may be partially explained by the cooling of skin by heat conduction to the air. A more feasible explanation is that the heat generated in the 65 μm thick layer dissipates throughout the epidermis. Indeed, if the thickness of the model epidermis is 1 mm, then the average temperature change of this layer will be 5 °C.

6.2 Modification of the optical parameters

In chapter 2 we briefly described the results of Torres *et al* (1994), who have cast doubt on the reliability of the optical parameters. They state

> spectrophotometric or other techniques that use broad light beams with integrating spheres may overestimate the absorption coefficient that leads to significant overestimation of predicted tissue temperature rises during laser irradiation.

It is therefore possible that the absorption parameters used in chapter 4 for the epidermis and blood are too high. In this section, we explore this possibility.

We assume that as the temperature of the blood increases, the haemoglobin continues to absorb the incident light. This may not be the case. The incident light may place the haemoglobin in an excited state, in which it does not absorb any of the incident light. Such a mechanism would allow the haemoglobin at the bottom of the vessel lumen to absorb more of the incident light, as it would no longer be shadowed by the overlying blood.

The concentration of red blood cells, and consequently the haemoglobin, may be lower in the vessels than in the arteries or veins. This would seem unlikely, as it is the red blood cells which are used to transport oxygen to the tissue. Reducing the concentration of these would affect the transport of oxygen.

Reducing the oxygen level will lower the absorption of yellow laser light in the haemoglobin. It has not been shown how the optical properties of blood change as the level of oxygen in the haemoglobin alters. Thus, we reduce the absorption coefficient of haemoglobin by a factor of three, and report the results.

The work of Torres *et al* (1994) shows that when spectrophotometric techniques are used to measure the optical properties of tissue, the calculated absorption coefficient may be too high. We therefore reduce the absorption coefficient of all three skin components by a factor of three and report the results.

We are interested to know what the effect of the scattering coefficient is. Two additional models are created, where the scattering coefficients for all three skin components are either doubled or divided by two.

Suppose a 1D optical propagation model was used when deriving the optical parameters. In this case, it will be necessary to use a 1D optical propagation model when these optical parameters are used to determine the distribution of absorbed light in the skin.

In the simulations reported in this section, a 3 mm beam diameter is used with a 2D or 1D scattering model. Our five variations on the reference model of skin are as follows:

1. The absorption coefficient (μ_a) for the haemoglobin is reduced by a factor of three. This change mimics the effect of reducing the amount of oxygen contained in the haemoglobin.

2. The absorption coefficients of the epidermis, dermis, and dermis are all reduced by a factor of three. This change was made on the basis of the experimental work of Torres *et al* (1994).

3. The scattering coefficients (μ_s) of the epidermis, dermis, and blood are all reduced by a factor of two.

4. The scattering coefficients of the epidermis, dermis, and blood are all increased by a factor of two.

5. The scattering coefficients of the epidermis, dermis, and blood are all set to zero. The scattering model is changed to 1D, as the optical parameters may have been derived from a 1D scattering model.

Surface plots of the absorption in the skin for the five different sets of parameters are reported in figures 6.1, 6.2, 6.3, 6.4, and 6.5.

Reducing the absorption coefficient for blood, or for all three skin components does reduce the absorption in the vessels, but by no more than 30%. This is unsurprising, as the light which enters the skin will scatter around until it is absorbed or manages to "escape". There will be more scattering events, so more light will leave the illuminated area.

Reducing the absorption coefficient for blood has reduced the difference in absorption between the top and bottom of the vessel. We show this effect in figure 6.6, where the absorption in all three skin components is reduced to one third of its

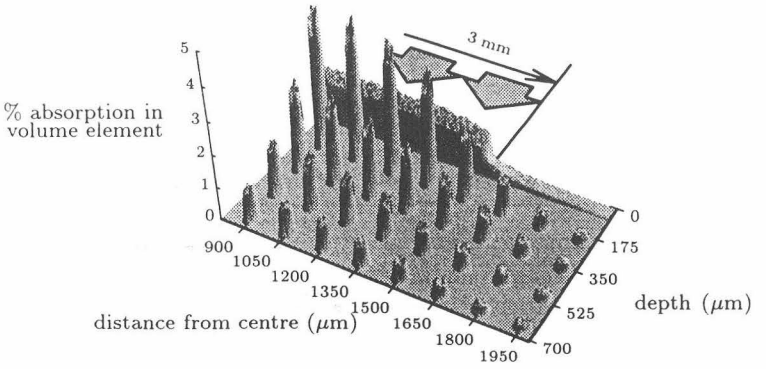

Figure 6.1. The absorption coefficients of the blood is reduced to one third of the original value.

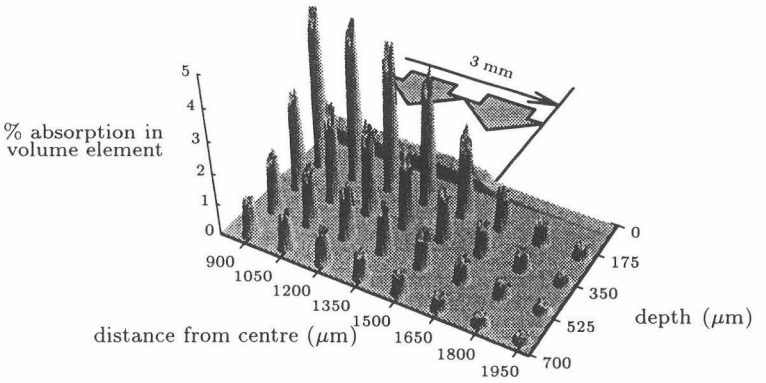

Figure 6.2. The absorption coefficients of all three skin components are reduced to one third of their original value.

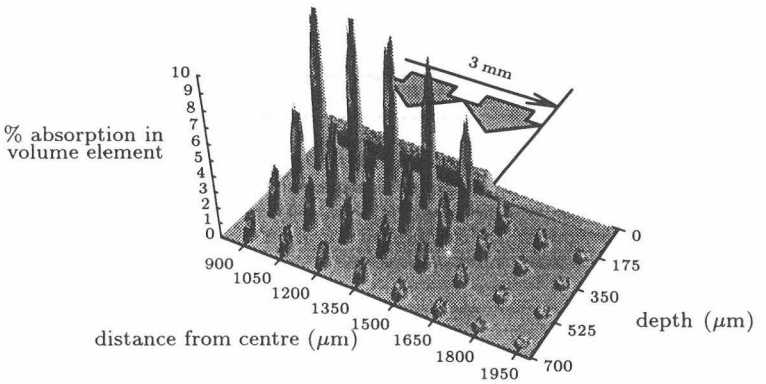

Figure 6.3. The scattering coefficients of all three skin components are reduced to half of their original value.

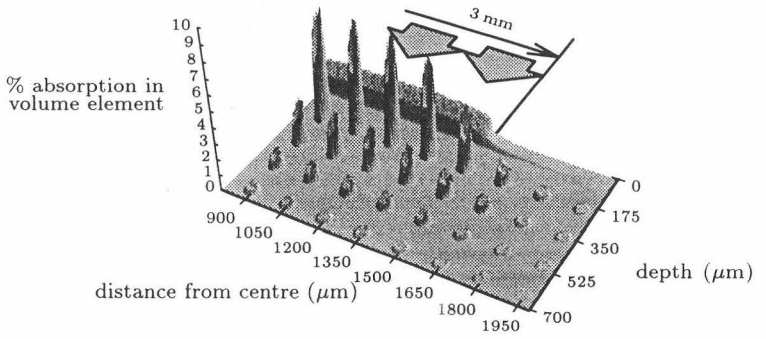

Figure 6.4. The scattering coefficients of all three skin components are doubled.

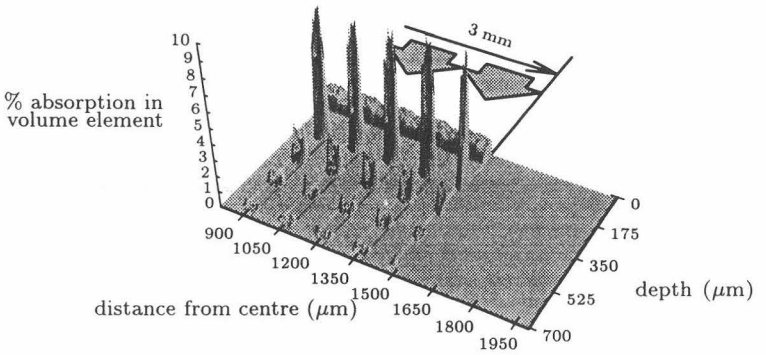

Figure 6.5. 1D optical propogation, no scattering.

original value. Included in this figure there is an contour plot of the evolution of temperature in the vessel following the use of a 0.4 ms illumination time. The peak temperature reached within the vessel is at the centre. There is minimal heating of the endothelial cells of the vessel wall. However, the calculated fluence is one quarter of the fluence that is typically used in the clinic.

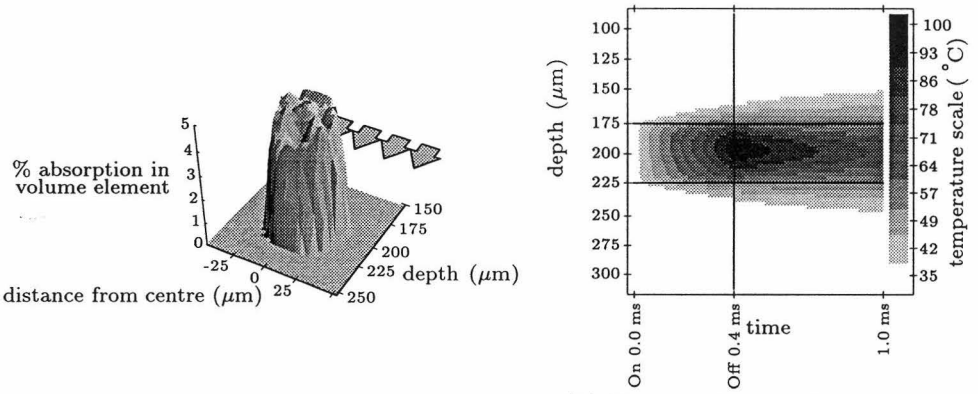

(a) Absorption in the central shallow vessel

(b) Temperature evolution in central shallow vessel. 0.4 ms, 1.53 J/cm^2

Figure 6.6. When the absorption coefficients of all three skin components are reduced to one third of their original value, figure (a) shows that the absorption in the central shallow vessel is almost uniform. We show the resultant evolution of temperature in the vessel if the illumination time is 0.4 ms in figure (b).

When the scattering coefficients of the skin components are halved, the absorption in the central shallow vessel is increased by 12%. Doubling the scattering coefficients reduces the absorption in the central shallow vessel by 10%. For both changes to the scattering parameters, there is a significant difference in absorption between the top and bottom of the vessel. The effect of 0.4 ms illumination times can be predicted from earlier work. An illumination time that is longer than 0.4 ms is necessary so there will be sufficient heating of the endothelial cells at the bottom of the vessel.

We note from a comparison of figures 6.4 and 6.3 that the absorption in all the vessels is higher when the scattering coefficients of the skin components is reduced by a factor of two. This reduces the average distance the particles travel between interactions. Consequently, the particles are less likely to scatter away from the illuminated region when the scattering coefficients are smaller. The fluence in the illuminated region is higher, so the absorption in the illuminated region is higher.

Finally, when the 1D optical propagation model with no scattering is used, the absorption in the central shallow vessel drops by 25%. A large fraction of the incident light is absorbed at the top of the vessel and a small fraction is absorbed at the

bottom. We show the absorption in the central shallow vessel in figure 6.7. Also shown is the temperature evolution in the vessel when the illumination time is 0.4 ms. There is, effectively, no heating of the endothelial cells at the bottom of the vessel.

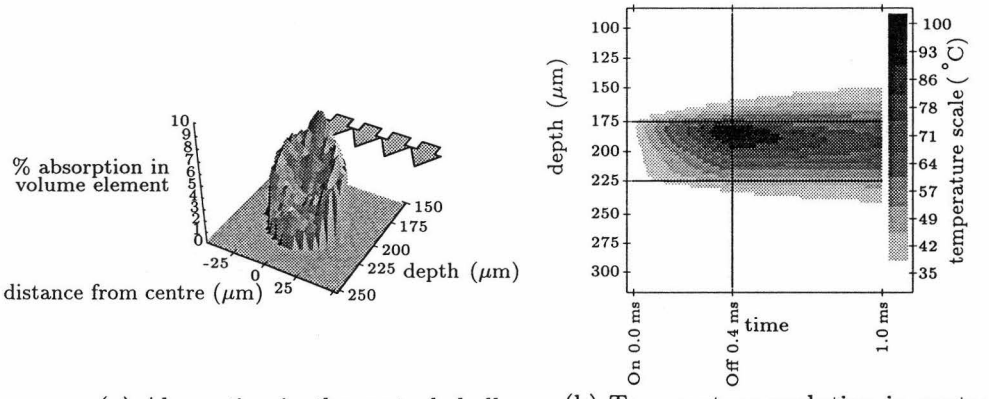

(a) Absorption in the central shallow vessel

(b) Temperature evolution in central shallow vessel. 0.4 ms, 1.3 J/cm^2

Figure 6.7. The scattering parameters are set to zero, and the light propagates in one dimension. Figure (a) shows that the most of the absorption in the central shallow vessel is at the top. We show the resultant evolution of temperature in the vessel if the illumination time is 0.4 ms in figure (b).

6.3 Conclusion

We have shown in the previous chapter that the predicted average temperature rise in the central shallow vessel is 420 °C when a fluence of 7.5 J/cm^2 is used. In this section, we give possible reasons for a temperature rise that is much higher than is obtained clinically.

One possible explanation for this overestimation of the temperature rise is the optical parameters are not correct. We changed the optical properties by a factor of two or three, yet the maximum reduction in the absorption in the blood vessels was 30%. With this reduction, the predicted average temperature rise in the central shallow vessel will be 300 °C when a fluence of 7.5 J/cm^2 is used. This is much higher than is expected from the clinical work. It is possible that the optical properties are incorrect, but it is unlikely that they are this far wrong.

The second possibility that was considered is that our representation of the epidermis is not appropriate. The results discussed in section 6.1 support this conclusion. A better representation would be to consider the epidermis as a layer with a thickness

of 1 mm. This layer is then subdivided into two layers. The bottom layer, which represents the melanin containing skin structures has a thickness of 65 μm. The optical properties of this layer would be the same as those used previously. The tissue that is represented by this top layer was described in subsection 2.1.1. The optical and thermal properties of the top layer, which represents the remainder of the epidermis, have not been reported.

The results in this chapter do not invalidate all of the results of the Monte Carlo technique, which were reported in chapter 4. We have shown in this chapter that our model of skin does not sufficiently limit the amount of light that reaches the vessels. Consequently, too much light reaches the vessels. The absorption in the vessels needs to be scaled down by some factor, which is determined by the optical properties of the top layer of the epidermis.

The top layer of the epidermis will scatter the incident light and so broaden the laser beam. We do not expect this effect to be significant when the spot diameter is larger than 3 mm. The light that travels through the epidermis will be more diffuse. Consequently, the difference in absorption between the top and bottom of the vessels will be less. Less light will reach the blood vessels as more of the beam will be backscattered out of the skin before passing through the epidermis.

In subsection 4.3.2, we examined the effect of the scattering model for spot diameters between 0.1 and 1.6 mm. These results are, unfortunately, misleading as the effect of the top layer of the epidermis is not included. This layer will broaden the incident beam and reduce the absorption in the vessels. Consequently, we expect that increasing the beam diameter from 1.3 mm (with constant fluence) will increase the absorption in the shallow vessels.

Chapter 7

Automated treatment devices

In this chapter, we describe the motivation for an automated treatment device, the various automated treatment devices in the literature, and the design considerations of the scanner in use at St. Georges Hospital.

When a port-wine stain is treated, the laser beam must be directed onto the skin in a controlled manner, so that the desired effect is obtained. The literature describes manual and automated methods.

With manual methods, the laser beam is typically passed down a fibre optic and onto the skin. The laser beam may be focussed by a lens when it leaves the fibre optic. The fibre optic is held in the surgeon's hand, who scans the laser beam over the port-wine stain or treats individual points in the port-wine stain.

Alternatively, a computer is used to control where the laser beam is incident on the skin, and the illumination time. There are several advantages for such a device, which are listed below in section 7.1.

A summary of the automated treatment devices in the literature is contained in section 7.2. Section 7.3 gives a complete description of the SCANALL system. This chapter concludes with a short discussion on automated treatment devices in section 7.4.

7.1 Why use an automated treatment device?

In this section, we briefly describe one method of treating port-wine stains. The problems with this manual technique are described. From this, the motivation and design criteria for an automated treatment device is given.

In 1985, my thesis advisor, Assoc. Prof. P.H. Butler watched Mr. E.P. Walker, a plastic surgeon, treat a port-wine stain with the light from an argon-ion laser. The

light was passed down a fibre, and Mr. Walker scanned the beam across the skin by moving the fibre. A rasterscan like pattern was created on the skin.

The speed of the fibre was not uniform, so a non uniform response was obtained. Some parts of the skin were overtreated and there was excessive blanching. Other parts of the skin did not blanch, indicating that these parts were not sufficiently treated.

Movement of the fibre over the port-wine stain is repetitive and tedious for the surgeon.

Theoretical work that was later carried out (Pickering *et al*, 1989b) showed that the illumination time should be in the range of 1-10 ms. With the manual technique described above, the minimum illumination time that could be obtained was 30 ms. Sometimes, depending on the laser power, the illumination time was 100 ms. Theoretical and clinical work shows that such illumination times are too long.

To provide a superior treatment which overcomes these difficulties an automated treatment device is needed. The design criteria for this device are given below:

1. Illumination times in the 1-10 ms range must be available to the user.

2. The system should be straightforward to operate.

3. Uniform treatment of the skin should be obtained.

With an automated device, it was hoped that information on the changes that occur in skin during treatment could be obtained.

7.2 Automated treatment devices in the literature

This section gives a brief review of the automated treatment devices listed in the literature. They fall into two types. The simple devices consist of a fibre optic that is moved over a region of tissue under the control of a computer. The region of tissue that can be treated is very small, less than 200 mm^2. The more complex devices direct the laser beam onto a mirror (or mirrors) and onto the patient. The mirror (or mirrors) are moved under the control of a computer. Movement of the mirror moves the laser beam, and so the spot on the patient.

With each of the scanners described, it is usually not possible for the entire port-wine stain to be treated without movement of the scanner or patient. The port-wine stain is usually split up into small areas. After each area has been treated, the patient or the device is then moved so that an adjacent area can be treated.

Hexascan^{TM}

The first automated treatment device reported in the literature is described by Rotteleur *et al* (1988). It consists of a handpiece with a scanning mechanism controlled by a microprocessor. A fibre optic is moved within the handpiece to one of 127 different positions. A hexagon shape is treated if all of the positions are used before the handpiece is moved. The spot diameter is 1 mm. For port-wine stains larger than the hexagon the handpiece is moved to an adjacent untreated region. This process is repeated until the entire area is treated. Following treatment, the hexagons are visible and unsightly.

This device provides illumination times between 30 and 990 ms. An argon-ion laser (488, 514 nm) is used as a light source. The maximum area of skin that can be treated before the handpiece must be moved is 139 mm^2. Typical treatment parameters are (Rotteleur *et al*, 1988)

1. Output Power:3-3.5 W
2. Pulse Length: 30-60 ms
3. Fluence:16-24 J/cm^2
4. Spot diameter: 1 mm

CC-Scan

Chambers *et al* (1990) describe a similar automated treatment device. The light from a continuous wave dye laser (575 nm) is passed through a fibre to a laser handpiece. Inside the handpiece, the fibre optic is moved by two stepper motors to scan a square of size 100 mm^2. The spot is moved in a rasterscan pattern so that the spot never travels over previously treated skin.

The exposure duration can be set between 300 and 5 000 ms. The laser power used is not mentioned, but the authors state that a continuous wave dye laser is used as a light source. The spot size is 1 mm.

Chambers *et al* (1990) did not describe the typical treatment parameters.

Scanall

We have described (Smithies *et al*, 1991) a scanning system with a single mirror that is under the control of a computer. Rotation of the mirror about two axis causes the spot to move on the patient.

This system is more complex that the Multiscan system described below as irregular shaped areas can be treated. The computer evaluates the shape of the lesion,

and will move the laser beam so that every point in the area is subjected to the laser beam once.

The maximum area that can be treated is 300 cm^2. Typical treatment parameters are as follows

1. Output Power:5 W
2. Illumination time: 4 ms
3. Fluence: 12 J/cm^2
4. Spot diameter: 0.3 mm

This system meets the design criteria set in section 7.1. Illumination times of 1-10 ms are available to the user, it is simple to operate and a uniform treatment is obtained.

With this scanner, our understanding of the skin processes involved has been improved. From observation of the treatment, a realistic model of blanching has been produced. This model is explained in subsection 8.2.3.

Further, we have been able to measure the rate at which the skin changes colour in response to the laser beam. These results are reported in chapter 9.

Multiscan

Laffitte *et al* (1992) describe a scanning system with galvanometric mirrors to scan the beam over a square area. The frequency doubled output of a Nd-YAG laser is used to produce 15 W of 532 nm light. The laser beam may pass over normal skin. Mordon *et al* (1993) reports that initially the normal skin was masked. However, it was demonstrated that the laser beam has no effect on normal skin so the mask is no longer used. The maximum area that can be treated is 300 cm^2. Laffitte *et al* (1992) state that the typical treatment parameters are as follows

1. Output Power:9 W
2. Fluence: 8-15 J/cm^2
3. Spot Diameter: 5 mm
4. scanning speed: 28 $cm\,s^{-1}$

The presented data is inconsistent. From the scanning speed and spot diameter the illumination time is 18 ms, so the fluence is 0.8 J/cm^2. It is likely that the spot diameter is in error, and is 0.5 mm. With this spot diameter, the illumination time is 1.8 ms, which gives a fluence of 8 J/cm^2.

7.3 The SCANALL system

In this section, we give a detailed description of the SCANALL system that was initially reported in the work of Smithies *et al.* (1991).

In subsection 7.3.1, we give an overview of the main components in the SCANALL system.

The mechanism for movement of the scanning mirror is described in subsection 7.3.2.

In subsections 7.3.3, 7.3.4, and 7.3.5, we calculate the path of the laser beam through the SCANALL system. These calculations show how the position of the pillar and angled mirrors must be adjusted so that optimum performance of the system is obtained.

In subsection 7.3.6, we describe how the patient is positioned so that treatment can commence.

To make the SCANALL system as simple as possible to use, several non trivial problems had to be solved when writing the computer program. We describe the solution to these problems in subsection 7.3.7.

We examine the types of laser that can be used with the SCANALL system in subsection 7.3.8.

Finally, in subsection 7.3.9 we describe in a qualitative manner the results that have been obtained with the SCANALL system. These results are compared with those obtained when the laser beam is manually scanned over the port-wine stain.

7.3.1 Overview of the SCANALL system

In figure 7.1, we show the SCANALL system in use. The patient is lying on a bed below the arm of the scanner. The laser beam is incident on the cheek of the patient, and this has resulted in a bright spot in the photograph. The surgeon, who is in control of the SCANALL system, is in the foreground. He is monitoring the effect of the laser beam on the port-wine stain, and has adjusted the illumination time so that the desired effect is obtained.

The path of light through the SCANALL system is shown in figure 7.2, which should be compared to the schematic diagram of the scanner unit, figure 7.3. The lens, scanning mirror drive unit, camera, fluorescent light, and camera mirror are fixed to an optical bench. The optical bench can slide along the track. Mounted to the track is the angled mirror. The track, optical bench, lens, scanning mirror drive unit, camera, fluorescent light, and camera mirror are collectively referred to as the

Figure 7.1. The SCANALL system is shown, delivering laser light onto the patient. The surgeon is sitting in the foreground, watching the effect of the laser beam on the patient's skin. In the background, the anaesthetist is monitoring the patients vital signs.

arm of the scanner unit.

The laser beam is generated within the laser cavity and is directed to the one end of the laser cabinet, where the pillar is mounted. At the base of the pillar, there is a mirror which reflects the laser beam in the upwards direction. This mirror is referred to in the text as the "pillar mirror". At the top of the pillar, the scanner arm is mounted in such a way that it can rotate around the pillar. The angled mirror, which rotates when the scanner arm is rotated, is used to deflect the beam along the scanner arm. The beam travels along the arm of the scanner, where it passes through the lens. The lens has a focal length of 800 mm, and it is used to focus the laser beam. At the end of the scanner arm, the scanning mirror is used to deflect the beam downwards onto the lesion that is to be treated.

The patient lies on an adjustable bed with the port-wine stain to be treated directly below the scanning mirror. The distance between the port-wine stain and the scanning mirror is such that the laser beam is focussed on the stain. A spot with a diameter of 0.3 mm is formed.

The video camera which is mounted above the scanning mirror is used to obtain an image of the lesion. The image is placed on the computer monitor. The computer text and graphics are superimposed over the image of the lesion on the monitor.

Figure 7.2. At the left end of this picture, one end of the laser is shown. The laser beam that is generated (green and yellow light), has been directed through two mirrors so that it travels along the arm of the scanner unit. It is focussed by lens to a point below the end of the scanner arm. This point is marked by the focus pendulum.

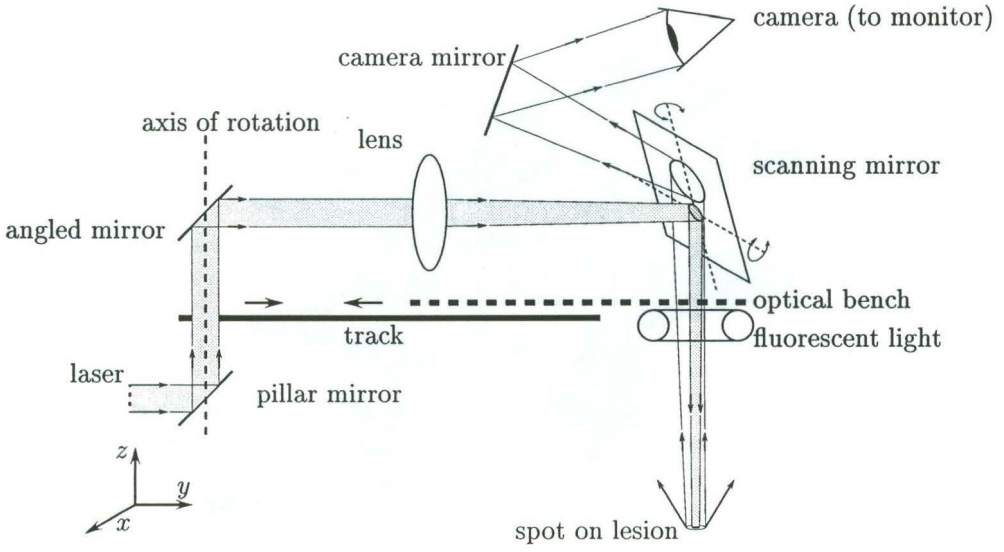

Figure 7.3. Schematic diagram that shows the path of light through the computer controlled scanning unit. The light is focussed onto the patient by the 800 mm focal length lens and scanned across the lesion by changing the orientation of the stepped mirror. An image of the lesion is obtained by the video camera and displayed on the computer monitor.

The position and shape of the lesion needs to be stored in the computer by the operator. This is achieved by stepping around the image of the lesion on the monitor, using a mouse. The position of the outline is recorded by the computer, which then evaluates the shape of the lesion and determines the path that the laser beam should take.

Once the computer has determined the path the spot should follow, treatment can commence. The shutters open, and the laser beam is incident on the port-wine skin. To move the spot, the orientation of the scanning mirror is adjusted by stepper motors that are controlled by the computer.

7.3.2 Scanning mirror

In this subsection, we describe in detail the mechanism used to move the scanning mirror.

Butler and van Halewyn (1988) describe in a US patent one method of moving the scanning mirror through the desired range of angles. Two stepper motors with a worm drive on their output are used to effect a rotation of the mirror about two perpendicular axes. As with almost any geared system, backlash is inevitable. Large springs were installed to remove the backlash, but this placed too much load on the motors. Consequently, the line spacing was uneven.

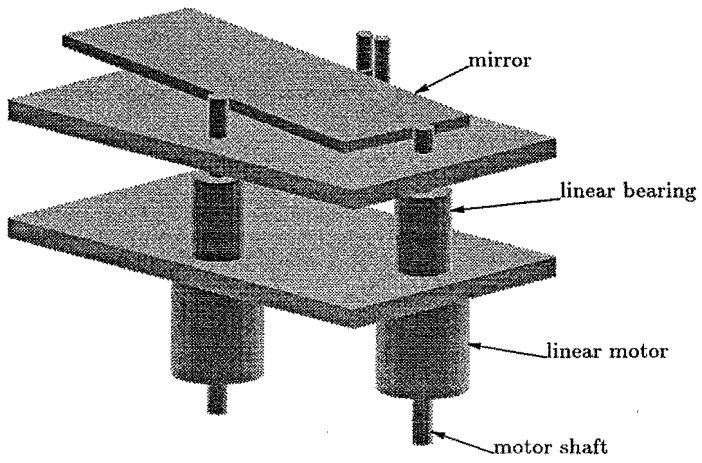

Figure 7.4. Schematic diagram of the scanning mirror drive mechanism. On two parallel aluminium plates the linear motors, linear bearings and mirror are mounted. Movement of the shaft in either motor causes the orientation of the mirror to change.

In 1991, a superior system was developed, which is shown schematically in figure 7.4. The scanning mirror is attached to a hemisphere, which rests in a seat. The

hemisphere is cut so that the mirror pivots about a point on the front surface of the mirror. Two linear stepper motors are attached to the top and side of the scanning mirror through universal joints. The shaft in each motor is is connected to a universal joint which is connected to the mirror. Thus, movement of the shaft in or out will rotate the scanning mirror about two perpendicular axis.

7.3.3 Path of light through the pillar

In this subsection and subsection 7.3.4, we calculate the path of the laser beam through the pillar and lens on the scanner arm. This calculation is necessary, as the following argument shows.

When the laser beam is activated, the spot would treat a point that is displayed on the monitor ($P(0,0)$). If the position of $P(0,0)$ is altered by changes in the position of the scanner arm, the system will be inaccurate. It will not be possible for the computer to "know" how many steps of the scanning mirror motors are required to move the spot from $P(0,0)$ to the lesion. If treatment does commence when the position of $P(0,0)$ has been altered, the region treated will be displaced from the region that was entered by the user.

Consider the angled mirror, which is shown in figure 7.5. It has been rotated around the x axis by an angle ω. This mirror is mounted on the track that the optical bench moves in and out on. When the arm is rotated, the angled mirror will rotate about the axis of rotation by an angle η.

The angle between the incident laser beam and the axis of rotation is ν. For simplicity, we describe the incident laser beam $\hat{\boldsymbol{i}}$, with the vector $(0, \sin\nu, \cos\nu)$.

The direction vector of the reflected laser beam, $\hat{\boldsymbol{r}}$ can be determined once the equation describing the normal to the mirror ($\hat{\boldsymbol{n}}$) is known after solving the following equation.

$$\hat{\boldsymbol{i}} \times \hat{\boldsymbol{n}} = \hat{\boldsymbol{r}} \times \hat{\boldsymbol{n}} \tag{7.1}$$

First, we must determine the normal to the angled mirror. If we take ω and η to be zero, then the normal is $(0,1,0)$. Rotation of the angled mirror about the x axis by an angle ω will rotate the vector normal to the angled mirror, giving

$$\begin{pmatrix} 0 \\ \cos\omega \\ -\sin\omega \end{pmatrix} = \begin{pmatrix} 1 & 0 & 0 \\ 0 & \cos\omega & \sin\omega \\ 0 & -\sin\omega & \cos\omega \end{pmatrix} \begin{pmatrix} 0 \\ 1 \\ 0 \end{pmatrix} \tag{7.2}$$

The result from equation (7.2) is rotated about the axis of rotation (the z axis) by

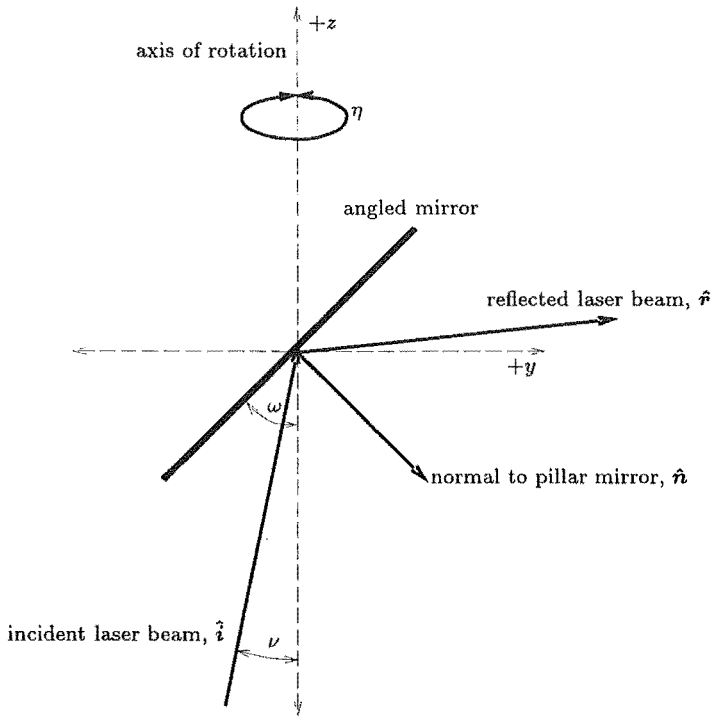

Figure 7.5. A schematic diagram of the angled mirror when a laser beam is incident on it. We use the angles described in this diagram when calculating the path of the reflected laser beam for different values of ν, ω, and η.

an angle of η when it is multiplied with the appropriate rotation matrix. Giving,

$$\begin{pmatrix} -\sin\eta\cos\omega \\ \cos\eta\cos\omega \\ -\sin\omega \end{pmatrix} = \begin{pmatrix} \cos\eta & -\sin\eta & 0 \\ \sin\eta & \cos\eta & 0 \\ 0 & 0 & 1 \end{pmatrix} \begin{pmatrix} 0 \\ \cos\omega \\ -\sin\omega \end{pmatrix} \tag{7.3}$$

On substituting for $\hat{\boldsymbol{i}}$ and $\hat{\boldsymbol{n}}$ into equation (7.1) and solving, we find that

$$r_x = -\cos\nu\,\sin 2\omega\,\sin\eta + \sin\nu\,\sin 2\eta\,\cos^2\omega \tag{7.4a}$$

$$r_y = \cos\nu\,\sin 2\omega\,\cos\eta + \sin\,\nu(1 - 2\cos^2\omega\,\cos^2\eta) \tag{7.4b}$$

$$r_z = \cos\nu\,\cos 2\omega + \sin\nu\,\cos\eta\,\sin 2\omega \tag{7.4c}$$

Suppose that ν is zero, the incident laser beam will be parallel to the axis of rotation. In this case, equations (7.4) will reduce to

$$r_{x0} = -\sin\eta\,\sin 2\omega \tag{7.5a}$$

$$r_{y0} = \cos\eta\,\sin 2\omega \tag{7.5b}$$

$$r_{z0} = \cos 2\omega \tag{7.5c}$$

Here, the subscript 0 indicates that ν is zero.

To examine where the beam goes when ν is not equal to zero, we note that the square of the distance between $\hat{\boldsymbol{r}}$ and $\hat{\boldsymbol{r}_0}$ is given by

$$(\hat{\boldsymbol{r}} - \hat{\boldsymbol{r}_0}) \cdot (\hat{\boldsymbol{r}} - \hat{\boldsymbol{r}_0}) = 4 \sin^2 \frac{\nu}{2} \tag{7.6}$$

As the arm rotates, the laser beam will always be a fixed distance away from $\hat{\boldsymbol{r}_0}$. In fact, the laser beam moves around the circle that is centred on $\hat{\boldsymbol{r}_0}$ as the arm rotates.

This calculation does not show what happens when the centre line of the laser beam is not coincident with the axis of rotation. We examine this with the following argument.

Suppose the centre of the beam is on the axis of rotation. The beam will be focussed at some point in space. If some fraction of the beam is removed, the remainder of the beam will still focus to the same point, regardless of the part of the beam removed. Thus, any beam that is parallel to the axis of rotation will focus to the same point. Therefore, the SCANALL system will operate correctly if the centre line of the laser beam is not coincident with the axis of rotation

This argument requires that the lens will always focus the beam to the same spot, regardless of the part of the lens used to focus the beam. In practice, the distance between the laser beam and the axis of rotation is small (5 mm) and the diameter of the lens is 80 mm. Consequently, the beam is always incident on the centre of the lens, so the lens can be regarded as ideal.

7.3.4 Optical bench

We calculate the path of the laser beam as it travels along the arm of the scanner unit in this subsection. From these results, and those in the previous subsection 7.3.3, we show how the pillar and angled mirrors should be adjusted. With these mirrors set correctly, the position at which the spot is focussed (relative to the camera) will not change when the arm of the scanner is rotated or extended.

In figure 7.6, we have drawn a schematic drawing of the path of the light through the scanner arm. The laser beam is reflected off the angled mirror, and heads towards the lens. It travels a distance l and then passes through the lens. The lens focusses the beam to a point at a distance r from the lens. We have ignored the scanning mirror as we want to find the effect of the angled mirror on where the laser beam is focussed.

We denote the angle between the y axis, or the optical axis and the laser beam by α. The work in the previous subsection 7.3.3, shows that such a representation is

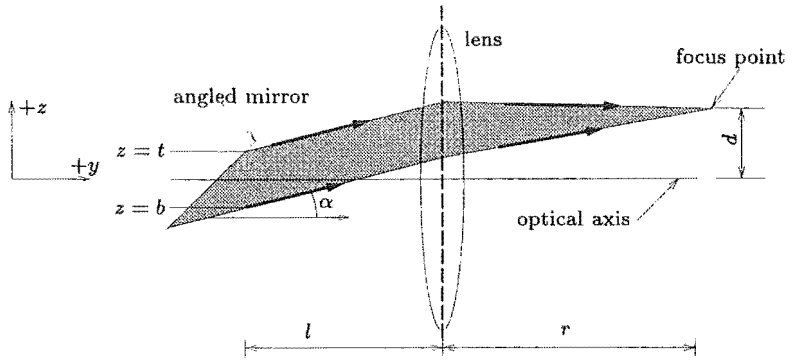

Figure 7.6. The path of an off-axis beam of light through the lens.

a simplification of what is experienced in reality. Arbitrarily, we place the origin of our coordinate system at the centre of the angled mirror.

In this calculation, we make two small approximations. First, effects due to spherical aberration are ignored. Second, $\tan\alpha = \alpha$. This second approximation is valid, as α is less than 0.03 radians.

In the notation of Gerrard and Burch (1975), we describe a ray of light that has been reflected off the angled mirror and is travelling to the right as

$$\begin{bmatrix} z \\ \alpha \end{bmatrix}_0 \tag{7.7}$$

This ray of light is a distance z form the optical axis (y axis) when $y = 0$.

At the point $y = l$, the angle between the optical axis, and the distance between the optical axis and the ray, is given by multiplying the matrix (7.7) with the following matrix,

$$\begin{bmatrix} 1 & l \\ 0 & 1 \end{bmatrix} \tag{7.8}$$

Similarly, to describe the effect of a lens of focal length f, the matrix describing the ray of light is multiplied by the matrix

$$\begin{bmatrix} 1 & 0 \\ \frac{-1}{f} & 1 \end{bmatrix} \tag{7.9}$$

The ray of light which has passed through the lens and reached the focus point will be described by the matrix

$$\begin{bmatrix} 1 & r \\ 0 & 1 \end{bmatrix} \begin{bmatrix} 1 & 0 \\ \frac{-1}{f} & 1 \end{bmatrix} \begin{bmatrix} 1 & l \\ 0 & 1 \end{bmatrix} \begin{bmatrix} z \\ \alpha \end{bmatrix}_0 \tag{7.10}$$

which is

$$\left[\begin{array}{c} (1-\frac{r}{f})z + (l+r-\frac{lr}{f})\alpha \\ -\frac{z}{f} + (1-\frac{l}{f})\alpha \end{array} \right]_{r+l} \tag{7.11}$$

We consider the two rays that represent the top and bottom of the laser beam at the angled mirror, $\left[\begin{array}{c} t \\ \alpha \end{array} \right]_0$ and $\left[\begin{array}{c} b \\ \alpha \end{array} \right]_0$. The point at which these rays intersect is the point at which the laser beam is focussed by the lens.

In a test of the algebra, we first take the simple case where the beam is parallel to the optical axis, so $\alpha = 0$. We require then that

$$(1-\frac{r}{f})t = (1-\frac{r}{f})b \tag{7.12}$$

From equation (7.12), we see that the point of focus will occur when $r = f$. As expected, these rays of light will intersect on the optical axis. Further, the point of intersection does not dependend on the value of t or b.

If we set α to some small value, then to find the focus point we require that

$$(1-\frac{r}{f})t + (l+r-\frac{lr}{f})\alpha = (1-\frac{r}{f})b + (l+r-\frac{lr}{f})\alpha \tag{7.13}$$

Again, we see that the point at which the beam is focussed will occur at $r = f$. It is not dependant on l, the distance between the lens and the angled mirror. Neither does it depend on the value of t or b, the distance from the optical axis to the top or bottom of the beam.

The position at which the focus point occurs is not on the optical axis, and d is given by

$$(1-\frac{r}{f})t + (l+r-\frac{lr}{f})\alpha \tag{7.14}$$

At the focus point, $r = f$ so equation (7.14) reduces to

$$d = f\alpha \tag{7.15}$$

Notice that the distance d is not dependant on the distance between the lens and angled mirror, or on the distance from the edge of the laser beam to the optical axis. Thus, extension of the scanner arm will leave the focus height and the distance d unchanged.

One further question remains, will the angle between the optical axis and the laser beam change when the arm is rotated? If it does change, then the position at which the spot is focussed will change as the arm is rotated.

To answer this question, we describe the optic axis with the vector $\hat{\boldsymbol{a}} = (-\sin\eta, \cos\eta, 0)$. The cosine of the angle between the optical axis and the laser beam is equal to the

dot product of the vectors representing the scanner arm and the laser beam. We note that

$$\begin{aligned}\hat{\boldsymbol{a}} \cdot \hat{\boldsymbol{r}} &= (-2\sin(\nu - 2\omega) - \sin(\nu - \eta - 2\omega) - \sin(\nu + \eta - 2\omega) \\ &\quad +2\sin(\nu + 2\omega) - \sin(\nu - \eta + 2\omega) - \sin(\nu + \eta + 2\omega))/4 \end{aligned} \tag{7.16}$$

From equation (7.16), we see that the angle between the arm of the scanner and the laser beam will change if the arm of the scanner is rotated and ν is non zero. If ν is zero, equation (7.16) reduces to

$$\hat{\boldsymbol{a}} \cdot \hat{\boldsymbol{r}} = \sin 2\omega = \cos\alpha \tag{7.17}$$

This implies that α is equal to $\pi/2 - 2\omega$.

In conclusion, we summarise the findings of this and the previous subsection.

1. The beam must be parallel to the axis of rotation, otherwise the position at which the spot is focussed will change.

2. The centre of the laser beam does not need to coincide with the axis about which the arm of the scanner is rotated.

3. When the laser beam is not parallel to the arm of the scanner, extension of the arm will leave the position at which the beam is focussed (relative to the video camera) unchanged.

4. The axis of the laser beam does not need to coincide with the centre of the lens.

7.3.5 Path of the laser spot on the lesion

In this section, we describe the calculation of the path of the laser spot on a flat surface below the scanning mirror. The results from this calculation show the relationship between the motor position and the position of the spot on the lesion.

The scanning mirror is shown in figure 7.7. Rotation of this mirror about either of the two axis drawn on the mirror will cause the spot to move on the patient. Initially, it was thought that the spot would move in a straight line. Experimental work, and the theoretical work in this subsection shows that this is false.

To calculate the path of the laser spot on the patient, we use the the coordinate system shown in figure 7.7. Also shown is the angles through which the mirror can rotate. It can rotate about the x axis by an angle θ. The mirror will rotate about a second axis, labelled R, by an angle ϕ.

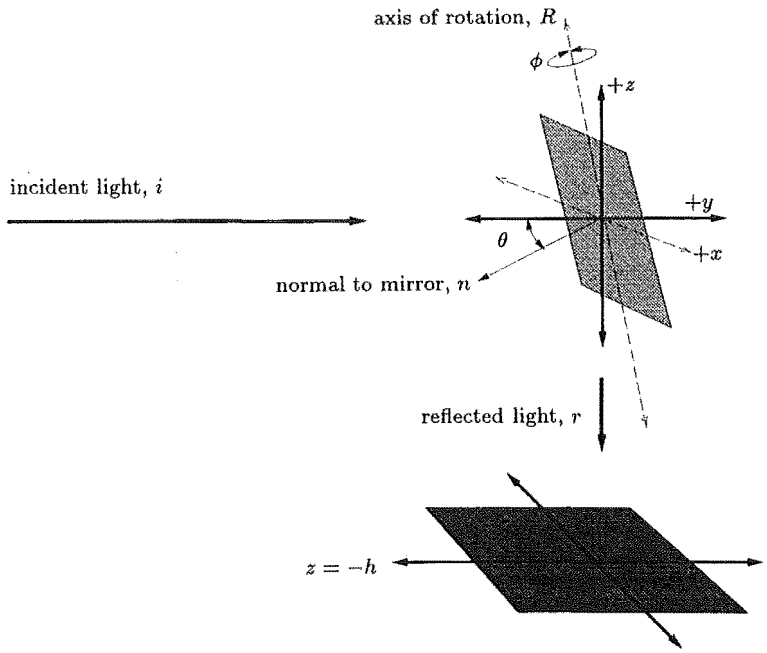

Figure 7.7. Schematic diagram of the scanning mirror, and the angles about which it can be rotated.

To calculate the path of the spot on the patient when the mirror is rotated about the x or R axis we proceed as before in section 7.3.3. Once the vector normal to the mirror surface has been found, the vector that describes the reflected beam can be calculated. From this, the point at which the spot intersects the plane below the scanning mirror can be determined.

The normal vector to the mirror when $\theta = 0$ and $\phi = 0$ is $(0, -1, 0)$. This vector is rotated by an angle ϕ about the axis R, and then rotated about the x axis by the angle θ. The normal vector after both rotations is given by the following equation,

$$\begin{pmatrix} \sin\phi \\ -\cos\phi\cos\theta \\ \sin\theta\cos\phi \end{pmatrix} = \begin{pmatrix} 1 & 0 & 0 \\ 0 & \cos\theta & -\sin\theta \\ 0 & \sin\theta & \cos\theta \end{pmatrix} \begin{pmatrix} \cos\phi & -\sin\phi & 0 \\ \sin\phi & \cos\phi & 0 \\ 0 & 0 & 1 \end{pmatrix} \begin{pmatrix} 0 \\ -1 \\ 0 \end{pmatrix} \quad (7.18)$$

Alternatively, the normal could have been calculated by rotating about the x axis first, and then about the R axis.

We note there is a sign difference in the matrix for rotation about the x axis in equations (7.2) and (7.18). This difference arises because the direction of rotation about the x axis has been reversed.

For simplicity, we take the normal vector of the incident beam to be $(0, 1, 0)$. With equation (7.1), we calculate $\hat{\boldsymbol{r}}$,

$$r_x(\phi,\theta) = -\sin 2\phi \cos\theta \tag{7.19a}$$
$$r_y(\phi,\theta) = 1 - 2\cos^2\phi \cos^2\theta \tag{7.19b}$$
$$r_z(\phi,\theta) = -\cos^2\phi \sin 2\theta \tag{7.19c}$$

The unit vector $\hat{\boldsymbol{r}}$ does not depend on where the laser beam is incident on the scanning mirror. The laser beam reflects of the scanning mirror at the point l_o, or (l_x, l_y, l_z). For simplicity, we will assume that l_o is (0,0,0).

The reflected beam travels along the line given by

$$l_o + t\hat{\boldsymbol{r}} \tag{7.20}$$

where t specifies one point on the line. It will intersect with a plane below the scanner unit at a height $-h$ when

$$t = \frac{-h}{r_k(\phi,\theta)} \tag{7.21}$$

Substituting equation (7.21) into equation (7.19d), the point of intersection on the plane at height $z = -h$ is

$$x(\phi,\theta) = \frac{-h\tan\phi}{\sin\theta} \tag{7.22a}$$
$$y(\phi,\theta) = \frac{h(1 - 2\cos^2\phi\cos^2\theta)}{\sin 2\theta \cos^2\phi} \tag{7.22b}$$
$$z(\phi,\theta) = -h \tag{7.22c}$$

This is plotted in figure 7.8 for when θ is in the range $[3\pi/16, 5\pi/16]$, ϕ is in the range $[-\pi/16, \pi/16]$, and $h = 400$ mm. Changes to ϕ cause the spot to move in an arc that is symmetric about the y axis. Increasing θ causes the spot to move to more negative values of y.

Extending the range of ϕ to $[-\pi/4, \pi/4]$ and θ to $[\pi/20, 9\pi/20]$, the result is as shown in figure 7.9. Increasing the maximum and minimum values of ϕ causes the spot to move further away from the y axis and to more positive values of y. Changing the angle θ from approximately 0 to almost $\pi/2$ moves the position of the arcs to more positive values of y and the size of the arcs decreases.

In figure 7.10 we show the results of an experiment where the laser beam was scanned over a section of cardboard. An illumination time of 1.6 ms was used. The spacing between the lines has been increased six fold, so that the position and shape of the lines is evident. The lines are not smooth and regular, which results from the stepped motion of the mirror. As in figure 7.8, the distance from the left end to

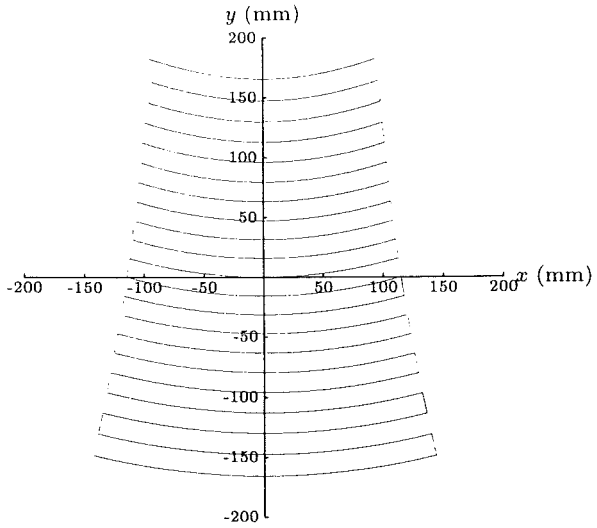

Figure 7.8. Path of the spot on a plane 400 mm below the scanning mirror. θ is in the range $[3\pi/16, 5\pi/16]$, and ϕ is in the range $[-\pi/16, \pi/16]$.

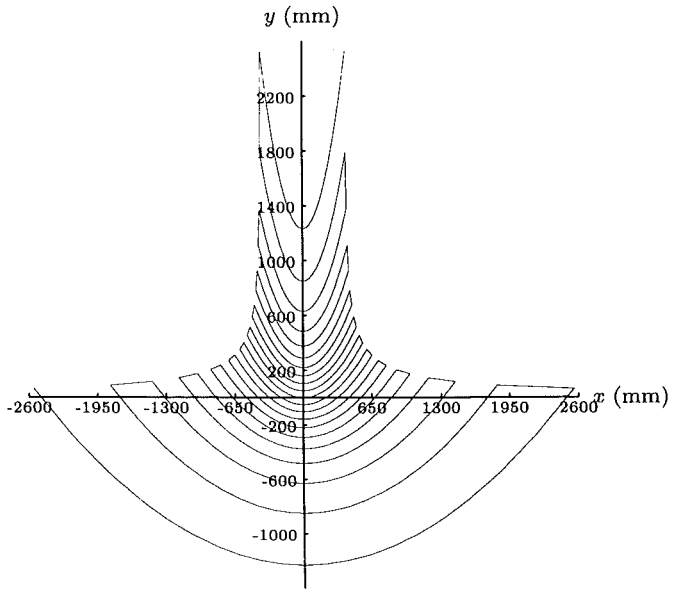

Figure 7.9. Path of the spot on a plane 400 mm below the scanning mirror when θ is in the range $[\pi/20, 9\pi/20]$ and ϕ is in the range $[-\pi/4, \pi/4]$.

the right end of the scan lines decreases as the spot moves up the page. However, the vertical lines at each end of the scanlines are in a different direction to those in figure 7.8.

The reason why the vertical lines are in the wrong orientation is uncertain. Analysis of the signals generated by the computer have proven that it is not a software problem. Tests have shown that the electronics which drives the motors generates the correct voltage levels in response to signals from the computer. Evaluation of the scanning mirror and drive mechanism reveals the presence of no backlash.

When the scanner is used with the standard scan pattern (2 steps between lines) to scan the laser beam over a square area of cardboard, the typical result obtained is shown in figure 7.11. An illumination time of 1.3 ms was used, so that the lines are thinner than those in figure 7.10. The scan lines are not smooth. At the end of the scan line, when the mirror is moved down, it seems to "oscillate" upwards and downwards after the movement.

The cause of the oscillation is probably due to the plastic universal links that connect the motor shaft to the mirror. Analysis of the dimensions involved shows the probable mechanism.

The distance from the universal link to the centre of the mirror is 40 mm and the distance from the mirror to the focus point of the laser beam is 400 mm. For the spot to move by 0.6 mm on the cardboard, the edge of the mirror must move a distance of 0.03 mm. It is probable that the length of the link alters when the motors move. For the link to extend by 0.03 mm, its length must alter by 0.08%.

7.3.6 Position of the lesion

For treatment to begin, the lesion that is to be treated must be below the scanning mirror. Also, the distance between the lesion and the scanner mirror must be set so that the laser beam is focussed on the lesion.

To meet the first requirement, the bed the patient lies on must be moved. Alternatively, the scanner arm is extended and/or rotated. When the patient is in the correct position, the lesion that is to be treated will be visible on the computer monitor.

Preferably, the patient is positioned so that the scan lines are approximately parallel to the lines of Langer in the skin. In this position, the gap between the scan lines is not obvious, and should not cause the patient embarrassment post treatment. Movement of the patient during treatment (as a result of breathing) can make the gap noticeable but in this position the effect is minimised.

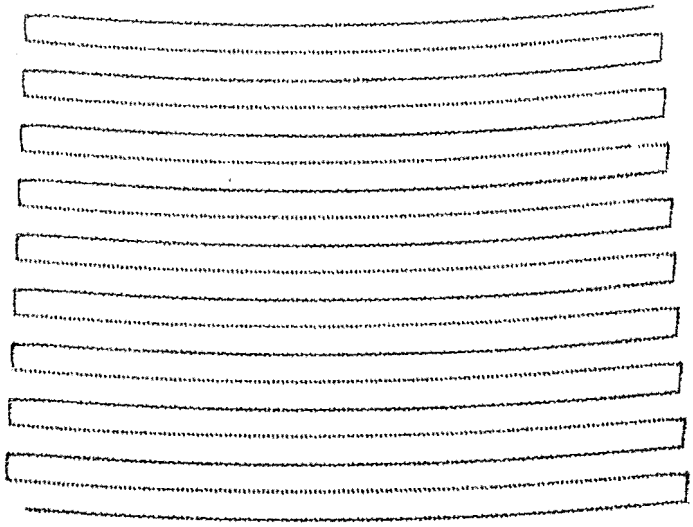

Figure 7.10. A full size diagram of the scan lines as obtained from an experiment. The scan lines are separated by 12 steps to aid comparison with the theoretical results, figure 7.8. The spot was scanned from left to right, starting at the bottom of the picture, moving upwards after each scan line was completed.

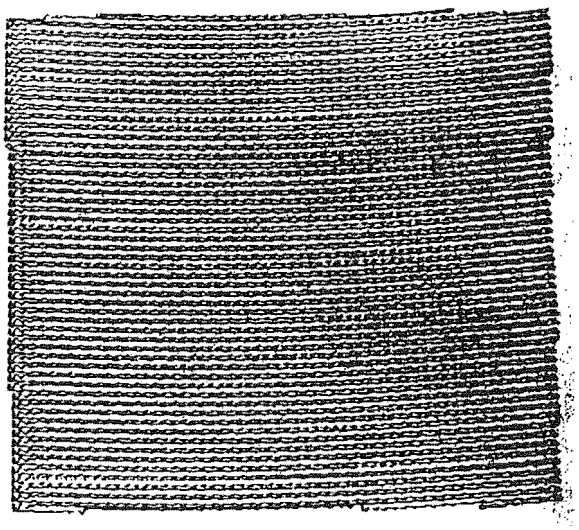

Figure 7.11. A full size diagram of the scan lines that the scanner creates on the patient. The scan lines are separated by 2 steps, or 0.6 mm.

Several methods have been used to ensure the lesion is at the correct height.

Initially, it was thought that the height of the bed the patient lies on should be adjusted until the image obtained by the camera is in focus. Unfortunately, the camera has a large depth of field, and the height could not be determined accurately enough.

Currently, a pendulum is suspended from the scanner arm. The bottom of the pendulum marks the height at which the laser beam is focussed. The height of the bed that the patient lies on is adjusted so that the port-wine stain is at the same height as the bottom of the pendulum. When this adjustment has been made, the pendulum is moved away from the treatment area.

Other methods for determining the correct height were discussed, but never tried. Similar to the dambusters during the second world war, two beams of collimated white light from either side of the scanning mirror should be directed downwards so that they intersect at the focus point. The light would have to be bright enough to be obvious, which would be uncomfortable for patients under a local anaesthetic. Alternatively, the use of two He Ne laser beams was considered dangerous because the anaesthetised patient does not have a blink response, or the eye protection may not be in place. The ultrasonic range finders similar to those in cameras are not suitable as the output beam is divergent and not capable of resolving structures such as a nose.

When setting the height of the lesion, a small error ($\pm$ 5 mm) is acceptable. With the long focal length of the lens, there is no appreciable change in the spot diameter over a distance of 10 mm at the focus point. This feature is useful when treating large areas as the distance between the scanning mirror and lesion will vary slightly. Therefore, the scanner can be used to treat an area such as the nose and cheek without the need to refocus during treatment.

7.3.7 Software

My supervisor, Assoc. Prof. P. H. Butler wrote, in PASCAL, the code that calculated the steps the motors should move for a given outline. This was translated into C by Bernie Mentink and installed on an Amiga B 2000 microcomputer. This code was extended by Bernie Mentink so that the user could enter the desired outline, treat the desired region, and store biographical information in the computer.

The code written by B. Mentink was for test purposes only. As such, it did not contain undo features, and was not "user-friendly".

Over the last four years, I have rewritten the program. It now contains 20 000

lines of program code, 2 000 lines of code describing the option boxes, and can be compiled into several different versions, depending on the preference of the user. Below, we describe the solution to the non-trivial problems encountered while making the program easier to use.

Entering the outline of the lesion to be treated

The code written by my supervisor to determine the path of the spot for a given outline requires that:

1. The lines in the outline do not cross.

2. The points in the outline are entered in a clockwise manner

For the program to be easy to use, it must prevent crossed lines from being entered and ensure the outline is in the correct direction.

During the outlining process, each line segment entered by the user is compared with the previous line segments that have been entered. If it does intersect with any of the previously entered line segments, the line segment entered and the previous line segment entered are deleted. This provides an undo facility for the user as the previously entered line segment can be deleted by entering a line segment that crosses another line segment.

To check if two line segments cross, the minimum and maximum x and y values are compared. The lines will not cross if the maximum y value of one segment is less than the minimum y value of the other segment. This is true for the x values also. For those lines segments where it is possible to cross, linear algebra techniques are then used. With this approach, the number of floating point operations required is minimised.

On completion of the outline, the entered lines must be ordered so the outline is in a clockwise direction. To check this, the cross product of each line and the next line in the outline is taken. The cross product generates a component along an axis which is at right angles to the entered line segments. This component is summed, and if the sum is positive, the order of all the lines in the outline is reversed.

Relating pixel position to motor position

For the computer to accurately scan the region marked on the screen, the computer must "know" how many steps of the scanning motors are required to bring the spot to a given pixel on the screen.

In the coordinate system used, the motor position $M(m_\phi, m_\theta)$ is $M(0,0)$ when the spot is incident on the pixel $P(0,0)$. This pixel is close to the centre of the screen. The position on the screen is described by the variables $P(p_x, p_y)$. Initially, it was assumed that the scan lines would be sufficiently straight for the following relationships to be valid:

$$m_\phi = a_x\, p_x \tag{7.4a}$$

$$m_\theta = b_y\, p_y \tag{7.4b}$$

From subsection 7.3.5, we see that m_ϕ and m_θ are functions of p_x and p_y. The accuracy of the scanning system was improved by using this result and making the approximation that:

$$m_\phi = a_x\, p_x + a_x x\, p_x\, p_x + a_{xy}\, p_x\, p_y + a_{xxy}\, {p_x}^2\, p_y + a_y\, p_y \tag{7.5a}$$

$$m_\theta = b_x\, p_x + b_{xx}\, p_x\, p_x + b_{xy}\, p_x\, p_y + b_{xxy}\, {p_x}^2\, p_y + b_{xyy}\, p_x\, {p_y}^2 + b_y\, p_y \tag{7.5b}$$

To determine the coefficients a and b, the mirror is moved to nine different points, and the laser beam is turned on briefly to mark the cardboard beneath the scanner. After each point is marked, the mirror is centred and the user marks on the screen with the mouse where the marked point appears.

From the nine sets of data $(m_\phi, m_\theta, p_x, p_y)$, the coefficients a and b are calculated. The major coefficients, a_x and b_y are determined using linear algebraic techniques from two of the data sets. The remainder of the coefficients are set to zero. The simplex technique is then used to adjust the values of all of the coefficients to bring the calculated values of m_ϕ and m_θ as close as possible to the experimental value.

7.3.8 Choice of laser

In this subsection, we describe the types of lasers that can be used with the SCANALL system. Further, we describe the motivation for the use of a copper vapour laser and the copper vapour laser currently in use.

From the preceeding subsections where we describe the path of the laser beam, it is clear that almost any type laser can be used. The scanning mirror can have the appropriate type of mirror fitted for non-visible wavelength lasers. However, it must reflect sufficient visible light for the camera to obtain an image of the lesion.

From theoretical calculations such as those in chapter 4 and the results of the clinical work described in chapter 8 we see that lasers that produce light at, or close to, the 577 nm wavelength are ideal for the treatment of port-wine stains. Several types of lasers are suitable,

1. argon pumped dye (577 nm)

2. flashlamp pumped dye (577, 585 nm)

3. krypton (568 nm)

4. copper vapour (578 nm)

Further, the laser must generate sufficient power so that the illumination time is as close as possible to the theoretical predicted optimum range of 1–10 ms. From clinical work, to obtain illumination times of 4 ms with a 0.3 mm spot, 5 W of laser power is required. The power density is 7 000 W/cm^2. With a pulsed dye laser, the maximum fluence available is 10 J/cm^2 when the diameter of the spot is 5 mm. The illumination time is 0.45 ms, so the average power density is 22 000 W/cm^2.

Wheeland (1993) mentions the krypton laser as a possible light source when treating port-wine stains. He notes that no long term studies of the effectiveness of this laser have been carried out. Further, he states that one advantage of this laser over the dye lasers is that exposure to toxic solvents and organic dyes can be avoided.

The copper vapour laser is the most efficient source of visible light currently available (Lewis, 1991). Two wavelengths are produced by this laser, 510.55 nm (60% of the power) and 578.21 nm (40% of the power). A further advantage is that this type of laser is cheap to operate (Ashley *et al*, 1991).

These results provided the motivation for the purchase of a copper vapour laser to treat port-wine stains. In 1985, the Quentron^{TM} QM91C copper vapour laser was installed in St. Georges Hospital to provide the optimum wavelength of light for the treatment of vascular lesions. Maximum output from this laser has been about 28 W. The light is generated as a rapid pulse train at a rate of 15 kHz. Each pulse is 0.000 02 hms long.

Initially, flat mirrors were installed at each end of the optical cavity, and the laser power is optimised. The laser beam has a large divergence, $>$ 10 mrad. When it was passed through the optics of the scanner and focussed to a spot the power density was sufficiently low that the illumination times were around 100 ms. This was unacceptably long, and unstable optics were installed. The divergence was reduced to 0.1 mrad (half angle) so the spot diameter is now 0.3 mm. With 5 W of laser power, the illumination time is around 4 ms.

7.3.9 Clinical results

In this subsection, we discuss the clinical results that have been obtained with the SCANALL system. These results are compared with those obtained from when the laser beam is scanned over the skin with a manual technique.

No long term study of the effectiveness of the SCANALL system have been completed, so we cannot show in a quantitative manner how effective it is. A further complication is that there have been several incremental improvements to the hardware and treatment technique, so a simple comparison is difficult. We do however describe some of the observations made by patients and the surgeon since the introduction of the SCANALL system.

The clinical results obtained after the treatment of four patients with port-wine stains is shown in figure 7.12.

The port-wine stains in figure 7.12a,b have been treated with the computer controlled scanner. In both cases, the spot diameter was 0.3 mm and the laser power was 4.5 W. The illumination times used were 11 and 15 ms for the port-wine stains in figures a) and b) respectively. The lines along which the spot travelled can only be determined on close inspection. This shows that no part of the lesion has been left untreated. Blanching is uniform across the surface of the lesion as the speed of the laser spot is constant.

The typical post treatment results of the fibre directed by hand can be compared with this. The port-wine stains in figure 7.12c (40 ms, 4.5 W) and figure 7.12d (130 ms, 2 W) have been treated with the optical fibre. The spot has an average diameter of 1.3 mm. Lines of un-treated skin can be observed between the lines of blanching and the blanching is not uniform. At the periphery of the lesion there is a tendency to over blanch the lesion as the surgeon slows the scan rate before changing direction. This indicates that the surgeon cannot control the speed and position of the fibre to the level required by the minimal blanching technique.

Patients who have undergone treatment with the SCANALL system and manual scanning of the fibre state that the degree of blistering post treatment is significantly less with the SCANALL system. The explanation for this is that there is much less damage to the non-vascular tissue when the SCANALL system is used as the illumination time is in the optimal range. There is negligible damage to the surrounding non vascular tissue with this system.

With the SCANALL system, the user has more control over the level of blanching obtained than with a manual system. This provides a question for the user, how much blanching is required? Certainly, blanching due to vessel constriction must be

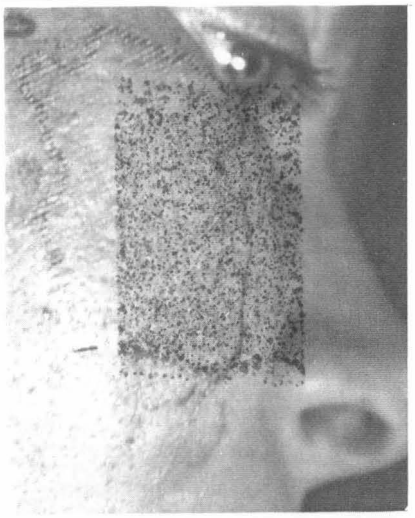

(a) 11 ms, 4.5 W, Scanall

(b) 15 ms, 4.5 W, Scanall

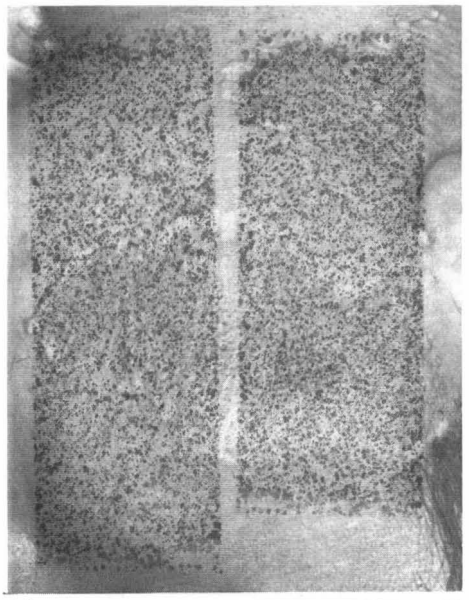

(c) 40 ms, 4.5 W, manual

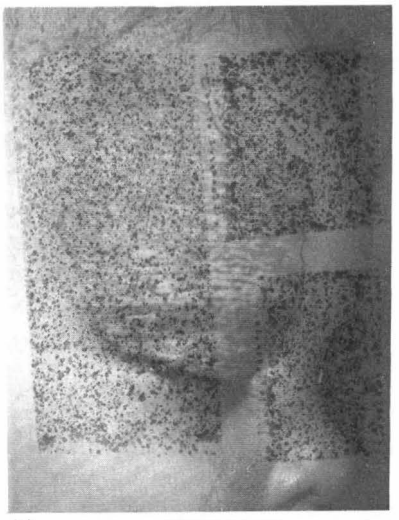

(d) 130 ms, 2 W, manual

Figure 7.12. Four examples of the results obtained when the light from a copper vapour laser is scanned over a port-wine stain. The lesions have been outlined with a green pen to highlight the border between lesional and non lesional skin. Figures a) and b) show two port-wine stains that have been treated with the computer controlled scanner. Figures c) and d) show the result after the laser beam has been passed down an optical fibre, which was manually scanned across the lesion.

obtained as this results from thermal damage to the ectatic vessels. Blanching that arises from changes in the optical properties of the epidermis is to be avoided, as damage to the epidermis is not required.

Rescanning the treated skin

Several workers have shown from histological studies that not all of the vessels in the skin contain blood (Barsky *et al.* 1980; Niechajev and Clodius, 1990). When the area is scanned once, not all of the capillaries in the skin are thermally damaged. The erythema observed after treatment is a result of the previously empty capillaries filling with blood. If the region is rescanned, more of the ectatic capillaries in the skin will be damaged. Thus, in one treatment session, significantly more vessels will be thermally necrosed.

However, with rescanning the region, more energy will be deposited in the epidermis. This increases the probability of untoward results.

Mehrtens (1994) recommended that port-wine stains can be rescanned, after cooling the epidermis. The cooling will help diminish the extent of damage to the epidermis. Following this suggestion, a trial on a 3 year old patient with a salmon pink port-wine stain was carried out. The port-wine stain covered the patients left temple, cheek, ear, and chin. This stain had received one previous laser treatment.

The cheek was scanned once. The entire temple region was scanned, cooled with an ice pack, scanned, and cooled with an ice pack. The entire stain was then dressed.

Three months later, the patient returned for a repeat treatment. The patient's father, a general practitioner, reported that there was significantly less blistering. Complete clearance of the port-wine stain on the temple was achieved, but not on the areas that were scanned once.

It is possible that the temple region would have given a similar response if it was scanned once. The cheek would need more treatments than the temple as port-wine stains on the cheek tend to be thicker. Following this test further clinical trials are being carried out to provide verification.

Our clinical procedure was modified as follows. Immediately after an area is scanned, the treated area is cooled with an ice pack for 10-20 seconds. This area is rescanned and then cooled.

Several patients have written, comparing the results from their last treatment session (where the area was rescanned) and previous sessions (the area was scanned once). With rescanning, there was a marked improvement in the colour of the port-wine stain.

7.4 Discussion

With an automated treatment device, it is possible to obtain a uniform response in the skin. No part of the stain is left untreated. In contrast, the manual technique produces a non uniform result and the possibility of over treatment of some areas exists. The uniformity of the results obtained with the scanner is a significant improvement in itself.

With an automated treatment device, the position of the spot and the illumination time is controlled more accurately than is possible with manual techniques. Thus, it is possible to investigate how the laser beam interacts with the skin. The results in chapter 9 are an example of this. We use this information to show the rate at which the colour of the skin changes from red to white.

Theoretical calculations, such as those described in chapter 5 show that the ideal illumination time is in the range of 1–10 ms. These calculations show that with such a short illumination time, there will be minimal damage to the dermal and epidermal tissue. Consequently, the level of blistering the patient experiences should be less than when the illumination time is 30 ms or longer. This result has been verified in our clinical experience.

The degree of blanching obtained can be adjusted by the surgeon so that the desired effect is obtained. With a manual technique, the control that the surgeon has on the result is limited. It is possible to examine the changes in the skin during laser treatment with the aid of filter glasses, such as those described by van Halewyn *et al* (1989).

The automated treatment device enables us to rescan an area of skin after it has been scanned. Consequently, the vessels which open up to deliver blood to the previously damaged vessels are also damaged. Initial results show that this has improved the efficacy of the treatment process.

The SCANALL system enables us to treat large areas quickly. From our experience, a port-wine stain that covers both cheeks, nose, chin, and the underside of the chin can be treated in 30 minutes. In addition to this, the patient must be anaesthetised, which requires a further 20 minutes.

7.5 Conclusion

The computer controlled scanner enables illumination times in the 1-30 ms range to be used in the treatment of vascular and hyperpigmented lesions. Theoretical

calculations and clinical results show that the use of these illumination times will give the optimal result.

Initial results obtained from the use of the scanner show that no part of the lesion is left untreated. With manual techniques, there is always an irregular gap between the lines along which the laser spot moves. The blanching obtained with the scanner is uniform, which indicates that the energy incident on the lesion is constant.

The scanner provides a significantly better treatment than the techniques currently available. It has the potential to become the treatment of choice both for port-wine stains.

Treatment with this computer controlled scanner is quick and free from boredom. A port-wine stain that covers both cheeks, nose, chin, and the underside of the chin can be treated in 30 minutes.

The degree of blanching obtained is controlled by the surgeon so that the required damage is inflicted on the blood vessels. Following treatment, the skin turns white in colour, and then red as the undamaged vessels open up to allow blood to reach the damaged tissue. When this happens, the area is rescanned, and the previously empty vessels are thermally damaged also. Initial clinical trials have shown this to be an improvement in the treatment of port-wine stains.

Chapter 8

Clinical Results

In this chapter, we examine and discuss the clinical results that have been reported in the literature. The effect of the illumination time and wavelength are examined.
Currently, the literature does not contain electron microscopy results for illumination times in the optimal range of 1-10 ms. Our results are reported.

In the first section, we describe the results from various wavelengths that have been described in the literature. These results show that yellow light (577-585 nm) is the optimum wavelength.

In section 8.2, we summarise the results in the literature for the various illumination times that have been used. Our theoretical calculations and theoretical calculations in the literature do show that illumination times in the 1–10 ms range will be ideal. We describe the processes that occur in the skin as a result of the laser treatment.

The SCANALL system, which is described in chapter 7 enables us to treat with an illumination time that is in the optimum range. We describe the changes in the skin which are observed following laser treatment, and those detected with electron microscopy in section 8.3.

Finally, we discuss the results contained in this chapter in section 8.4.

8.1 Wavelength

Many types of lasers producing different wavelengths have been used in an endeavour to find one which gives the best results. The carbon dioxide laser (10 600 nm), argon-ion laser (488-514 nm), ruby laser (694 nm), Nd:YAG laser (1 064 nm), dye laser(577,

585 nm) and copper vapour laser (511, 578 nm) have all been used with varying degrees of success. In the following paragraphs, we describe the results obtained with each type of laser.

It was as early as 1981 that Anderson and Parrish (1981b) suggested on the basis of theoretical calculations that yellow light (577 nm) should be used. The theoretical calculations of others supported this argument, yet it was not for another ten years that authors were in general agreement that yellow light should be used. We suspect that the wavelength used is determined more by the types of laser available to the clinician than by the results of research.

8.1.1 Carbon dioxide laser (CO_2)

Buecker *et al* (1984), and Tan *et al* (1986) have reported the histological changes in port-wine stains after treatment with a CO_2 laser. In both cases, the damage was non-specific. Buecker *et al* (1984) reported that there was acute coagulation necrosis, extending 0.4 to 0.5 mm into the dermis. Tan *et al* (1986) reported that the epidermis was absent, probably sloughed off. There was denaturation in the collagen, especially in the upper dermis.

These histological changes are predictable, as the light generated by the CO_2 laser is not selectively absorbed in any of the structures in the skin. van Gemert *et al* (1986) calculated the distribution of the CO_2 laser light within the skin. It was strongly absorbed in the epidermis, with almost no light reaching the vessels. Consequently, damage to the skin will be a result of heat conduction from the epidermis.

Ratz and Bailin (1987) supported the use of the CO_2 laser for the treatment of port-wine stains. The authors state that, "Generally, much deeper damage to the reticular dermis is necessary before a hypertrophic scar will develop". From this claim, the authors seem to be saying that damage to the epidermis is acceptable. They later state that, "The carbon dioxide laser, however, if used properly, vaporises the target tissue and generates little thermal damage below or beyond the layer of tissue that has been removed." Anderson (1987) points out that if the top layer of the skin must be necrosed, a contact electrical heater would provide at a fraction of the cost a similar, equally controllable histological result.

8.1.2 Nd:YAG laser

This laser uses a neodymium doped crystal of yttrium, aluminium and garnett to produce a beam at the the 1 064 nm wavelength (Rosenfeld and Sherman, 1986). The

beam is not heavily absorbed by blood or water, so the beam will not be strongly attenuated by the upper layers of the skin. It is not selectively absorbed by any one structure in the skin, so non-specific damage will result from the use of this laser.

Landthaler *et al* (1986) treated the dorsal aspects of the ears of white guinea pigs with this laser and examined the changes in the epidermis, dermis, and blood vessels. A spot diameter of 1 mm was used. The laser power was between 20 and 85 W and the illumination time set between 100 and 500 ms so that the fluence was in the range of 1000 to 1500 J/cm^2. There was damage to the epidermis, dermis and obliteration of the vessels. Reducing the laser power to 10 W with an illumination time of 100 ms (120 J/cm^2) led to moderate coagulation of the epidermis and dermis, with obliteration of the vessels.

From chapter 5, we see that such illumination times are very long as there is sufficient time for the heat generated in the vessels to be conducted to, and damage, all of the surrounding dermal tissue. However, this wavelength is not preferentially absorbed in the blood, so reducing the illumination time will not affect the distribution of damage within the skin.

The fluence, which is the amount of energy deposited on the skin, was exceptionally high. Depositing hundreds, or thousands of joules per square centimetre must be regarded as unwise as there will be sufficient energy to thermally necrose the entire skin.

Rosenfeld and Sherman (1986) used this laser in 81 treatments of 39 lesions. The lesions consisted of capillary, cavernous, combined capillary–cavernous hemangiomas, port–wine stains, arteriovenous malformations, lymphangiomas, multiple telangiectasias, and one case of Klippel–Trenaunay–Webber syndrome. The laser power used ranged from 15 to 100 W, with an illumination time of 100 to 500 ms. The higher powers were used with lesions such as the cavernous haemangioma, a lesion that contains blood vessels over 1 mm in diameter. Two cases of hypertrophic scarring and one of hyperpigmentation were reported, so the probability of scarring in any one treatment is 4%.

Dixon and Gilbertson (1986) reports the use of the Nd:YAG laser for the treatment of the large nodules within nodular port-wine stains. The laser power used was 20–40 W, with a 2 mm spot diameter, illumination time of 200 ms, and the fluence was between 100 and 200 J/cm^2. The endpoint obtained was shrinkage, little blanching, and the immediate appearance of brown to black spots representing the larger coagulated vessels with an overall brown to black appearance. The incidence of scarring was the same as obtained when these workers used the argon-ion laser.

Adams *et al* (1987) compared the Nd:YAG laser and the argon-ion laser. They adjusted the treatment parameters for both lasers so that blanching was obtained with the minimum laser power. The probability of scarring was significantly higher with the Nd:YAG laser.

8.1.3 Argon-ion laser

Several authors, (for example, see Goldman *et al*, 1976; Noe *et al*, 1980; Dixon *et al*, 1984a; Finley *et al*, 1984; Carruth and Shakespeare, 1986) have reported the use of the blue/green light generated by the argon-ion laser to treat port-wine stains. All report non vascular specific damage within the skin. As Goldman *et al* (1976) states, "The mechanism of the laser reaction is, for the most part, a superficial, non specific thermal coagulation necrosis. There is, in brief, superficial necrosis, thrombosis, and at times, extravasation of blood. The deeper vascular plexus are not affected. These changes produce blanching of the skin colour through a change in the optical quality of the tissue".

When Dixon *et al* (1984a) treated a group of 73 patients with the argon-ion laser, 38% developed scars after treatment with fluences of 47 ± 2 J/cm^2. The treatment technique used required that "good" blanching is obtained. In the subsequent group of 73 patients, care was taken in selecting the areas for treatment. The fluence used ranged from 29 to 61 J/cm^2. The incidence of scarring was reduced to 13.7%. These findings reflect those of Noe *et al* (1980), who showed that some patients are more likely to undergo scarring, and should not be treated.

Carruth and Shakespeare (1986) described a slightly different technique, where the minimum laser power is used to obtain blanching. Use of this "minimal blanching power technique" reduced the incidence of scarring to less than 2%. The fluence used ranged between 15 and 25 J/cm^2.

Both studies were not clear in what was meant by the incidence of scarring figure reported. It seems that both studies reported the fraction of those treated who have developed scars, and not the probability of developing scars in any one treatment session.

The probable reason for the difference in the rate of scarring obtained is that Carruth and Shakespeare (1986) used a much lower fluence, and so there was less heating (and consequent damage) of the non-vascular tissue.

Part of the explanation for the different results obtained may be due to the location of the two studies. The study by Carruth and Shakespeare (1986) was conducted in the United Kingdom, while the study of Dixon *et al* (1984a) was carried out in

Salt Lake City, U.S.A. We expect then that the patients in one study will be more "tanned", and so these patients will have a higher melanin content in the epidermis. These patients will have a higher risk of scarring as the melanin content determines the fraction of the beam absorbed in the epidermis, and thus the heating of the epidermis.

In a comparison of the copper vapour and the argon-ion laser, Neumann *et al* (1992) showed that there was necrosis of the epidermis with a fluence of 10 J/cm^2 when the argon-ion laser was used. Below this fluence, no change was observed. Increasing the fluence increased the extent of the damage into the tissue. The damage was never vessel selective. In contrast, use of the copper vapour laser with a fluence of 10 J/cm^2 resulted in vessel selective damage, sparing the epidermis. These clinical results could have been predicted using the theoretical results in subsection 4.3.9. A high proportion of the incident beam from the argon-ion laser is absorbed in the epidermis, while a lower proportion is absorbed in the vessel. Shifting the wavelength to 578 nm will reduce the absorption and subsequent damage in the epidermis.

As van Gemert *et al* (1991a) notes, the argon-ion laser is used with illumination times that are much longer than optimal; there is sufficient time for the conduction of heat from the vessel to the surrounding tissue. This will cause non-selective damage in the dermis.

The argon-ion laser cannot be considered as the ideal light source, even if the illumination time was reduced to the optimal range, because too much of the blue/green light produced is absorbed in the epidermis.

8.1.4 Lasers producing yellow light

Many authors have reported the results from when dye, pulse dye, and copper vapour lasers are used to produce yellow light (577–585 nm wavelength). The difference in the results arises from the illumination time used, which is explained in the following section. In this subsection, we will endeavour to summarise the results obtained.

Light close to the absorption peak of haemoglobin at the 577 nm wavelength has been predicted to be optimal, see, for example, Anderson and Parrish (1981b) and van Gemert and Welch (1987). When yellow light is used, energy deposition in the epidermis is minimised, while maximising the temperature increase in the blood vessels.

Greenwald *et al* (1981) used a flashlamp pumped dye laser to treat the volar aspect of the forearm of 10 Caucasian subjects. The pulse width was 0.000 35 ms (full width at half maximum) with a spot diameter of 1 mm. At 3–5 J/cm^2, purpuric

macules and papules were noted but the epidermis appeared intact. Histologically, the primary alterations were virtually exclusively vascular in nature and basically involved the superficial vascular plexus.

Cotterill (1986) used a continuous wave dye laser and a spot diameter of 1 mm. Typically, the laser power was 0.5 W, with an illumination time between 500 and 5 000 ms. With these parameters, the fluence was between 32 and 320 J/cm^2. The fluence was adjusted until the skin appeared to blanch.The purple, mature port-wine stain responded particularly well, whilst the pink, easily compressible lesion responds poorly, it if all. The overall incidence of scarring is less than 1%.

Carruth and Shakespeare (1986) describe the use of a continuous wave dye laser at 577 nm to treat port-wine stains. The spot size was 1 mm, illumination times were between 20 and 5 000 ms, and the laser power was from 0 to 1.2 W. The authors adjusted the fluence to the minimum setting where blanching of the stain was obtained. Overall, the incidence of scarring was 1%, and the authors state that this is lower than the reported figures for when a Nd:YAG, argon-ion or CO_2 laser is used. Following treatment, some superficial crusting inevitably follows treatment, and some patients may develop a frank blister.

Pickering *et al* (1990b) reports the results that were obtained prior to the installation of the SCANALL system in our treatment clinic. A copper vapour laser (578 nm) was used, with a spot diameter of 1.3 mm and laser power between 1 and 5 W. The illumination time was proportional to the inverse of the laser power and was between 30 and 300 ms. Depending on the laser power, the illumination time was adjusted to obtain minimal blanching of the lesion. These results showed that when the laser power is high, a better treatment (less scarring, more long term colour change) is obtained.

Tan *et al* (1986) used a flash lamp-pumped tunable dye laser (577 nm, 0.36 ms, 3 mm spot diameter) to treat port-wine stains. Unlike the previous results quoted in this subsection, the skin turned purple after treatment, not white. Slight edema was observed in the papillary dermis and around the vessels.

In 1990, Tan *et al.* recommended the use of 585 nm, rather than 577 nm, as there is an improved depth of penetration. On the basis of a clinical trial with fifteen patients, they claimed that there was an improved rate of clearance. As Neumann *et al* (1992) points out, this clinical data is interesting, but remains to be proven in a larger clinical trial.

8.2 The effect of the illumination time

In the following paragraphs, we describe the clinical changes observed after treatment with yellow light and various illumination times. The processes occurring in the skin are described. We first summarise these results on the time line shown in figure 8.1. This figure helps to show where the clinical results fit into the overall picture.

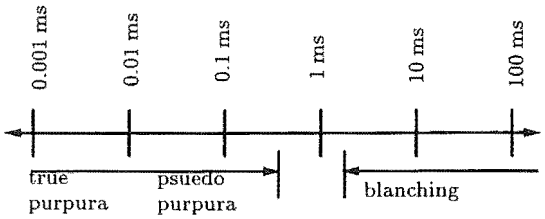

Figure 8.1. The clincial results that are immediately observed with various illumination times.

8.2.1 Illumination times less than 0.01 ms

Following treatment with illumination times in this range, purpura is obtained. Purpura, as defined by Miller and Keane (1987), is the extravasation of red blood cells throughout the dermis. The skin is purple in colour.

Anderson and Parrish (1981b) used an illumination time of 0.000 3 ms on normal skin with spot diameter 1 mm, 577 nm wavelength, and a fluence of 1–5 J/cm^2. Changes in the skin were almost entirely vascular in nature, involving the superficial vascular plexus. Clusters of tightly aggregated erythrocytes with an orange hue were observed in the superficial vascular plexus. Endothelial and transmural necrosis associated with rupture and haemorrhage was manifest.

Hulsbergen-Henning *et al* (1984) used illumination times of 0.001 ms, 2 mm spot diameter, 577 nm wavelength, and a fluence of 0.5–3 J/cm^2. A brown-red spot appeared one minute after treatment, which faded over the next four weeks. Damage to the epidermis was absent, although a blister was present in the basal layer of the heavily pigmented patient. Immediately after treatment, tearing of the vessel wall was evident. Forty eight hours after treatment, histology showed no damage to the vessel wall, although erythrocyte extravasation to a depth of 0.9 mm was observed. Six months after treatment, there was no long term fading of the port-wine stain.

The results from modelling show that with such short illumination times there is insufficient time for the conduction of heat from the blood to the endothelial cells in

the vessel wall. Consequently, there is no thermal damage to these cells. The tears in the vessel wall due to steam formation will heal and the vessel will remain enlarged.

In summary, purpura is observed after use of 0.001 ms illumination times. The vessels are ruptured, allowing erythrocytes to be spread through the dermis. Thermal necrosis of the endothelial cells in the vessel walls is absent. Hulsbergen-Henning *et al* (1984) suggests that steam has formed within the vessel, the steam expands and causes the vessel to rupture.

8.2.2 Illumination times of 0.3–0.5 ms

With illumination times of 0.3 ms, the skin turns a purple colour after treatment. The blood vessels are not ruptured, and there is minimal extravasation of the erythrocytes. Several authors mistakenly refer to this as purpura. For example, see Tan *et al* (1986), and Garden *et al* (1986). A more accurate description would be to describe the skin as "purpura like", or "purpuric colour". Perhaps the best description would be to say that the skin has a purple colour after treatment. This does not use the word purpura, which has connotations of vessel rupture.

Others have criticised the use of the word purpura. From the clinical and histological results obtained after treatment of port-wine stains, Verkruysse *et al* (1993b) have argued that the term *purpura* should not be used to describe the blue-gray colour obtained. However, they did not suggest an alternative name.

Garden *et al* (1986) showed that with exposure times of 350 ms, wavelength of 577 nm, energy density of 4 J/cm^2, the skin on the volar forearm of fair caucasians turned purple in colour. They showed that the purple colour observed is a result of the formation of an intravascular coagulumn, and not the extravasation of erythrocytes.

Morelli *et al* (1986) reported the results obtained with a 3 mm spot diameter, 577 nm wavelength, an illumination time of 0.3 ms, and a fluence of 6.5–10 J/cm^2. Within minutes after illumination, the skin turned a dusky, grey-blue colour. Within blood vessels, there were multiple foci of agglutinated erythrocytes, fibrin, and platelet thrombi extending as deep as the mid-reticular dermis. There was focal epidermal intercellular edema when damaged vessels were near the dermal-epidermal junction.

Many authors have reported encouraging results after the use of these illumination times, (for example, see Tan *et al*, 1989; Sheehan-Dare and Cotterill, 1994). Modelling shows that there is minimal, if any, damage to the tissue surrounding the vessels. However, these theoretical results show that there may be insufficient damage to the wall of the vessel.

8.2.3 Illumination times of 4 ms

The treatment of port wine stains with the SCANALL system described in chapter 7 has been observed with the rare earth doped safety glasses described by van Hálewyn *et al* (1989). These glasses provide nearly full colour vision. The explanation for the changes observed have been published in Marini *et al* (1992).

The skin is seen to blanch at the treatment point, that is within a matter of tens of milliseconds or less. At the same time, or very shortly after, bands of erythema are formed on both sides of the treatment line.

A different response is sometimes obtained when treating ectatic capillaries where a sclerosing agent has been used to collapse larger vessels in the vicinity of the laser treatment. In this situation lines of black or brown are observed.

Theoretical work, such as that in chapter 6, shows that when the haemoglobin absorbs the yellow laser light, heat will be conducted from the erythrocytes to the endothelial cells of the vessel walls on a timescale of approximately 3 ms. The next step is that the selective permeability of the endothelial cell membrane is irreparably lost. The sudden influx of water carried by the Na^+ ions redistributing according to their concentration gradient causes the cells to rapidly enlarge. Since the surrounding dermal structure prevents centrifugal expansion, expansion occurs centripetally, blocking the lumen. When the vessel lumen is almost entirely occluded, the blanching effect is obtained. These steps are shown in figure 8.3.

In the sclerosed case, we propose that the some of the escape channels are predamaged and swollen. There is haemoconcentration and the haemoglobin denatures *in situ*. The blood cells are stationary and colour of the vessel changes to black or brown. The effect is shown in figure 8.2.

When the laser beam causes thermal damage to the endothelial portion of the vessel structure, vasodilating agents are immediately released by these cells as part of the series of events occurring during an acute inflammatory process. These agents will dilate the adjacent capillaries, causing a band of erythema on either side of the laser track. The timescale for this is related to the flow rate of blood in the capillaries (typically 3 mm/sec), as shown in figure 8.4. These dilated vessels, congested with erythrocytes, present a better target for the returning computer guided laser beam.

When the illumination time is set so that the vessel constriction process is observed, there is minimal blistering following treatment. If the illumination time is increased by 20%, erythema is not observed following treatment. The blanching obtained is more pronounced. Following treatment, there is more blistering of the skin. When the illumination time is increased, more energy is deposited on the skin, and

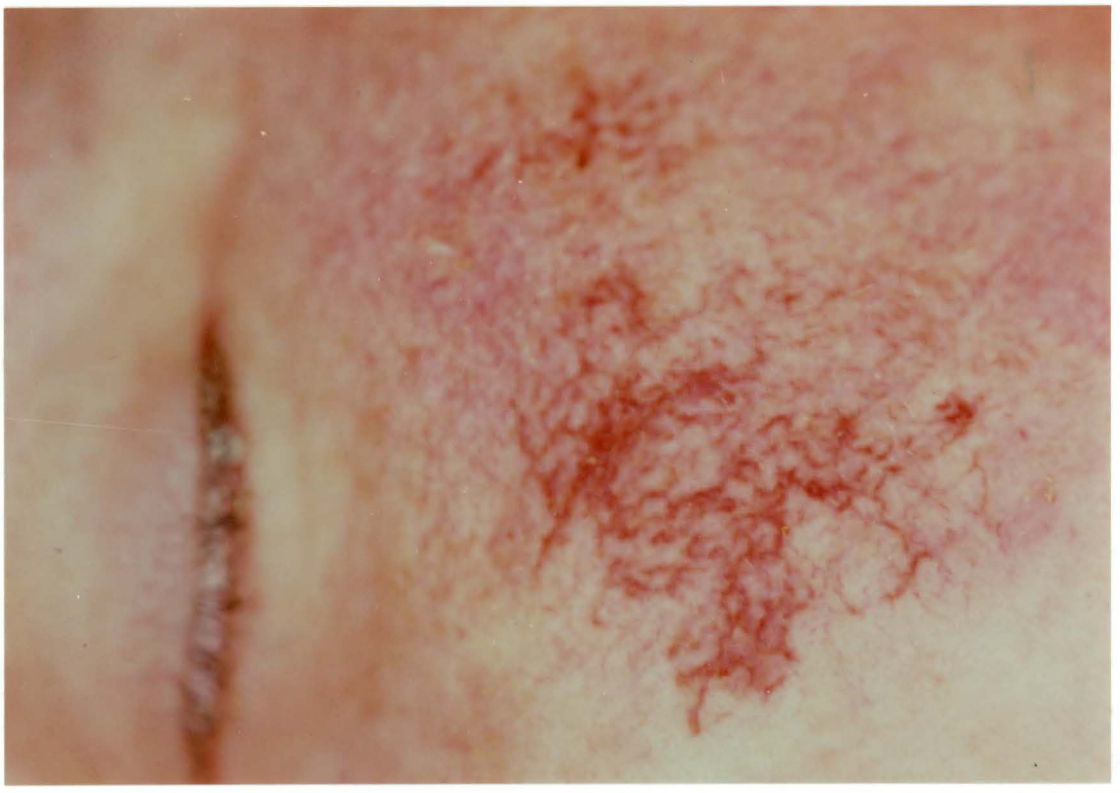

Figure 8.2. Photograph of the purpura like reponse of sclerosed vessels after copper vapour laser treatment.

consequently the epidermis absorbs more energy. This has caused sufficient thermal damage so that the changes in the underlying vessels are no longer observable.

8.2.4 Illumination times longer than 20 ms

With these illumination times, theoretical modelling shows that there will be non-specific damage to the tissue surrounding the vessels. This finding is reflected in the literature review below.

The literature shows that blanching of the skin occurs with these illumination times. Several mechanisms are involved, depending on the degree of blanching obtained.

Arndt (1984) obtained total whitening of the skin when the illumination time was between 50 and 200 ms. The fluence was between 20 and 40 J/cm^2. Histological work showed that there was non specific necrosis of the epidermal and dermal tissue. The blanching response was likened to that of egg white when cooked.

Walker *et al* (1989) used a 1.3 mm spot size, 578 nm wavelength and laser power of 1.6–3.6 W. The illumination times used were between 100 and 150 ms, with a fluence between 11 and 25 J/cm^2. The exact dose depended on when the skin first appeared

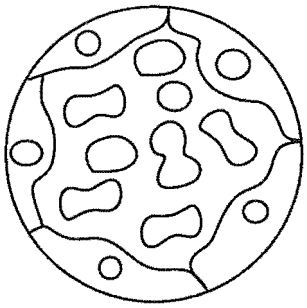

(a) Ectatic blood vessel with red blood cells shown.

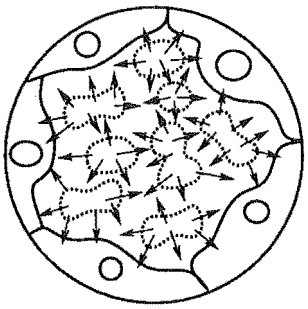

(b) Absorption of the laser light heats red blood cells, which are damaged. Heat flows outward.

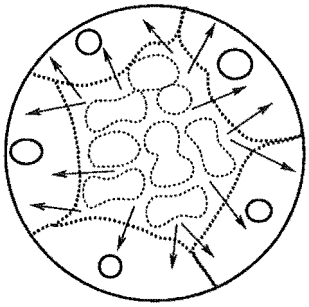

(c) Endothelial walls damaged, the osmotic pressure allows the flow of Na^+ ions and water into the cells.

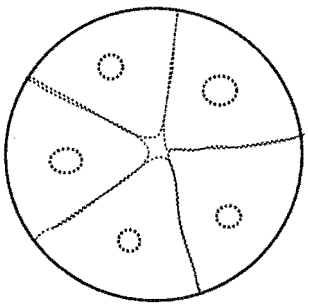

(d) Damaged endothelial cells swell to exclude red blood cells, and occlude the lumen.

Figure 8.3. Sequence of thermal damage to ectatic capillary during and immediately after heating by 578 nm laser illumination.

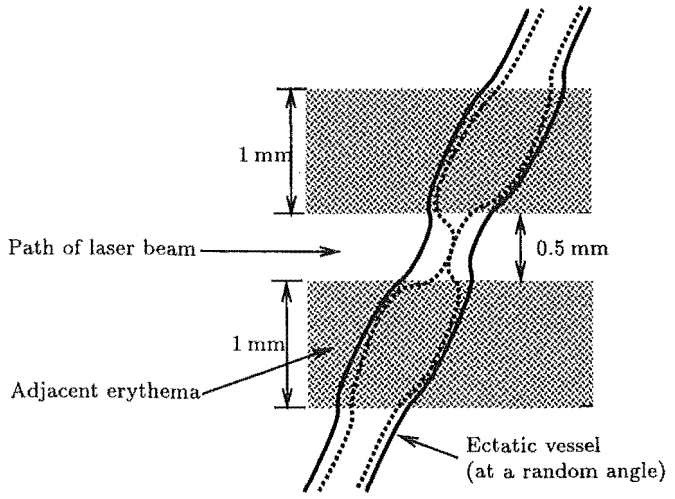

Figure 8.4. Erythema as a result of laser treatment at 578 nm.

to blanch, this minimal blanching being the endpoint. No haemorrhage was observed and occasionly red blood cells were ruptured.

Orenstein and Nelson (1990) used a 0.1 mm spot diameter, 577 nm wavelength, laser power of 0.7-1 W, and illumination times between 50 and 100 ms. Individual vessels were treated with the laser beam. The treated site appeared blanched, surrounded by erythema as a result of vasodilation induced by local hyperthermia. The blanched areas overlying the treated blood vessels formed a series of tiny superficial crusts, which required five to six days before complete healing.

From the results described above, it is understandable why the blanching endpoint has been linked to "nonselective damage of the vessel wall, dermis, and epidermis." (Mordon *et al*, 1993). Two causes of the blanching response are provided in the literature.

Goldman *et al* (1976), Sheehan-Dare and Cotterill (1993), and Neumann *et al* (1992) have linked the blanching response with a change in the optical properties of the overlying tissue. Consequently, the underlying vessels are no longer observable as light cannot penetrate through the damaged epidermis.

Dinehart *et al* (1993) observed the illuminated vessels with magnification and reported that they constrict. The illumination time used was not stated, but from the text we infer that it was 200 ms.

We conclude that the vessels constrict as a result of the incident laser beam when the exposure time is longer than 4 ms. This will not be observed if sufficient energy is absorbed in the epidermis so that the optical properties are changed.

8.3 Electron microscopy, 4 ms illumination times

We are particularly interested in the use of illumination times in the optimal range of 1-10 ms, as predicted by our modelling. The results from these computer models state that with illumination times in the range of 1-10 ms there will be minimal damage to the surrounding non-vascular tissue, but the endothelial cells of the vessel wall will be thermally necrosed. In this section, we report the electron microscopy (EM) changes in port-wine stains following treatment with 3.6 ms illumination times. These results have been submitted for publication (Smithies *et al*, 1995).

8.3.1 Method

Two consenting patients with dark red port-wine stains who had not previously received treatment for their port-wine stains participated in this study.

Rotteleur *et al* (1988) describe thermal accumulation, where the heat generated at a previously treated point in the skin is conducted to the point currently being treated. They note that this effect causes variability in the results obtained. To reduce this, the scan lines are separated by one spot diameter.

Pickering *et al* (1990a) showed that increasing the power density decreased the illumination time required to obtain blanching. They used a spot size of 1.3 mm, laser power of 5 W, illumination time of 40 ms, and a power density of 370 W/cm^2. If the illumination time is to be in the millisecond range the power density required will be an order of magnitude higher. To obtain the requisite power density, the spot diameter was reduced to 0.3 mm as the available power is limited to 5 W.

The desired response was transient blanching. This endpoint is the same as that used by Laffitte *et al* (1992). The skin that the laser beam has just passed over has paled in colour. This blanching or paling is transient as erythema is observed after treatment. Erythema occurs because the previously empty vessels have dilated and allowed blood to flow into the skin in response to the thermal injury. Whitening is then observed, as intra-cellular fluid has leaked from the damaged vessels. This is the "Triple Response", which is described in more detail by Ganong (1965).

The presence of transient blanching implies that the optical properties of the epidermis have not been substantially altered as erythema is observed. Further, the initial blanching seen indicates that there has been constriction of the ectatic vessels in the port-wine stain due to thermal damage.

On the day that the biopsies were taken, the laser power was 5 W ($\pm$ 10%) as measured with a Scientech 364 power meter. Setting the illumination time to 3.6 ms provided the desired endpoint. From the illumination time, spot size, spot separation, and laser power we calculate that the fluence was 10 J/cm^2.

When setting the illumination time, it was noted that an illumination time of 4.2 ms resulted in permanent blanching. This was undesirable, as it indicates the presence of damage to the non-vascular components in the skin. An illumination time of 3.0 ms had no effect. This too was undesirable, as the vessels remain undamaged.

5 mm punch biopsies were taken pre-treatment, immediately post-treatment and 24 hours after treatment. The biopsies were fixed in 2.5% glutaraldehyde buffered with PIPES, post-fixed in 2% osmium tetroxide, stained with 2% aqueous uranyl acetate, dehydrated through alcohol series and flat–embedded in resin (Spurr, 1969).

Semi-thin (1 μm) and ultra-thin (silver-gold) transverse sections were cut on a LKB ultrotome III using a diamond knife (DuPont). Semi-thin sections for use with light microscopy were stained with toluidine blue and viewed in a Zeiss Axioskop

microscope. The ultra-thin sections for electron microscopy were stained in lead citrate, mounted on uncoated 100 mesh or coated slot grids and viewed in a Philips CM12 electron microscope operated at 100 kV.

Depth measurements were carried out using an interfaced MIA image analysis computer. The maximum distance from the epidermal/dermal boundary that thermally necrosed vessels were found was recorded. This has been defined by Tan *et al* (1988) as the penetration depth.

8.3.2 Results

Epidermis

The principal absorber of visible light in the epidermis is melanin. This pigment will absorb a fraction of the beam, causing the epidermis to rise in temperature. The junction of the epidermis and dermis is rich in melanin (Wood and Bladon, 1985), and this part of the epidermis will experience a larger temperature rise than other parts. When the fluence is 10 J/cm^2 few, if any, changes are observed in the epidermis (fig 8.5). These cells are normal in appearance with no discernable loss of structure.

Red blood cells

The laser light is strongly absorbed by the red blood cells, which accounts for the pronounced damage observed, as shown in figure 8.6. Vacuoles, or holes, have appeared in the red blood cells, which is indicative of the formation of steam. The walls of the red blood cells have been damaged, indicating that these cells are no longer viable.

No agglutination of the red blood cells was observed. Most of the vessels were empty after treatment. It is possible that the blood could have leeched out during the processing stages. This is a problem when obtaining specimens (Niechajev and Clodius, 1990).

Vessels

The heat generated in the red blood cells is conducted to the vessel walls, causing thermal necrosis of the vessel walls. In fig 8.7, two endothelial cells of a vessel at a distance of 150 μm from the epidermal/dermal boundary are shown. The uneven black lines indicate the boundary of the nucleus of each cell. The nucleus of each cell has one break in the boundary. Inside the nucleus of these cells, there is chromatin aggregation and nuclear vacuolation. This is evident in the figure from the lack of structure.

Twenty four hours after treatment, the vessels contained large numbers of platelets. The vessel walls were infiltrated with collagen and platelets. These signs show that

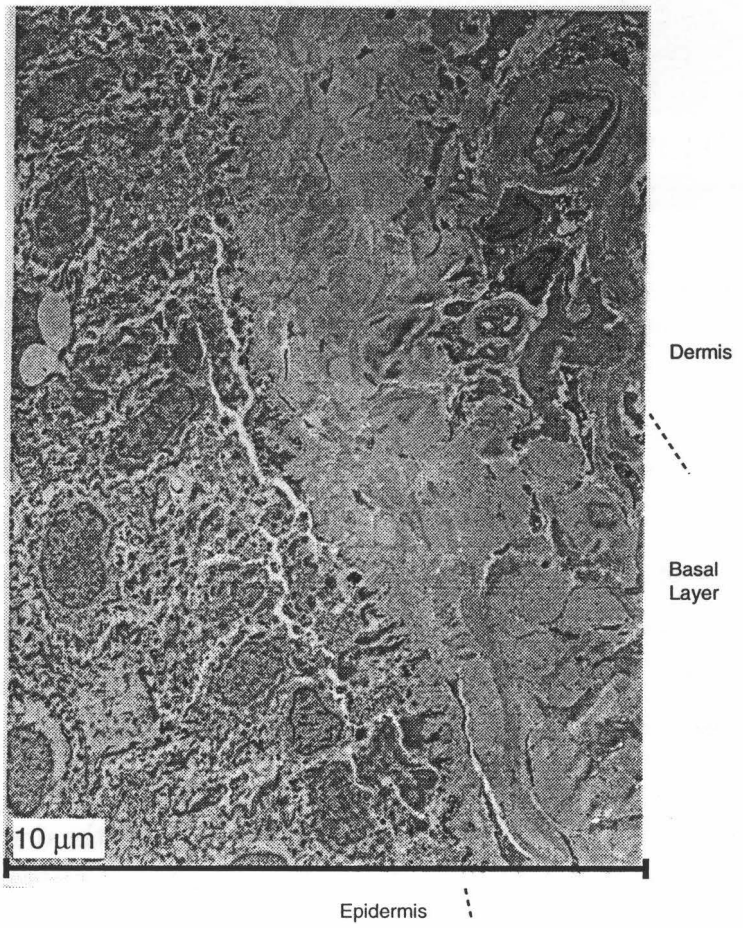

Figure 8.5. The epidermal/dermal junction 24 hours after treatment.

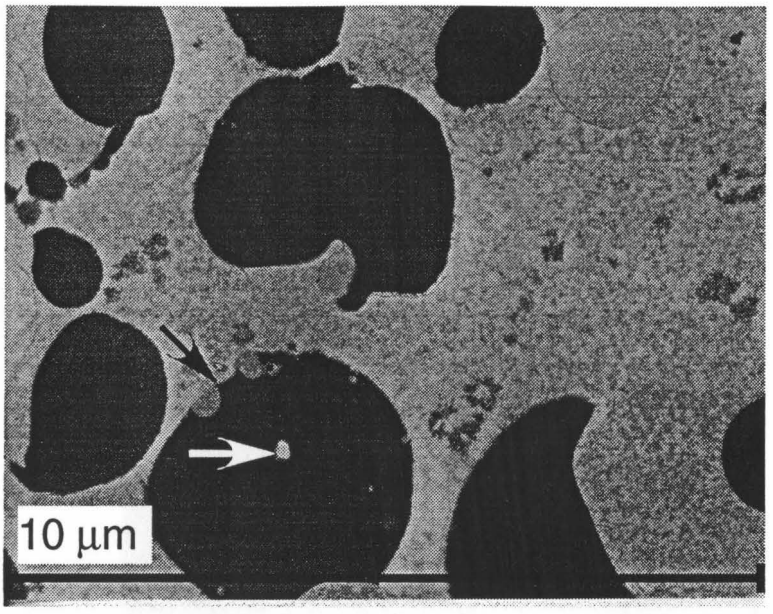

Figure 8.6. Damaged red blood cells immediately following treatment with an illumination time of 3.6 ms. The boundary of the red blood cells are blurred (black arrow). Vacuoles (white arrow) have formed inside the red blood cells.

the vessel has been irreversibly damaged and will no longer contain blood.

For all patients, the severity of the damage to the vessels decreased with increasing depth. At a distance of 150 μm from the epidermal/dermal boundary there was severe damage to the vessel walls. The severity of the damage decreased as the depth of the vessels increased. At a distance of 500 μm there was no discernable ultrastructural changes to the vessel walls. This finding is unsurprising. The theoretical work in chapter 4 shows that the shallow vessels attenuate the laser beam, reducing the amount of light that reaches the deeper vessels. Consequently, the degree of damage in the deeper vessels will be less than in the shallow vessels.

There was minimal conduction of heat away from the vessels. The results showed that non-vascular components in the skin such as the nerve fibres were undamaged following treatment.

8.4 Discussion

In this section, we discuss the clinical issues when port-wine stains are treated. We examine the endpoint obtained, the appropriate wavelength, and the illumination time.

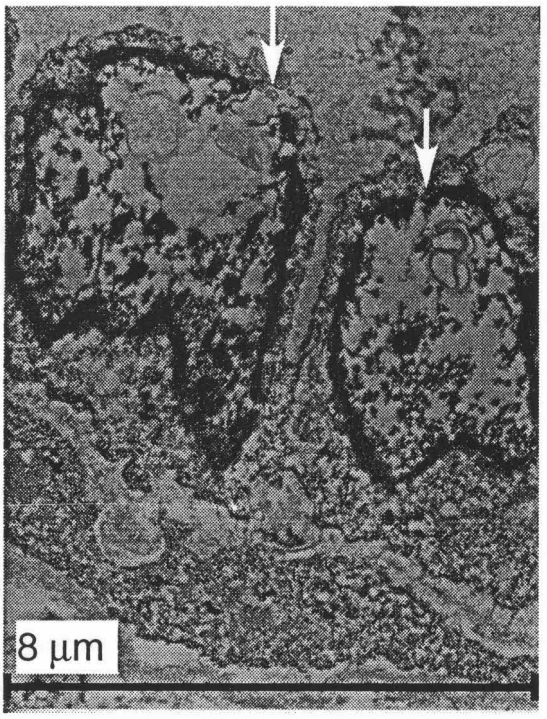

Figure 8.7. Two damaged endothelial cells of a vessel at a distance of 150 μm from the epidermal/dermal boundary immediately after treatment. These cells have been thermally necrosed. The boundary of the nucleus of both cells is shown by the uneven black line. White arrows are used to mark breaks in the boundary.

8.4.1 End point of treatment

In this subsection, we propose an explanation of why the purpuric like endpoint is obtained with illumination times of 0.4 ms, while blanching is obtained with exposure times of 4 ms or longer.

Purpura, which is obtained after illumination times around 0.001 ms, has been described in the literature. The steam generated in the red blood cells has caused rupture of the vessels in the skin. There is extravasation of the red blood cells throughout the dermis. Following treatment, there is no long term colour change. These clinical findings are in agreement with the results from computer modelling.

With illumination times in the 0.3-0.5 ms range, 3-5 mm spot diameter, psuedo purpura is obtained. There is minimal extravasation of the red blood cells. After treatment, the vessels contain a coagulum of agglutinated erythrocytes, fibrin, and platelet thrombi.

The damage mechanism of Marini *et al* (1992) proposes that the endothelial cells swell in response to the thermal damage inflicted. This explains the transient blanching response obtained following treatment with a 0.3 mm spot diameter, 4 ms illumination time. If this mechanism is correct, one would expect it to occur with 0.4 ms illumination times.

With sub-millisecond illumination times, the spot diameter is in the 3-5 mm range. Consequently, more of the vessels in the skin are damaged during the laser pulse. The damage extends further into the skin, so some of the vessels which carry blood from the deeper dermis to (or from) the port-wine stain are damaged also.

We propose that the endothelial cells do expand following treatment with sub-millisecond illumination times as a result of thermal damage. However, the blood is contained within the treated vessels as there are insufficient "escape routes" for all the blood in the treated area to leave the treated area following treatment.

Thus, with a smaller spot there will be more escape routes for the blood following treatment. Consequently, the fluence would have to be increased (assuming constant illumination time), to ensure that sufficient vessels were treated so the blood is contained in the treated area. Tan *et al* (1988) has examined the effect of spot size on the skin of albino guinea pigs. The wavelength was 577 nm, illumination time was 0.36 ms, with the spot sizes 1, 3, and 5 mm. The fluences required to cause a blue-gray discolouration were 27.0, 6.0, and 4.0 J/cm^2, the higher fluences for the smaller spot sizes.

Broska *et al* (1994) report the private communication of Geronemus, R. and Applebaum, J. who obtained good objective clearing of telangiectasias with much less purpura when

a a 2 or 3 mm spot diameter is used with a flashlamp pumped dye laser. However, these results are preliminary. Presumably, the purpura referred to is the purple colour in the treated spots, and not the overall appearance of the skin.

This explanation for the processes that occur in the skin with sub-millisecond illumination times is supported by the results obtained when treating telangiectasisas in our clinic. A sclerosing agent is injected into the larger vessels, which causes these vessels to constrict. The skin is then scanned with the laser beam, which thermally damages the smaller vessels. Often, the blue-gray colour associated with purpura is obtained. The blood in the treated skin cannot leave the treated site, and so the purpuric like colour is obtained.

8.4.2 Wavelength

In this subsection, we discuss the issues involved in the debate over the appropriate wavelength.

The results from theoretical calculations are clear: yellow light at or close to the 577 nm absorption peak of haemoglobin will be ideal for treating port-wine stains. This is in agreement with the clinical results in the literature which have been quoted in subsection 8.1.4.

There is some disagreement. Ratz and Bailin (1987) has argued that the CO_2 laser can be used to treat port-wine stains. The sentiments expressed have been repeated in Sheehan-Dare (1993). He states that the pulsed dye laser may not be the most effective treatment, and that a considerable proportion of lesions do not respond. On the basis of his experience, lesions that do not blanch on pressure (which are often dark in colour and raised) respond poorly. With these, the 532 nm output from a frequency doubled Nd:YAG laser in conjunction with an automated treatment device (Laffitte *et al*, 1992) would be more appropriate.

Deeper cavernous areas or hyper-trophic tissue may require more non-specifically destructive treatment with alternative lasers such as the Nd:YAG or CO_2 lasers to improve the appearance.

He continues,

> Mathematical modelling can determine theoretically ideal laser variables for treating port-wine stains. The work has made great contribution to our understanding of the subject, although the structural diversity of port-wine stains confounds the best attempts at mathematical modelling and there is no substitute for good clinical assessments and comparisons

of different laser systems.

In making these statements, R. A. Sheehan-Dare has highlighted several difficulties in the interpretation of the results obtained from computer models and clinical work.

It is improbable that the absorption properties of blood will change significantly between individuals. This is dependant on the level of oxygen carried by haemoglobin, a protein molecule that is contained in the red blood cells. The absorption spectrum of visible light in the epidermis depends on the concentration of melanin on the epidermis. We expect then that there will be some variation between individuals, but not enough to support the use of a laser that does not produce yellow light.

For the regions where there is hyper-trophic tissue and nodules, the problem is two fold. The ectatic capillaries have to be removed, along with the raised tissue to obtain the desired result. An ablating type of laser, (for example CO_2 laser) is necessary to remove the surplus tissue. In our clinic, such raised areas are removed with surgery.

When a very high fraction of the skin is blood, which is the case with cavernous areas, more laser light is required so that the required level of damage to the vessels occurs. Many of the vessels in the skin have a diameter that is sufficiently large that exposure times of 0.45 ms will not cause the required thermal damage. Consequently, the pulsed dye laser will be ineffective for such lesions. We expect that satisfactory treatment results for these lesions can be obtained when longer exposure times are used. Longer exposure times can be obtained with minimal damage to the surrounding tissue when automated treatment device is used.

8.4.3 Illumination time

We have described the effect of the illumination time in section 5.5. The effect of the illumination time is poorly understood by various authors in the literature. In this subsection, we give two examples of this lack of understanding.

Tan *et al* (1990b) compared the effects of the pulsed dye laser (578 nm) and a copper vapour laser (578 nm) on pig skin. With the pulse dye laser, the exposure time was 0.4 ms. There was minimal damage to the non vascular tissue. This is to be expected from the theoretical results described previously. With the copper vapour laser, the illumination times were greater than one second. From the theoretical results in chapter 5, we estimate that the use of this illumination time will cause widespread heating (and damage) of the the non vascular tissue. In this study, Tan

et al. erroneously attributed the widespread damage obtained to the design characteristics of the laser, and not to the excessively long illumination times.

A second example is in the review article by Wheeland (1993). When describing the effects of the argon-ion laser, he states,

> Virtually all of these negative effects can be blamed on a lack of precision in the laser-tissue interaction that results from the exposure of skin to energy from the argon-ion laser. The most likely reason for these effects is the fact that the argon-ion laser emits its energy at a trough in the absorption spectrum of oxyhemoglobin. This reduces the potential confinement of the thermal injury to blood vessels, and allows heat to be distributed more widely throughout the dermis.

An alternative way of putting this would be to say that when the wavelength is not 577 nm, there will be damage to the non-vascular tissue.

When describing thermal relaxation time, he repeats the comment found in numerous places in the literature and states, "as long as the duration of the laser pulse is shorter than the thermal relaxation time for the blood vessels found in the port-wine stain, the thermal injury can be effectively restricted just to the blood vessels." This statement is contradictory to the previous statement that we quoted, yet both were found in the same paper.

8.5 Conclusion

The use of yellow light (577-585 nm) for the treatment of port-wine stains is supported. This wavelength is strongly absorbed by the blood and less strongly absorbed by the epidermis. The use of yellow light will cause vascular specific damage, provided the illumination time is in the 0.3-10 ms range.

When the endothelial cells of vessel walls are thermally damaged, they expand, which removes the blood from the treated area. It may not be possible for the blood to be removed from the treated area as the "escape route" for the blood is blocked. In this case, the blood is trapped in the treated area and the skin turns a purpuric colour.

The purpuric colour has been erroneously described by some authors as purpua, which implies that there is rupture of the blood vessels. We describe the clinical effect as psuedo purpura.

EM results show that with illumination times of 3.6 ms, 5 W of yellow (578 nm) light, spot size 0.3 mm, thermal damage has been confined to the blood vessels.

There are minimal changes in the epidermis. Damaged vessels are found to a depth of 0.5 mm into the dermis. Following treatment, the skin blanches as the damaged capillaries constrict, removing the blood in the damaged vessel. Erythema is then observed, as the previously empty capillaries have dilated in response to the thermal damage caused.

Increasing the energy incident on the skin from the level required to cause transient blanching results in permanent blanching of the skin. In this case, the erythema that results from treatment cannot be observed as the optical properties of the epidermis have changed. These changes are tempory as the damaged epidermis heals, and the red colour associated with a port-wine stain returns.

Chapter 9

Measurement of the time before blanching commences

> We measure the time elapsed before the colour of the skin starts to change from red to white.
> As the skin changes colour, less light will be absorbed in the skin, and so more laser light will be scattered out of the skin. A qualitative measure of the amount of scattered light is obtained with a photodiode.

The laser beam passes through the scanner and is incident on the skin surface. Some is reflected off the skin surface. Some light travels into the skin, and is then backscattered out of the skin. The scattered and backscattered light will be referred to in this text as the "remitted light". It is the purpose of this chapter to describe how a photodiode is used to provide a qualitative measure of the quantity of remitted light. The results obtained are reported.

Prior to the introduction of the computer controlled scanner, the laser beam was passed down a fibre and through a handpiece. The handpiece was scanned across the skin by hand. During treatment, the light level in the room is observed to change rapidly. This was thought to be caused by the skin blanching beneath the laser spot, and so more light will be remitted from the skin. Two questions were asked, "1)Can the change in light level be used to tell us the rate at which the skin changes colour?", and "2)Can a feedback device for the SCANALL system be devised that moves the spot when the skin below the spot has blanched?".

The computer controlled scanning device described in chapter 7 is used to scan the laser beam across port-wine stain skin. A photodiode is used to obtain a qualitative measure of the amount of remitted light during the scanning procedure. In section 9.1

we describe the equipment that was used to measure of the amount of remitted light. The results obtained from the equipment are described in section 9.2. A discussion of these results is contained in section 9.3. Finally, in section 9.4 we summarise the results obtained.

9.1 The recording system

The various components of the system that was used to give a quantitative measure of the amount of remitted light is given in this section. We first give an overall picture of the various components in the system in subsection 9.1.1. In subsection 9.1.2 there is a detailed description of the unit which measures the light level. The technique used to record the data generated is described in subsection 9.1.3. We describe the results of the various tests to check the reliability of the system in subsection 9.1.4.

9.1.1 Overview of the measurement system

The layout of the equipment necessary to record the quantity of remitted light is shown in figure 9.1.

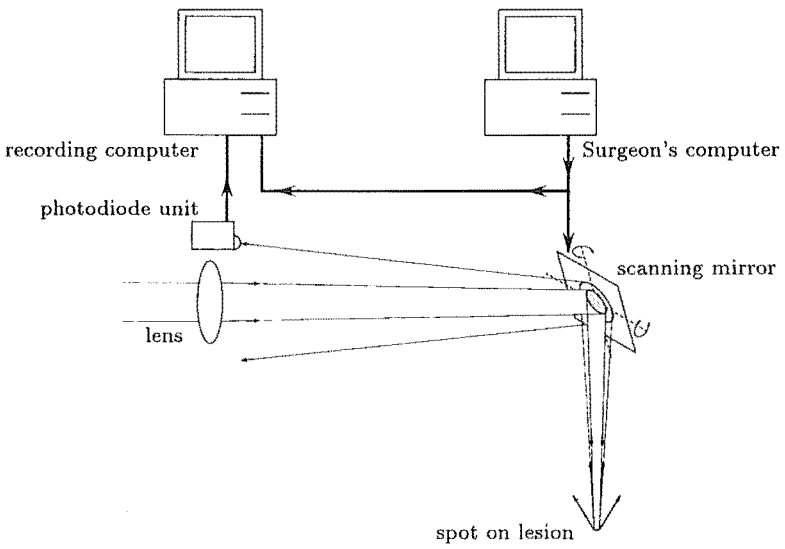

Figure 9.1. The apparatus used to record the reflected light during laser treatment with the computer controlled scanner.

As noted in subsection 7.3.8, the output of the copper vapour laser is quasicontinuous, that is, every 67 μs a 20 ns pulse of light is generated. If the average power of the beam is 5 W, then the average power in each pulse is 17 000 W. Such a high peak

power is advantageous as the light detecting system need only detect the magnitude of the peak levels and the effect of ambient light can be ignored.

The laser light is focussed by the lens and reflected off the stepped mirror onto the lesion. Some of the remitted light passes back through the scanner, where it is detected by the photodiode unit.

The photodiode unit is adjacent to the lens (figure 9.1) as this will minimise the effect that movement of the scanning mirror has on the light level detected.

The signals generated by the photodiode unit are recorded by an Amiga B2000 computer, referred to in figure 9.1 as the recording computer. The time at which each pulse occurs is recorded. If either of the two stepper motors began to move when a light pulse occurred, this also is recorded. The information obtained was stored in a text file for later processing and display.

9.1.2 Photodiode unit

A high speed photodiode (MRD500, 5 ns rise time) is used to measure the amplitude of the laser pulse. The best method to measure the voltage induced in a photodiode is to connect the two input leads of an op-amp to the anode and cathode of the photodiode (DuPuy, 1989). The op-amp used (NE5539N, 15 ns rise time), keeps the voltage across the photodiode constant so the capacitance in the photodiode does not increase the response time.

Initially, it was unknown how the output of the op-amp changed when the laser pulse was present. Various trials were carried out to determine this. We describe the results from one trial below. From these results, the appropriate circuit was constructed to process the output of the op-amp. Different levels of laser light were directed onto the photodiode and the output of the op-amp was measured with a high speed digital storage oscilloscope. Two results are shown in figure 9.2. In these results, the photodiode and op-amp were not enclosed in a copper box. Consequently, electrical noise generated by the laser is detected by the photodiode. This is shown by the small oscillations which last for 1 μs after the large spike.

The height of the pulse depends on the quantity of light incident on the photodiode. Small variations in the base line are present, which is a result of the analogue to digital (a/d) noise in the oscilloscope. With this result, the complete photodiode unit could be designed, and a simplified version of the circuit is shown in figure 9.3.

The maximum voltage produced by the op-amp is stored in the capacitor. This analogue value is read by the analogue to digital chip, which digitizes the signal and places it on eight data lines that connect to the computer. The data ready line is

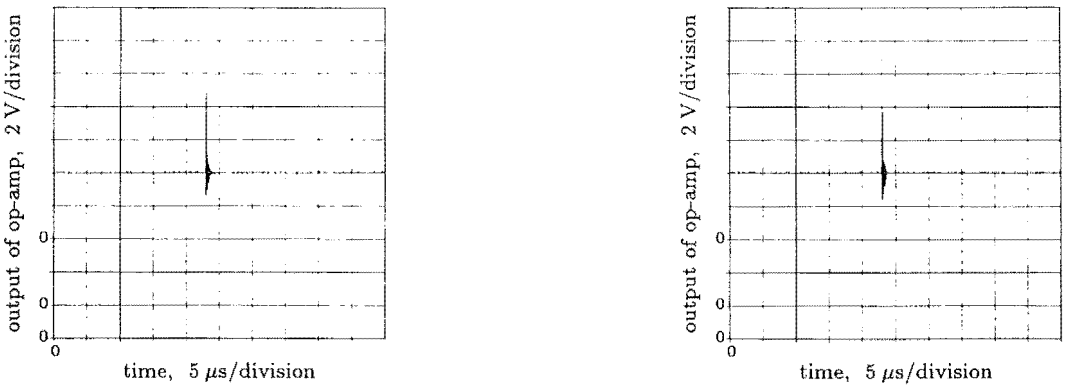

(a) Medium light level (b) High light level

Figure 9.2. The signal produced by the op-amp for two different light levels.

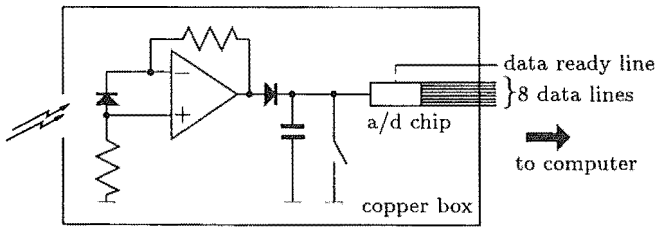

Figure 9.3. Schematic diagram of the circuit used in the photodiode unit.

set "low", to indicate the presence of data. After 50 μs, all nine data lines are set "high" and the capacitor is discharged, ready for the next laser pulse. During the 50 μs interval the computer must detect the "low" state of the data ready line and read the data on the eight data lines. When the next pulse of the laser beam occurs, this process is repeated.

The analogue to digital converter, op-amp and photodiode are mounted in a copper box to prevent electrical noise generated by the laser affecting the result.

9.1.3 Recording computer

We describe in this subsection the steps taken to ensure that the recording computer obtained every data element generated by the photodiode unit.

The recording computer is a multitasking machine, and it is inevitable that the CPU will not be available to read every data element generated by the photodiode unit. For this reason, all interrupts to the CPU on the recording computer were turned off, ensuring that the amplitude of every light pulse detected is recorded.

A machine code subroutine was written to read information from the photodiode unit, the surgeon's computer, and the system clock (720 kHz). From this information, we can determine the time elapsed between the start and finish of any section of data.

When the interrupts are turned off, a machine code subroutine has access to fourteen registers. In comparison, a subroutine written in a high level language such as C on this computer has access to four registers. Access to an additional ten registers makes the program quick enough that it can read every data pulse generated by the photodiode unit.

9.1.4 System testing

We describe in this subsection the tests carried out to ensure the system operated correctly.

First, the computer program was tested to see if it would miss any of the data points generated by the photodiode unit. When a 19 kHz data signal is read by the computer, 53 seconds is required to read 1 million data points, as expected. The laser generates pulses of light at a rate of 15 kHz, so the computer must be able to detect all of the data points.

The photodiode unit was tested for linearity. Various surfaces were placed beneath the laser spot and then half of the laser beam was occluded. As expected, the reading produced dropped by 50%. When the laser beam is incident on a mirror, the

photodiode unit produced a maximal value. This value is considerably higher than the value obtained during the laser treatment of port-wine stains. The photodiode unit was found to be linear up to this value.

The electrical noise generated by the laser was not detected by the photodiode unit. No signal is produced when the laser beam is blocked. The results obtained were consistent and repeatable, a further proof that the photodiode unit was unaffected by the electrical noise generated by the laser.

The uniformity of the output was checked by placing a piece of steel under the laser beam. The optical properties of the steel should not change, yet small variations in the output are observed (figure 9.4). Some digitisation noise is present, and there are fluctuations in the laser power. These fluctuations occur on a timescale of tens of milliseconds, and are small in size (± 2%).

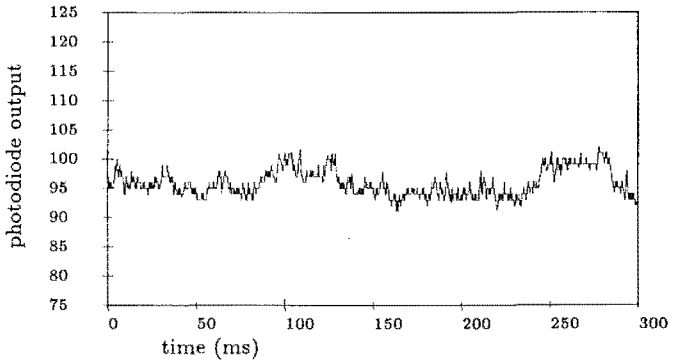

(a) 300 ms of data

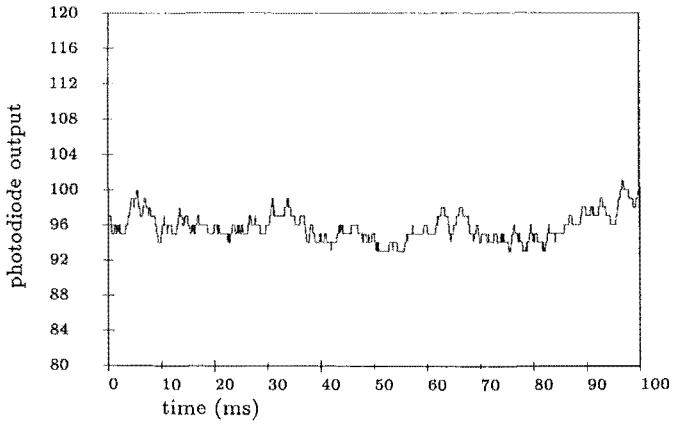

(b) The first 100 ms of data in figure (a) is expanded

Figure 9.4. Reflected light levels while the spot is stationary on a piece of steel.

9.2 Results

In this section, we describe the results for two different treatment modes with the computer controlled scanner.

The two treatment modes used are shown in figure 9.5. The scanning treatment mode is the same as that used when treating port-wine stains. The spot diameter is 0.3 mm, and the distance between the centre of adjacent scan lines is 0.6 mm. For the spot treatment mode, the spot was quickly moved 4.8 mm (16 steps) to an adjacent untreated point on the skin and held stationary for a period long enough to cause the skin to blanch underneath the spot. Where the spot is quickly moved over the port-wine stain, no changes in the port-wine stain are observed. In all cases reported here, the laser power is between 4 and 5 W.

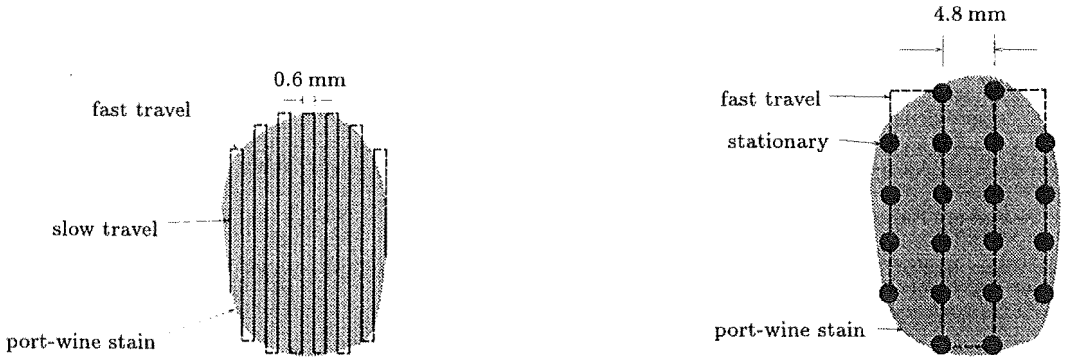

(a) Standard scanning pattern

(b) Spot treatment

Figure 9.5. The difference between the two scan patterns used to determine the rate at which the skin responds to the laser beam.

9.2.1 Scanning

The remitted light levels during the treatment of many patients were recorded. In figure 9.6 there is a sample result, recorded over a period of 2.13 seconds. In this graph, 32 000 data points are plotted.

The height of the line depends on the quantity of light detected. Across the bottom, there is an almost solid black line. This black line is made up of many narrow vertical lines, each of which indicates when the surgeon's computer generates the command for the horizontal stepper motor to move by one step. On this scale the individual horizontal steps are not resolved. Immediately above this black line there are five pairs of short vertical lines. These lines indicate when the command is

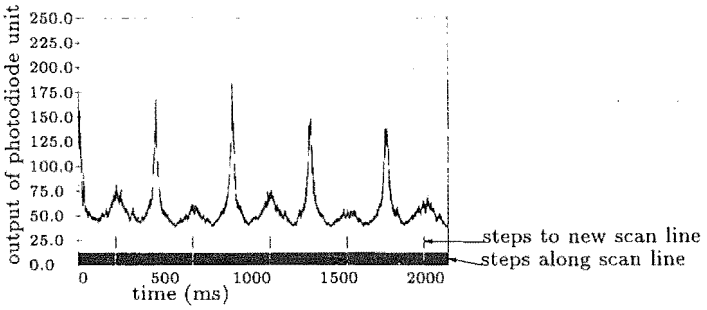

Figure 9.6. Remitted light levels during a 2130 ms interval while scanning the nose of the patient.

generated for the vertical stepper motor to move by one step. (It takes the stepper motors 1 ms to move one step from when the command is generated.)

At 250 ms, the spot is incident on the cheek to the side of the nose. The cheek is perpendicular to the laser beam. As the spot travels horizontally, towards the bridge of the nose, the angle between the skin and the beam alters. Less light is remitted back to the photodiode unit and the value plotted is reduced. After 600 ms, the spot is incident on the bridge of the nose. The skin is perpendicular to the beam and a peak value is recorded. This process is reversed as the spot travels down the other side of the nose. At 850 ms, the vertical stepping motor moves the spot, ready to begin the next horizontal scan line.

We note that the reading obtained when the spot is on the bridge of the nose is twice as high as when the spot is on the cheek. This difference is probably due to the colour difference in the two areas. The bridge of the nose is paler than the cheek, and more light will be remitted.

To show what is happening on the millisecond time scale a small section of the data in figure 9.6 is plotted in figure 9.7.

Every 4.5 ms, the horizontal stepper motor moves the mirror by one step. It takes the motor approximately 1 ms to complete the move. When this stepper motor begins to move, there is a short vertical line at the bottom. There is considerable variation in the output, which is not related to the movement of the stepper motors. The cause of the variation is discussed in section 9.3.

Figure 9.7 is typical of the data obtained when scanning port-wine stains. If the skin blanched underneath the laser spot, we expect that more light would be reflected from the skin. Consequently, the detected light level would rise. Analysis of figure 9.7 shows that the light level does not increase during the time the spot is stationary. In the many seconds of data obtained during the scanning of port-wine stains, no

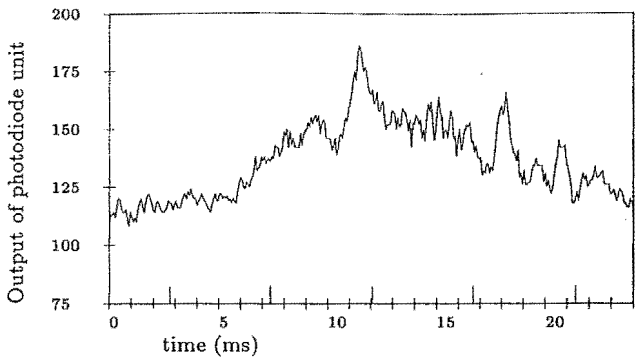

Figure 9.7. Remitted light levels during a 30 ms interval while scanning the nose of the patient.

exception to this rule was found.

We conclude that the skin does not blanch underneath the laser spot. To measure the time required for the skin to blanch, the spot needs to be stationary on a point for much longer. If the exposure time for regular scanning was dramatically increased, there would be a large area of skin that is overtreated. So that a large, representative area of skin could be treated with long exposure times without excessive damage the spot treatment mode was devised and used. The results from this technique are reported in the next subsection.

9.2.2 Spots

The spot technique was used on three different port-wine stains which are described in table 9.1. In figure 9.8 we show the typical response to this mode of scanning. There are many points of white skin within the treated area. Each point corresponds to where the spot was stationary for many milliseconds.

The photodiode results obtained for the three port-wine stains are shown in figures 9.9, 9.10, and 9.11. A running average of 50 was used when processing the data in these figures to remove the noise in the signal. The variation in the output with movement of the spot is clear.

These figures give an overall picture of what is happening. They should be interpreted in the same manner as figure 9.6. Figure 9.11 is similar to figure 9.6 in that the light levels detected by the photodiode unit rise and fall as laser beam moves along each scan line. This is not apparent with figures 9.9 and 9.10 as the scan lines for these two patients were much shorter.

Each of the above graphs shows data collected over period larger than 1.2 seconds.

patient	colour of port-wine stain
A	red
B	purple
C	light red

Table 9.1. The three port-wine stains that received treatment with the spot mode of scanning

Figure 9.8. The pattern observed on the skin after individual points on the skin have been illuminated by the laser beam for more than 40 ms. (Patient A)

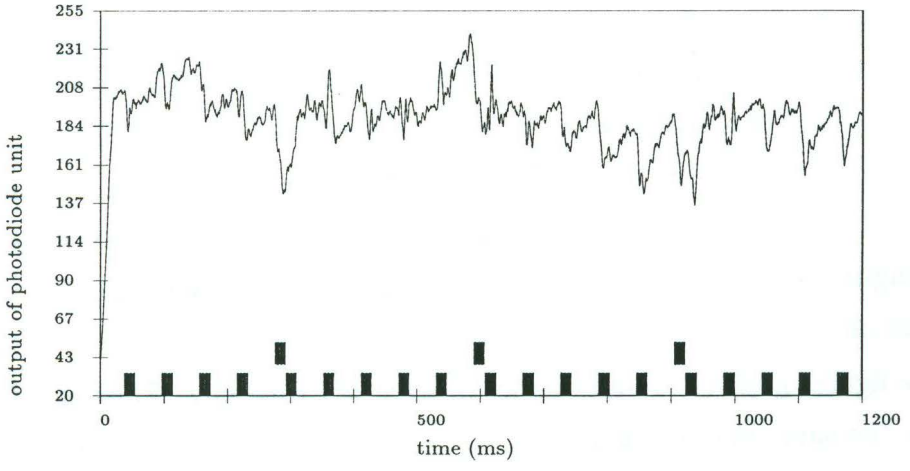

Figure 9.9. Remitted light levels with the spot scanning strategy while scanning a red port-wine stain. Each solid line at the bottom of the graph represents 16 moves of the stepper motors, which moved the spot a distance of 4.8 mm. (Patient A)

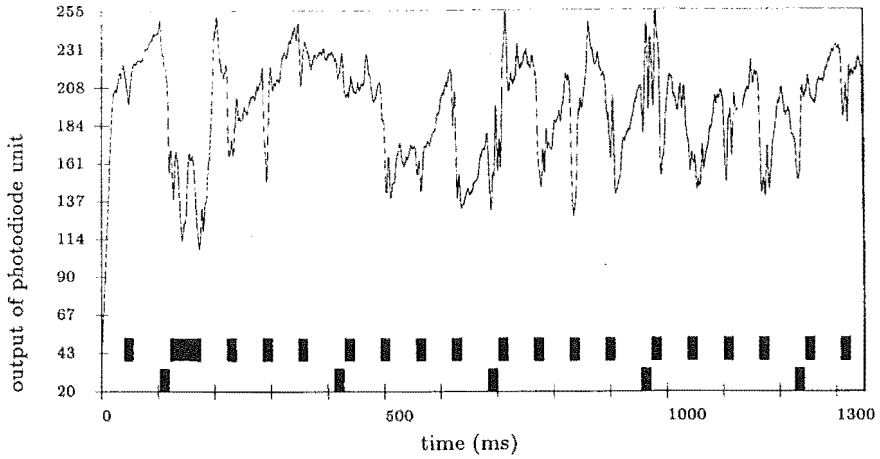

Figure 9.10. Remitted light levels with the spot scanning strategy while scanning a thick purple port-wine stain. (Patient B)

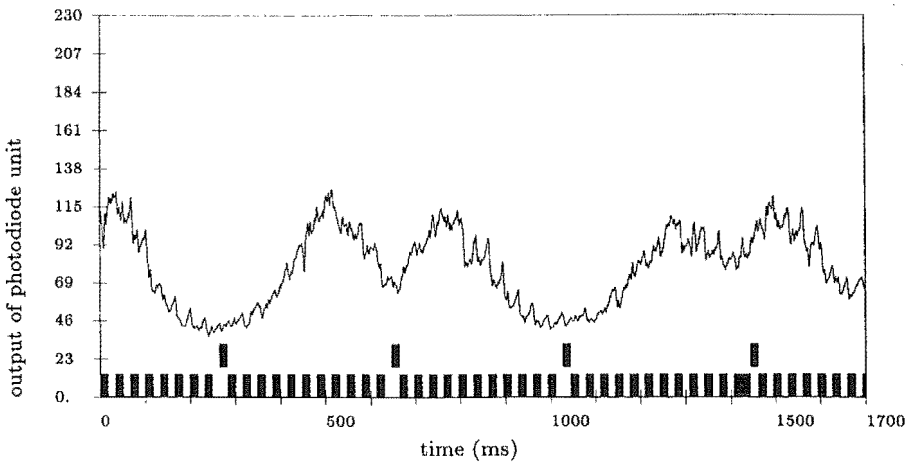

Figure 9.11. Remitted light levels with the spot scanning strategy while scanning a light red port-wine stain. (Patient C)

This corresponds to more than 18000 data points per graph. To show what is happening to the detected light level when the spot is stationary for some of the spots, we have expanded a section of data from figure 9.11 and displayed it in figure 9.12. The last move pulse of every group of moves is highlighted by the long vertical line through the data. As before, a running average of 50 was used when processing this data to remove the noise present in the data.

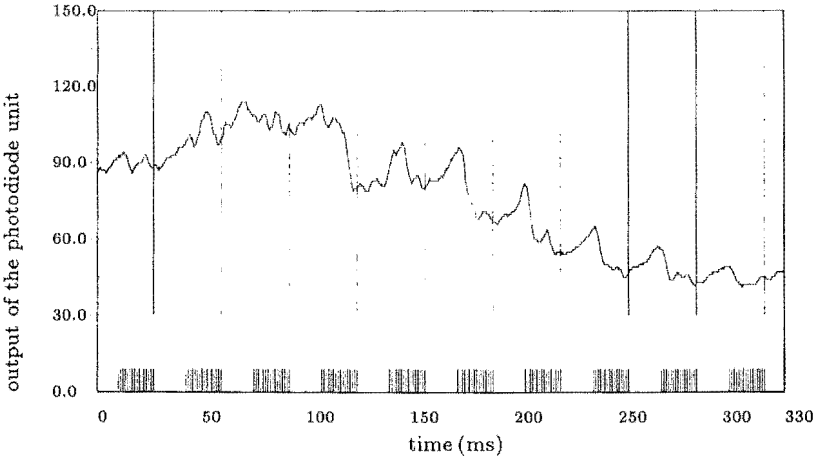

Figure 9.12. Remitted light levels with the spot scanning strategy while scanning a light red port-wine stain. On this scale, individual motor moves can be seen.

The classification of the data for the spots treated is given in table 9.2. The interpretation of the three columns at the right end of the table is given later. Combining the results for the three port-wine stains that were treated: there was a definite rise in 161, no detectable change in 15, and in no spot was there a detectable decrease.

From table 9.2, for most spots (91%), when the spot is stationary on the skin the level of light detected by the photodiode rises. This rise is linked to the blanching response of the skin. Further analysis of the data is carried out to determine the time before the data obtained rises after the spot is stationary. It is uncertain why there is no detectable rise for the 9% of the spots obtained.

The skin that was treated is not uniform. For example, we see that in figure 9.8, there are many fine lines of white inside the red port-wine stain. If the spot is incident on one of these lines, the level of remitted light will be higher than when it is incident on red skin. The increase in the light level, which is associated with blanching, will be less. Further, it may be masked by the noise present. The data for these spots will be interpreted as flat because there is no detectable rise or fall.

For the remaining 161 spots, we require a method to analyse the data obtained. A visual inspection of the data obtained reveals that, generally, the level of light

detected rises at some time after the spot is stationary. We are interested in finding what this time is, as it is presumed that at this time the blanching process commences. The method that is used to analyse the data obtained must meet the following requirements:

1. The raw, unsmoothed data is used so that the results are not affected by the smoothing technique.

2. The same technique must be applied to the data for every spot.

3. It should be simple and straightforward to operate.

Whatever technique is chosen, the data must be broken up into short sections, each section containing the data for one spot on the skin. A typical section is shown in figure 9.13, which was taken from figure 9.12. There is a gap of 1.1 ms between move pulses. As in figure 9.12, the last move pulse of a group of moves is highlighted by a vertical line. The data has not been smoothed to remove the variation in the signal. The variation between data points is magnified by reducing the range in the vertical axis.

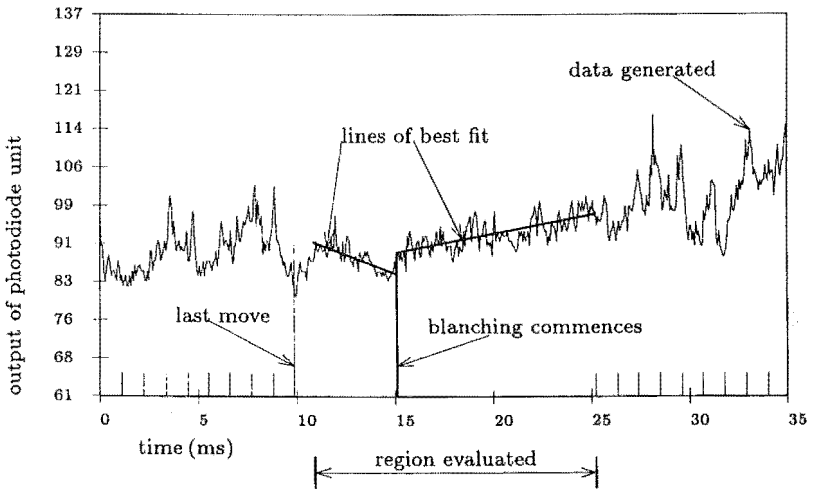

Figure 9.13. Remitted light levels during the treatment of one spot on a light red port-wine stain. Blanching has started 4.3 ms after the spot is stationary.

A computer program was written to process the data obtained. The algorithm used is explained in the following paragraphs with the aid of figure 9.13. This algorithm was chosen as it is relatively simple to implement. In section 9.3.1 we explain why this particular algorithm was chosen, and other possible algorithms.

Only the data in the time interval where the spot is stationary is used. Data obtained when the spot is moving is ignored. Thus, the data from 1 ms after the last

patient	number spots	observable decrease	flat	observable increase	evaluated by computer	evaluated by eye	could not interpret
A	16	0	1	15	13	0	2
B	15	0	0	15	10	5	0
C	145	0	14	131	91	19	21

Table 9.2. The number of of spots acquired from each of the three patients treated. We list the number of these spots that could not be interpreted, or reinterpreted.

move pulse in one group of move pulses to the first move pulse of the next group of moves was used. When calculating the point at which blanching commences in figure 9.13, 231 points were considered.

We make the assumption that the change in the remitted light level is linear in the time intervals before and after blanching commences. The region before blanching commences, and the region after blanching commences, will each be represented by a line. For the 231 points considered, there will be 229 possible pairs of lines to represent the data.

Every line that was used to represent the data was fitted to the data with the linear regression technique. This technique provides χ^2, which is a measure of the "goodness of fit". The χ^2 value for the pre and post blanching line was added together, and the pair of lines with the smallest total was used.

In figure 9.13, blanching occurs 5.3 ms after the last move pulse. One millisecond should be subtracted from the interval between the last move pulse and the point at which blanching commences to correct for the delay between the move pulse and the laser beam coming to rest. From the data in this graph, it is 4.3 ms after the spot is stationary on the skin that blanching commences.

Example results of the processing are given in figures 9.14, 9.15 and 9.16 for nine spots. These figures show how the fitted lines generated by the computer are affected by the noise in the data.

Where the computer program produced a value which is inconsistent with that estimated by a visual inspection, the estimated value is given. The method of estimation is given below. First, we explain why the computer program gave results for some spots which is inconsistent with that obtained from a visual inspection. Some spots contained so much noise that it was uncertain where blanching commenced. These spots were ignored. We list the number of spots for each patient where the time before blanching was measured by the computer, estimated, or could not be determined in table 9.2.

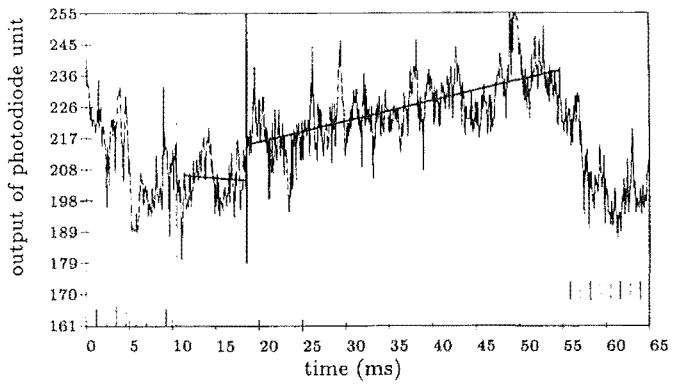

(a) Blanching commences after 6.9 ms.

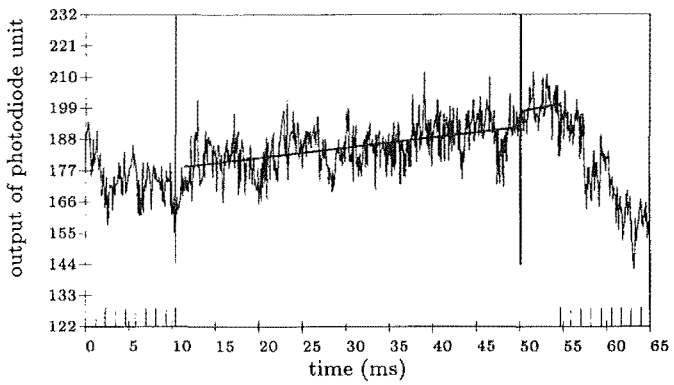

(b) Blanching was calculated to commence after 37.8 ms. The data in this graph does not represent an increase in light level after the spot is stationary. This spot was ignored, as the presence of noise has hidden the change which results from the skin blanching.

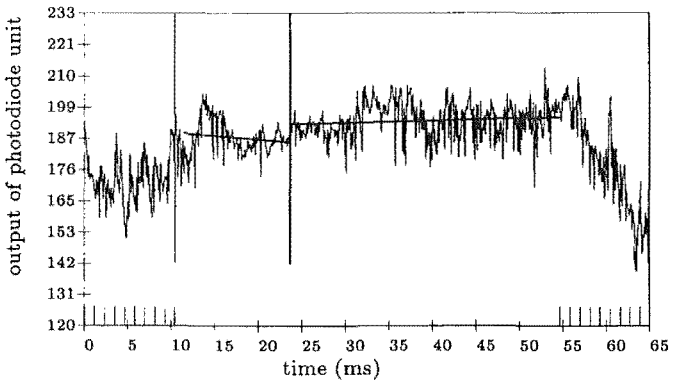

(c) Blanching was calculated to commence after 12.0 ms. The presence of noise has obscured the onset of blanching. This spot is described as flat, with no detectable rise.

Figure 9.14. Photodiode results for three spots on a red port-wine stain (patient A).

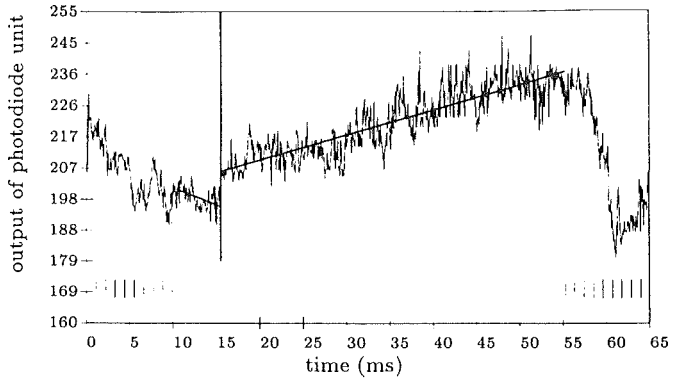

(a) Blanching commences after 4.7 ms

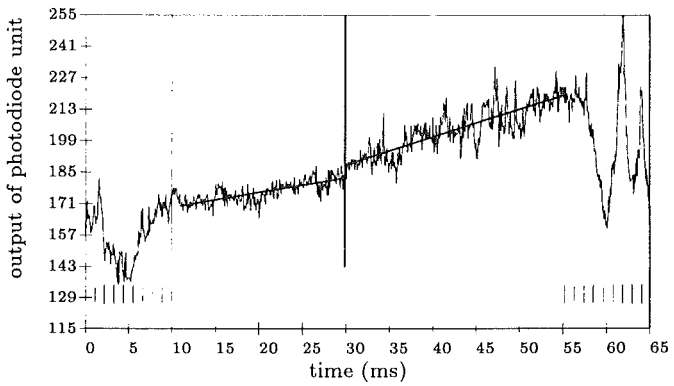

(b) Blanching was calculated to commence after 19.5 ms. The rate of increase in the light level becomes larger over a period of time. The initial increase occurs 10 ms after the last move pulse, which is where the blanching was assumed to start.

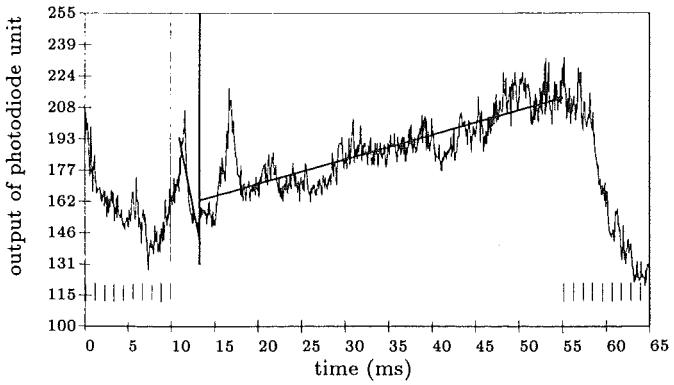

(c) Blanching was calculated to commence after 2.4 ms. The noise spike at t=12 ms was ignored. Blanching was assumed to commence 5 ms after the last move pulse.

Figure 9.15. Photodiode results for three spots on a purple port-wine stain (patient B).

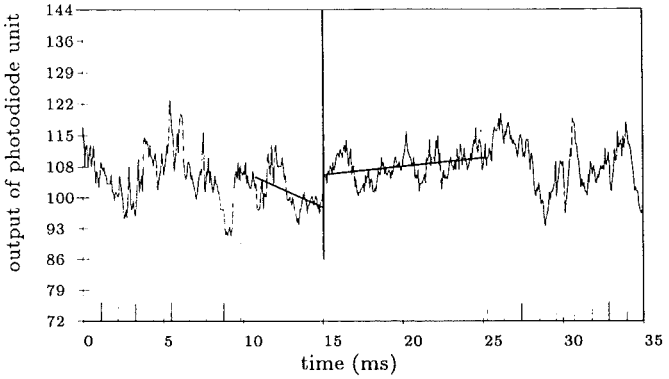

(a) Blanching commences after 4.4 ms.

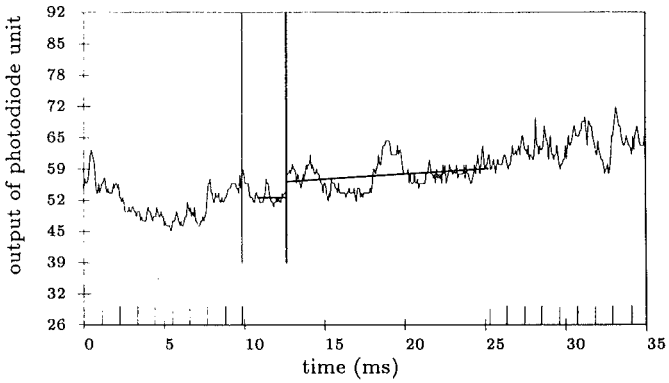

(b) Blanching was calculated to commence after 1.8 ms. It is not until 8 ms after the last move pulse that there is a sustained increase in the light level. At this point, blanching was assumed to start.

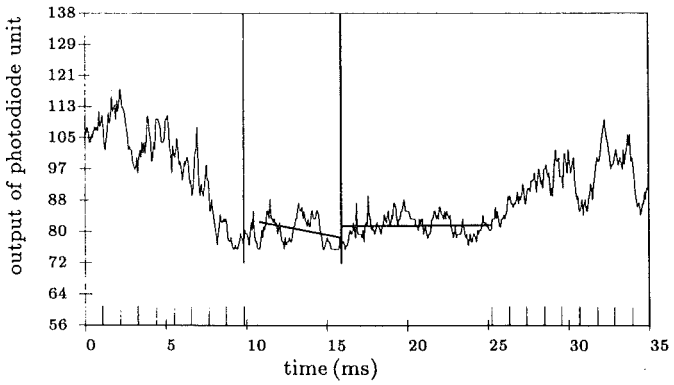

(c) Blanching was calculated to commence after 5.2 ms. There is no sustained rise in the data obtained while the spot is stationary. The data from this spot does not indicate the presence of blanching.

Figure 9.16. Photodiode results for three spots on a light red port-wine stain (patient C).

In most cases, the linear regression technique provided results that were consistent with those obtained by a visual inspection. Listed below are the reasons why the linear regression technique provided results that were different to those obtained by a visual inspection.

1. The data obtained from the photodiode had no net rise, but the computer would still fit two lines to the data. An example of this is in figure 9.16c.

2. The noise in the data was such that it was uncertain where the blanching started. Figure 9.14b is a typical example. The data obtained increases with time which is a product of the blanching obtained.

3. An initial noise spike that lasts several milliseconds, such as that shown at t=12 ms in figure 9.15c, may have an undue effect on the output of the regression routine.

4. The rate of increase in the data obtained increases with time. Consequently, the line fitting routine incorrectly determined the position where blanching commences. An example of this is shown in figure 9.15b.

5. Noise spikes, such as those at t=16 ms in figure 9.15c should be ignored.

The noise in the data cannot be attributed to the photodiode unit. In subsection 9.1.4 we showed that some analogue to digital noise was present, and that the output of the laser varied slightly over a time scale of tens of milliseconds. The noise level in the data increases with high light levels, which happens when the laser beam is normal to the skin surface. With high light levels, a larger fraction of the light detected by the photodiode unit has been reflected from the surface of the skin, and not remitted from inside the skin.

One cannot argue that the noise is introduced by the photodiode unit when the light level is high. In figures 9.4 and 9.13, the light level is close to 100 for both graphs. The noise is present when the laser beam is incident on skin, but not when the laser beam is incident on steel.

A more complex approach to the analysis of the data is required for some of the spots. This approach must be able to ignore noise spikes that last for several milliseconds, such as the one shown at $t = 14$ ms in figure 9.16b. It was decided that the best (and easiest) approach was to visually inspect the data. The data obtained fell into three groups, which we describe below.

kept: Used the output from the line fitting routine where it appeared to correctly determine the point at which blanching commenced. The time before blanching commenced as determined by a visual inspection was identical to that determined by the computer program in figures 9.14a, 9.15a, and 9.16a. From table 9.2, we see that the results from the computer program matched those from a visual inspection for 71% of the spots obtained.

ignored: Noise obscured the transition from pre blanching to post blanching. An example of this is given in figure 9.14b. Those where there is no sustained rise in the data.

reprocessed: Those where the computer program produced a result that was not consistent with that obtained from a visual inspection. We have explained why this happens previously.

Of the 127 spots that were used, the time before blanching commences is provided in the histograms in figure 9.17.

9.3 Discussion

In this section we discuss the results that were obtained with the photodiode unit.

First, we explain why the data from the spot treatment strategy was processed by the computer in the manner described. Other techniques are explained. We examine the causes of the noise that is present in the results. Our measurements show the time required for the skin to change colour for laser power of 5 W. We discuss what would happen when the laser power is altered. Finally, we examine the possibility of using the photodiode unit as the basis in a feedback mechanism for the SCANALL system.

9.3.1 Analysis of the data

In this subsection, we discuss the method used to interpret the data obtained from the spot mode of treatment. Other possible interpretations on the data are discussed.

When the laser beam enters the skin, some is absorbed in the blood vessels and in the melanin rich components of the epidermis. The remainder is backscattered out of the skin. From the results of the Monte Carlo technique, (chapter 4), we see that the maximum fluence will be close to the centre of the laser beam near the surface of the

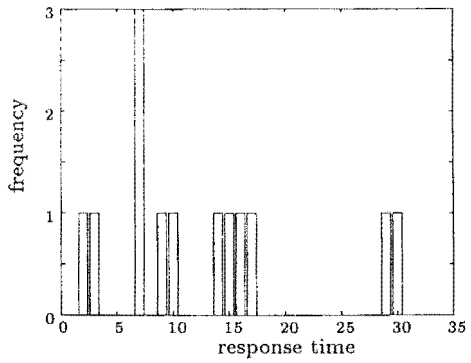

(a) Patient A. Average 12.9 ms.

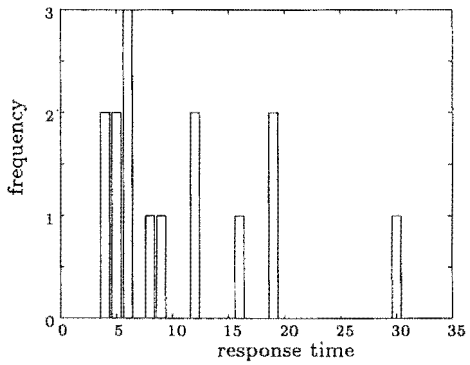

(b) Patient B. Average 10.9 ms.

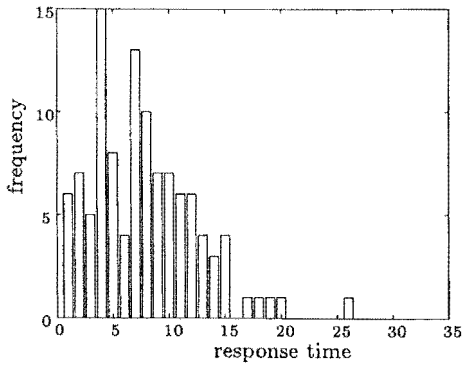

(c) Patient C. Average 7.8 ms.

Figure 9.17. The time required for the three port-wine stains to blanch.

skin. The blood vessels in this region will be the first to respond to the laser beam as the heating in these vessels will be maximised. These vessels constrict, removing blood from the illuminated area. Consequently, laser light will no longer be absorbed in these vessels, and the light will spread further into the skin.

The level of remitted light detected by the photodiode will increase with time as the blood is removed from the skin. With time, the skin will approach the steady state and there will be no further increase in the level of remitted light. Thus, the relationship between the light level detected and time is probably logarithmic. During the initial rise, we approximate it by a linear relationship as it is relatively simple to implement.

This description of the blanching process (due to vessel constriction) assumes that the optical properties of the epidermal and dermal layers are constant. From the clinical work described in chapter 8, we see that the optical properties of the epidermal layer will change so more light is scattered by the epidermis. Consequently, the light will not reach the underlying vessels.

With this description, we have a theoretical model of the data that will be generated. This is shown in figure 9.18.

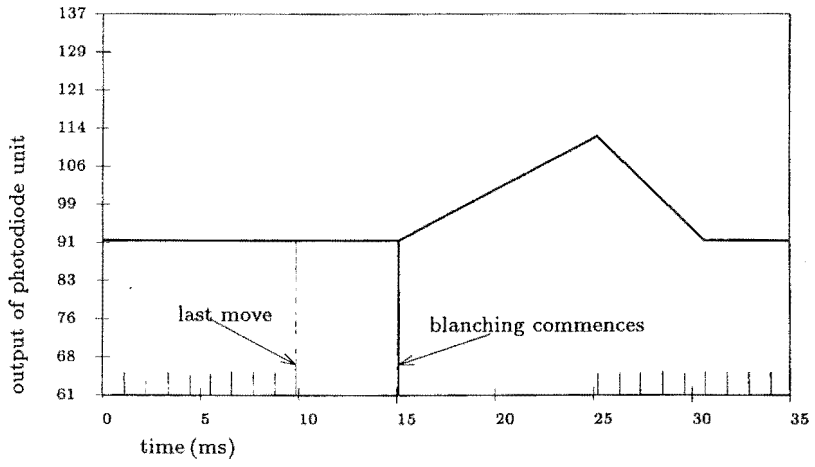

Figure 9.18. The expected output of the photodiode unit when blanching occurs.

The light level is unchanged during the time interval that the spot is moving quickly over skin (which does not cause the skin to blanch) and before blanching commences. When the spot moves again at t=25 ms, the light level decreases as the laser beam is moved away from the blanched region, towards untreated skin. It is not until t=28 ms that the spot is on unblanched skin, but more light is scattered through the adjacent blanched spot than through the unblanched skin. Consequently, the

level detected by the photodiode unit is higher than the baseline level. At t=35 ms, the spot is far away from blanched regions of skin and the baseline level of light is detected.

The results of the model shown in figure 9.18 assume that the skin is uniform, so the remitted light levels detected while the spot is stationary prior to blanching will be identical to those obtained when the spot moves over unblanched skin. This is not the case.

To find the point at which blanching commences, we therefore fit two lines to the data as explained in 9.2.2. However, if the vessels at the centre of the spot blanch in less than one millisecond this technique will not be valid. The rise in the light level detected by the photodiode due to the blanching of these vessels will not be detected as it is masked by the presence of noise. Thus, figure 9.13 should be interpreted as shown in figure 9.19.

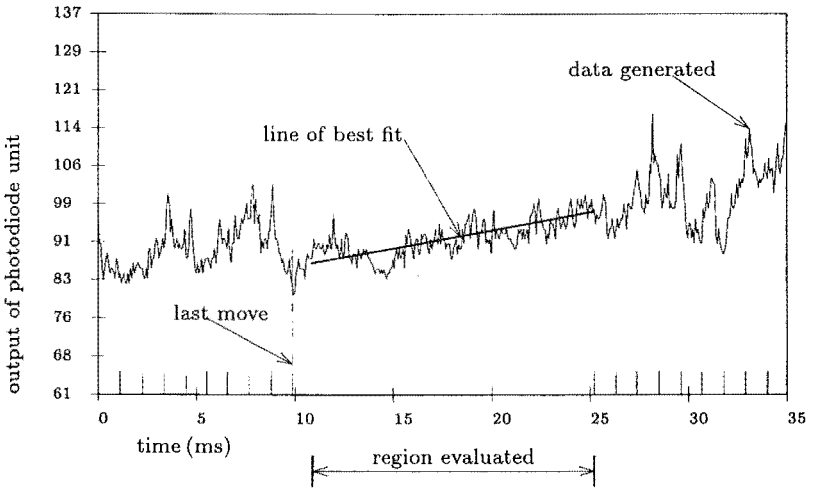

Figure 9.19. Alternative interpretation of figure 9.13.

If it is valid to fit two lines to the data, a superior fitting program is necessary. Such a program should fit the lines so that they join, as shown in figure 9.20. Where the lines join would not be required to coincide with the data from the photodiode unit. If the data was required to coincide with the point where the lines intersected, the presence of noise at the intersection point would have an untoward effect on the calculated result.

9.3.2 Noise in the results

The explanation for the presence of the noise in the output of the photodiode unit relies upon the comparison of figures 9.4 and 9.13. If the spot is incident on skin,

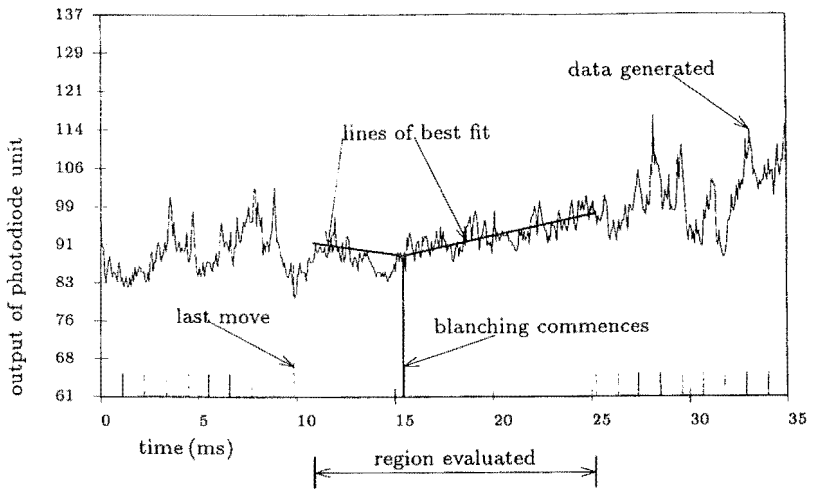

Figure 9.20. The lines that are fitted to the data join at the point where blanching commences. The point at which the lines join need not coincide with a data point.

there is noise in the result, which does not happen when the spot is incident on steel.

We noted that when looking through the data that the noise is less when the spot is near the end of the scan line. In this position, the laser beam is far away from normal incidence. Further, most of the light detected by the photodiode unit will be light that has backscattered out of the skin. When the laser beam is at normal incidence, most of the light detected by the photodiode unit has been reflected from the surface of the skin.

From this observation we suggest that some of the noise in the detected light levels is due to the optical properties of the epidermis changing beneath the laser spot.

The time scale of the noise is such that it cannot be related to movement of the patient, or the flow of blood through the illuminated area.

From figure 7.11, we see that there is oscillation of the scanning mirror along an axis that causes the spot to move to the left and right of the scan line. This effect will move the spot on the patient after the motors are stationary. Consequently, the region of skin illuminated will alter and the level of remitted light may change as a result. This may account for the large noise spikes that are observed immediately after the stepper motors stopped for some of the spots.

9.3.3 Time before the onset of blanching

We have shown that some parts of skin blanch in less than 3 ms. Blanching on these time scales was not detected with the scan mode of treatment as the noise in the results obscured the rise in the detected light levels.

With the spot treatment mode, the spot is stationary on a point for much longer than during normal treatment. More energy is deposited in a point on the skin, so the temperature change in the tissue will be higher. As the rate at which damage is inflicted is temperature related, we expect the changes in the skin to happen over a shorter time period with this treatment mode. The times determined here are probably shorter than what happens during normal scanning.

The time required for the region to blanch must depend on the power density of the incident beam. With a lower power density, less energy is deposited in the vessels. The time before the critical temperature at which damage occurs will be longer, so the response time of the port-wine stain will be longer. Increasing the power density should reduce the time before the onset of blanching.

The histograms in figure 9.17 show the range in response times for each port-wine stain. This may be a result of variations between different points on the port-wine stain. As Niechajev and Clodius (1990) stated in a histological study of port-wine stains, "Extreme differences in abnormal vessel size, mean vascular area per visual field, and the percentage of vascular area filled with red blood cells were repeatedly noted in different regions in the same patient." The angle of incidence of the laser beam will affect the times determined. With a larger angle of incidence, the light has to travel further to reach the blood vessels. Less light will reach the vessels, and so the response time will be slower.

9.3.4 Feedback device for the SCANALL system

During the design and development phases of the SCANALL system, it was hoped that information on when the skin blanches could be used to control the speed of the laser spot across the port-wine stain. The theory was that when the skin blanches, or whitens, the level of light remitted from the skin should increase. At this time the spot should be moved to an adjacent point on the skin.

When the SCANALL system was introduced, the flickering light level was still observed, even though the response time of the eye is much longer than the illumination time used. From this, we realised that the flickering light levels are due to variations in the skin texture and angle of the laser beam, and not to the blanching of the skin below the spot. To see if the skin blanches below the spot, we need to measure the quantity of remitted light.

The high level of noise in the result has made it difficult to determine when blanching commences. This may be overcome by placing several photodiode units at the end of the scanner arm. The recording computer should use the results from the

unit with the lowest noise level.

A further problem is that there are times when the angle between the spot and the skin is such that no blanching occurs. When this happens, the spot could conceivably stop for several seconds while the computer waits for blanching to commence. This possibility must be avoided.

Even if the problems outlined above could be overcome, a feedback system based on a photodiode remains impracticable. During treatment with the SCANALL system, the surgeon observes the effect of the laser beam on the skin beside and behind the spot. This information is not available to the recording computer.

9.4 Conclusion

During the treatment of port-wine stains with a copper vapour laser the light levels in the room are recorded with a fast photodiode. Analysis of this information has determined the time taken before the colour of the skin starts to change from red to white.

The results indicate that port-wine stains do not respond instantaneously to the laser beam. With a 5 W laser beam, 0.3 mm spot diameter the skin begins to change 7 milliseconds after the spot is first incident on the skin.

The noise that is present in the data indicates that the optical properties of the top layer of the skin change in the hundreds of microseconds time scale.

When the laser beam is scanned across the skin, the rapidly changing levels in the quantity of remitted light are attributed to variations in the skin. Measurement of the remitted light levels cannot be used to determine the appropriate speed of the laser spot across the skin.

Chapter 10

Conclusion

In this thesis we have endeavoured to describe the optimal treatment of port-wine stains. We have described theoretical and clinical results which show that the optimal illumination time is in the range of 1-10 ms.

The passage of light through skin was modelled with the Monte Carlo technique (Smithies and Butler, 1995). In this simulation, we used a model of skin that is superior to those previously published in the literature. We used the published optical properties of the individual components of skin to describe the passage of light through our model. The results are consistent with those that we would expect. For example, absorption in the vessels decreases as the depth of the vessel increases. The shallow vessels absorb more than the deeper vessels.

Moving the wavelength away from the absorption peak at 577 nm decreases the absorption in the shallow vessels. This change makes the absorption pattern in the vessel more uniform, so there is more heating at the bottom of the vessel. We predict that this difference is important when the pulsed dye laser is used to treat port-wine stains with sub-millisecond illumination times. Our results show that there is an increase in absorption in the deeper vessels, but that this is not important.

Thus, the optimal wavelength is 577 nm, provided the illumination time is in the 1-10 ms range. The use of this wavelength maximises the heating in the blood filled vessels relative to the heating in the epidermis.

The necessary fluence calculated from the Monte Carlo simulation is one fifth of that used in the clinic. The literature shows that some of the optical parameters may be too high. We show the effect of adjusting these parameters. Even quite drastic reductions in the absorption properties of the blood does not significantly reduce the absorption in the blood filled vessels. The more likely cause of the difference between the calculated and clinical temperature rise is that the description of the epidermis

that is used in the literature is inadequate. Additional information about the optical characteristics of the shallow layers of the epidermis is needed to further improve the model.

Our results predict that the pulsed dye laser (0.4 ms illumination time) will be ineffective when used to treat large vessels. We showed that the endothelial cells at the bottom of the vessel will not be damaged. Clinical trials have verified this finding. For the endothelial cells at the bottom of the vessel to be damaged, the illumination time needs to be in the optimal range of 1-10 ms.

These illumination times can be obtained when an automated treatment system is used to scan the laser beam across the skin. This system, which was described by Smithies *et al* (1991), provides a uniform result with the minimum of untoward damage. This system is not tedious to use as large areas can be treated in the minimum of time.

When this automated treatment device is used to treat port-wine stains with illumination times of 4 ms, transient blanching is observed. We have published these observations (Marini *et al*, 1992). The transient blanching observed results from the damaged endothelial cells of the blood filled vessels expanding towards the centre of the vessel, which removes blood from the treated area. Blanching is transient because the previously empty vessels have dilated and allowed blood to flow into the skin in response to the thermal injury. Observation of the erythema implies that the optical properties of the epidermis have not been sufficiently changed so that it is turned opaque.

Electron microscopy results show that with illumination times of 4 ms there is minimal damage to the surrounding non vascular tissue. Few, if any, changes are observed in the epidermis. Following treatment, the cells in the epidermal are normal in appearance with no discernable loss of structure. These changes were predicted from our theoretical calculations. We have submitted these results for publication (Smithies *et al*, 1995).

Published histological studies report that some of the vessels in the skin are empty. During laser treatment with yellow light, the empty vessels will not be heated. These vessels will not be damaged. These empty vessels will be treated in a subsequent treatment session if they contain blood. Initial anecdotal evidence has shown that after the laser beam has been scanned over a port-wine stain, the region should be cooled with an ice pack and then rescanned. This will increase the number of vessels thermally damaged in any one treatment session.

The blanching response commences several milliseconds after the illumination

time period has ended. We show that some parts of the port-wine stain respond more quickly than other parts. This finding is expected, as the histological work of Niechajev and Clodius (1990) shows there is considerable variation of the structure within a port-wine stain. This work has been submitted for pulication (Mehrtens *et al*, 1995).

Acknowledgements

Throughout the course of my Ph.D., there are many people who have helped me in various ways. First, and perhaps most importantly to my parents, many thanks for your emotional and financial support during the last six years.

To my wife Cindy, I am very grateful for the many hours that you spent discussing aspects of my work and proofreading various documents.

I must thank Anne Segedin and David Baird for your considered advice and encouragement to undertake this Ph.D. You inspired me to do more than teach physics at high school.

I am grateful for the assistance supplied by John Pickering, a fellow student, who helped me to become a competent user of the computer system in this department.

The assistance and discussions that I received from Nathan Mehrtens has been invaluable. I am thankful for your help.

The technical staff in the Physics and Astronomy Department have been a real encouragement. Aside from the numerous comments, "Why have you not finished yet?", they supplied very good advice on many occasions. In particular, I want to thank Stephen Hemmingsen and Ross Ritchie for your help.

When the power supply of the laser that we use in our clinic failed in 1990, and the best efforts of Phil Butler and myself did not fix it, things looked bleak. I appreciated the support supplied by friends, in particular Wayne & Pam Arnold, David & Karen Baird, and Don & Pat Kempt.

Peter Walker, it has been my pleasure to work with you in the operating theatre at St. Georges Hospital. Your generous, quiet spoken nature has made it a delight to work with you. Thankyou also to the anaesthetists (principally Sue Newton) and staff. Your encouragement and jokes were always in the best of taste.

Finally, to my supervisor, Phil Butler. Thank you for the hours you spent examining the various papers that I have written. The question you often asked, "What does this mean?" has stimulated a marked improvement in my writing style. Your considered advice has been helpful on many occasions.

In every Ph.D., there are financial aspects. I am grateful for the scholarship supplied by Medical Laser Developments Ltd., which supported me for most of my Ph.D.. Further, I am grateful for the financial assistance this company provided so that I could travel to a conference in the U.S.A. The Physics and Astronomy Department have assisted me to attend two conferences, the 1992 NZIP conference in Auckland and the Australasian College of Physical Scientists and Engineers in Medicine conference in Auckland 1994.

While writing these acknowledgements, I am mindful of the many people who have supported me over the last six years who have not been mentioned. To these people, many thanks for your help.

Finally, thank you to my daughter Sarah without whose help this thesis would have been finished somewhat sooner.

References

Adams S J, Swain C P, Mills T N, Bown S G, and Salmon P R 1987 The effect of wavelength, power and treatment pattern on the outcome of laser treatment of port-wine stains *British Journal of Dermatology* **117** 487–94

Anderson R R and Parrish J A 1981a The optics of human skin *Journal of Investigative Dermatology* **77** 13–9

——— 1981b Microvasculature can be selectively damaged using dye lasers: A basic theory and experimental evidence in human skin *Lasers in Surgery and Medicine* **1** 293–76

Anderson R R 1987 Carbon dioxide lasers: A broader perspective (letter) *Archives Dermatology* **123** 566–7

Arndt K A 1984 Treatment techniques in argon laser therapy *Journal American Academy Dermatology* **11** 90–7

Ashley S, Brooks S G, Wright H, Gehani A A, and Rees M R 1991 Acute effects of a copper vapour laser on atheroma *Lasers in Medical Science* **6** 23–7

Balasubramanium J A and Bowman H F 1976 *Thermal conductivity and thermal diffusivity of biomaterials. A simultaneous measurement technique* American Society of Medical Engineering, Publication 76-WA/Bio-5

Barsky S H, Rosen S, Geer D E, and Noe J M 1980 The nature and evolution of port wine stains: A computer-assisted study *Journal of Investigative Dermatology* **74** 154–7

Bracewell R N 1978 *The Fourier Transform and Its Applications* (Tokyo: McGraw–Hill, Inc)2

Broska P, Martinho E, and Goodman M M 1994 Comparison of the argon tunable dye laser with the flashlamp pulsed dye laser in treatment of facial telangiectasia *Journal of Dermatological Surgery and Oncology* **20** 749–53

Buecker J W, Ratz J L, and Richfield D F 1984 Histology of port-wine stain treated with carbon dioxide laser *Journal American Academy Dermatology* **10** 1014–9

Burton A C 1934 Application of the theory of heat flow to study of energy metabolism *J Nutr.* **7** 473–533

Buslenko N P, Golenko D I, Shreider Y A, Sobol' I M, and Sragovich V G 1966 *The Monte Carlo Method* (Oxford: Pergamon Press)

Butler P H and van Halewyn C H 1988 *Apparatus for moving a mirror* US patent no 4,750,486

Carruth J A S and Shakespeare P G 1986 Toward the ideal treatment for the port wine stain with the argon laser: Better prediction and an "optimal" technique *Lasers in Surgery and Medicine* **6** 2–4

Carruth J A S, van Gemert M J C, and Shakespeare P G 1992 The Argon Laser in the Treatment of the Port-Wine Stain Birthmark in *Management and Treatment of benign cutaneous vascular lesions* , edited by Tan O T chap 4, pages 53–67(Philadelphia: Lea & Febiger)

Carslaw H S and Jaeger J C 1967 *Conduction of heat in solids* (Oxford: Clarendon Press)

Cashwell E D and Everett C J 1959 *A Practical Manual on the Monte Carlo Method for Random Walk Problems* (New York: Pergamon Press)

Chaffee E E and Lytle I M 1980 *Basic Physiology and Anatomy* (Philadelphia/Toronto: J.B. Lippencott Company)

Chambers I R, Clark D, Bainbridge C, Balakrishnan C, and Piggot T A 1990 Automation of laser treatment of port wine stains (technical note) *Physics in Medicine and Biology* **35** 1025–8

Cheong W F, Prahl S A, and Welch A J 1990 A review of optical properties of biological tissues *IEEE Journal of Quantum Electronics* **QE-26** 2166–85

Çilesiz I F and Welch A J 1994 Optical properties of human aorta: Are they affected by cryopreservation? *Lasers in Surgery and Medicine* **14** 396–402

Cotterill J A 1986 Preliminary results following treatment of vascular lesions of the skin using a continuous wave tunable dye laser which emits at 577 nm *Clinical and Experimental Dermatology* **11** 628–35

Dinehart S M, Waner M, and Flock S 1993 The copper vapor laser for treatment of cutaneous vascular and pigmented lesions *Journal of Dermatological Surgery and Oncology* **19** 370–5

Dixon J A and Gilbertson J J 1986 Argon and neodymium YAG laser therapy of dark nodular port wine stains in older patients *Lasers in Surgery and Medicine* **6** 5–11

Dixon J A, Huether S, and Rotering R 1984a Hypertrophic scarring in argon laser treatment of port-wine stains *Plastic and Reconstructive Surgery* **73** 771–9

Dixon J A, Rotering R H, and Huether S E 1984b Patient's evaluation of argon laser therapy of port wine stain, decorative tattoo, and essential telangiectasia *Lasers in Surgery and Medicine* **4** 181–90

Doughty N A 1990 *Lagrangian Interaction* (Sydney: Addison-Wesley)

DuPuy D L 1989 Measuring solar luminosity with a photodiode *American Journal of Physics* **57** 826–8

Erez A and Shitzer A 1980 Controlled destruction and temperature distributions in biological tissues subjected to monoactive electrocoagulation *Transactions of the ASME* **102** 42–9

Finley J L, Arndt K A, Noe J, and Rosen S 1984 Argon laser-port-wine stain interaction immediate effects *Archives Dermatology* **120** 613–9

Fitzpatrick R E, Lower N J, Goldman M P, Borden H, Behr K L, and Ruiz-Esparza J 1994 Flashlamp-pumped pulsed dye laser treatment of port-wine stains *Journal of Dermatological Surgery and Oncology* **20** 743–8

Freund J E and Walpole R E 1987 *Mathematical Statistics* (London: Prentice/Hall International, Inc)

Gagge A P, Winslow C E A, and Herrington L P 1938 The influence of clothing on the physiological reactions of the human body to varying environmental temperatures *American J of Physiology* **124** 30–50

Ganong W F 1965 *Review of Medical Physiology* (California: Lange Medical Publications)2

Garden J M, Tan O T, Kerschmann R, Boll J, Furumoto H, Anderson R R, and Parrish J A 1986 Effect of dye laser pulse duration on selective cutaneous vascular injury *Journal of Investigative Dermatology* **87** 653–7

Gerrard A and Burch J M 1975 *Introduction to Matrix Methods in Optics* (London: John Wiley & Sons)

Ginsbach G 1991 A tool for the evaluation of colour in port wine stains *Lasers in Medical Science* **6** 49–52

Glasstone S and Edlund M C 1953 *The elements of nuclear reactor theory* (London: MacMillan)

Goldman L, Dreffer R, Rockwell R J, and Perry E 1976 Treatment of portwine marks by an argon laser *Journal of Dermatological Surgery* **2** 385–8

Goldsmith L A, editor 1983 *Biochemistry and Physiology of the Skin* (Oxford: Oxford University Press)

Gouw H S, Evans J H, and Veitch A R 1991 Optimum laser parameters for port-wine stain treatment *Journal of Clinical Laser Medicine & Surgery* **10** 524–32

Graaff R, Dassel A C M, Koelink M H, de Mul F F M, Aarnoudse J G, and Zijlstra W G 1993 Optical properties of human dermis *in vitro* and *in vivo Applied Optics* **32** 435–47

Greenwald J, Rosen S, Anderson R R, Harrist T, MacFarland F, Noe J, and Parrish J A 1981 Comparitive histological studies of the tunable dye (at 577 nm) laser and argon laser: The specific vascular effects of the dye laser *Journal of Investigative Dermatology* **77** 305–10

Hammersley J M and Handscomb D C 1964 *Monte Carlo Methods* (London and Colchester: Spottiswoode, Ballantyne & Co Ltd)

Hanks P, editor 1986 *Collins Dictionary of the English Language* (London: Glasgow & Collins)

Hasegawa Y, Yamada Y, Tamura M, and Nomura Y 1991 Monte Carlo simulation of light transmission through living tissues *Applied Optics* **30** 4515–20

Henriques F C 1947 Studies of thermal injury V. The predictability and the significance of thermally induced rate processes leading to irreversible epidermal injury *Archives of Pathology* **43** 489–502

Henyey L G and Greenstein J L 1941 Diffuse radiation in the galaxy *Astrophysical Journal* **93** 70–83

Hulsbergen-Henning J P, van Gemert M J C, and Lahaye C T W 1984 Clinical and histological evaluation of portwine stain treatment with a microsecond-pulsed dye-laser at 577nm *Lasers in Surgery and Medicine* **4** 375–80

Ishimaru A 1977 Theory and application of wave propogation and scattering in media *Proceedings of the IEEE* **65** 1030–61

——— 1978 *Wave propagation and scattering in random media vol I*) (New York: Academic)

Jacobs A H and Walton R G 1976 The incidence of birthmarks in the neonate *Pediatrics* **58** 218–22

Jacques S L, Alater C A, and Prahl S A 1987 Angular dependence of HeNe laser light scattering by human dermis *Lasers in the Life Sciences* **1** 309–33

Jarrett A 1973 The epidermis in *The Physiology and Pathophysiology of the Skin* , edited by Jarrett chap 1, pages 1–44(London: Academic Press)

Kahn H 1954 Use of different Monte Carlo sampling techniques in *Symposium on Monte Carlo Methods* , edited by Meyer H A pages 146–90University of Florida(New York: John Wiley & Sons, Inc)

Karvonen S L, Vaajalahti P, Marenk M, Janas M, and Kuokkanen K 1992 Birthmarks in 4346 Finnish newborns *Acta Dermato-Venereologica* **72** 55–57

Keijzer M, Star W, and Storchi P 1988 Optical diffusion in layered media *Applied Optics* **27** 1820–4

Keijzer M, Jacques S L, Prahl S A, and Welch A J 1989 Light distributions in artery tissue: Monte Carlo simulations for finite-diameter laser beams *Lasers in Surgery and Medicine* **9** 148–54

Keijzer M, Pickering J W, and van Gemert M J C 1991 Laser beam diameter for port wine stain treatment *Lasers in Surgery and Medicine* **11** 601–5

Knuth D E 1971 *The Art of Computer Programming* (Massachusetts: Addison-Wesley)

Kubelka P 1948 New contributions to the optics of intensely light-scattering materials. Part I *Journal of the Optical Society of America* **38** 448–57

Laffitte F, Mordon S, Chavoin J P, Bonafé J L, and Costagliola M 1992 The frequency–doubled Nd-YAG laser with automatic scanning in the treatment of port–wine stains: A preliminary report *Lasers in Medical Science* **7** 341–9

Lahaye C T W and van Gemert M J C 1985 Optimal laser parameters for port wine stain therapy: A theoretical approach *Physics in Medicine and Biology* **30** 573–87

Landthaler M, Haina D, Brunner R, Waidelich W, and Braun-Falco O 1986 Effects of argon, dye and Nd:Yag lasers on epidermis, dermis and venous vessels *Lasers in Surgery and Medicine* **6** 87–93

Lanigan S W and Cotterill J A 1989 Psychological disabilities amongst patients with port wine stains *British Journal of Dermatology* **121** 209–15

Leider M and Buncke C M 1954 Physical dimensions of the skin: determination of the specific gravity of skin, hair and nail *Archives of Dermatology and Syphiology* **69** 563–9

Lewis R R 1991 The operating regime of longitudinal discharge copper vapour lasers *Optical and Quantum Electronics* **23** S493–S512

Marini L, Butler P H, Smithies D J, and Walker E P 1992 A theoretical model of the blanching response after copper vapour laser treatment of telangiectasia *British Journal of Dermatology* **127** 189–90

Marples M J 1965 *The ecology of the human skin* (Illinois: Charles C Thomas)

Mehrtens N W, Smithies D J, Butler P H, and Walker E P 1995 The blanching process due to copper vapour laser treatment of port-wine stains *Submitted to Phys. Med. Bio*

Mehrtens N W 1994 *The Interaction of Light with Skin* Masters thesisDepartment of Physics and AstronomyUniversity of Canterbury, New Zealand

Miller B F and Keane C B 1987 *Encyclopedia and Dictionary of Medicine, Nursing, and Allied Health* (Philadelphia: WB Saunders Company)

Miller I D and Veitch A R 1993 Optical modelling of light distributions in skin tissue following laser irradiation *Lasers in Surgery and Medicine* **13** 565–71

Montagna W 1956 *The structure and function of skin* (New York: Academic Press)

Mordon S R, Rotteleur G, Brunetaud J M, and Apfelberg D B 1993 Rationale for automatic scanners in laser treatment of port wine stains *Lasers in Surgery and Medicine* **13** 113–23

Morelli J G, Tan O T, Garden J, Margolis R, Seki Y, Boll J, Carnery J M, Anderson R R, Furumoto J, and Parrish J A 1986 Tunable dye laser (577 nm) treatment of port wine stains *Lasers in Surgery and Medicine* **6** 94–9

Mudgett P S and Richards L W 1971 Multiple scattering calculations for technology *Applied Optics* **10** 1485–501

Neumann R A, Knobler R M, Leonhartsberger H, and Gebhart W 1992 Comparative histochemistry of port-wine stains after copper vapor laser (578 nm) and argon laser treatment *Journal of Investigative Dermatology* **99** 160–7

Neumann R A, Leonhartsberger H, Böhler-Sommeregger K, Knobler R M, Kokoschka E M, and Hönigsmann H 1993 Results and tissue healing after copper-vapor laser (at 578 nm) treatment of port wine stains and facial telangiectasias *British Journal of Dermatology* **128** 306–12

Niechajev I A and Clodius L 1990 Histology of port-wine stain *European Journal of Plastic Surgery* **13** 79–85

Noe J M, Barsky S H, Geer D E, and Rosen S 1980 Port wine stains and the response to argon laser therapy: Successful treatment and the predictive role of color, age, and biopsy *Plastic and Reconstructive Surgery* **65** 130–6

Ohmori S and Huang C K 1981 Recent progress in the treatment of portwine staining by the argon laser: some observations on the prognostic value of relative spectro-reflectance (RSR) and the histological classification of the lesions *British Journal of Plastic Surgery* **34** 249–57

Ohtsuka H 1990 Port wine stain: Distribution patterns on the face and neck *Archives of Pathology* **24** 409–13

Orenstein A and Nelson J S 1990 Treatment of facial vascular lesions with a 100-μ spot 577-nm pulsed continuous wave dye laser *Annals of Plastic Surgery* **23** 310–6

Osburn K, Schosses R H, and Everett M A 1987 Congenital pigmented and vascular lesions in newborn infants *Journal American Academy Dermatology* **16** 788–92

Parrish J A and Deutsch T F 1984 Laser photomedicine *IEEE Journal of Quantum Electronics* **QE-20** 1386–96

Pickering J W and van Gemert M J C 1991 585 nm for the laser treatment of Port-Wine Stains: A possible mechanism (letter) *Lasers in Surgery and Medicine* **11** 616–618

Pickering J W, Butler P H, Ring B J, and Walker E P 1989a Computed temperature distributions around ectatic capillaries exposed to yellow (578 nm) laser light *Physics in Medicine and Biology* **34** 1247–58

——— 1989b Thermal profiles of blood vessels heated by a laser *Australasian Physical & Engineering Sciences in Medicine* **12** 11–5

——— 1990a Copper vapour laser treatment of port wine stains: A patient questionaire *Lasers in Medical Science* **5** 43–9

Pickering J W, Walker E P, Butler P H, and van Halewyn C N 1990b Copper vapour laser treatment of port-wine stains and other vascular malformations *British Journal of Plastic Surgery* **43** 273–82

Pickering J W, Walker E P, and Butler P H 1991 The facial distribution of port wine stains on patients presenting for treatment. *Annals of Plastic Surgery* **27** 550–2

Pickering J W, Prahl S A, van Wieringen N, Beek J F, Sterenborg H J C M, and van Gemert M J C 1993 Double–integrating–sphere system for measuring the optical properties of tissue *Applied Optics* **32** 399–410

Pickering J W 1990 *Modelling the Laser Treatment of Vascular Lesions* Ph.D. thesis University of Canterbury

Prahl S A 1988 *Light Transport in Tissue* Ph.D. thesis University of Texas at Austin

Profio A E 1979 *Radiation Shielding and Dosimetry* (New York: John Wiley & Sons)

Ratz J L and Bailin P L 1987 The case for the use of the carbon dioxide laser in the treatment of port-wine stains *Archives Dermatology* **123** 74–5

Rosenfeld H and Sherman R 1986 Treatment of cutaneous and deep vascular lesions with the ND:YAG laser *Lasers in Surgery and Medicine* **6** 20–3

Rotteleur G, Mordon S, Buys B, Sozanski J P, and Brunetaud J M 1988 Robotized scanning laser handpiece for the treatment of port wine stains and other angiodysplasias *Lasers in Surgery and Medicine* **8** 283–7

Rushmer R F 1972 *Structure and Function of the Cardiovascular System* (Philadelphia: W.B. Saunders Company)

Ryan T J 1973 The blood vessels of the skin in *The physiology and pathophysiology of the skin* , edited by Jarret A (London: Academic Press)

Rydh M, Malm M, Jernbeck J, and Dalsgaard C J 1991 Ectatic blood vessels in port-wine stains lack innervation: Possible role in pathogenesis *Plastic and Reconstructive Surgery* **87** 419–22

Shakespeare P G, Hambleton J, and Carruth J A S 1991 Skin surface temperatures during argon and tunable dye laser therapy of port wine stains *Lasers in Medical Science* **6** 29–34

Sheehan-Dare R A and Cotterill J A 1993 Copper vapour laser treatment of port wine stains: clinical evaluation and comparison with conventional argon laser therapy *British Journal of Dermatology* **128** 546–9

——— 1994 Copper vapour laser (578 nm) and flashlamp-pumped pulsed tunable dye laser (585 nm) treatment of port wine stains: results of a comparative study using test sites *British Journal of Dermatology* **130** 478–82

Sheehan-Dare R A 1993 Laser treatment of port wine stains *British Medical Journal* **306** 394–395

Smithies D J and Butler P H 1995 Modelling the distribution of laser light in port-wine stains with the Monte Carlo method *Physics in Medicine and Biology* **40** 701–33

Smithies D J, Butler P H, Pickering J W, and Walker E P 1991 A computer controlled scanner for the laser treatment of vascular lesions and hyperpigmentation *Clinical Physics and Physiological Measurement* **12** 261–7

Smithies D J, Butler P H, Day W T, and Walker E P 1995 The effect of the illumination time when treating port-wine stains. *submitted to Lasers in Medical Science*

Smoller B R and Rosen S 1986 Port-wine stains a disease of altered neural modulation of blood vessels? *Archives Dermatology* **122** 177–9

Spurr A R 1969 A low-viscosity epoxy resin embedding medium for electron microscopy *Journal of Ultrastructure Research* **26** 31–43

Star W M, Marijnissen J P A, and van Gemert M J C 1988 Light dosimetry in optical phantoms and in tissues: I Multiple flux and transport theory *Physics in Medicine and Biology* **33** 437–54

Tait J H 1964 *An introduction to neutron transport theory* Mathematical Physics Series(London: Longmans)

Takata A N 1974 Development of criterion for skin burns *Aerospace Medicine* **45** 634–7

Tan O T and Stafford T J 1992 EMLA for laser treatment of portwine stains in children *Lasers in Surgery and Medicine* **12** 543–548

Tan O T, Carney M, Margolis R, Seki Y, Boll J, Anderson R R, and Parrish J A 1986 Histologic response of port-wine stains treated by argon, carbon dioxide, and tuneable dye lasers *Archives Dermatology* **122** 1016–22

Tan O T, Motomedi M, Welch A J, and Kurban A K 1988 Spotsize effects on guinea pig skin following pulsed irradiation *Journal of Investigative Dermatology* **90** 877–81

Tan O T, Sherwood K, and Gilchrest B A 1989 Treatment of children with port-wine stains using the flashlamp-pulsed tuneable dye laser *New England Journal of Medicine* **320** 416–21

Tan O T, Morrison P, and Kurban A K 1990a 585 nm for the treatment of port-wine stains *Plastic and Reconstructive Surgery* **86** 1112–7

Tan O T, Stafford T J, Murray S, and Kurban A K 1990b Histologic comparison of the pulsed dye laser and the copper vapor laser effects on pig skin *Lasers in Surgery and Medicine* **10** 551–8

Tan O T 1992 Pulsed Dye Laser Treatment of Adult Port-Wine Stains in *Management and treatment of benign cutaneous vascular lesions* , edited by Tan O T chap 6, pages 83–99(Philadelphia: Lea & Febiger)

Torres J H, Welch A J, Çilesiz I F, and Motamedi M 1994 Tissue optical property measurements: Overestimation of absorption coefficient with spectrophotometric techniques *Lasers in Surgery and Medicine* **14** 249–57

van Gemert M J C and Welch A J 1987 Treatment of port-wine stains: Analysis *Medical Instrumentation* **21** 213–7

van Gemert M J C, de Kleijn W J A, and Hulsbergen-Henning J P 1982 Temperature behaviour of a model port-wine stain during argon laser coagulation *Physics in Medicine and Biology* **27** 1089–104

van Gemert M J C, Welch A J, and Amin A 1986 Is there an optimal treatment for port wine stains? *Lasers in Surgery and Medicine* **6** 76–83

van Gemert M J C, Jacques S L, Sterenborg H J C M, and Star W M 1989 Skin optics *IEEE Transactions on Biomedical Engineering* **36** 1146–54

van Gemert M J C, Carruth J A S, and Shakespeare P G 1991a Has the argon laser ever been used optimally for the treatment of port wine stain birthmarks? *Lasers in Medical Science* **6** 371

van Gemert M J C, Welch A J, Miller I D, and Tan O T 1991b Can physical modelling lead to an optimal laser treatment strategy for portwine stains? in *Laser Applications in Medicine and Biology , vol 5)* , edited by Wolbarsht M L (New York: Plenum Press)

van Gemert M J C, Pickering J W, and Welch A J 1992 Modelling Laser Treatment of Port-Wine Stains in *Management and treatment of benign cutaneous vascular lesions* , edited by Tan O T chap 2, pages 24–47(Philadelphia: Lea & Febiger)

van Gemert M J C 1992 Modelling Laser Treatment of Portwine Stains: Fact or Fiction *Journal of Clinical Laser Medicine & Surgery* pages 1–5

van Halewyn C N, Miles C, Butler P H, Holdsworth J, and Walker E P 1989 Rare-earth doped eyewear provide for safer laser surgery (letter) *British Journal of Dermatology* **120** 470–1

Verkruysse W, Pickering J W, Beek J F, Keijzer M, and van Gemert M J C 1993a Modelling the effect of wavelength on the pulsed dye laser treatment of port wine stains *Applied Optics* **32** 393–8

Verkruysse W, Trelles M A, and Pickering J W 1993b Defining purpura *Journal American Academy Dermatology* **28** 666

Wagner K D and Wagner R F 1990 The necessity for treatment of childhood port-wine stains *Cutis* **45** 317–318

Walker E P, Butler P H, Pickering J P, Day W A, Fraser R, and van Halewyn C N 1989 Histology of port wine stains after copper vapour laser treatment *British Journal of Dermatology* **121** 217–23

Waner M, Dinehart S M, Wilson M B, and Flock S T 1993 A comparison of copper vapor and flashlamp pumped dye lasers in the treatment of facial telangiectasia *Journal of Dermatological Surgery and Oncology* **19** 992–998

Welch A J, Wissler E H, and Priebe L 1980 Significance of blood flow in calculations of temperature in laser irradiated tissue *IEEE Transactions on Biomedical Engineering* **BME-27** 164–6

Welch A J, Yoon G, and van Gemert M J C 1987 Practical models for light distribution in laser-irradiated tissue *Lasers in Surgery and Medicine* **6** 488–93

Welch A J 1984 The thermal response of laser irradiated tissue *IEEE Journal of Quantum Electronics* **QE-20** 1471–81

Wheeland R G 1993 Treatment of port-wine stains for the 1990s *Journal of Dermatological Surgery and Oncology* **19** 348–56

Wilson B C and Adam G 1983 A Monte Carlo model for the absorption and flux distributions of light in tissue *Medical Physics* **10** 824–30

Witt A N 1977 Multiple scattring in reflection nebulae I. A monte carlo approach *Astrophysical Journal Supplement Series* **35** 1–6

Wood E J and Bladon P T 1985 *The Human Skin* (London: Arnold)

Yoon G, Welch A J, Motomedi M, and van Gemert M J C 1987 Development and application of three-dimensional light distribution model for laser irradiated tissue *IEEE Journal of Quantum Electronics* **QE-23** 1721–33